SPECTROSCOPIC STUDIES ON THE MOLECULAR STRUCTURAL CHANGES OF PLASTICS AND PLASTICIZERS AT MODEL ENVIRONMENTAL INTERFACES

by

Jeanne Marie Hankett

A dissertation submitted in partial fulfillment
of the requirements for the degree of
Doctor of Philosophy
(Chemistry)
in the University of Michigan
2015

Doctoral Committee:

Professor Zhan Chen, Chair
Professor Robert T. Kennedy
Professor Kenichi Kuroda
Professor Mark E. Meyerhoff

DEDICATION

To Mom & William
Your love and support are the world to me.

In loving memory of Dad
…I did it!

ACKNOWLEDGEMENTS

My journey through graduate school has been far different from anything I could have expected. From academic highlights to work disappointments, to personal struggles, excitement, seemingly insurmountable challenges, fun adventures, stressors, and good and poor health, it was friends, family, colleagues and mentors that saw me through it all. As I step back, the phrase "it takes a village to earn a PhD" is indeed nothing short of the truth. I am incredibly thankful for the kind words, inspiration, advice, pep talks, collaborations, nonchalant conversations, and shared emotions I have experienced throughout the past five years.

I am extremely grateful to my advisor Dr. Zhan Chen, first of course, for letting me join his lab, fostering enthusiasm, skills, leadership and independence, and challenging me with difficult problems, questions, concepts, and projects not only in research, but in academics and beyond. You have given me so many opportunities for growth. Thank you for supporting my off-the-wall ideas, and reining me in when they went too far. Thank you for all your coaching, strategizing, and instruction. You have made me a better scientist and a much stronger individual.

I am also grateful for the faculty, students, and staff of the Chemistry Department and science departments here at UM. From research to classes, there has always been a drive to foster excellence in a positive manner. I have received so much support and positive challenges from so many people! My committee members especially, Dr. Robert Kennedy, Dr. Kenichi

Kuroda, and Dr. Mark Meyerhoff have given incredible support, guidance, direction, counseling and insights for which I am extremely grateful.

And of course I cannot forget to mention my great thanks to the elite five friends/coworkers/scientists-in-arms/cohorts/confidants/adventurers that are the former lab mates and now doctors from the Chen lab: Jesse Zhang, Joshua Jasensky, Yuwei Liu, Lauren Soblosky, and Bei Ding. All of you are simply awesome. The amount that we have learned from each other in a few short years is mind boggling. Thank you so much for helping the new confused lab member, re-teaching me basic solving skills, and sharing both great and tough times. I have loved our journey together and I look forward to more adventures in the future! Dr. Xiaoxian Zhang, you have been a great collaborator, friend, and confidant. I consider myself lucky to have worked on some of the same projects with you; you made collaboration easy! And all the rest of the members of our lab that I have overlapped with, it has been a pleasure getting to know and work with everyone! I am happy to call all of you friends and I am super grateful to have worked in a lab that has such camaraderie.

I am grateful to the many collaborators I have had the pleasure of working with during my time here at UM, especially Dr. Xiaolin Lu, Dr. Alexander Welle, and Dr. Melissa Duhaime. I have learned so much from our work together and have had so many wonderful opportunities to expand my research, knowledge, and skill set by collaborating with you. It has been a joy both professionally and personally to work with you. Thanks as well to all the members of the Water Center Great Lakes Microplastics team! To work with so many wonderful people has truly been a blessing.

I give my utmost thanks to the physical therapy team at UM clinic, especially Roseanne Crompton, Maria Pap, and Angie Abner. Through my many injuries and struggles, your expertise, care and support has kept me moving throughout these years, and has allowed me to finish my studies!

Last, but never least, I am forever grateful to my amazing and wonderful emotional support team: my family and friends. I want to thank my Mom, Dad, Will, Ali, Brian, grandpa Bob, Will's father Rod, friends Danny Rudnick, Laura Horan, Michael Logli and many more friends too numerous to mention I have made along the way. All of you have transformed my life from surviving to thriving even during hardship. Mom, your love and prayers have kept me afloat in seemingly impossible times. Will, you have been my partner and supporter through academic and personal struggles, devastating loss, ridiculously fun times, class work, research collaboration, and everything in between. Thank you for everything!

To keep myself from repeating endlessly, I have met **so** many wonderful people through my PhD journey that have influenced me greatly. Although I may not list them by name, they have positively impacted my life. Thank you, thank you!!!

TABLE OF CONTENTS

LIST OF FIGURES

LIST OF TABLES

ABSTRACT

The mainstream introduction and development of plastics has been integral in the formation of modern urban infrastructures and has allowed for the advancement of medical, electronic, and industrial technologies. Some plastics first mass produced nearly a century ago like poly(vinyl chloride) (PVC) and poly(styrene) (PS) are still widely utilized with global annual production exceeding tens of millions of tons. The long term and widespread use of these two plastics make them some of the most studied anthropogenic materials to date. However, there remain some major holes in understanding how the institution of these plastics affects the environment at a molecular level, likely due to a lack of appropriate analytical techniques to gain this information. Herein, the work in this thesis develops a wide understanding of how phthalate-plasticized PVC plastics interact with the surrounding environment at a molecular level. Plastic and plasticizing phthalate behaviors at air, water and silica interfaces were elucidated using a combination of spectroscopic surface sensitive techniques including sum frequency generation (SFG) vibrational spectroscopy, x-ray photoelectron spectroscopy, and time-of-flight secondary ion mass spectrometry. Both molecular surface and bulk changes of plastics exposed to a variety of harsh chemical environments were determined using select analytical techniques. In contrast to traditional plastics research, plastics were probed *in situ* and in real time at the molecular level without disturbing the integrity of the plastic whenever feasible.

Studies on the natural state of phthalate-plasticized PVC surfaces and on molecular effects of heat and water contact on PVC plastics revealed that phthalates can be present on plastic surfaces even when a low percentage of these plasticizers are added to PVC. Applied heat was found to induce dramatic phthalate leaching over hours, and water contact induced permanent changes to the surfaces of PVC plastics from both molecular restructuring and phthalate leaching. Surface phthalates were found to leach into water and permanently transfer to new surfaces through water contact in only minutes. Additionally, the molecular mechanisms and effects of treatments we designed to reduce phthalate leaching or degrade phthalates in plastic: plasma and short wave UV light treatments, respectively, were deduced. Air plasma treatment was found to induce drastic chemical changes to the surface of PVC plastics dominated by PVC chains including scission, chlorine removal, oxygen deposition, and minor surface crosslinking, while the bulk of the plastic remained intact. Exposure of plastics to short wave UV light was determined to be a potentially efficient means of phthalate removal for disposed plastics, resulting in phthalate degradation on the surface and throughout the plastic, with most toxic molecules removed after 5 h of exposure and little damage to PVC chains. Short wave/H_2O_2 treatments led to competing radical reactions with PVC chains over phthalates and increased molecular surface disorder, and long wave UV exposure and long wave/H_2O_2 treatments induced only very minor chemical reactions in and on phthalate-plasticized PVC films.

In later studies, we turned our attention to understanding how PS plastics adsorb and desorb local environmental toxins at a molecular level. Using analytical techniques SFG spectroscopy and quartz crystal microbalance in combination with new environmental point-source experimental models, we revealed how marine and human toxins nonylphenols (NP)s

deposit and order differently on PS plastics when the plastic is located above a calm water surface versus over land. NPs were found to remain much more highly ordered on PS if they were originally deposited under humid conditions, even after agitation of the plastic surface by moving water and re-exposure to air. Interestingly, a similar order of NPs were found to deposit on PS plastic under both model land and surface lake conditions though the theoretical availability of NPs was at ppm concentrations near dry land and ppt concentrations near a lake surface. By understanding how plastics release and adsorb toxins at a molecular level we can predict what sort of surface and bulk changes will occur before any microscopic or macroscopic changes to the plastic can be observed and more accurately gauge the impact of currently implemented plastics on a wide variety of ecosystems. Ultimately this information aids in the future design and formulation of newer, more environmentally friendly plastics.

CHAPTER 1

INTRODUCTION

1.1 Motivation and Background

As a whole, the plastic industry has revolutionized modern life around the world. As early as 1922, plastics became available to the Western public at large, in the form of Bakelite, the first synthetic thermosetting polymer. Bakelite's uses quickly expanded and could be found in industrial components, electrical wiring, household items and even toys.[1,2] The successful mass production and application of synthetic Bakelite products sparked the plastic revolution of the 1930s-1950s. Within only several decades, a thriving worldwide market for synthetic polymer materials was born.[1] Since this era, there has been great drive to develop better, cheaper, stronger, and more versatile plastics. As plastic synthesis and production technology progressed, more structurally complex polymers and plastics were devised in a self-feeding, ever progressing cycle. Better plastics = better technologies = greater ability to synthesize new plastics. Molecules and materials found to yield beneficial structural and physical properties were added during production, and plastics soon came to be known as the standard for endurance and affordability. The formulation of products with appropriate flexibility, porosity, color, strength, weight, and shelf-life allowed for the invention of millions of modern devices, everyday items and conveniences which could not be fabricated with traditional materials. [3,4]

Unfortunately, there were many oversights in the midst of the plastic economic explosion which impact us today. Consequently, it has been well demonstrated that the mainstream introduction of billions of tons of these ultra-durable, non-native materials has a rather large negative impact on the environment at both a macroscopic and molecular scale.[5-16] Take for example, the story of a single family of plastic: poly(vinyl chloride) or PVC, which will be a major focus of research in this thesis. PVC is considered one of the first generation commercial plastics, developed in the late 1800s and manufactured in the 1920s.[3] Along with poly(styrene) (PS), poly(propylene) (PP), and poly(ethylene terephthalate) (PET), PVC was commercially produced during the plastic revolution and has become a major player in the plastic market today. The formulation of PVC plastic has remained relatively unchanged in the last few decades and PVC is still widely used for industrial purposes, household items, wiring, tubing and cables, paints, medical devices, children's toys, and vinyl flooring, among thousands of other applications.

PVC, if manufactured without additional plasticizing compounds, forms rather rigid and/or brittle materials. As such, it is not too difficult to conjecture why it took several decades for PVC use to popularize; there simply wasn't any well known method to make PVC supple. It wasn't until the 1930s, when the molecule bis-2-ethyhexyl phthalate, otherwise known as di-2-ethylhexyl phthalate (DEHP), became commercially available, that PVC became an international plastic leader.[1,4,17] The molecular structures of PVC and DEHP can be seen below in Figure 1.1.

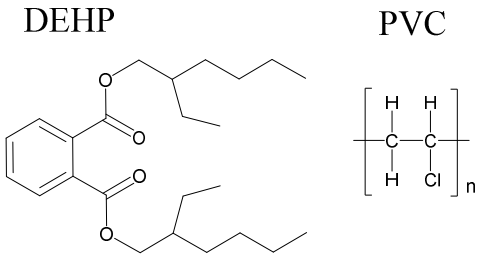

Figure 1.1. Molecular structures of di-2-ethylhexyl phthalate (DEHP) (left), and poly(vinyl chloride) (PVC) (right).

DEHP belongs to a class of small, non-covalently bound phthalate plasticizers that are still used to achieve appropriate PVC plastic elasticity and pliability for different applications. When phthalates were first introduced as a cost-effective, relatively simple means to plasticize PVC plastics, negative interactions between these molecules and living organisms were relatively unknown. Both the ease of plastic manufacture and the low cost of phthalate synthesis led to the mass production of millions of tons of phthalate plasticized PVC products per year.

Today we know that phthalates are suspected human and marine toxins, suspected human carcinogens, and proven rodent endocrine disruptors and have been well documented to pervade urban and rural environments. In fact, many scientific studies have demonstrated correlations of increased phthalate levels in surrounding environments and in living organisms with adverse health effects in animals and humans.[18-59]

One of the most famous studies on phthalate toxicity was conducted by EPA toxicologists in 2000. Louise Parks and researchers determined that the introduction of 750 mg/kg/day of DEHP to fetal and postnatal male rats resulted in inhibited testosterone production, reduced anogenital distance, and reduced testis weight. Ultimately this meant that exposure to DEHP induced malformations in male rats.[59] Interestingly, in contrast to the induced androgenic effects from relatively low dose exposure, the lethal DEHP dose (LD-50) for rodents is quite

high. The oral LD-50 for rats, for example, is 30,000 mg/kg, leading researchers to label DEHP as a rodent reproductive toxin rather than an acute toxicant.[60]

More current research has revealed that phthalates may have negative impacts on reproductive health of humans as well as rodents. To list a couple quick examples, strong associations between increased concentrations of active metabolites of DEHP in male urine and increased sperm DNA damage have been reported[35] as well as increases in cell oxidative stress associated with increased DEHP exposure.[32,33,39] In response to the plethora of toxicity findings, some countries have banned the use of phthalates in various consumer products in favor of more expensive, but less toxic plasticizers. Many countries, however, either due to lack of facilities and financial means, political discourse, or more complicated reasons, still utilize high concentrations of phthalates as plasticizers. This includes the United States, where strict regulations limit the use of phthalates in certain types of children's toys, but the use of phthalates in medical equipment and devices is currently allowed.[61,62] As a result, new PVC products are often plasticized up to 75% by weight of phthalates, with DEHP leading the charge in plasticizer market share. Since phthalates are persistently applied in the PVC industry and have been utilized for decades, it is extremely important to further understand the impact of both PVC and phthalates on the environment and living ecosystems.

By and large, PVC and phthalates, and all of the molecules studied in this thesis for that matter, have been well characterized, including toxicological studies, examination of bulk and/or macroscopic properties, and bulk degradation as previously cited in this introduction and listed here.[9,19,32,35,45,46,51,56,58-93] Information on the negative impacts of PVC, PS, PET and other common plastics have changed hands from scientists to the public at large through the generations. Ask the average American middle school child why we recycle plastics, and he or

she will likely rattle off stories of plastics cluttering beaches, trapping fish, and piling up in landfills. Yet still, after almost hundreds of years of using PVC and common plastics, there remain some fundamental missing pieces of information about how plastics, plasticizers, and plastic components interact with and influence surrounding matter. That is, previous to this research, there existed very little understanding of the *surface* behaviors of these molecules, likely due to a lack of appropriate analytical techniques to gain this information.

Thus, we reach the first focus of this thesis: studying the surface molecular level behaviors of phthalates and simple PVC plastics *in situ* in a variety of different environments [90-94] which until now have remained mostly unknown.[4,18,22,44,99,100] A large section of this research focus is dedicated to evaluate the potential for non-covalently bound phthalates to interact with living organisms, undergo chemical reactions, or segregate and accumulate at a molecular level under various environmental conditions. Additionally we study the molecular level changes of plastics from various purposely applied leaching and/or surface treatments. These studies allow us to better evaluate the risks encountered with these materials and to evaluate new sustainable treatment methods that minimize phthalate contact with living organisms.

Of course, the interaction of toxin molecules from plastics with surrounding matter is only one of many ways that plastics pervade areas far outreaching their intended applications. A second focus in this thesis shifts gears to study how and why plastics *adsorb* environmental toxins under different conditions. Rather than focus on the molecular components that make up a plastic like PVC, I study molecules from the surrounding environment interacting with the surfaces of common plastic PS. This revolution-era plastic often finds its way into natural ecosystems, where there is potential for various complicated interactions with wildlife. Mainly,

the plastics can break into smaller pieces, upset flora and fauna balance, and release and collect toxins.

My molecular level studies take us to a narrow section of the field of plastic/toxin interactions: evaluating how hydrophobic plastics that end up in fresh-water ecosystems may play a key role in toxin distribution through uptake and release of toxins in different environmental platforms.[7,8,15,16,101-125] It has been previously established that there is enormous potential for hydrophobic microplastics like PS to interact with industrial runoff and contaminants in the Great Lakes.[5,6,8,104,110,120,126-130] By studying the molecular level interactions between toxins and plastics in aquatic ecosystems in real time and *in situ*, we aid in explaining how and why microplastics interrupt ecosystem balance at a very fundamental level. Therefore as an environmentally relevant model, the molecular level interactions of nonylphenols (NPs), human and aquatic toxins commonly found in the Great Lakes, with PS under different model conditions were examined in this thesis.

To summarize, much of the work in this thesis is investigative in nature, aiming to scrutinize environmental risks as well as evaluate green methods to prevent negative interactions between plastics and the surrounding matter. I strongly believe that research efforts should focus on better understanding currently used toxic plasticizers and remediation efforts in addition to developing future safe plasticizers and plastics. There are many ways to study the impact of commonly used plastics on the environment, and thousands of avenues of research topics within this field. Here, I aim to show progress in one of those avenues: filling a large knowledge gap regarding the environmental impacts of widely utilized polymeric materials by focusing on *in situ* molecular level characterizations of phthalates, PVC, NPs, and other common plastics at environmentally relevant surfaces and interfaces.

Finally, this leaves us now with an analytical question of how we were able to gain these surface molecular level insights. *In situ* molecular level studies of plastic surfaces and interfaces were accomplished by using a nonlinear optical technique called sum frequency generation (SFG) vibrational spectroscopy which will be described in detail in the following sections. In turn, we generated a broad picture on molecular interactions and behaviors of our systems of study overall by combining information obtained from SFG with that of other analytical techniques such as coherent anti-Stokes Raman scattering (CARS), secondary ion mass spectrometry (SIMS), and Fourier transform infrared spectroscopy (FTIR), among others. The utilization of SFG was crucial to these studies, revealing molecular-level changes in plastics that can vastly impact biota but cannot be observed with traditional analytical techniques due to detection limitations and/or destructive analyses.

With SFG, we could focus specifically on studying surface changes of plastics in air, water, under humidity, and at solid interfaces, which is greatly warranted since plastic surfaces directly contact and interact with living organisms during the plastic's use and after disposal. And by focusing on studying molecules on surfaces and interfaces of plastics *in situ*, we gain a deeper fundamental understanding of the effects of harsh chemical treatments applied during and after manufacture, the ability to predict the effectiveness of plastic treatments, and the risk of direct exposure to surface toxic molecules under various environmental stressors. In closing, my hope here is that this research, though extremely narrow in the scope of polymer studies, may help reveal the structures of surfaces and interfaces of currently manufactured plastics, and aid in designing safer future surface treatments and plastics.

1.2 Introduction to Sum Frequency Generation Vibrational Spectroscopy

SFG is the main technique utilized in these studies to conduct the aforementioned surface and interface studies *in situ*. SFG is a truly surface sensitive second order nonlinear optical process capable of providing molecular vibrational information for molecules where centrosymmetry is broken, i.e. at surfaces and interfaces.[131-134] The interfacial sensitivity of SFG is provided by the selection rule which is different from linear vibrational spectroscopy. Because SFG is a second order nonlinear optical process, the signal intensity is proportional to the square of the second order nonlinear optical susceptibility of the material $\chi^{(2)}$ under the electric dipole approximation. The selection rule under the electric dipole approximation for the SFG process states that no SFG signal will be generated for materials with inversion symmetry. However, at surfaces and interfaces where centrosymmetry is broken, SFG signal may be generated. Most bulk materials have inversion symmetry and therefore do not generate SFG signal.

SFG has been demonstrated to be a very powerful spectroscopic technique over the past couple decades to probe environmental and polymeric interfaces without disturbing the systems of study (i.e. no destruction of sample or vacuum required), an advantage over many traditional analytical instruments.[135-170] A number of other techniques were utilized in this thesis work to complement SFG data and to generate a better picture of molecular behaviors, including coherent anti-Stokes Raman scattering (CARS), contact angle goniometry, x-ray photoelectron spectroscopy (XPS), time-of-flight mass spectrometry (ToF-SIMS), and Fourier transform infrared spectroscopy (FTIR). CARS and ToF-SIMS will be described later in this chapter.

The SFG process may occur when two pulsed laser beams, one with a tuneable IR frequency ω_{IR}, and the other with a fixed visible frequency ω_{VIS}, overlap spatially and temporally

at a surface or interface. SFG can probe interfaces that are accessible to laser light including air/film interfaces, film/water interfaces, film/film interfaces, and film/optical substrate interfaces *in situ* and in real time at sub-monolayer sensitivity. An SFG signal can be generated at a specific direction given by phase matching conditions with a frequency $\omega_{SFG} = \omega_{IR} + \omega_{VIS}$. The intensity of this sum frequency signal is resonantly enhanced when the tuneable IR frequency equals that of a vibrational transition of a molecule. Thus, SFG signal intensity plotted against the input IR frequency provides a vibrational spectrum consisting of vibrational peaks contributed by molecular vibrational modes of molecules.

In general, the SFG process is considered a combination of both IR absorption and anti-Stokes Raman scattering. By applying different polarization combinations of the input and output laser beams, SFG can be used to elucidate molecular orientation or ordering information at interfaces and/or information on the number of molecules or molecular groups present, which will be discussed in detail later. The following two sections of this chapter describe SFG experimental setup and theory in detail.

1.3 SFG Experimental Details

The SFG systems used for the presented studies were commercially available from EKSPLA (Vilnius, Lithuania), composed of a pico-second Nd:YAG laser, a harmonic unit with two KD*P crystals, an optical parametric generation (OPG)/optical parametric amplification (OPA) and difference frequency generation (DFG) system based on LBO and $AgGaS_2$ (or GaSe) crystals and a detection system. The output of the Nd:YAG laser is a 20 Hz 20 ps 1064 nm near-IR beam. The visible input 532 nm beam for SFG experiments is generated by frequency-doubling a portion of this 1064 nm beam. The OPG and OPA can generate a signal beam (420 to

680 nm) and an idler beam (740 to 2300 nm). The idler beam and the 1064 nm pump beam are used in the DFG to generate a tunable mid-IR light (from 1000 cm^{-1} to 4300 cm^{-1}). For SFG experiments, the input visible and IR pulse energies are both ~100 μJ. The incident angles of the visible and the IR input are 60° and 55° versus the surface normal, respectively. The diameters of both input beams at the surface are about 500 μm. The SFG signal from the surface passes through a monochromator, is collected by a photomultiplier tube and processed with a gated integrator. The powers of both beams are monitored by two photodiodes and this power information can be used for data normalization. The schematic of the SFG laser system can be found in Figure 1.2 and the energy diagram of the SFG process as well as an illustration of generic sample setups can be found in Figure 1.3. To conduct SFG analysis, all samples analyzed in this thesis were held on an optical substrate like a fused silica or CaF_2 window or right angle prism at the sample stage.

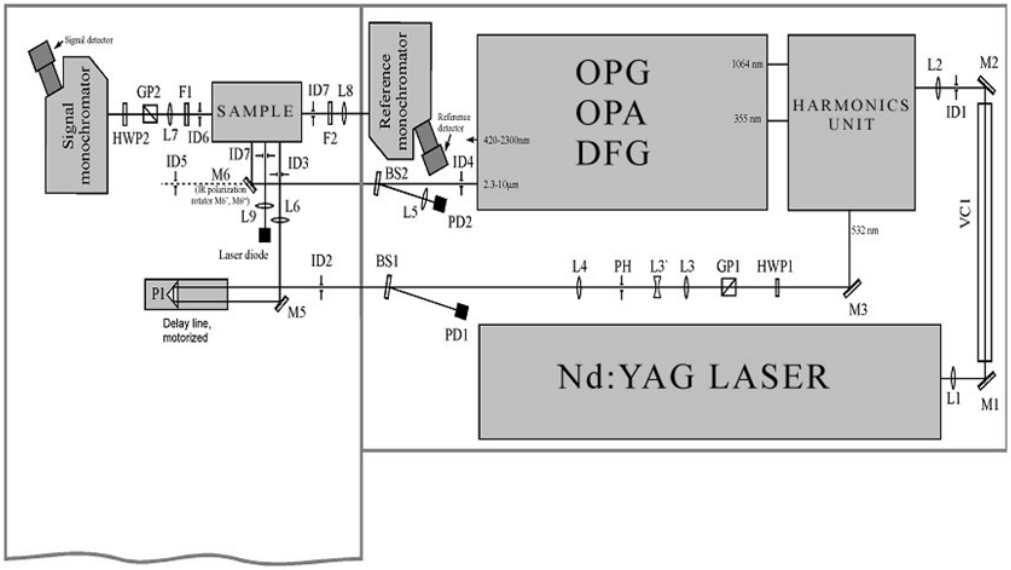

Figure 1.2. Schematic of the SFG laser system illustrating the Nd:YAG laser unit, Harmonics unit, OPG/OPA/DFG, sample stage and monochromator (from EKSPLA laser manual).

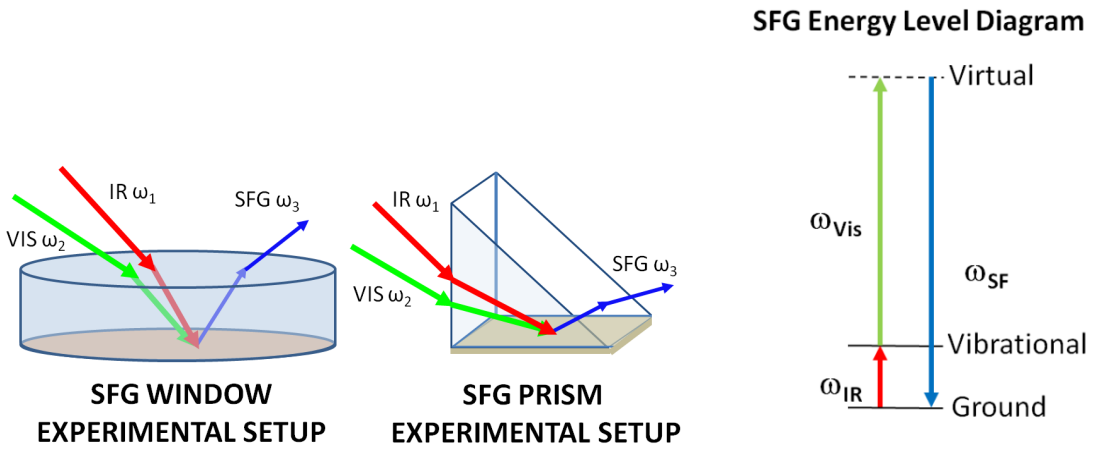

Figure 1.3. Illustration of two common SFG sample geometries using window and prism optical substrates with spin coated polymer (left) and the SFG energy level diagram (right).

1.4 Additional Information on SFG Signal Contributions

As previously stated, SFG is a coherent optical process involving two input (visible and infrared) beams and one output (sum) beam. In a generic sense the SFG signal intensity can be described as proportional to the intensities of the input IR and visible beams (I_{IR} and I_{vis}) and the effective second order nonlinear susceptibility ($\chi_{eff}^{(2)}$)[171]:

$$I_{SFG} \propto \left|\chi_{eff}^{(2)}\right|^2 I_{IR} I_{vis} \qquad \textbf{Eq. 1.1}$$

More specifically, the output sum frequency intensity obtained experimentally in the reflection mode can be described as[171,172]:

$$I(\omega) = \frac{8\pi^3 \omega^2 \sec^2 \beta}{c^3 n_1(\omega_1) n_1(\omega_2) n_1(\omega)} \left|\chi_{eff}^{(2)}\right| I_1(\omega_1) I_2(\omega_2) AT \qquad \textbf{Eq. 1.2}$$

where β is the output sum frequency reflection angle, $n_i(\omega_i)$ is the frequency (ω_i) dependent refractive index of the medium, $I_1(\omega_1)$ and $I_2(\omega_2)$ are the intensities of the input visible and IR fields, respectively, T is the input beam pulse-width, A is the overlapping area of the two

input beams at the sample surfaces or/and interfaces, and $\chi_{eff}^{(2)}$ is once again the effective second-order nonlinear optical susceptibility.

Since each beam can be adjusted to either an s- or p-polarization, $\chi_{eff}^{(2)}$ with different polarization combinations can be experimentally measured, such as ssp (s-polarized sum frequency signal, s-polarized visible beam, and p-polarized IR beam), sps, pss, and ppp polarization combinations.[172] As such, for an isotropic interface in the x-y plane, the effective second order nonlinear optical susceptibility components can be related to the second order nonlinear optical susceptibility components of the sample in the lab-fixed coordinating system. With the coordinate system defined as xy plane = the surface or interface of interest, z perpendicular to the surface/interface, and xz plane = plane of incoming and outgoing laser beams, we have:

$$\chi_{eff,ssp}^{(2)} = L_{yy}(\omega)L_{yy}(\omega_1)L_{zz}(\omega_2)\sin\beta_2\chi_{yyz} \qquad \textbf{Eq. 1.3}$$

$$\chi_{eff,sps}^{(2)} = L_{yy}(\omega)L_{zz}(\omega_1)L_{yy}(\omega_2)\sin\beta_1\chi_{yzy} \qquad \textbf{Eq. 1.4}$$

$$\chi_{eff,pss}^{(2)} = L_{zz}(\omega)L_{yy}(\omega_1)L_{yy}(\omega_2)\sin\beta\chi_{zyy} \qquad \textbf{Eq. 1.5}$$

$$\begin{aligned}\chi_{eff,ppp}^{(2)} = &-L_{xx}(\omega)L_{xx}(\omega_1)L_{zz}(\omega_2)\cos\beta\cos\beta_1\sin\beta_2\chi_{xxz}\\ &-L_{xx}(\omega)L_{zz}(\omega_1)L_{xx}(\omega_2)\cos\beta\sin\beta_1\cos\beta_2\chi_{xzx}\\ &+L_{zz}(\omega)L_{xx}(\omega_1)L_{xx}(\omega_2)\sin\beta\cos\beta_1\cos\beta_2\chi_{zxx}\\ &+L_{zz}(\omega)L_{zz}(\omega_1)L_{zz}(\omega_2)\sin\beta\sin\beta_1\sin\beta_2\chi_{zzz}\end{aligned} \qquad \textbf{Eq. 1.6}$$

For an isotropic non-chiral surface, there are only seven non-zero tensor components of second-order nonlinear susceptibility (χ_{yyz}, χ_{yzy}, χ_{zyy}, χ_{xxz}, χ_{xzx}, χ_{zxx}, and χ_{zzz}) within the surface-fixed coordinate system. β, β_1 and β_2 are the output angles for the sum frequency signal, input

angle of the visible beam and input angle of the infrared beam, respectively and ω, ω_1 and ω_2 are frequencies of the sum frequency beam, the visible beam and the IR beam, respectively. L_{ii}s are (i=x, y, or z) the Fresnel coefficients responsible for the local field correction of the two input and one output beams. For a single surface or interface embedded between two semi-infinite media, L_{ii}s can be written as[172-174]:

$$L_{xx}(\omega) = \frac{2n_1(\omega)\cos\gamma}{n_1(\omega)\cos\gamma + n_2(\omega)\cos\beta} \qquad \textbf{Eq. 1.7}$$

$$L_{yy}(\omega) = \frac{2n_1(\omega)\cos\beta}{n_1(\omega)\cos\beta + n_2(\omega)\cos\gamma} \qquad \textbf{Eq. 1.8}$$

$$L_{zz}(\omega) = \frac{2n_2(\omega)\cos\beta}{n_1(\omega)\cos\gamma + n_2(\omega)\cos\beta} \cdot \left(\frac{n_1(\omega)}{n'(\omega)}\right)^2 \qquad \textbf{Eq. 1.9}$$

For all the sum frequency, visible and IR beams, such equations responsible for the local field correction are valid. Here, β is the beam input or output angle, γ is the refracted angle in the medium 2, and $n'(\omega)$ is the refractive index of the surface or interfacial layer. An SFG spectrum can be fitted to deduce $\chi^{(2)}_{eff}$ components obtained experimentally, using the following equation, a sum of Lorentzians:

$$\chi^{(2)}_{ijk} = \chi_{NR} + F_{ijk}\sum_q \frac{A_q}{\omega_2 - \omega_q + i\Gamma_q} \qquad \textbf{Eq. 1.10}$$

Where χ_{NR} is the non-resonant background arising from the electric polarization of the surface or interface and the adjacent media, F_{ijk} is the Fresnel coefficient responsible for the local field correction, and A_q, ω_q, and Γ_q are the strength, resonant infrared frequency, and damping coefficient of the q_{th} vibrational mode, respectively.

$\chi^{(2)}$ itself can be described as related to the molecular second order nonlinear polarizability (or hyperpolarizability), $\beta_{ijk}^{(2)}$, through a coordinate transformation [175]:

$$\chi_{IJK}^{(2)} = \frac{N}{\varepsilon_0} \sum_{IJK=x,y,z} \left\langle R_{Ii} R_{Jj} R_{Kk} \right\rangle \beta_{ijk}^{(2)} \qquad ijk = a,b,c \qquad \textbf{Eq. 1.11}$$

Where N is the number of surface molecules, ε_0 is the vacuum permittivity, R is a transformation matrix to change from the molecular frame to the laboratory frame. The macroscopic susceptibility is therefore an average of the molecular hyperpolarizability of all molecules. Thus, $\chi^{(2)}$ is directly related to both the number of molecules/molecular groups at a surface or interface as well as the hyperpolarizability.

Contributions of $\chi_{eff}^{(2)}$ for various vibrational molecular groups can be compared quantitatively. It is from the comparison of $\chi_{eff}^{(2)}$ contributions (generated by fitting SFG spectra) of particular functional group(s) that information on molecular vibrational group ordering or orientation may be deduced, taking into account specific assumptions regarding the system of interest. Molecular orientation and ordering analysis of different functional groups such as methyl (CH_3),[172,176,177] methylene (CH_2), [178,179] and aromatic C-H stretches,[180-184] have been discussed in length in previous publications and will not be repeated here.

Because the systems probed in this thesis are mainly polymeric in nature with microscopically rough and/or disordered surfaces, C-H functional groups tend to adopt multiple orientations on a surface or interface. The determination of such multiple orientation(s) of CH_2 or CH_3 groups at an interface can be very challenging, if not impossible to deduce correctly. As such, much of the ordering analysis of C-H functional groups and corresponding molecules has been completed in a qualitative, rather than quantitative, manner.

This can be performed (using the CH_2 functional group as an example), by comparing the $\chi^{(2)}_{eff}$ values of a CH_2(s) peak and a CH_2(as) peak collected a specific polarization combination, and generating a $\chi^{(2)}_{eff(s),ssp}/\chi^{(2)}_{eff(as),ssp}$ value from fitted SFG peaks. After taking into account local Fresnel coefficients, the $\chi^{(2)}_{eff}$ ratio may be translated to $\chi^{(2)}_{(s)yyz}/\chi^{(2)}_{(as)yyz}$. An orientation curve can be plotted consisting of $\chi^{(2)}_{(s)yyz}/\chi^{(2)}_{(as)yyz}$ as a function of CH_2 group tilt angle on a surface (assuming that the twist angle can be averaged out). The tilt angle may be plotted as a delta distribution of angles. Normally a specific angle for the CH_2 group will be chosen if the calculated $\chi^{(2)}_{(s)yyz}/\chi^{(2)}_{(as)yyz}$ value falls within the limits of the plot. However, for polymer surfaces, where one surface angle for C-H groups may not be realistic, a range of values or possible orientations may be given. This can be accomplished by using a Gaussian distribution of angles versus $\chi^{(2)}$ ratio, and/or by giving a qualitative description of surface C-H group ordering. E.g. the calculated $\chi^{(2)}$ ratio from the CH_2 group falls within a Gaussian distribution plot such that we can state the CH_2 groups tend to lie down on the surface of the polymer, or the CH_2 groups stand up towards the surface normal. These qualitative conclusions can also be made by studying at the ratio of the intensity of the plotted peaks, provided the peak intensity ratios are reasonable in nature and if fit, the peaks generate normal $\chi^{(2)}_{eff}$ values.

A similar qualitative approach can be taken when studying the ordering of CH_3 functional groups (in that case comparing $\chi^{(2)}_{eff(s),ssp}/\chi^{(2)}_{eff(s),ppp}$) and aromatic phenyl or phenol functional groups (e.g. is there any signal from the C-H stretching modes of these aromatic groups in ssp or ppp spectra? If not, the rings likely lie down flat on a surface, are completely disordered, or are not present on the surface).

The previous descriptions related to Equations 1.1-1.11 correspond to a single surface or interface which can generate the SFG signals. However, it is possible to generate SFG signals for a polymer film at two interfaces simultaneously, such as the film/optical substrate interface and the film/air interface. When this occurs, any orientation or ordering analysis needs to take into account signal interferences from the two interfaces. Another equation is needed to consider the contributions from both interfaces, which will be discussed in Chapter 5.

1.5 Discussion of Model Systems and SFG Limitations

The research of this thesis involves the investigation of simple PVC plastics under simple environmental models. The plastic and environmental models were designed using minimal chemical components. At the same time, it was vital to design the models accurately enough to mimic real life situations so that the information gained from these experiments would provide meaningful results. The simplification of model plastics and environments was performed so that spectroscopic experiments could be easily replicated and results easily interpreted, especially in the case of SFG experiments.

A normal PVC plastic product, for example, contains fillers such as dyes, UV absorbers, and fire retardants in addition to the plasticizer and polymer itself. Each component mentioned can consist of molecules with C-H group functionalities. If any of the C-H components from fillers are present on the surface of the compounded plastic, they may yield SFG signals in the C-H region of vibrational spectra which overlap with signals from phthalates and/or PVC. As such, it would be difficult or impossible to distinguish which SFG signals come from what component of the plastic, and the surface behaviors of the plastic and plasticizer may not be isolated. Additionally, some PVC plastics are opaque, colored, and/or not optically flat materials. In such

cases, SFG signals from the surface or interface of the plastics would likely be difficult to collect, due to optical scattering, light absorption, and/or inaccessibility to laser light. Thus, clear PVC plastics consisting solely of plastic and plasticizer were utilized for all PVC-based experiments.

This may raise questions regarding the interpretation of experimental results and the applicability of SFG for plastic studies. Certainly, we can assert that there are some consequences of our model approach to studying plastic surfaces and interfaces. Without fillers, chemical reactions and molecular reordering may occur on a faster scale. Therefore, the observation of such events in real time may closely mimic behaviors of highly plasticized clear PVC products, but may not relate well to other opaque PVC materials. In turn, the simplification of environments surrounding the plastics, such as model freshwater or toxin exposure can omit molecules normally present in real life situations. Experiments using model chemical environments were performed in house, rather than obtaining data in the field. Therefore the complicated interaction mechanics between trace amounts of ions, molecules, and/or radicals present in "real" environments cannot always be inferred.

Thus, we can conclude overall that SFG is an excellent technique to study model plastic surfaces and interfaces under various model stimuli, and results can be interpolated to form general conclusions about the molecular behaviors of industrial and consumer plastics. As will be shown in this thesis, fundamental molecular level studies on plastic yield vital insights which help progress plastic science and engineering. However, SFG may not be well suited to study certain types of "real" plastics for applied engineering or formulation purposes due to the increased complexity of surface components.

1.6 Introduction to Coherent Anti-Stokes Raman Scattering

Briefly, CARS is also a nonlinear optical spectroscopy, but unlike SFG it is not a surface sensitive analytical technique. Some details regarding the CARS process are outlined in the next few paragraphs.[185-187] The CARS signal intensity can be expressed as:

$$I_{CARS} \propto \left|\chi^{(3)}\right|^2 I_p I_s I_{pr} \qquad \textbf{Eq. 1.12}$$

Where I_p, I_s and I_{pr} are intensities of the pump, Stokes and probe beams respectively, and $\chi^{(3)}$, the third order nonlinear susceptibility term, has the nonresonant $\chi_{NR}^{(3)}$ and resonant $\chi_R^{(3)}$ contributions described as:

$$\left|\chi^{(3)}\right|^2 = \left|\chi_{NR}^{(3)} + \chi_R^{(3)}\right|^2 = \left|\chi_{NR}^{(3)} + \sum_i \frac{A_i}{\Omega_i - \left(\omega_p - \omega_s\right) + i\Gamma_i}\right|^2 \qquad \textbf{Eq. 1.13}$$

The resonant contribution is modeled as the sum of Lorentzians with signal strength or amplitude A_i, frequency Ω_i, and linewidth Γ_i. The resonant susceptibility $\chi_R^{(3)} \propto N$, where N is the number of molecules probed. Thus, similar to $\chi_R^{(2)}$, $\chi_R^{(3)}$ is related to the number of molecules, but this includes molecules throughout the entirety of the sample probed with laser light rather than only molecules at a surface or interface. The energy level diagram for the CARS process is found in Figure 1.4.

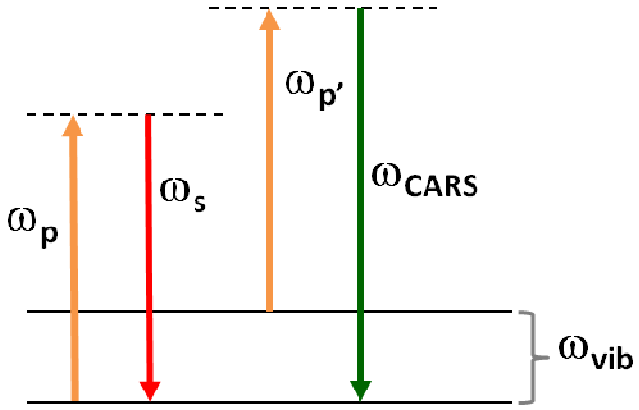

Figure 1.4. Energy level diagram of the CARS process where ω_p is the pump beam, ω_s is the Stokes beam, $\omega_{p'}$ is the probe beam and ω_{CARS} is the resulting CARS signal. Note the pump and the probe beam are the same.

1.7 CARS Experimental Details

As described previously in Chapter 5 of Dr. Chi Zhang's thesis[188], CARS spectra can be collected on the same SFG spectrometer with some optical modifications. The signal output from the OPG/OPA SFG system is used as the Stokes beam, and the 532 nm visible beam as the pump/probe beam. The pulse energies for the pump/probe and Stokes beams are ~300 μJ and ~100 μJ respectively. An additional delay line is used to generate temporal overlap of the input beams on the sample when changing from SFG to CARS spectroscopy. The CARS signal is generated at a different angle compared to the SFG signal. A He-Ne laser is used to track the CARS signal, which is collected by the same monochromator and PMT as in SFG. Flip mirrors are used to change between SFG and CARS spectral collections. CARS has the advantage of orders of magnitude higher collection rates than traditional Raman scattering due to the fact that it is a coherent technique. Also, CARS signals can be directly compared to SFG signals as both are vibrational techniques, making it easy to probe bulk and surface properties of a thin film

material in the same environment. More details on the utilization of SFG and CARS spectroscopy can be found in Chapter 2 of this thesis.

1.8 Introduction to Time-of-Flight Secondary Ion Mass Spectrometry

ToF-SIMS is another surface sensitive technique, but provides different information than SFG, mainly the presence and quantity of surface ions which can be correlated to quantitative measurements of surface molecules and molecular fragments. In the ToF-SIMS process, a primary pulsed ion beam is applied onto a surface held under ultra high vacuum (UHV), which releases secondary atoms, molecules and ions. This secondary process occurs in less than 10^{-12} seconds. Under UHV, only ions 1-2 nm below the surface will reach the time-of-flight mass analyzer and generate a mass spectrum consisting of lines of mass-to-charge-ratios (m/z). Either positive or negative ions may be analyzed. ToF-SIMS gives a wide mass range and high mass resolution for up to hundreds of thousands of lines. Appropriate data analysis programs may be used to identify patterns from specific molecules or ion fragments. ToF-SIMS typically has a ppm to ppb detection limit, making it one of the highest sensitivity mass spectrometry techniques available.[189-192] The Tof-SIMS data in this thesis were collected in static mode, focusing the ion beam on a large surface area (500x500μm) and spectra were collected in minutes. Further details regarding ToF-SIMS instrumentation and experiments can be found in Chapter 4.

1.9 Presented Research

This thesis marks the first time phthalates and NPs have been studied *in situ* at the molecular level at surfaces and buried interfaces using nonlinear optical spectroscopy. Additionally, this thesis applies a unique combination of analytical techniques and experiments to generate molecular information on interfacial and bulk phthalate behaviors and chemical

reactions. An understanding of phthalate behaviors in air and at buried interfaces under various chemical environments was successfully developed, several chemical treatments for phthalate removal/leaching control in plasticized PVC were designed, and the molecular level effects of such treatments were elucidated. The molecular level behaviors of NPs on plastics were studied, and a model for a lake environment was designed so that the effects of water content on the adsorption and desorption of NP onto plastic could also be determined.

In Chapter 2, the basic surface molecular structures of PVC plasticized with phthalates were examined, elucidating the phthalate surface content at equilibrium under standard atmospheric conditions, and probing the molecular effects of an up-and-coming phthalate leaching application, air plasma treatment. Results from Chapter 2 illustrate the near simultaneous use of SFG and CARS spectroscopy to give *in situ* information on molecular content and ordering on plastic surfaces and throughout the bulk of plastics, respectively.

Chapter 3 focuses on studying the effects of UV light on phthalate plasticized PVC at a molecular level to gain a better understanding of the changes in and on PVC plastics exposed to sunlight or UV lamps before the plastics demonstrate microscopic or macroscopic stress. Specifically, short wave and long wave UV light was applied to plastics and the molecular changes on the surface of the plastic and throughout the bulk of plastic were examined using SFG, FTIR, and HPLC/MS among other techniques. Herein a basic degradation of phthalates in plastic was determined for the first time, and the stable degradation products identified.

Chapter 4 expands upon the UV work in the previous chapter. A new phthalate degradation technique was developed and evaluated based off of success with short wave UV exposure experiments, with the purpose of minimizing the threat of phthalate leaching from

plastics intended for disposal or recycling. The degradation of phthalates in and on PVC through exposure of hydrogen peroxide and UV light versus UV light alone was directly compared. Stable surface molecular products were identified by ToF-SIMS and SFG, and products in the plastic were determined as well. A more complicated phthalate degradation scheme under short wave UV light and standard atmospheric conditions was proposed.

The research focus shifts in Chapter 5 from studying PVC surfaces in air to the water/plastic interface and discriminating SFG signals from multiple interfaces. An understanding of how the molecular surface of PVC and plasticized PVC changes from water contact was developed and SFG signals simultaneously collected from the top and bottom of a thin film plastic were distinguished through multiple interface calculations. The effects of phthalate bulk content on the surface structures of PVC plastics in water were determined, and the transfer of phthalates from plastic to new polymer surfaces through water contact was observed in a matter of minutes, a rate much faster than traditional leaching experiments. The multiple interface signal interface calculations in Chapter 5 help quantitatively explain why SFG signals from a variety of thin films often appear different under different experimental geometries.

Lastly, Chapter 6 studies the deposition and desorption of the prolific environmental toxin NP, on plastics under different model environments: dry land mass and near a lake surface. Focus was held on understanding how microplastics in lakes collect and transfer toxins like NPs through an ecosystem. The role of humidity and water content on the molecular ordering behaviors of NP, the amount of deposition from air to plastic, and the permanence of deposition under various stressors on poly(styrene) plastic were determined using SFG, QCM, and ATR-

FTIR. An SFG sample chamber was introduced for use in future trace analysis gas-deposition projects.

1.10 References

1. Meikle, J. L. *American Plastic: A Cultural History*; Rutgers University Press, 1995.
2. Lokensgard, E. *Industrial Plastics: Theory and Applications*; Cengage Learning, 2008.
3. Wilkes, C. E.; Summers, J. W.; Daniels, C. A.; Bernard, M. T. *PVC Handbook*; Hanser Gardner Publications Inc.: Cincinnati, OH, 2005.
4. Wypych, G. *Handbook of Plasticizers*; Chemtech Publishing: Toronto, 2004.
5. Teuten, E.; Rowland, S.; Galloway, T.; Thompson, R. *Environ. Sci. Technol.* **2007**, *41*, 7759.
6. Teuten, E.; Saquing, J.; Knappe, D.; Barlaz, M.; Jonsson, S.; Bjorn, A.; Rowland, S.; Thompson, R.; Galloway, T.; Yamashita, R.; Ochi, D.; Watanuki, Y.; Moore, C.; Viet, P.; Tana, T.; Prudente, M.; Boonyatumanond, R.; Zakaria, M.; Akkhavong, K.; Ogata, Y.; Hirai, H.; Iwasa, S.; Mizukawa, K.; Hagino, Y.; Imamura, A.; Saha, M.; Takada, H. *Philos. Trans. R. Soc. Lond. B. Biol. Sci.* **2009**, *364*, 2027.
7. Eerkes-Medrano, D.; Thompson, R. C.; Aldridge, D. C. *Water Res.* **2015**, *75*, 63.
8. Wagner, M.; Scherer, C.; Alvarez-Munoz, D.; Brennholt, N.; Bourrain, X.; Buchinger, S.; Fries, E.; Grosbois, C.; Klasmeier, J.; Marti, T.; Rodriguez-Mozaz, S.; Urbatzka, R.; Vethaak, A.; Winther-Nielsen, M.; Reifferscheid, G. *Env. Sci. Eur.* **2014**, *26*, 12.
9. Ekelund, M.; Azhdar, B.; Gedde, U. W. *Polym. Degrad. Stab.* **2010**, *95*, 1789.
10. Halden, R. U. *Annu. Rev. Public Health* **2010**, *31*, 179.
11. Lardjane, N.; Belhaneche-Bensemra, N. *J. Appl. Polym. Sci.* **2009**, *111*, 525.
12. Oehlmann, J.; Schulte-Oehlmann, U.; Kloas, W.; Jagnytsch, O.; Lutz, I.; Kusk, K. O.; Wollenberger, L.; Santos, E. M.; Paull, G. C.; Van Look, K. J. W.; Tyler, C. R. *Philos. Trans. R. Soc. Lond., Ser. B: Biol. Sci.* **2009**, *364*, 2047.
13. Roy, W. R. In *Handbook of Plasticizers*; Wypych, G., Ed.; Chemtec Publishing: 2004, p 591; The Environmental Fate of Plasticizers: Ch 18.
14. Barnes, D.; Galgani, F.; Thompson, R.; Barlaz, M. *Philos. Trans. R. Soc. Lond. B. Biol. Sci.* **2009**, *364*, 1985.
15. Besseling, E.; Wegner, A.; Foekema, E.; van den Heuvel-Greve, M.; Koelmans, A. *Environ. Sci. Technol.* **2013**, *47*, 593.
16. Browne, M.; Crump, P.; Niven, S.; Teuten, E.; Tonkin, A.; Galloway, T.; Thompson, R. *Environ. Sci. Technol.* **2011**, *45*, 9175.
17. Seymour, R. B.; Deanin, R. D.; Meeting, A. C. S. *History of Polymeric Composites*; Taylor & Francis, 1987.
18. Cao, X. L. *Compr. Rev. Food Sci. F* **2010**, *9*, 21.
19. Colombani, J.; Herbette, G.; Rossi, C.; Joussot-Dubien, C.; Labed, V.; Gilardi, T. *J. Appl. Polym. Sci.* **2009**, *112*, 1372.
20. Rahman, M.; Brazel, C. S. *Prog. Polym. Sci.* **2004**, *29*, 1223.
21. Hopewell, J.; Dvorak, R.; Kosior, E. *Philos. Trans. R. Soc. Lond., Ser. B: Biol. Sci.* **2009**, *364*, 2115.
22. Kovacic, P. *Med. Hypotheses* **2010**, *74*, 626.
23. Zieminski, K. F.; Peppas, N. A. *J. Appl. Polym. Sci.* **1983**, *28*, 1751.
24. Amberg-Müller, J. P.; Hauri, U.; Schlegel, U.; Hohl, C.; Brüschweiler, B. J. *J. Con. Prot. Food Safety* **2010**, *5*, 429.
25. Api, A. M. *Food Chem. Toxicol.* **2001**, *39*, 97.
26. Bakir, A.; Rowland, S. J.; Thompson, R. C. *Environ. Pollut.* **2014**, *185*, 16.

27. Buchta, C.; Bittner, C.; Heinzl, H.; Hocker, P.; Macher, M.; Mayerhofer, M.; Schmid, R.; Seger, C.; Dettke, M. *Transfusion* **2005**, *45*, 798.
28. Chen, C. W.; Chen, C. F.; Dong, C. D. *Soil. Sediment. Contam.* **2013**, *22*, 119.
29. Christiansen, S.; Boberg, J.; Axelstad, M.; Dalgaard, M.; Vinggaard, A. M.; Metzdorff, S. B.; Hass, U. *Reprod. Toxicol.* **2010**, *30*, 313.
30. Doyle, T. J.; Bowman, J. L.; Windell, V. L.; McLean, D. J.; Kim, K. H. *Biol. Reprod.* **2013**, *88*, 112.
31. Ehrlich, S. R.; Meeker, J. D.; Williams, P. L.; Wright, D.; Petrozza, J.; Hauser, R. *Fertil. Steril.* **2010**, *94*, S73.
32. Ferguson, K. K.; Loch-Caruso, R.; Meeker, J. D. *Environ. Res.* **2011**, *111*, 718.
33. Ferguson, K. K.; Loch-Caruso, R.; Meeker, J. D. *Environ. Sci. Technol.* **2012**, *46*, 477.
34. Frederiksen, H.; Skakkebaek, N. E.; Andersson, A. M. *Mol. Nutr. Food Res.* **2007**, *51*, 899.
35. Hauser, R.; Meeker, J. D.; Singh, N. P.; Silva, M. J.; Ryan, L.; Duty, S.; Calafat, A. M. *Hum. Reprod.* **2007**, *22*, 688.
36. Herreros, M. A.; Gonzalez-Bulnes, A.; Inigo-Nunez, S.; Letelier, C.; Contreras-Solis, I.; Ros-Rodriguez, J. M.; Encinas, T. *Theriogenology* **2010**, *73*, 141.
37. Huang, M. Z.; Ma, Y. W.; Wang, Y.; Wan, J. Q.; Zhang, H. P. *Bioresour. Technol.* **2010**.
38. Jaeger, R. J.; Rubin, R. J. *Fed. Proc.* **1970**, *29*, A411.
39. Kasahara, E.; Sato, E. F.; Miyoshi, M.; Konaka, R.; Hiramoto, K.; Sasaki, J.; Tokuda, M.; Nakano, Y.; Inoue, M. *Biochem. J.* **2002**, *365*, 849.
40. Kamrin, M. A. *J. Toxicol. Env. Heal. B* **2009**, *12*, 157.
41. Koch, H. M.; Calafat, A. M. *Philos. Trans. R. Soc. Lond., Ser. B: Biol. Sci.* **2009**, *364*, 2063.
42. Latini, G. *Clin. Chim. Acta* **2005**, *361*, 20.
43. Li, N.; Wang, D.; Zhou, Y.; Ma, M.; Li, J.; Wang, Z. *Environ. Sci. Technol.* **2010**, *44*, 6863.
44. Martino-Andrade, A. J.; Chahoud, I. *Mol. Nutr. Food Res.* **2010**, *54*, 148.
45. Meeker, J. *Drug Metab. Rev.* **2009**, *41*, 24.
46. Meeker, J. D. *Arch. Pediatr. Adolesc. Med.* **2012**, *166*, 952.
47. Meeker, J. D.; Calafat, A. M.; Hauser, R. *J Expo Sci Environ Epidemiol* **2012**, *22*, 376.
48. Meeker, J. D.; Calafat, A. M.; Hauser, R. *J. Androl.* **2009**, *30*, 287.
49. Meeker, J. D.; Calafat, A. M.; Hauser, R. *Environ. Health Perspect.* **2007**, *115*, 1029.
50. Meeker, J. D.; Ferguson, K. K. *Environ. Health Perspect.* **2011**, *119*, 1396.
51. Meeker, J. D.; Hu, H.; Cantonwine, D. E.; Lamadrid-Figueroa, H.; Calafat, A. M.; Ettinger, A. S.; Hernandez-Avila, M.; Loch-Caruso, R.; Tellez-Rojo, M. M. *Environ. Health Perspect.* **2009**, *117*, 1587.
52. Mendiola, J.; Meeker, J. D.; Jorgensen, N.; Andersson, A. M.; Liu, F.; Calafat, A. M.; Redmon, J. B.; Drobnis, E. Z.; Sparks, A. E.; Wang, C.; Hauser, R.; Swan, S. H. *J. Androl.* **2012**, *33*, 488.
53. North, M. L.; Takaro, T. K.; Diamond, M. L.; Ellis, A. K. *Ann. Allergy, Asthma Immunol.* **2014**, *112*, 496.
54. Rael, L. T.; Bar-Or, R.; Ambruso, D. R.; Mains, C. W.; Slone, D. S.; Craun, M. L.; Bar-Or, D. *Oxid. Med. Cell Longev.* **2009**, *2*, 166.
55. Sathyanarayana, S.; Karr, C. J.; Lozano, P.; Brown, E.; Calafat, A. M.; Liu, F.; Swan, S. H. *Pediatrics* **2008**, *121*, E260.

56. Staples, C. A.; Peterson, D. R.; Parkerton, T. F.; Adams, W. J. *Chemosphere* **1997**, *35*, 667.
57. Suzuki, Y.; Niwa, M.; Yoshinaga, J.; Mizumoto, Y.; Serizawa, S.; Shiraishi, H. *Environ. Int.* **2010**, *36*, 699.
58. Tetz, L. M.; Cheng, A. A.; Korte, C. S.; Giese, R. W.; Wang, P. G.; Harris, C.; Meeker, J. D.; Loch-Caruso, R. *Toxicol. Appl. Pharmacol.* **2013**, *268*, 47.
59. Parks, LG; Ostby, JS; Lambright, CR; et al. *Toxicol. Sci.* **2000**, 58, 339
60. Bis-2-ethylhexyl phthalate; MSDS No. Fluka 36735 [Online]; Sigma Aldrich, St. Louis, MO, June 8, 2015.
61. The Consumer Product Safety Improvement Act of 2008 (CPSIA); Title 1: Children's Product Safety, Section 108: Prohibition on Sale of Certain Products Containing Specified Phthalates. http://www.cpsc.gov/PageFiles/129663/cpsia.pdf.
62. 112th Congress of the United States of America. Jan. 5, 2011. Section 5: Application of Phthalates Limit. Amendment of USC 2057c. H.R. 2715-8. http://www.cpsc.gov/PageFiles/129663/cpsia.pdf.
63. Andrady, A. L.; Hamid, H.; Torikai, A. *Photoch. Photobio. Sci.* **2011**, *10*, 292.
64. Balabanovich, A. I.; Denizligil, S.; Schnabel, W. *J. Vinyl Addit. Techn.* **1997**, *3*, 42.
65. Chen, C.-Y. *Water Air Soil Poll.* **2009**, *209*, 411.
66. Decker, C. *Eur. Polym. J.* **1984**, *20*, 149.
67. Ding, X.; An, T.; Li, G.; Chen, J.; Sheng, G.; Fu, J.; Zhao, J. *Res. Chem. Intermed.* **2008**, *34*, 67.
68. Duval, E.; Achibat, T.; Boukenter, A.; Varrel, B.; Calemczuk, R.; Salce, B. *J. Non-Cryst. Solids* **1995**, *190*, 258.
69. Park, C. G.; Kim, J. C. *Desalin. Water Treat.* **2012**, *47*, 163.
70. Hollande, S.; Laurent, J. L. *Polym. Degrad. Stab.* **1997**, *55*, 141.
71. Ito, R.; Seshimo, F.; Haishima, Y.; Hasegawa, C.; Isama, K.; Yagami, T.; Nakahashi, K.; Yamazaki, H.; Inoue, K.; Yoshimura, Y.; Saito, K.; Tsuchiya, T.; Nakazawa, H. *Int. J. Pharm.* **2005**, *303*, 104.
72. Kaczmarek, H.; Kowalonek, J.; Szalla, A.; Sionkowska, A. *Surf. Sci.* **2002**, *507*, 883.
73. Määttä, J.; Koponen, H. K.; Kuisma, R.; Kymäläinen, H. R.; Pesonen-Leinonen, E.; Uusi-Rauva, A.; Hurme, K. R.; Sjöberg, A. M.; Suvanto, M.; Pakkanen, T. A. *Appl. Surf. Sci.* **2007**, *253*, 5003.
74. Okamoto, Y.; Hayashi, T.; Toda, C.; Ueda, K.; Hashizume, K.; Itoh, K.; Nishikawa, J.; Nishihara, T.; Kojima, N. *Chemosphere* **2006**, *64*, 1785.
75. Tawabini, B. S.; Al-Suwaiyan, M. S. *J. Environ. Eng. Sci.* **2004**, *3*, 289.
76. Torikai, A.; Hasegawa, H. *Polym. Degrad. Stab.* **1999**, *63*, 441.
77. Xu, B.; Gao, N. Y.; Cheng, H.; Xia, S. J.; Rui, M.; Zhao, D. D. *J. Hazard. Mater.* **2009**, *162*, 954.
78. Zhang, K. H.; Cao, W. L.; Zhang, J. C. *Appl. Catal., A* **2004**, *276*, 67.
79. Balandier, M.; Decker, C. *Eur. Polym. J.* **1978**, *14*, 995.
80. Bowley, H. J.; Gerrard, D. L. *Polym. Degrad. Stab.* **1988**, *20*, 257.
81. Burgos, N.; Jiménez, A. *Polym. Degrad. Stab.* **2009**, *94*, 1473.
82. Chen, C. Y. *Water Air Soil Poll.* **2010**, *209*, 411.
83. Chung, Y. C.; Chen, C. Y. *Water Air Soil Poll.* **2009**, *200*, 191.
84. Denizligil, S.; Schnabel, W. *Angew. Makromol. Chem.* **1995**, *229*, 73.
85. Fahmi, M. M.; Mohamed, N. A. *Polym. Degrad. Stab.* **2007**, *92*, 733.

86. Fang, C.-R.; Yao, J.; Zheng, Y.-G.; Jiang, C.-J.; Hu, L.-F.; Wu, Y.-Y.; Shen, D.-S. *Int. Biodeterior. Biodegrad.* **2010**, *64*, 442.
87. Gibb, W. H.; Maccallu.Jr *Eur. Polym. J.* **1971**, *7*, 1231.
88. Kaczmarek, H.; Galka, P.; Wrzyszczynski, A.; Olszewski, K.; Janota, H. *Polimery* **2009**, *54*, 202.
89. Khan, M. H.; Jung, J. Y. *Chemosphere* **2008**, *72*, 690.
90. Skowronski, T. A.; Rabek, J. F.; Ranby, B. *Polym. Photochem.* **1984**, *5*, 77.
91. Szarka, G.; Domjan, A.; Szakacs, T.; Ivan, B. *Polym. Degrad. Stab.* **2012**, *97*, 1787.
92. Vinhas, G. M.; Souto-Maior, R. M.; Lapa, C. M.; de Almeida, Y. M. *Materials Research* **2003**, *6*, 497.
93. Zhao, X.-K.; Yang, G.-P.; Wang, Y.-J.; Gao, X.-C. *J. Photochem. Photobiol. A: Chem.* **2004**, *161*, 215.
94. Hankett, J. M.; Collin, W. R.; Chen, Z. *J. Phys. Chem. B* **2013**, *117*, 16336.
95. Hankett, J. M.; Liu, Y. W.; Zhang, X. X.; Zhang, C.; Chen, Z. *J. Polym. Sci. Part B: Polym. Phys.* **2013**, *51*, 311.
96. Hankett, J. M.; Lu, X. L.; Liu, Y. W.; Seeley, E.; Chen, Z. *PCCP* **2014**, *16*, 20097.
97. Hankett, J. M.; Welle, A.; Lahann, J.; Chen, Z. *J. Appl. Polym. Sci.* **2014**, *131*.
98. Hankett, J. M.; Zhang, C.; Chen, Z. *Langmuir* **2012**, *28*, 4654.
99. Oehlmann, J.; Schulte-Oehlmann, U.; Kloas, W.; Jagnytsch, O.; Lutz, I.; Kusk, K.; Wollenberger, L.; Santos, E.; Paull, G.; Van Look, K.; Tyler, C. *Philos. Trans. R. Soc. Lond. B. Biol. Sci.* **2009**, *364*, 2047.
100. Muncke, J. *Sci. Total Environ.* **2009**, *407*, 4549.
101. Andrady, A. L. *Mar. Pollut. Bull.* **2011**, *62*, 1596.
102. Bakir, A.; Rowland, S.; Thompson, R. *Mar. Pollut. Bull.* **2012**, *64*, 2782.
103. Bakir, A.; Rowland, S.; Thompson, R. *Environ. Pollut.* **2013**, *185C*, 16.
104. Castañeda, R. A.; Avlijas, S.; Simard, M. A.; Ricciardi, A. *Can. J. Fish. Aquat. Sci.* **2014**, *71*, 1767.
105. Claessens, M.; De Meester, S.; Van Landuyt, L.; De Clerck, K.; Janssen, C. *Mar. Pollut. Bull.* **2011**, *62*, 2199.
106. Cole, M.; Lindeque, P.; Fileman, E.; Halsband, C.; Goodhead, R.; Moger, J.; Galloway, T. *Environ. Sci. Technol.* **2013**, *47*, 6646.
107. Cole, M.; Lindeque, P.; Halsband, C.; Galloway, T. *Mar. Pollut. Bull.* **2011**, *62*, 2588.
108. Collignon, A.; Hecq, J.; Glagani, F.; Voisin, P.; Collard, F.; Goffart, A. *Mar. Pollut. Bull.* **2012**, *64*, 861.
109. Dekiff, J.; Remy, D.; Klasmeier, J.; Fries, E. *Environ. Pollut.* **2014**, *186*, 248.
110. Eriksen, M.; Mason, S.; Wilson, S.; Box, C.; Zellers, A.; Edwards, W.; Farley, H.; Amato, S. *Mar. Pollut. Bull.* **2013**, *77*, 177.
111. Frias, J. P. G. L.; Sobral, P.; Ferreira, A. M. *Mar. Pollut. Bull.* **2010**, *60*, 1988.
112. Fries, E.; Dekiff, J.; Willmeyer, J.; Nuelle, M.; Ebert, M.; Remy, D. *ESPI* **2013**, *15*, 1949.
113. Gouin, T.; Roche, N.; Lohmann, R.; Hodges, G. *Environ. Sci. Technol.* **2011**, *45*, 1466.
114. Harrison, J.; Sapp, M.; Schratzberger, M.; Osborn, A. *Mar Technol Soc J* **2011**, *45*, 12.
115. Hidalgo-Ruz, V.; Gutow, L.; Thompson, R.; Thiel, M. *Environ. Sci. Technol.* **2012**, *46*, 3060.
116. Imhof, H.; Ivleva, N.; Schmid, J.; Niessner, R.; Laforsch, C. *Curr. Biol.* **2013**, *23*, R867.
117. Ivar do Sul, J.; Costa, M. *Environ. Pollut.* **2014**, *185*, 352.
118. Lorena Rios Mendoza, P. J. *Environ. Chem.* **2015**, *Just Accepted*.

119. Setala, O.; Fleming-Lehtinen, V.; Lehtiniemi, M. *Environ. Pollut.* **2014**, *185*, 77.
120. Teuten, E. L.; Saquing, J. M.; Knappe, D. R. U.; Barlaz, M. A.; Jonsson, S.; Bjorn, A.; Rowland, S. J.; Thompson, R. C.; Galloway, T. S.; Yamashita, R.; Ochi, D.; Watanuki, Y.; Moore, C.; Pham, H. V.; Tana, T. S.; Prudente, M.; Boonyatumanond, R.; Zakaria, M. P.; Akkhavong, K.; Ogata, Y.; Hirai, H.; Iwasa, S.; Mizukawa, K.; Hagino, Y.; Imamura, A.; Saha, M.; Takada, H. *Philos. Trans. R. Soc. Lond., Ser. B: Biol. Sci.* **2009**, *364*, 2027.
121. Ugolini, A.; Ungherese, G.; Ciofini, M.; Lapucci, A.; Camaiti, M. *Estuar. Coast. Shelf Sci.* **2013**, *129*, 19.
122. Van Cauwenberghe, L.; Vanreusel, A.; Mees, J.; Janssen, C. *Environ. Pollut.* **2013**, *182*, 495.
123. Von Moos, N.; Burkhardt-Holm, P.; Kohler, A. *Environ. Sci. Technol.* **2012**, *46*, 11327.
124. Wright, S.; Thompson, R.; Galloway, T. *Environ. Pollut.* **2013**, *178*, 483.
125. Zarfl, C.; Fleet, D.; Fries, E.; Galgani, F.; Gerdts, G.; Hanke, G.; Matthies, M. *Mar. Pollut. Bull.* **2011**, *62*, 1589.
126. Bennett, E. R.; Metcalfe, C. D. *Environ. Toxicol. Chem.* **2000**, *19*, 784.
127. Kavanagh, R. J.; Balch, G. C.; Kiparissis, Y.; Niimi, A. J.; Sherry, J.; Tinson, C.; Metcalfe, C. D. *Environ. Health Perspect.* **2004**, *112*, 898.
128. Li, H.; Helm, P. A.; Metcalfe, C. D. *Environ. Toxicol. Chem.* **2010**, *29*, 751.
129. Zbyszewski, M.; Corcoran, P.; Hockin, A. *J. Great Lakes Res.* **2014**, *40*, 288.
130. Teuten, E. L.; Rowland, S. J.; Galloway, T. S.; Thompson, R. C. *Environ. Sci. Technol.* **2007**, *41*, 7759.
131. Shen, Y. R. *The Principles of Nonlinear Optics*; Wiley: New York, 1984.
132. Shen, Y. R. *Nature* **1989**, *337*, 519.
133. Chen, Z.; Shen, Y. R.; Somorjai, G. A. *Annu. Rev. Phys. Chem.* **2002**, *53*, 437.
134. Lambert, A. G.; Davies, P. B.; Neivandt, D. J. *Appl. Spec. Rev.* **2005**, *40*, 103.
135. Chen, C.; Clarke, M. L.; Wang, J.; Chen, Z. *PCCP* **2005**, *7*, 2357.
136. Chen, C.; Even, M. A.; Wang, J.; Chen, Z. *Macromolecules* **2002**, *35*, 9103.
137. Chen, C.; Wang, J.; Chen, Z. *Langmuir* **2004**, *20*, 10186.
138. Chen, C.; Wang, J.; Woodcock, S.; Chen, Z. *Langmuir* **2002**, *18*, 1302.
139. Chen, Z. *Prog. Polym. Sci.* **2010**, *35*, 1376.
140. Chen, Z.; Shen, Y. R.; Somorjai, G. A. *Annu. Rev. Phys. Chem.* **2002**, *53*, 437.
141. Chen, Z.; Ward, R.; Tian, Y.; Baldelli, S.; Opdahl, A.; Shen, Y. R.; Somorjai, G. A. *J. Am. Chem. Soc.* **2000**, *122*, 10615.
142. Chen, Z.; Ward, R.; Tian, Y.; Eppler, A. S.; Shen, Y. R.; Somorjai, G. A. *J. Phys. Chem. B* **1999**, *103*, 2935.
143. Even, M. A.; Chen, C. Y.; Wang, J.; Chen, Z. *Macromolecules* **2006**, *39*, 9396.
144. Kim, J.; Opdahl, A.; Chou, K. C.; Somorjai, G. A. *Langmuir Letters* **2003**, *19*, 9551.
145. Koffas, T. S.; Amitay-Sadovsky, E.; K, J.; Somorjai, G. A. *J. Biomater. Sci. Polym. Ed.* **2004**, *15*, 475.
146. Kondo, T.; Nomura, K.; Murou, M.; Gemmei-Ide, M.; Kitano, H.; Noguchi, H.; Uosaki, K.; Ohno, K.; Saruwatari, Y. *Colloids Surf. B. Biointerfaces* **2012**, *100*, 126.
147. Kristalyn, C. B.; Lu, X.; Weinman, C. J.; Ober, C. K.; Kramer, E. J.; Chen, Z. *Langmuir* **2010**, *26*, 11337.
148. Lu, X.; Chen, Z.; Xue, G.; Wang, X. *Front. Chem. China* **2010**, *5*, 435.

149. Lu, X. L.; Clarke, M. L.; Li, D. W.; Wang, X. P.; Xue, G.; Chen, Z. *J. Phys. Chem. C.* **2011**, *115*, 13759.
150. Lu, X. L.; Han, J. L.; Shephard, N.; Rhodes, S.; Martin, A. D.; Li, D. W.; Xue, G.; Chen, Z. *J. Phys. Chem. B* **2009**, *113*, 12944.
151. Lu, X. L.; Li, D. W.; Kristalyn, C. B.; Han, J. L.; Shephard, N.; Rhodes, S.; Xue, G.; Chen, Z. *Macromolecules* **2009**, *42*, 9052.
152. Lu, X. L.; Xue, G.; Wang, X. P.; Han, J. L.; Han, X. F.; Hankett, J.; Li, D. W.; Chen, Z. *Macromolecules* **2012**, *45*, 6087.
153. Miyamae, T.; Nozoye, H. *J. Photochem. Photobiol. A: Chem.* **2001**, *145*, 93.
154. Miyamae, T.; Yamada, Y.; Uyama, H.; Nozoye, H. *Appl. Surf. Sci.* **2001**, *180*, 126.
155. Ni, H. G.; Li, X. H.; Hu, Y. Y.; Zuo, B.; Zhao, Z. L.; Yang, J. P.; Yuan, D. X.; Ye, X. Y.; Wang, X. P. *J. Phys. Chem. C.* **2012**, *116*, 24151.
156. Noguchi, H.; Hiroshi, M.; Tominaga, T.; Ping Gong, J.; Osada, Y.; Uosaki, K. *PCCP* **2008**, *10*, 4987.
157. Prasad, S.; Zhu, H.; Kurian, A.; Badge, I.; Dhinojwala, A. *Langmuir* **2013**, *29*, 15727.
158. Shi, Q.; Ye, S.; Spanninga, S. A.; Su, Y. L.; Jiang, Z. Y.; Chen, Z. *Soft Matter* **2009**, *5*, 3487.
159. Wang, J.; Chen, C.; Buck, S. M.; Chen, Z. *J. Phys. Chem. B* **2001**, *105*, 12118.
160. Wei, X.; Zhuang, X.; Hong, S.; Goto, T.; Shen, Y. R. *Phys. Rev. Lett.* **1999**, *82*, 4256.
161. Ye, H. K.; Gu, Z. Y.; Gracias, D. H. *Langmuir* **2006**, *22*, 1863.
162. Ye, S. J.; Liu, G. M.; Li, H. C.; Chen, F. G.; Wang, X. W. *Langmuir* **2012**, *28*, 1374.
163. Zhang, C.; Hankett, J.; Chen, Z. *ACS Appl Mater Interfaces* **2012**, *4*, 3730.
164. Ebben, C. J.; Ault, A. P.; Ruppel, M. J.; Ryder, O. S.; Bertram, T. H.; Grassian, V. H.; Prather, K. A.; Geiger, F. M. *J. Phys. Chem. A* **2013**, *117*, 6589.
165. Lu, R.; Gan, W.; Wu, B.; Chen, H.; Wang, H. *J. Phys. Chem. B* **2004**, *108*, 7297.
166. Stokes, G. Y.; Buchbinder, A. M.; Gibbs-Davis, J. M.; Scheidt, K. A.; Geiger, F. M. *Vib. Spectro.* **2009**, *50*, 86.
167. Stokes, G. Y.; Chen, E. H.; Walter, S. R.; Geiger, F. M. *J. Phys. Chem. A* **2009**, *113*, 8985.
168. Voges, A. B.; Al-Abadleh, H. A.; Musorrariti, M. J.; Bertin, P. A.; Nguyen, S. T.; Geiger, F. M. *J. Phys. Chem. B* **2004**, *108*, 18675.
169. Wang, T.; Li, D. W.; Lu, X. L.; Khmaladze, A.; Han, X. F.; Ye, S. J.; Yang, P.; Xue, G.; He, N. Y.; Chen, Z. *J. Phys. Chem. C.* **2011**, *115*, 7613.
170. Ye, S. J.; Majumdar, P.; Chisholm, B.; Stafslien, S.; Chen, Z. *Langmuir* **2010**, *26*, 16455.
171. Hirose, C.; Akamatsu, N.; Domen, K. *Appl. Spectrosc.* **1992**, *46*, 1051.
172. Zhuang, X.; Miranda, P.; Kim, D.; Shen, Y. *Phys. Rev. B* **1999**, *59*, 12632.
173. Shen, Y. R. *Annu. Rev. Phys. Chem.* **1989**, *40*, 327.
174. Feller, M. B.; Chen, W.; Shen, Y. R. *Phys. Rev. A: At. Mol. Opt. Phys.* **1991**, *43*, 6778.
175. Moad, A. J.; Simpson, G. J. *J. Phys. Chem. B* **2004**, *108*, 3548.
176. Hirose, C.; Yamamoto, H.; Akamatsu, N.; Domen, K. *J. Phy. Chem.* **1993**, *97*, 10064.
177. Wang, J.; Chen, C.; Buck, S. M.; Chen, Z. *J. Phys. Chem. B* **2001**, *105*, 12118.
178. Hirose, C.; Akamatsu, N.; Domen, K. *J. Chem. Phys.* **1992**, *96*, 997.
179. Gan, W.; Zhang, Z.; Feng, R.; Wang, H. *J. Phys. Chem. C* **2007**, *111*, 8726.
180. Duffy, D. C.; Davies, P. B.; Bain, C. D. *J. Phy. Chem.* **1995**, *99*, 15241.
181. Gautam, K. S.; Schwab, A. D.; Dhinojwala, A. *Phys. Rev. Lett.* **2000**, *85*, 3854.

182. Harp, G. P.; Rangwalla, H.; Yeganeh, M. S.; Dhinojwala, A. *J. Am. Chem. Soc.* **2003**, *125*, 11283.
183. Lu, X.; Han, J.; Shephard, N.; Rhodes, S.; Martin, A. D.; Li, D.; Xue, G.; Chen, Z. *J. Phys. Chem. B* **2009**, *113*, 12944.
184. Lu, X.; Spanninga, S. A.; Kristalyn, C. B.; Chen, Z. *Langmuir* **2010**, *26*, 14231.
185. Druet, S. A.; Taran, J. P. *Prog. Quant. Electr.* **1981**, *7*, 1.
186. Cheng, X.; Xie, X. S. *J. Phys. Chem. B* **2004**, *108*, 827.
187. Evans, C. L.; Xie, X. S. *Annu. Rev. Anal. Chem.* **2008**, *1*, 883.
188. Zhang, C., PhD Thesis, Physical Chemistry, University of Michigan, 2014.
189. Benninghoven, A. *Angew. Chem.* **1994**, *33*, 1023.
190. Mahoney, C. M. *Mass Spectrom. Rev.* **2010**, *29*, 247.
191. Schwarz, S. A.; Wilkens, B. J.; Pudenzi, M. A. A.; Rafailovich, M. H.; Sokolov, J.; Zhao, X.; Zhao, W.; Zheng, X.; Russell, T. P.; Jones, R. A. L. *Mol. Phys.* **1992**, *76*, 937.
192. Karim, A.; Slawecki, T. M.; Kumar, S. K.; Douglas, J. F.; Satija, S. K.; Han, C. C.; Russell, T. P.; Liu, Y.; Overney, R.; Sokolov, O.; Rafailovich, M. H. *Macromolecules* **1998**, *31*, 857.

CHAPTER 2

STUDIES ON PLASTICIZED PVC SURFACE AND BULK STRUCTURES: EFFECTS OF AIR PLASMA TREATMENT

2.1 Background and Motivation

In this Chapter, the effects of air plasma treatment and heating on molecular surface and bulk structures of PVC plastics are elucidated. SFG was used to probe the molecular surface structures of thin films of PVC containing various weight percentages of the phthalate plasticizer DEHP (See Figure 1 in previous Chapter), before plastic annealing, after annealing and after exposure to air plasma. The plasticized PVC film bulk structures were probed using an additional nonlinear optical spectroscopy, CARS, before and after treatments as well. SFG and CARS spectra were collected *in situ* from samples in the same environment, using the same instrumentation. In this manner the surface and bulk vibrational molecular changes of plastics from plasma treatment and/or annealing could be directly compared and the surface behaviors of DEHP elucidated. Additional techniques x-ray photoelectron spectroscopy (XPS) and contact angle goniometry were applied as well to generate a broader picture of molecular level chemical changes. The contents in this chapter have been adapted with permission from the following publication: Hankett, J. M.; Zhang, C.; Chen, Z. "Sum Frequency Generation and Coherent Anti-Stokes Raman Spectroscopic Studies on Plasma-Treated Plasticized Polyvinyl Chloride Films" *Langmuir* **2012**, *28*, 4654-4662. Copyright 2012 American Chemical Society.

Recalling from the first Chapter of this thesis, PVC plastics that are plasticized with DEHP have a great potential for phthalate exposure through leaching. Millions of tons of DEHP-plasticized PVC are currently in use across the globe, and millions more tons of disposed plastics are scattered throughout urban and rural ecosystems.[1-7] The leaching of DEHP from PVC into the surrounding environment is highly undesirable since extensive research has revealed DEHP and other phthalates have negative influences on human health and biological ecosystems. Particularly, in recent years it has been discovered that DEHP is rapidly metabolized to mono-ethylhexyl phthalate (MEHP) in the human body and it is this molecule that behaves as the active toxic metabolite of DEHP. Several studies indicate that MEHP may damage human endothelial cells and sperm cells, among others.[8-17] Many more researchers have focused on other biological and medical effects associated with exposure to phthalates, and means to reduce phthalate environmental exposure. This includes studying bio-degradation mechanisms of phthalates, degradation mechanisms of phthalates in bulk media especially in solutions, and leaching of phthalates from the bulk media into external environments (e.g., measured by chromatograph and mass spectrometry).[1-29]

Here a study is presented on one potential means to reduce plasticizer exposure, surface plasma treatment. Plasma treatment has previously shown promise for increasing the hydrophilicity of PVC plastic surfaces, for cross-polymerization to prevent phthalate migration and leaching in plastics, and as a means to accelerate PVC degradation for environmentally friendly material disposal. Plasma treatment has been applied in both laboratory and industrial stages for many plastic applications, including medical equipment.[30-35] While plasma treated materials have demonstrated improved properties towards biocompatibility and reduced plasticizer leaching in laboratory tests, little is known regarding the induced chemical changes on

plastics from this applied process and the surface behaviors of phthalates in general.[36-38] It is especially important to understand the surface chemical changes that are induced by plasma treatment on plastic materials and phthalate plasticizers as a multitude of organisms can contact the treated plastic surfaces, and phthalate plasticizers leach into the environment through surfaces.

Previous to this research there were no *in situ* studies explicitly probing the molecular changes from plasma treatment of plastic and plasticizer molecules on the surface compared to those in the bulk using a non-destructive truly surface sensitive technique. Particularly, FTIR, ATR-FTIR and Raman have been used to probe PVC materials treated with various forms of plasma.[30-34] These techniques, however, yield molecular information beyond surface layers (≥200 nm). We studied the molecular changes of PVC plastics from plasma treatment using SFG and CARS spectroscopies nearly simultaneously, probing the surface molecular changes of DEHP plasticized PVC after plasma treatment, and the bulk structural changes of the plastics, respectively. Recall also from the introduction that SFG is a powerful optical spectroscopy with intrinsic surface sensitivity, and the ability to probe environmental and polymeric interfaces with submonolayer surface sensitivity under atmospheric conditions.[39-60] SFG has previously been proven a sound technique to study polymer surfaces exposed to plasma, radicals and UV-light.[61-65] For our materials of study, DEHP was added by weight to PVC materials and several different weight percentages of DEHP in plastic were studied in order to better understand the surface molecular behaviors of phthalates on PVC.

To briefly summarize, this Chapter aims to demonstrate success in: gaining a fundamental understanding of surface segregation and ordering of DEHP molecules on plasticized PVC, determining whether or not plasma treatment truly only affects surface layers of

plastics, and lastly, presenting the utility of an instrumental setup to study the surface and the bulk molecular structural changes of plastics from harsh treatments nearly simultaneously with SFG and CARS probing the same samples in the same environment. The research in this Chapter laid a foundation for future studies on the surface and bulk structures of plasticized PVC films under different harsh environmental conditions including oxygen plasma, argon plasma, UV light, UV light with present reactive radicals, and exposure to water and other aqueous conditions like solvents.[45,66-70]

2.2 Experimental Methods

2.2.1 Materials

Tetrahydrofuran (THF), ≥99.9% purity, concentrated sulfuric acid (reagent grade), potassium dichromate and poly(vinyl) chloride (Mw 62,000, Mn 35,000), in pellet form, were obtained from Sigma Aldrich (St. Louis, Mo). Bis(2-ethylhexyl) phthalate (analytical standard) was obtained from Fluka (St. Louis Mo).

2.2.2 Sample Preparation

The PVC pellets were dissolved in THF to prepare thin films for spectroscopic studies. A 30:1 weight ratio of THF:PVC was used to prepare all films. DEHP was added by weight percent to PVC. Solutions were mixed using a vortex mixer (Vortex-Genie 2T, Scientific Industries Inc.) until clear. Fused silica windows (ESCO Products, Inc.) were used for SFG measurements and cleaned by first soaking in organic solvent for several hours, rinsing with deionized water, drying with nitrogen gas, and then were left to soak in a concentrated sulfuric acid bath saturated containing potassium dichromate overnight. After the acid bath, windows

were rinsed with deionized water again and dried with nitrogen gas before sample preparation. Both silica windows and microscope glass slides were used as substrates for polymer films for contact angle measurements. No differences were found in surface water contact angles when the different substrates were used.

A P-6000 spin coater (Speedline Technologies) was used to prepare all polymer/plasticizer films. Samples were spin coated at 3000 rpm for 30 s on windows and glass slides. PVC films were prepared with varying weight percentages of DEHP at: 0 wt%, 5 wt%, 10 wt%, 25 wt% and 65 wt% of the total PVC/DEHP mass. Selected films were annealed in an Isotemp lab oven (Fisher Scientific) at 76˚C overnight to study the effects of annealing on the plastic films' surface structure. To ensure THF was removed from non-annealed samples in this Chapter and in all following PVC-based experiments, films were dried with a stream of nitrogen and FTIR of the films were obtained to confirm lack of solvent signals.

2.2.3 Instrumentation

Static water contact angle measurements were conducted using a CAM 100 Optical Contact Meter (KSV Instruments). At least three samples of each type of polymer blend were used for contact angle goniometry measurements and four spots were taken per sample on average. Millipore deionized water was used for the measurements. Film thickness measurements were obtained using a Dektek3 Profilometer (Veeco). Film thicknesses averaged around 150-200 nm. Air plasma treatment was completed using a lab-built glow discharge plasma cleaner held under low vacuum. Discharge was maintained between two parallel Ti plates using an AC high voltage at 700 V.

X-ray photoelectron spectroscopy (XPS) was performed at the University of Michigan's Electron Microbeam Analysis Laboratory using a Kratos AXIS Ultra DLD XPS with a

monochromatic Al source that gives an energy resolution better than 0.5 eV measured from the pure Ag 3d peak. Charge neutralization was applied during XPS measurements.

SFG was used to obtain molecular information on the surface structures of these PVC plastics in air before and after plasma exposure. Details of the SFG system used for this study were presented in the previous Chapter and will not be repeated again. SFG spectra were collected using the ssp polarization combination which consists of an s-polarized output signal, s-polarized visible input beam and p-polarized IR input beam.

To compare molecular vibrational signals on surfaces to the bulk of plasticized polymers, CARS spectroscopy was also used in this study. CARS capability was added to our SFG system as was previously reported.[71] Instead of using the frequency tunable mid-IR input beam applied in SFG, we used the frequency tunable visible beam generated from the OPG/OPA system as the Stokes beam and the 532 nm input beam as the pump/probe beam for CARS experiments and spectra were collected using the ssss polarization combination. CARS spectra were collected from a sample using our SFG system in the same environment. The experimental stage setup for both SFG and CARS is described in more detail in the next section. The collection of SFG or CARS spectra can be controlled by flipping mirrors on the laser table, and aligning beams onto the sample surface. To ensure the temporal overlap on the sample, an additional delay line was used in the CARS experiments. In this study, both SFG and CARS spectroscopies examined molecules in the C-H stretching frequency range (2700-3100 cm^{-1}).

2.2.4 SFG and CARS Experimental Setup

Both SFG and CARS spectra were collected using the reflection geometry. With the SFG setup, this means that the window was held film-face down in a custom made substrate holder such that the visible and IR beams first had to penetrate the substrate to overlap spatially and temporally

upon the film surface. The reflected signal beam was then directed to the monochromator. To perform CARS measurements, the sample must be flipped face-up in the sample holder, and the reflected signal from the top of the sample was directed to the monochromator. CARS measurements were obtained in a face-up reflection geometry so the generation of non-resonant signals from silica was avoided. A schematic of the two experimental sample setups can be found in Figure 2.1.

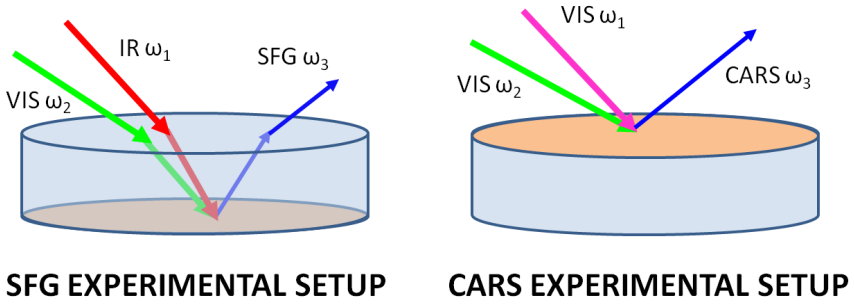

Figure 2.1. Schematic of experimental geometries for SFG measurements (left) and CARS measurements (right) on the same sample

2.3 Results and Discussion

2.3.1 Choosing Appropriate Film Thicknesses

A film thickness of ~200 nm was chosen for PVC films studied in Chapters 2-5. This decision was made after carefully analyzing films of different thicknesses deposited on silica windows. 200 nm was determined to be an ideal thickness for SFG measurements for the following reasons: first, the thickness and appearance of the film could easily be reproduced using a simple weight ratio of 30:1 THF: PVC and then spin coating the solution. Second, a thickness of 200 nm was thick enough to allow the phthalate, when mixed in with PVC in

solution and then spin coated, to function as a plasticizer. If the film was much thinner than 200 nm (100 nm or below) according to early SFG results the phthalate molecules would separate from a layer of polymer and function as a new layer of material, rather than inserting between polymer chains. Therefore the surface behaviors of the phthalate would not reflect that of a phthalate plasticizer. Third, if the plastics were much thicker than 200 nm (275 nm or higher), the surfaces of the films were not optically flat, especially when a high weight percentage of phthalate was added. This would result in light scattering from the film, loss of signal from scattering, and also yield a more disordered surface at a molecular level, giving a low signal to noise ratio when data was obtained on the SFG instrument.

2.3.2 SFG and CARS Analysis of Non-annealed PVC Films

SFG spectra were obtained on the surfaces of pure and plasticized PVC materials in an effort to understand the surface structures of these materials and determine how increasing phthalate bulk percentages affects surface molecular ordering and content. SFG spectra were collected from pure PVC, PVC that contained 5 wt%, 10 wt%, 25 wt%, or 65 wt% DEHP, and pure DEHP in air (Figures 2.2 and 2.3). The pure PVC spectrum can be found in Figure 2.2. The PVC SFG spectrum is dominated by a CH_2 symmetric stretching signal (CH_2(s)) located at about 2920 cm^{-1} which was assigned in accordance with literature studies.[72,73] It is important to note that the symmetric stretch of CH_2 groups in polymers with aliphatic chains usually occurs at ~2850 cm^{-1} in SFG spectra, but the local environment surrounding these types of CH_2 groups is much different than for PVC, and it is the difference in local environment that yields a different peak center for the PVC CH_2(s) mode. As an example, "normal" aliphatic chains, like those in poly(ethylene), contain CH_2 groups that are located directly next to one other but in PVC, CH_2 groups appear in every other position along the backbone. In addition to the cited IR papers

which used isotope labeling studies to identify the peak center of the CH_2(s) stretch, further evidence for our assignment can be found in an IR paper studying polyvinyl alcohol (PVA). The CH_2 groups in PVC have similar environments as those in PVA, which generates symmetric stretching signals at ~2910 cm^{-1}.[74] In addition to the dominant CH_2(s) peak in PVC spectra, there is also a weak and broad signal at 2880 cm^{-1} which we believe is a methyl symmetric stretch (CH_3(s)) originating from the methyl end groups of PVC chains.[75]

In comparison, the SFG spectrum collected from the pure DEHP surface is markedly different from that collected from the pure PVC surface. The DEHP SFG spectrum is dominated by a CH_3(s) stretch at 2880 cm^{-1} and a Fermi resonance (generated from both the CH_3(s) symmetric stretching and the overtone of the CH_3 bending mode) at 2945 cm^{-1}. A third peak at 2860 cm^{-1} can also be observed, assigned to a CH_2(s) stretch (Figure 2.3).

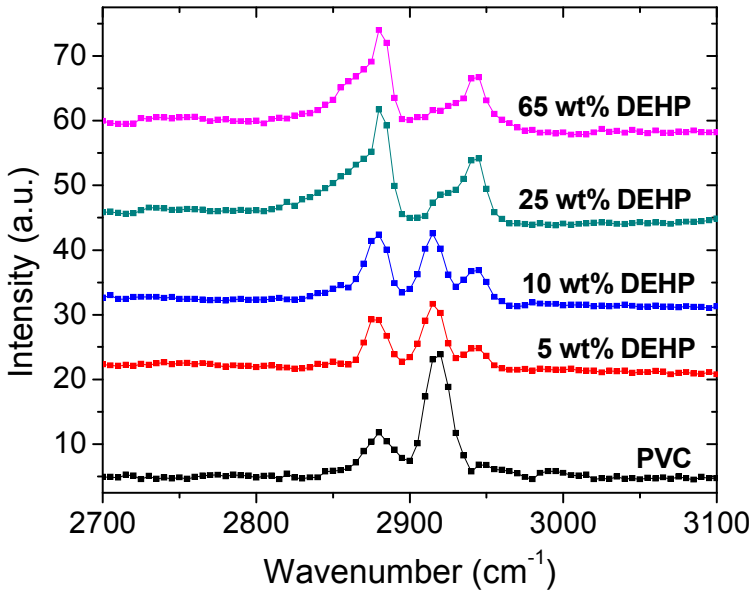

Figure 2.2. SFG ssp spectra of PVC films with 0 wt%, 5 wt%, 10 wt%, 25 wt% and 65 wt% DEHP.

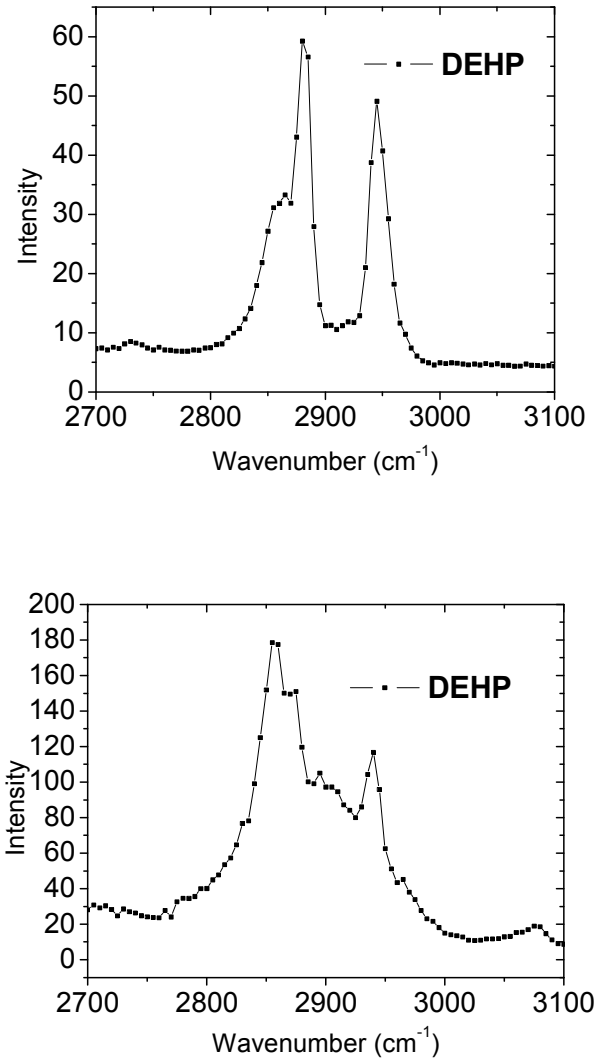

Figure 2.3. SFG ssp (top) and CARS ssss (bottom) spectrum of pure DEHP.

Figure 2.2 displays SFG spectra collected from the surfaces of DEHP plasticized PVC with the different percent loadings of DEHP in PVC. Looking first at the SFG spectrum of the sample with the lowest weight percent DEHP bulk loading (5 wt%), the dominant peak remains the CH_2(s) stretch of PVC. However, signals indicative of the CH_3 groups of DEHP are clearly observed as small peaks. This illustrates that the DEHP plasticizer is present on the surfaces of these films even though a very small amount was added to the bulk of the plastic. With the

addition of 10 wt% DEHP, the ratio of the intensity of the CH_2(s) to CH_3(s) peak is about equal, indicating that more DEHP is present on the film surface compared to the 5 wt% DEHP sample.

At the two higher weight percent loadings (25 wt% and 65 wt%), the DEHP signals dominate the spectra, indicating that the surfaces contain even more DEHP molecules. At 25 wt% DEHP, the PVC peak at 2920 cm^{-1} can still be observed from the surface as a shoulder in the spectrum, suggesting that the DEHP molecules do not entirely cover the plastic surface. At 65 wt% DEHP, only DEHP signals are observable, indicating that the surface consists only of DEHP molecules. Looking closer, a clear trend is observed of the relative peak signal intensities in spectra from small to large percent bulk loading of DEHP. The 2880 cm^{-1} and 2940 cm^{-1} peaks gradually increase in intensity and the 2920 cm^{-1} signal gradually decreases in intensity as more bulk DEHP is added. This demonstrates that the surface coverage of DEHP increases while the surface coverage of PVC decreases with the increased bulk DEHP content. We can confidently say that the increase in the 2880 cm^{-1} signal arises from DEHP molecules rather than PVC molecules, because the SFG CH_3(s) peak from DEHP is much narrower than the CH_3(s) PVC peak.

To compare the presence of DEHP on the film surfaces to the bulk mixtures, CARS spectra of these films were collected as well (Figure 2.4). Unsurprisingly, the CH_2 signal of PVC (2920 cm^{-1}, CH_2(s) stretch) dominates all percent bulk loadings except 65 wt% DEHP. For the this sample, in addition to the PVC CARS peak, DEHP peaks are clearly present at 2860 cm^{-1} (CH_2(s) stretch), 2880 cm^{-1} (CH_3(s) stretch; shoulder), 2945 cm^{-1} (Fermi resonance), and 2970 cm^{-1} (CH_3 asymmetric stretch (CH_3(as)). These signals are also present in the CARS spectrum of pure DEHP (Figure 2.3). CARS and SFG spectra reveal that the bulk composition of the films

may be different from the surface and that the bulk CARS signal is closely related to the percent loadings of DEHP prepared.

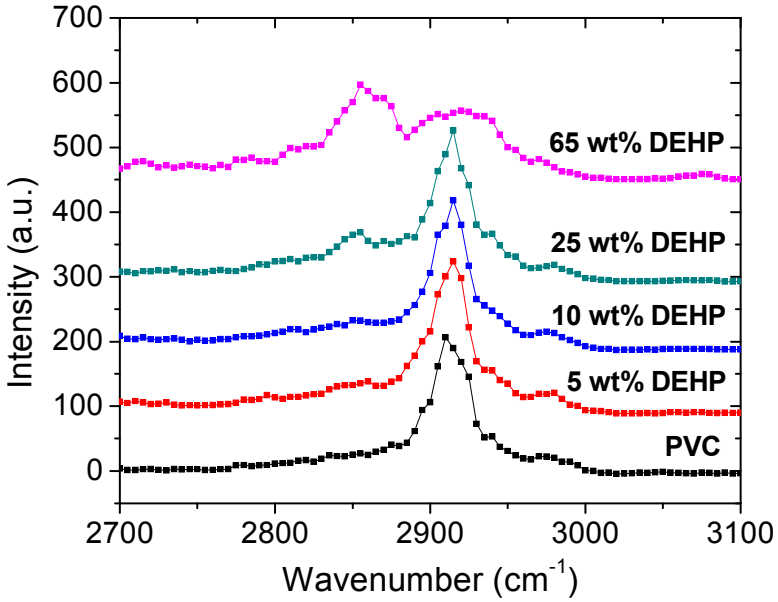

Figure 2.4. CARS ssss spectra of PVC films with 0 wt%, 5 wt%, 10 wt%, 25 wt% and 65 wt% DEHP.

2.3.3 SFG and CARS Analysis of Plasma Treated Non-annealed PVC Films

The SFG spectra of PVC plastic surfaces obtained after exposure of individual samples to glow discharge atmospheric plasma for five seconds can be found in Figure 2.5. For the pure PVC sample after plasma treatment, the SFG spectrum is dominated by a very wide peak at 2930 cm^{-1}. A weak signal at 2875 cm^{-1} can also be observed. The spectrum is markedly different compared to the spectrum collected before plasma treatment, where the main peak is centered at 2920 cm^{-1} and much narrower in width, and the 2875 cm^{-1} signal is larger. It can be reasonably assumed that the decrease of the 2875 cm^{-1} signal is due to the surface coverage of methyl end groups decreasing or the methyl groups becoming more disordered (more evidence for this

conclusion will be given in later sections). However, explaining the appearance of the broad 2930 cm^{-1} peak is more complicated.

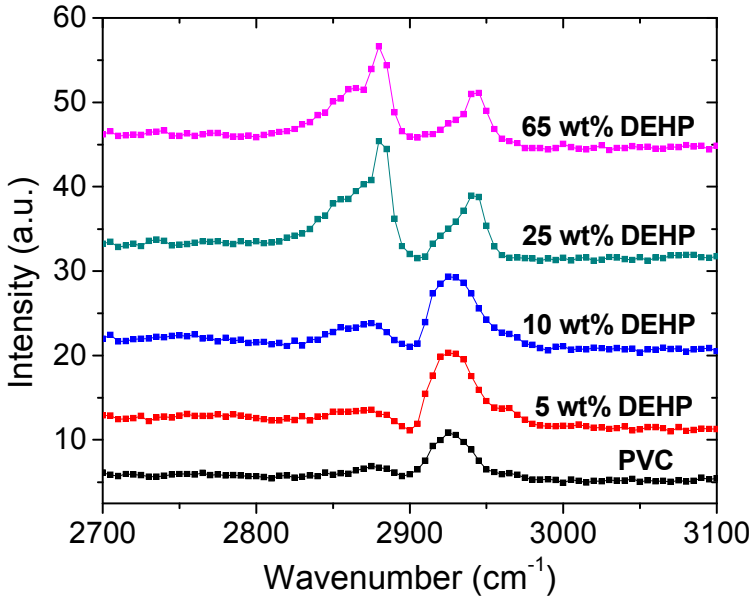

Figure 2.5. SFG ssp spectra of PVC films after plasma treatment with 0 wt%, 5 wt%, 10 wt%, 25 wt% and 65 wt% DEHP.

The increased peak width at 2930 cm^{-1} suggests that dramatic surface changes occurred from plasma treatment; the environment surrounding the methylene groups in PVC may undergo some changes due to the plasma treatment and/or spectral interference plays a role. The spectral interference may occur if chemical reactions changed the surface of the film such that a new peak is now present near 2920 cm^{-1} (i.e. 2940 cm^{-1}) which can lead to peak overlap. As a result, a broad peak with a shifted peak center could appear. In addition to spectral overlap, previous research has indicated that plasma treatment and other radical reactions on PVC may remove chlorine atoms from the polymer chains, which could shift the CH_2(s) peak center to a higher wavenumber and/or broaden the signal due to the increased types of environments surrounding the methylene groups (if only some of the chlorine atoms are removed).

Lastly, previous research also suggested that radical reaction can easily result in PVC chain scission. If such processes occurred on the plastic surface, additional CH_3 groups would be present that could yield signals at 2940 cm^{-1} (Fermi resonance).[30,31,33] Because these newly created methyl groups are different from the original methyl end groups, they may not be ordered in the same manner and not necessary have strong 2880 cm^{-1} CH_3(s) signals. SFG alone cannot concretely explain why the PVC surface appears to be much different after plasma treatment. A second surface sensitive analytical technique, XPS, was used to confirm the cause for the SFG spectral changes.

The SFG spectra collected from the PVC films with 5 wt% and 10 wt% DEHP after the plasma treatment also show the appearance of the very broad peak at 2930 cm^{-1}. In addition, signals at 2855 cm^{-1}, 2880 cm^{-1}, and 2960 cm^{-1} (small shoulder) can be resolved. The peak shift of the 2920 cm^{-1} signal to 2930 cm^{-1} and the peak width increase are likely due to the same reasons as discussed above for the pure PVC sample. A small dip at around 2900 cm^{-1} may be due to interference between a non-resonant signal and the 2930 cm^{-1} signal. Again, signal decrease of the 2880 cm^{-1} peak is observed for these samples after plasma treatment, due to surface chemical changes on the plastic. Thus, we believe that plasma treatment induced similar surface changes on the pure PVC sample and the mixed PVC samples containing 5 wt% and 10 wt% DEHP. The PVC samples containing higher DEHP bulk loading, 25 wt% and 65 wt% DEHP content, showed no visible spectral changes before and after plasma treatment. As previously mentioned, DEHP dominates the surfaces of these two samples. Therefore this may indicate that plasma treatment does not affect DEHP methyl groups on PVC surfaces to any major extent.

CARS spectra reveal no differences before and after plasma treatment for all samples (Figure 2.6). This indicates that the bulk of the polymer film does not exhibit structural changes after sample exposure to plasma. When directly comparing SFG spectra to CARS spectra, we can confirm that only a surface layer reaction occurred and only the surface layers of the films were affected while the bulk remained undisturbed.

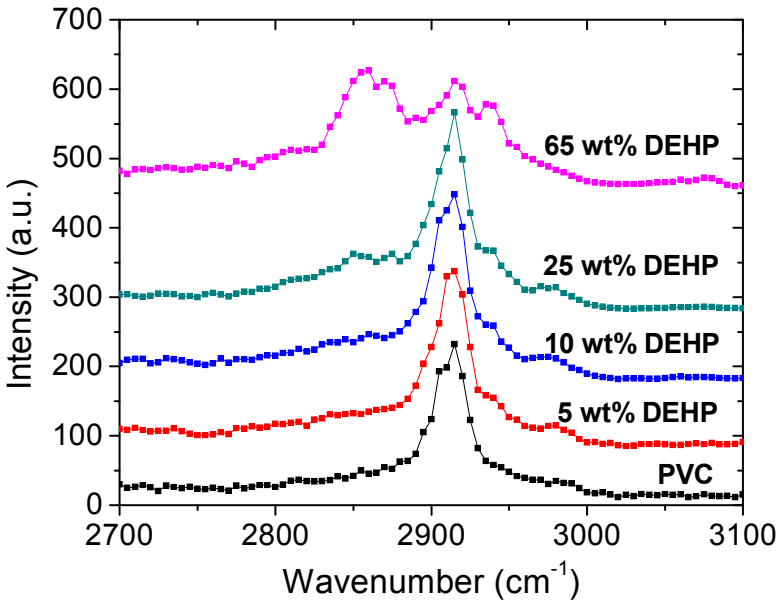

Figure 2.6. CARS ssss spectra of PVC films after plasma treatment with 0 wt%, 5 wt%, 10 wt%, 25 wt% and 65 wt% DEHP.

2.3.4 SFG and CARS Analysis of Annealed PVC Films

To ensure that sample surfaces reached equilibrium, sample films were annealed in an oven overnight at 76 °C. SFG and CARS spectra (Figures 2.7 and 2.8) were obtained to compare the surface and bulk structures, respectively, of the annealed films to non-annealed films (Figures 2.2 and 2.4). While the SFG spectra are markedly different for some samples before and after annealing, the CARS spectra of all the samples are similar. First for pure PVC,

the SFG spectrum collected after annealing shows the CH_2(s) 2920 cm^{-1} peak intensity decreases, indicating that the annealing induces surface methylene group reordering. Likely they tilt more toward the surface (i.e., the PVC backbones stand up more on the surface), which would yield smaller ssp SFG signals. In addition, SFG spectral reveal a disappearance of the 2880 cm^{-1} CH_3(s) signal, indicating that the end methyl groups either retreat to the bulk (point away from the air interface) or become randomly ordered on the surface. For the plastic samples that contain 5 wt% and 10 wt% DEHP, SFG spectra are markedly different from those collected before annealing. After annealing, only spectral features from DEHP can be observed, indicating that the surfaces are now covered with DEHP molecules. This demonstrates that at equilibrium, DEHP segregates to the PVC surface.

SFG spectra were collected from PVC films with 25 wt% and 65 wt% DEHP after annealing. These spectra exhibit similar features to those collected before annealing. However, similar to the pure PVC sample, the overall SFG signal intensities for the 25 wt% and 65 wt% samples decreased after annealing, likely indicating that DEHP molecules now have a broader orientation distribution (the DEHP methyl groups are less ordered on the surface).

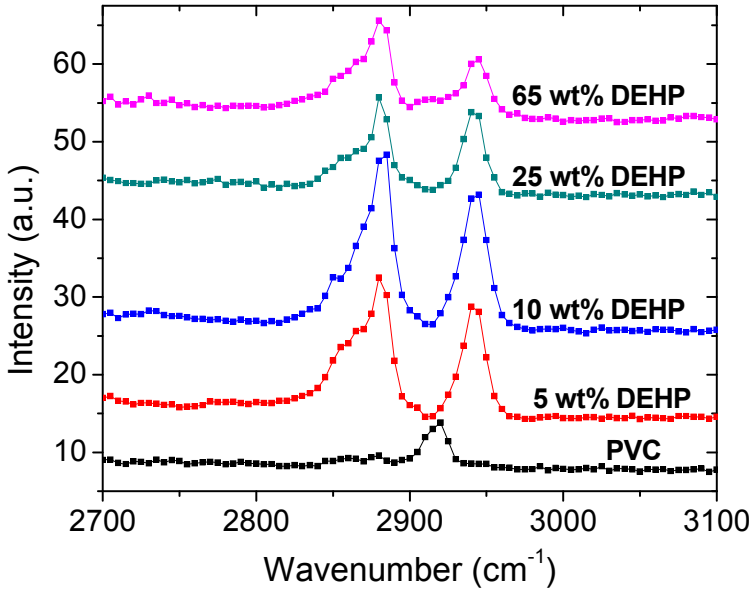

Figure 2.7. SFG ssp spectra of annealed PVC films with 0 wt%, 5 wt%, 10 wt%, 25 wt% and 65 wt% DEHP.

It is important to further discuss the effects of molecular group ordering on SFG signal intensity for these sample types. As can be observed in Figure 2.7, the SFG signals of 5 wt% and 10 wt% DEHP samples are stronger than those from the 25 wt% and 65 wt% DEHP samples. We believe this signal intensity change between sample types is directly related to the ordering of DEHP molecules on the plastic surfaces. As discussed previously, before annealing, the surfaces of 5 wt% and 10 wt% DEHP in bulk PVC consist of both DEHP and PVC molecules. However, after annealing, these two surfaces are dominated by DEHP due to upward movement of DEHP molecules from the plastic matrix to the surface. Since the total amount of DEHP in PVC is small for these two samples, it is highly likely that after annealing, DEHP molecules barely cover the top layer of the sample. Thus, methyl groups can order well, and "stand up" at the air interface (due to drives to lower the free energy of the system), generating strong signals. However, for 25 wt% and 65 wt% DEHP samples, both before and after annealing, the top layers

of the samples are crowded with DEHP molecules. The crowded methyl groups do not have as much room to reorder, and can adopt a number of different orientations, generating weaker SFG signals. This ordering theory can explain the relative signal intensity changes found in Figures 2.2 and 2.7. CARS spectra of the annealed films (Figure 2.8) are comparable to non-annealed films except for the 65 wt% DEHP sample. The structure of DEHP molecules in the bulk may have slightly varied after annealing which can be detected by polarized CARS.

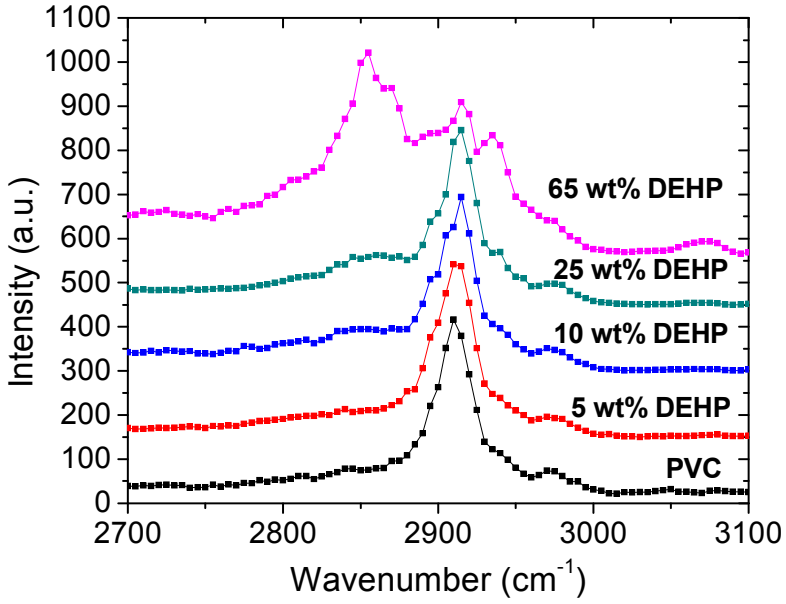

Figure 2.8. CARS ssss spectra of annealed PVC films with 0 wt%, 5 wt%, 10 wt%, 25 wt% and 65 wt% DEHP.

2.3.5 SFG and CARS Analysis of Plasma Treated Annealed PVC Films

First, studying the SFG spectrum of annealed pure PVC after plasma treatment, there is an obvious increase in peak width of the main peak, and an overall increase in this peak's intensity as well (Figure 2.9). The peak width increase is similar to what was observed with the non-annealed samples after plasma treatment, and must be caused by the same surface changes

that were previously discussed. The signal intensity increase indicates the methylene groups on the surface have reordered and are now more perpendicular to the air interface because the PVC backbones lie down flatter on the surface.

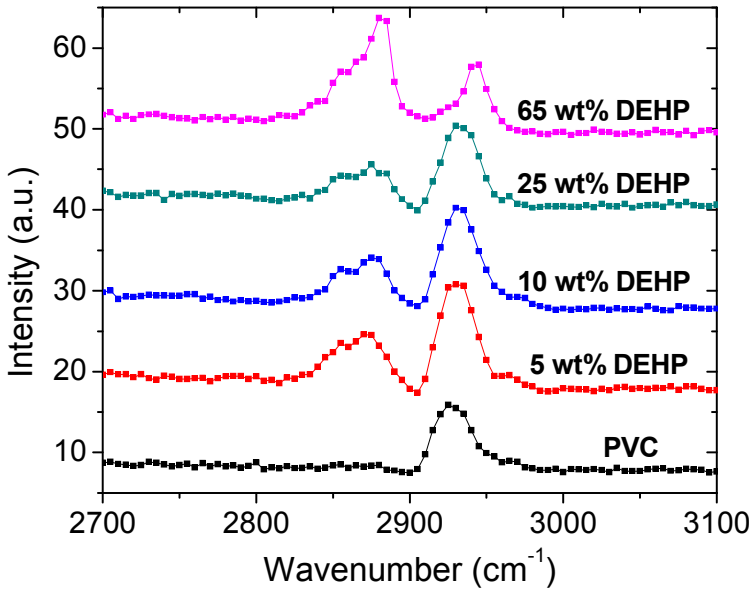

Figure 2.9. SFG ssp spectra of annealed PVC films with 0 wt%, 5 wt%, 10 wt%, 25 wt% and 65 wt% DEHP after exposure to glow discharge plasma.

Next, looking at SFG spectra collected from DEHP plasticized PVC with 5 wt%, 10 wt% and 25 wt% DEHP after plasma treatment, there are marked spectral differences compared to spectra collected before plasma treatment. A shift of the 2920 cm^{-1} peak is apparent, and a decrease in the 2875 cm^{-1} peak compared to the wide 2930 cm^{-1} peak is obvious. This may have occurred because the plasma treatment could have exposed more sub-surface PVC, since annealing changed the surface structure of these plasticized films (recall surface signal changes for the 5wt% and 10 wt% samples after annealing). However, the two DEHP signals (2875 and 2860 cm^{-1}) can still be observed, demonstrating that some surface coverage of DEHP remains. Similar to the pure annealed PVC sample, plasma exposure may also have oriented CH_2 groups

along the surface normal in these samples. Evidence of such lies in the fact that although the PVC signal at 2920 cm^{-1} was not observed before plasma treatment, after plasma treatment PVC generates strong signals near 2920 cm^{-1}.

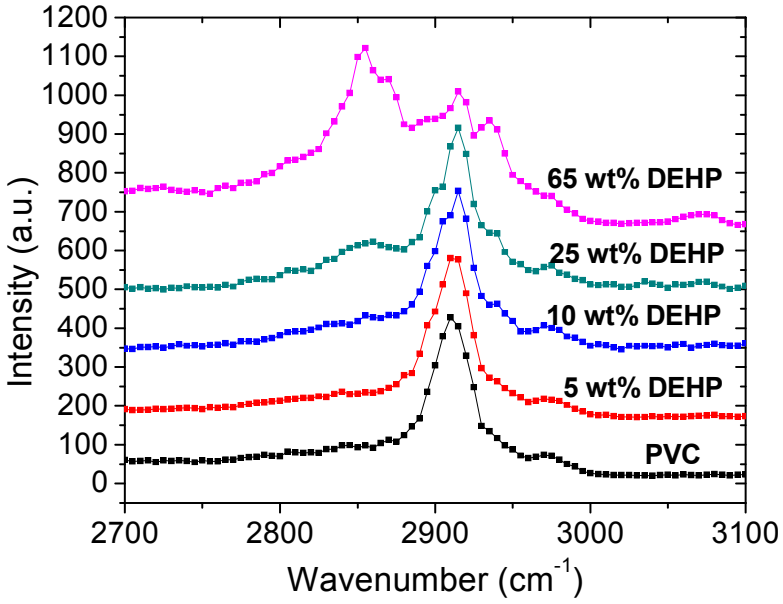

Figure 2.10. CARS ssss spectra of annealed PVC films with 0 wt%, 5 wt%, 10 wt%, 25 wt% and 65 wt% DEHP after exposure to glow discharge plasma.

In contrast, SFG spectra collected from the 65 wt% DEHP sample surface after plasma treatment are similar to those before plasma treatment. This means that plasma treatment does not substantially alter surface DEHP structure, similar to what was observed from the non-annealed samples. Compared to the other plasticized samples, the 65 wt% samples contain more DEHP, and therefore the surface DEHP layer must be much thicker such that plasma treatment could not expose bulk PVC to the surface. CARS spectra demonstrate no change in bulk molecular vibrational signals before and after plasma treatment for annealed samples (Figure 2.10).

2.3.6 Analysis of Surface Hydrophilicity Changes with Contact Angle Goniometry

To substantiate the SFG results, contact angle measurements were obtained for the pure PVC and 25 wt% DEHP samples. Table 2.1 displays the water contact angles on annealed, non-annealed and plasma-treated films. With water contact angle goniometry, a higher contact angle indicates an increase in surface hydrophobicity. Before plasma treatment, non-annealed films demonstrate an increase in contact angle after 25 wt% DEHP has been added to the plastic. This highly suggests that the hydrophobic methyl groups of the plasticizer are present on the surface, which is well correlated to SFG data, where on the surface of non-annealed PVC with 25 wt% DEHP, the SFG signal is dominated by DEHP CH_3 groups. In addition, the contact angles on annealed and non-annealed pure PVC surfaces exhibit differences, and SFG spectra show spectral differences after annealing. The annealed and non-annealed PVC with 25 wt% DEHP samples generate similar SFG spectra, showing similar surface structure and the water contact angles on these two surfaces are also similar.

Both annealed and non-annealed films (pure PVC and PVC with 25 wt% DEHP, Table 2.1) demonstrate changes in contact angle after plasma treatment. Recall the SFG spectra of annealed and non-annealed pure PVC changes after plasma treatment with an increase or decrease in the 2920 cm^{-1} peak, respectively, due to the orientation change of CH_2 groups versus the surface normal. The major contact angle decreases for both annealed and non-annealed pure PVC after plasma treatment are more likely induced by increased oxygen content on the surface rather than CH_2 orientation. The annealed PVC sample containing 25 wt% DEHP also generates a very different SFG spectrum after the plasma treatment. However, the non-annealed PVC with 25 wt% DEHP loading exhibits a similar spectrum before and after treatment, and their contact angles have the least difference of all samples after plasma treatment. Again, the contact angle

decrease measured here is likely due to oxygen deposition which has been observed after plasma treatment in literature[76] but could not be confirmed solely using the SFG spectra detected in the C-H stretching frequency region. This hypothesis was further tested using XPS, as outlined below.

Table 2.1. Water contact angles for plastic films with varying percent loadings of DEHP before and after exposure to glow discharge plasma

Water Contact Angle Results for Films				
	Non-Annealed		Annealed	
	PVC	25 wt% DEHP	PVC	25 wt% DEHP
Before Plasma	~80-82°	~88°	~86°	~86-87°
After Plasma	~52-54°	~63-66°	~52-53°	~48-50°

2.3.7 Analysis of Chemical Content and Bonding Changes with XPS

XPS spectra were collected at bonding energies near the O 1s peak, Cl 2p peak, and the C 1s peak signals for two sample types: the non-annealed PVC films and the non-annealed 25 wt% DEHP films both before and after plasma treatment, as shown in Figure 2.11. Before plasma treatment, on the non-annealed PVC surface, almost no O 1s signal can be detected but both the C 1s and Cl 2p peaks are clearly visible. In addition, there is a doublet formation on the C 1s peak. This indicates that there are two forms of carbon present (or two different types of carbon bonds). The carbon bonded to a more electronegative element yields a peak center at a higher bonding energy and thus the appearance of the peak doublet could be representative of both the carbon of CCl bonds in PVC and the carbon bonded to hydrogen atoms in the PVC CH_2 group. For the PVC surface with 25 wt% DEHP loading, the O 1s signal can be clearly detected (Figure 2.11). Since our SFG results indicated that on this surface DEHP dominates, which contains C=O groups, our SFG and XPS data are well correlated

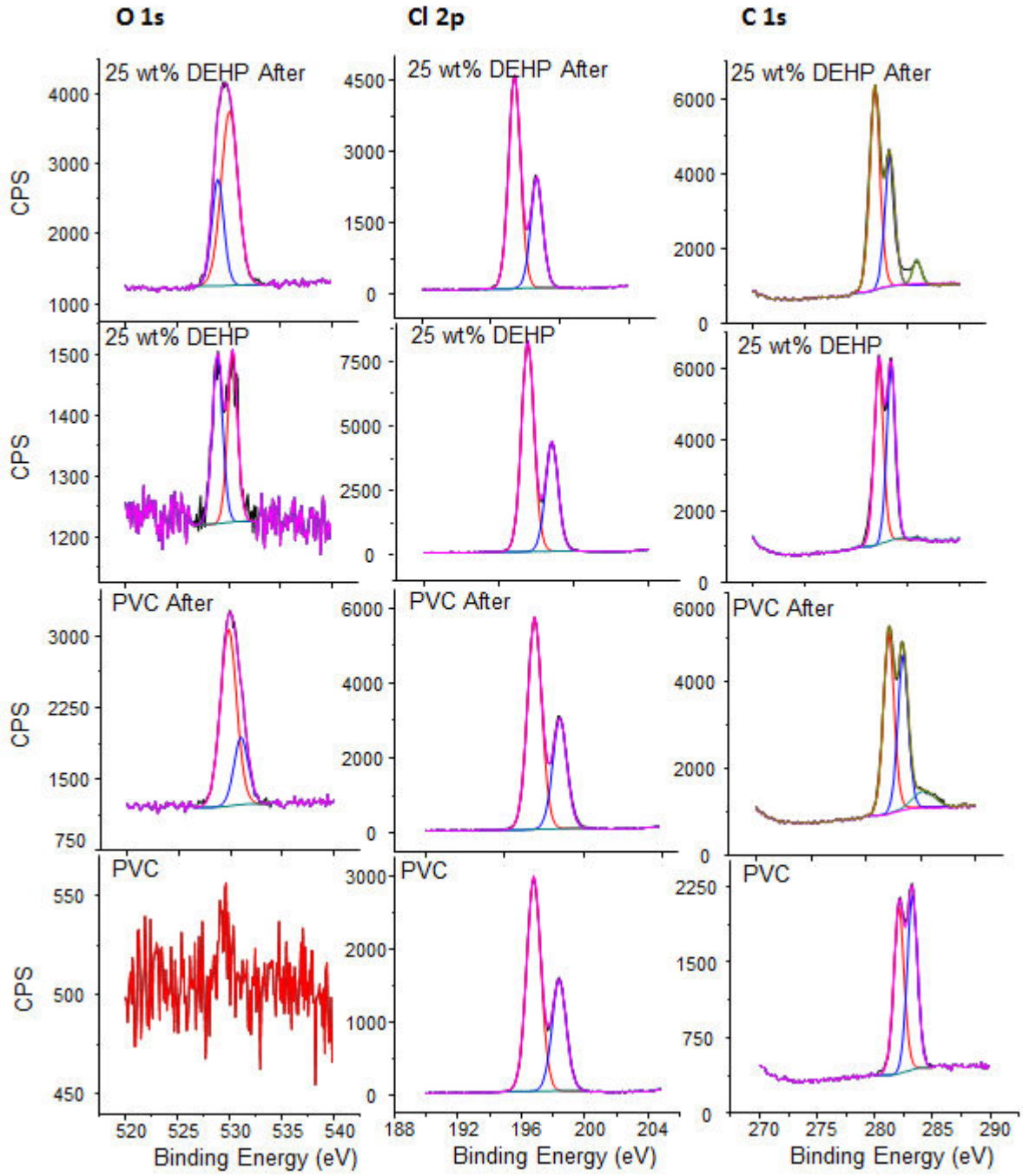

Figure 2.11. Fit XPS spectra for O1s, Cl 2p & C 1s in PVC films and PVC films plasticized with 25 wt% DEHP before and after exposure to glow discharge plasma.

After plasma treatment, the removal of chlorine atoms and the addition of oxygen atoms on the surface of PVC and plasticized PVC with 25 wt% DEHP were confirmed with XPS

spectra. The intensity ratio of the O 1s peak vs. the C 1s peak increases substantially for both PVC and 25 wt% DEHP plasticized PVC after plasma treatment as can be seen in Table 2.2.

Table 2.2 XPS peak area ratios calculated for elements in PVC and plasticized PVC films before and after exposure to glow discharge plasma.

Peak Area Ratios				
PVC	Cl 2p/C 1s	0.41	O 1s/C 1s	N/A
	Cl 2p/C 1s After Treatment	0.30	O 1s/C 1s After Treatment	0.17
DEHP 25 wt%	Cl 2p/C 1s	0.39	O 1s/C 1s	0.023
	Cl 2p/C 1s After Treatment	0.20	O 1s/C 1s After Treatment	0.22

In contrast, the intensity ratio of the Cl 2p peak decreases with respect to the C 1s peak after plasma treatment. In addition, after plasma treatment the lower bonding C 1s energy peak (C of CH_2) is more intense than the higher bonding C 1s energy peak (C of CHCl), whereas previously the higher bonding energy peak is of greater intensity. This C 1s peak shape change also suggests that chlorine removal occurred. Finally, the appearance of a third C 1s peak suggests a new form of carbon bonding is present after plasma treatment, perhaps due to new bonding between C and O on the surface. Therefore, XPS data can help to interpret the contact angle decrease reported in the previous section and can be correlated to the SFG spectral changes as well.

2.4 Conclusions

In this Chapter, the surface properties and molecular content of PVC and plasticized PVC films were characterized *in situ* using SFG for the first time, giving us a much broader understanding of surface phthalate availability and molecular behaviors on plastics. The effects of annealing PVC plastics and applying glow discharge plasma treatment were analyzed at a molecular level using SFG and CARS. SFG spectra revealed that DEHP is present on lab-

synthesized film surfaces at low concentrations and CARS spectra revealed there is a difference between molecular signatures on surfaces compared to the bulk of the film, indicating that the distribution of phthalates is different on the surface than over the majority of plastic. SFG and CARS data also revealed annealing facilitates the surface segregation of DEHP. After annealing, DEHP molecules dominate the surface even if only 5 bulk wt% of DEHP was added to PVC. Annealing also seems to affect the bulk structure of PVC that contain substantial amount of plasticizers as revealed by CARS.

From a realistic perspective, some of the annealing results are a bit surprising. It is well known that the non-covalently bound phthalates will migrate out of PVC plastics over years, and that the addition of heat to these plastics will accelerate plasticizer leaching. However, these materials almost always have a phthalate concentration much higher than 5 wt%. Our results indicate that even though the percentage of phthalate in the PVC plastic is small, it is likely that surface DEHP molecules will be present increasing numbers as the plastic ages.

In addition to evidence of leaching after annealing, spectral data revealed interesting chemical changes to PVC plastics exposed to plasma. SFG revealed some bond breaking and molecular surface rearrangement when PVC was exposed to plasma but the vibrational signatures of plasticizer methyl bonds remained similar before and after plasma exposure. CARS signals remained the same after the plasma treatment, indicating that the plasma treatment only affects surface structures. Because the entirety of surface chemical reactions could not be explored using SFG and CARS signals in the C-H stretching frequency range, we applied XPS and contact angle measurements to substantiate our data. The contact angle results suggest the addition of hydrophilic groups to the film surface after plasma treatment. XPS results indicate

chlorine is extracted from PVC chains and new surface bonds or functionalities were formed containing oxygen after the plasma exposure.

To evaluate the effectiveness of a plastic leaching treatment, the success in preventing plasticizer leaching at a macroscopic level must be weighed against any detrimental effects to the plastic itself. The intention of leaching treatments is to maintain the desired physical properties of a plastic by preventing loss of the molecules that provide plastic flexibility and pliability. Thus, by understanding the molecular level chemical and structural changes induced by leaching treatments, we can help predict which treatments may be most effective for PVC materials. Lastly, this work demonstrates SFG and CARS can successfully be applied to observe molecular changes from a surface-sensitive chemical reaction, giving us a platform to study surface and bulk molecular changes of plastics exposed to different chemical environments where traditional surface sensitive techniques (i.e. XPS) cannot be used.

2.5 References

1. Lorz, P. M.; F.K., T.; Enke, W.; Jackh, R.; Bhargava, N.; Hillesheim, W. In *Ullmann's Industrial Encyclopedia*; Wiley-VCH Verlag GmbH & Co: 2007.
2. Ekelund, M.; Azhdar, B.; Gedde, U. W. *Polym. Degrad. Stab.* **2010**, *95*, 1789.
3. Xu, B.; Gao, N. Y.; Cheng, H.; Xia, S. J.; Rui, M.; Zhao, D. D. *J. Hazard. Mater.* **2009**, *162*, 954.
4. Jaeger, R. J.; Rubin, R. J. *Lancet* **1970**, *2*, 778.
5. Jaeger, R. J.; Rubin, R. J. *Lancet* **1970**, *2*, 35.
6. Rael, L. T.; Bar-Or, R.; Ambruso, D. R.; Mains, C. W.; Slone, D. S.; Craun, M. L.; Bar-Or, D. *Oxid. Med. Cell Longev.* **2009**, *2*, 166.
7. Oehlmann, J.; Schulte-Oehlmann, U.; Kloas, W.; Jagnytsch, O.; Lutz, I.; Kusk, K. O.; Wollenberger, L.; Santos, E. M.; Paull, G. C.; Van Look, K. J. W.; Tyler, C. R. *Philos. Trans. R. Soc. Lond., Ser. B: Biol. Sci.* **2009**, *364*, 2047.
8. Ehrlich, S. R.; Meeker, J. D.; Williams, P. L.; Wright, D.; Petrozza, J.; Hauser, R. *Fertil. Steril.* **2010**, *94*, S73.
9. Ferguson, K. K.; Loch-Caruso, R.; Meeker, J. D. *Environ. Sci. Technol.* **2012**, *46*, 477.
10. Hauser, R.; Meeker, J. D.; Singh, N. P.; Silva, M. J.; Ryan, L.; Duty, S.; Calafat, A. M. *Hum. Reprod.* **2007**, *22*, 688.
11. Meeker, J. D. *Arch. Pediatr. Adolesc. Med.* **2012**, *166*, 952.
12. Meeker, J. D.; Calafat, A. M.; Hauser, R. *J. Androl.* **2009**, *30*, 287.
13. Martino-Andrade, A. J.; Chahoud, I. *Mol. Nutr. Food Res.* **2010**, *54*, 148.
14. Api, A. M. *Food Chem. Toxicol.* **2001**, *39*, 97.
15. Muncke, J. *Sci. Total Environ.* **2009**, *407*, 4549.
16. Fang, C.-R.; Yao, J.; Zheng, Y.-G.; Jiang, C.-J.; Hu, L.-F.; Wu, Y.-Y.; Shen, D.-S. *Int. Biodeterior. Biodegrad.* **2010**, *64*, 442.
17. Zhao, X.-K.; Yang, G.-P.; Wang, Y.-J.; Gao, X.-C. *J. Photochem. Photobiol. A: Chem.* **2004**, *161*, 215.
18. Ding, X.; An, T.; Li, G.; Chen, J.; Sheng, G.; Fu, J.; Zhao, J. *Res. Chem. Intermed.* **2008**, *34*, 67.
19. Bajt, O.; Mailhot, G.; Bolte, M. *Appl. Catal. B Environ.* **2001**, *33*, 239.
20. Mailhot, G.; Sarakha, M.; Lavedrine, B.; Caceres, J.; Malato, S. *Chemosphere* **2002**, *49*, 525.
21. Mendiola, J.; Meeker, J. D.; Jorgensen, N.; Andersson, A. M.; Liu, F.; Calafat, A. M.; Redmon, J. B.; Drobnis, E. Z.; Sparks, A. E.; Wang, C.; Hauser, R.; Swan, S. H. *J. Androl.* **2012**, *33*, 488.
22. Tetz, L. M.; Cheng, A. A.; Korte, C. S.; Giese, R. W.; Wang, P. G.; Harris, C.; Meeker, J. D.; Loch-Caruso, R. *Toxicol. Appl. Pharmacol.* **2013**, *268*, 47.
23. Koch, H. M.; Calafat, A. M. *Philos. Trans. R. Soc. Lond., Ser. B: Biol. Sci.* **2009**, *364*, 2063.
24. Wang, X. L.; Lin, Q. X.; Wang, J.; Lu, X. G.; Wang, G. P. *Ecol. Eng.* **2013**, *51*, 10.
25. Staples, C. A.; Peterson, D. R.; Parkerton, T. F.; Adams, W. J. *Chemosphere* **1997**, *35*, 667.
26. Kamrin, M. A. *J. Toxicol. Env. Heal. B* **2009**, *12*, 157.
27. Latini, G. *Clin. Chim. Acta* **2005**, *361*, 20.

28. Sathyanarayana, S.; Karr, C. J.; Lozano, P.; Brown, E.; Calafat, A. M.; Liu, F.; Swan, S. H. *Pediatrics* **2008**, *121*, E260.
29. Buchta, C.; Bittner, C.; Heinzl, H.; Hocker, P.; Macher, M.; Mayerhofer, M.; Schmid, R.; Seger, C.; Dettke, M. *Transfusion* **2005**, *45*, 798.
30. Audic, J. L.; Poncin-Epaillard, F.; Reyx, D.; Brosse, J. C. *J. Appl. Polym. Sci.* **2001**, *79*, 1384.
31. Kumagai, H.; Tashiro, T.; Kobayashi, T. *J. Appl. Polym. Sci.* **2005**, *96*, 589.
32. Wen, X. Q.; Liu, X. H.; Liu, G. S. *Vacuum* **2010**, *85*, 406.
33. Xiao-jing, L.; Guan-jun, Q.; Jie-rong, C. *Appl. Surf. Sci.* **2008**, *254*, 6568.
34. Li, R.; Chen, J. *Chin. Sci. Bull.* **2006**, *51*, 615.
35. Slowe, M.; Novak, I.; Vesel, A.; Junkar, I.; Lehocky, M.; Saha, P.; Chodak, I. *Int. J. Polym. Anal. Charact.* **2009**, *14*, 641.
36. Wypych, G. *Handbook of Plasticizers*; Chemtech Publishing: Toronto, 2004.
37. Cao, X. L. *Compr. Rev. Food Sci. F* **2010**, *9*, 21.
38. Kovacic, P. *Med. Hypotheses* **2010**, *74*, 626.
39. Shen, Y. R. *The Principles of Nonlinear Optics*; Wiley: New York, 1984.
40. Shen, Y. R. *Nature* **1989**, *337*, 519.
41. Chen, Z.; Shen, Y. R.; Somorjai, G. A. *Annu. Rev. Phys. Chem.* **2002**, *53*, 437.
42. Geiger, F. M. *Annu. Rev. Phys. Chem.* **2009**, *60*, 61.
43. Stokes, G. Y.; Buchbinder, A. M.; Gibbs-Davis, J. M.; Scheidt, K. A.; Geiger, F. M. *Vib. Spectro.* **2009**, *50*, 86.
44. Tarbuck, T. L.; Ota, S. T.; Richmond, G. L. *J. Am. Chem. Soc.* **2006**, *128*, 14519.
45. Hankett, J. M.; Liu, Y. W.; Zhang, X. X.; Zhang, C.; Chen, Z. *J. Polym. Sci. Part B: Polym. Phys.* **2013**, *51*, 311.
46. Chen, Z. *Polym. Int.* **2007**, *56*, 577.
47. Zhang, C.; Myers, J. N.; Chen, Z. *Soft Matter* **2013**, *9*, 4738.
48. Voges, A. B.; Al-Abadleh, H. A.; Musorrariti, M. J.; Bertin, P. A.; Nguyen, S. T.; Geiger, F. M. *J. Phys. Chem. B* **2004**, *108*, 18675.
49. Callahan, K. M.; Casillas-Ituarte, N. N.; Xu, M.; Roeselova, M.; Allen, H. C.; Tobias, D. J. *J. Phys. Chem. A* **2010**, *114*, 8359.
50. Liu, D. F.; Ma, G.; Allen, H. C. *Environ. Sci. Technol.* **2005**, *39*, 2025.
51. Xu, M.; Liu, D. F.; Allen, H. C. *Environ. Sci. Technol.* **2006**, *40*, 1566.
52. Bisson, P.; Xiao, H.; Kuo, M.; Kamelamela, N.; Shultz, M. J. *J. Phys. Chem. A* **2010**, *114*, 4051.
53. Kristalyn, C. B.; Lu, X.; Weinman, C. J.; Ober, C. K.; Kramer, E. J.; Chen, Z. *Langmuir* **2010**, *26*, 11337.
54. Lu, X. L.; Spanninga, S. A.; Kristalyn, C. B.; Chen, Z. *Langmuir* **2010**, *26*, 14231.
55. Shi, Q.; Ye, S.; Kristalyn, C. B.; Su, Y.; Jiang, Z.; Chen, Z. *Langmuir* **2008**, *24*, 7939.
56. Lu, X. L.; Han, J. L.; Shephard, N.; Rhodes, S.; Martin, A. D.; Li, D. W.; Xue, G.; Chen, Z. *J. Phys. Chem. B* **2009**, *113*, 12944.
57. Zhang, C.; Shephard, N. E.; Rhodes, S. M.; Chen, Z. *Langmuir* **2012**, *28*, 6052.
58. Lu, X. L.; Li, D. W.; Kristalyn, C. B.; Han, J. L.; Shephard, N.; Rhodes, S.; Xue, G.; Chen, Z. *Macromolecules* **2009**, *42*, 9052.
59. Miyamae, T.; Akiyama, H.; Yoshida, M.; Tamaoki, N. *Macromolecules* **2007**, *40*, 4601.
60. Miyamae, T.; Yokoyama, H.; Han, S.; Ishizone, T. *e-J. Surf. Sci. Nanotech.* **2006**, *4*, 515.
61. Zhang, D.; Dougal, S. M.; Yeganeh, M. S. *Langmuir* **2000**, *16*, 4528.

62. Miyamae, T.; Nozoye, H. *J. Photochem. Photobiol. A: Chem.* **2001**, *145*, 93.
63. Miyamae, T.; Yamada, Y.; Uyama, H.; Nozoye, H. *Surf. Sci.* **2001**, *493*, 314.
64. Miyamae, T.; Yamada, Y.; Uyama, H.; Nozoye, H. *Appl. Surf. Sci.* **2001**, *180*, 126.
65. Ye, H.; Gu, Z.; Gracias, D. H. *Langmuir* **2006**, *22*, 1863.
66. Zhang, X.; Zhang, C.; Hankett, J. M.; Chen, Z. *Langmuir* **2013**, *29*, 4008.
67. Zhang, X.; Chen, Z. *Langmuir* **2014**.
68. Hankett, J. M.; Collin, W. R.; Chen, Z. *J. Phys. Chem. B* **2013**, *117*, 16336.
69. Hankett, J. M.; Welle, A.; Lahann, J.; Chen, Z. *J. Appl. Polym. Sci.* **2014**.
70. Hankett, J. M.; Lu, X. L.; Liu, Y. W.; Seeley, E.; Chen, Z. *PCCP* **2014**, *16*, 20097.
71. Zhang, C.; Wang, J.; Khmaladze, A.; Liu, Y. W.; Ding, B.; Jasensky, J.; Chen, Z. *Opt. Lett.* **2011**, *36*, 2272.
72. Krimm, S.; Shipman, J. J.; Folt, V. L.; Berens, A. R. *J. Polym. Sci. Part A* **1963**, *1*, 2621.
73. Enomoto, S.; Asahina, M. *J. Polym. Sci. Part A* **1966**, *4*, 1373.
74. Wei, X.; Zhuang, X.; Hong, S.; Goto, T.; Shen, Y. R. *Phys. Rev. Lett.* **1999**, *82*, 4256.
75. Snyder, R. G.; Strauss, H. L. *J. Phys. Chem.* **1982**, *86*, 5145.
76. Ghoranneviss, M.; Shahidi, S.; Wiener, J. *Plasma Science and Technology* **2010**, *12*, 204.

CHAPTER 3

SURFACE AND BULK CHANGES OF PLASTICIZED PVC FROM ENVIRONMENTAL UV LIGHT EXPOSURE

3.1 Background and Motivation

This Chapter studies the molecular changes of phthalate plasticized poly(vinyl chloride) (PVC) thin films due to long and short wave UV exposure. Surface technique SFG was utilized to determine molecular ordering and content changes on PVC films after UV exposure. SIMS data complemented SFG data, confirming the identity of surface products formed on the plastics. The molecular changes throughout the majority of the plastic were determined using select analytical techniques, and compared to the surface molecular changes to identify competing chemical reactions within the plastic matrix. Lastly, a degradation scheme for phthalate molecules exposed to short wave UV light was devised. The results from this Chapter have been adapted with permission from: Hankett, J.M.; Collin, W. R.; Chen, Z. "Molecular Structural Changes of Plasticized PVC after UV Light Exposure" *J. Phys. Chem. B* **2013**, *117,* 16336-16344, Copyright 2013 American Chemical Society. Figure 3.6 has been published in the supplemental information file of: Hankett, J.M.; Welle, A.; Lahann, J.; Chen, Z. **"**Evaluating UV/H_2O_2 Exposure as a DEHP Degradation Treatment for Plasticized PVC" *J. App. Polym. Sci.* **2014**, *131,* 40649 (1-10), Publisher John Wiley and Sons, Copyright Wiley Periodicals, Inc. 2014, and used with permission as well.

An understanding of molecular-level changes of PVC plastics from UV exposure is desirable since PVC products are often used under UV light, due to their macroscopic durability compared to other plastics. This underlying stability, involving extremely slow degradation processes, is highly desirable during the plastic's use under harsh chemical environments. Phthalate plasticized PVC materials may be exposed to sunlight or UV lights for polymer curing or disinfecting/germicide in areas including but not limited to the medical industry, academic or industrial laboratories, the common household, and across a wide gambit of industrial settings.[1-5] However, while the macroscopic integrity of PVC plastic may remain for years after exposure to UV light, the plastic contents and structure may change at a molecular scale, and thus, the interactions of plastics with the surrounding environment may change.

Previous to this research, little was known of the microscopic behaviors of plasticizer and plastic molecules on plastic surfaces as compared to the bulk after harsh conditions like UV exposure.[4] Understanding such molecular behaviors gives us key insights into how plastic surfaces can be altered even if macroscopic changes from compounded chemical reactions are not observable. As stated previously in this thesis, phthalates are known rodent endocrine disruptors, suspected marine toxins and suspected human carcinogens and toxins. Thus it is of vital importance to understand the molecular behaviors of plasticized PVC at surfaces and observe how UV light may change the potential for exposure to such molecules.[3,6-11] In addition, the molecular structure of phthalates aid in separating PVC chains for plasticizing purposes but are highly susceptible to degradation under harsh environmental conditions. [12] The ester linkage connecting the alkyl chains to the phenyl ring can readily undergo radical reaction. Cleavage of this linkage may yield a variety of different products and would ultimately eliminate the plasticizing effect of this molecule.

Because bulk analytical studies have been performed to examine the degradation of pure PVC plastics or pure phthalate due to UV light but typically require *ex situ* analyses, either through the form of sample destruction or analysis under non-standard conditions, we believe this study aids in closing an important information gap on the molecular content and structural changes of plastic surfaces from UV exposure. [13-22] Previous studies also often included photocatalysts purposely designed to degrade plastic components and do not study effects solely from UV exposure[15-17,22-29]. Even fewer bulk analysis studies have been performed on the photodegradation of plastic/phthalate plasticizer matrix rather than separated components,[30-33] leaving many questions about the molecular changes in UV irradiated PVC bulk unanswered. Consequently, the molecular-level effects of short and long wave UV on DEHP in plastic were not well understood. To the best of our knowledge, no study previously existed that probed UV-exposed phthalate-plasticized PVC at the molecular level in air using a truly surface sensitive technique. Reported here is a study on both the surface and bulk molecular behaviors of plasticizing phthalates before and after exposure to UV irradiation. A battery of carefully chosen surface sensitive and bulk analytical techniques were applied to better understand the effects of UV on plasticizing phthalate molecules at an air interface and throughout the plastic. Once again, this study utilizes bis-2-ethyhexyl phthalate (DEHP) to plasticize the PVC materials. As a refresher, the molecular structures of PVC and DEHP are shown in Figure 3.1.

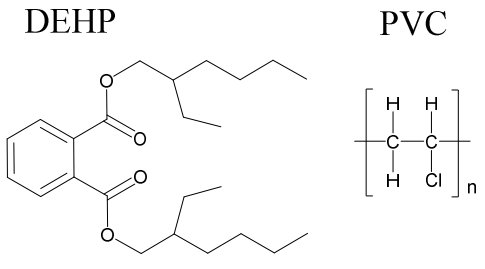

Figure 3.1. Molecular structures of di-2-ethylhexyl phthalate (DEHP) (left), and poly(vinyl chloride) (PVC) (right).

In this Chapter the molecular structural changes in and on PVC films with 0, 10 and 25 wt% DEHP due to exposure to 254 nm short wave or 365 nm long wave UV are analyzed. These wavelengths are commonly used for germicidal applications and polymer/epoxy curing, respectively and are also wavelengths present in sunlight. We utilized SFG to probe the surface of the films non-destructively. In addition, we determined the hydrophilicity changes on film surfaces after UV exposure with contact angle goniometry (CA). To probe molecular changes in the bulk of the plastic, Fourier transform infrared spectroscopy (FTIR) was used, as well as high performance liquid chromatography coupled with mass spectrometry (HPLC/MS) using a novel plasticizer extraction method, and gel permeation chromatography (GPC).

3.2 Experimental Methods

3.2.1 Materials

Poly(vinyl chloride) (M_w 62,000; M_n 35,000) in pellet form, tetrahydrofuran (THF) ≥99.9% purity, concentrated sulfuric acid (reagent grade) and potassium dichromate were purchased from Sigma Aldrich (St. Louis, MO). Bis 2-ethylhexyl phthalate (analytical standard) was obtained from Fluka (St. Louis, MO), and acetonitrile (99.9% purity, HPLC grade) was purchased from Acros Organics (Pittsburg, PA).

3.2.2 Sample Preparation

3.2.2.1 General Sample Preparation

Fused silica windows (ESCO Products, Inc.) used for SFG measurements were sequentially cleaned using a concentrated sulfuric acid bath saturated with potassium dichromate

overnight, rinsed with deionized water, dried under nitrogen gas, and then further cleaned by exposing windows to a glow discharge air plasma for 4 min using a PE-50 series Plasma System (Plasma Etch, Inc.) to remove any remaining organic material before sample preparation. For FTIR experiments, calcium fluoride windows (ESCO Products, Inc.) were used as substrates. Calcium fluoride windows were first soaked in THF and then cleaned using a dilute Alconox soap solution, rinsed with Milli-Q deionized water, dried under nitrogen gas, and further cleaned with the same glow discharge plasma as previously mentioned. Glass slides used for contact angle measurements and plasticizer extraction were dusted with nitrogen gas and also plasma cleaned before sample preparation.

PVC pellets were dissolved in THF (weight ratio of THF:PVC = 30:1) to prepare the PVC-based thin films. DEHP was added by weight percent to PVC. Solutions were mixed using a vortex mixer (Vortex-Genie 2T, Scientific Industries Inc.) until clear. Sample films of ~200 nm thick were spin coated at 3000 rpm for 30 s on silica windows, calcium fluoride windows, or glass slides using a P-6000 spin coater (Speedline Technologies).

3.2.2.2 UV Treatment for SFG Spectral Analysis

SFG spectra were first collected from PVC or PVC/DEHP thin films deposited on fused silica as reference spectra in air. Films were placed in a blacked out chemical hood and exposed to either a 60 watt short wave UV (254 nm) lamp (Cole Palmer, Inc.) at about 30 cm from the film surface ($I = 53\ W/m^2$) or a 100 watt long wave UV (365 nm) lamp (Ted Pella, Inc.) at about 30 cm from the film surface ($I = 88\ W/m^2$) for 30, 60, 90, or 300 min. After UV exposure, SFG spectra were obtained again at the air interface.

3.2.2.3 Notes about Intensity of UV Applied to Materials Compared to Sunlight

While the intensities of the UV lamps used in this and the following chapter's studies are comparable to intensities used in laboratories and industrial settings for photoactivation and/or germicidal applications, they are more intense than natural sunlight. Natural UV at ground level consists of about 3% of the sun's total irradiance since the emission of light is essentially blackbody radiation. Therefore, when the sun is at zenith, the total amount of UV (100 nm-400 nm) irradiance is about 32 W/m^2 or less, according to the American Society for Testing and Materials (ASTM) Terrestrial Reference Spectra for Photovoltaic Performance Evaluation (Document ASTM G-173-03 can be found online free of charge to the public). In contrast, our lamps irradiate at 53 or 88 W/m^2 at a single wavelength. Thus the samples would need to be exposed to sunlight for much longer times in order to receive the same number of photons from a given treatment time via UV lamp.

3.2.2.4 Sample Preparation and Extraction for HPLC/MS Analysis

A novel sample preparation and extraction method was developed to analyze pure plasticizer and plasticizer reaction products via HPLC/MS. 25 wt% DEHP films were spin coated on glass slides, which were first cut to 1 cm x 1.5 cm and plasma cleaned on both sides. After spin coating, the bottom of the glass slides were wiped off with ethanol using a Kimwipe and placed on plasma cleaned 2.54 cm x 7.62 cm glass slides in preparation for UV treatment. Twenty-eight samples each were exposed to long or short wave UV for 300 min. To extract DEHP and related compounds, fourteen slides exposed to short wave UV were immersed in ~5 ml acetonitrile for 30 min. After immersion, these slides were removed and the remaining fourteen slides were immersed for 30 min in the same 5 ml solution. The top half of this solution was removed by glass pipette and placed in a glass vial for HPLC injection. As a standard, 2.5

wt% pure DEHP was added to acetonitrile, mixed with a vortex mixer and further diluted for injection. The same procedure was used for the twenty-eight samples exposed to the long wave UV.

3.2.2.5 Sample Preparation and Reactions for GPC Analysis

Pure PVC was dissolved by THF in a 20 mL glass vial in the same manner as other experiments. The THF was evaporated from PVC by a stream of nitrogen gas for about 30 min, leaving a thin (on the order of microns) film of PVC on the bottom of the vial. The open vial was placed under long or short wave UV lamps for 300 min. After 300 min the vial was removed from UV light and the PVC was re-dissolved in THF at the same concentration as regular sample preparation methods. As a control, pure PVC was dissolved in THF in the same vial type and used for injection without any UV exposure.

3.2.3 Instrumentation

3.2.3.1 FTIR

A Nicolet 6700 FTIR spectrometer was used to study bulk structures of plastic films before and after UV exposure. The FTIR sample stage was purged with nitrogen gas prior to and during the data collection procedure. Spectra were obtained of pure PVC and 25 wt% DEHP films spin coated on calcium fluoride windows from 400 cm^{-1} to 4000 cm^{-1} before UV exposure and after 1 h or 5 h of short or long wave UV exposure. The spectra were corrected for atmospheric water interferences and baseline anomalies and have a presented range of 1000-3200 cm^{-1}.

3.2.3.2 SFG

SFG has been widely applied to gather molecular level information on molecular changes of a variety of polymers at interfaces including air, water, and other buried interfaces.[34-45] The details of SFG theory and setup have been extensively outlined in previous papers from our lab[46-49] and in the introduction section of this thesis. The SFG experiments conducted for this Chapter were taken using the ssp (s-polarized signal, s-polarized 532 nm input beam and p-polarized tunable frequency IR input beam) polarization combination in face-down geometry. All SFG spectra were obtained at the same visible beam power.

3.2.3.3 HPLC/MS

HPLC/MS analyses were performed on an Agilent 1200 LC coupled to a G2710AA MSD, running the following ACN:H_2O:AcOH gradient on a Phenomenex Gemini 3µ C18 110A 50 x 2mm column at 0.4 ml/min: 0-4min: 0-100%B; 4-9min: 100%B; 9-15min: 0%B; where A is 90:10:0.1 H_2O:MeOH:AcOH and B is 10:90:0.1 H_2O:MeOH:AcOH. The analyte injection volume was 2.0 µL. HPLC-MS was conducted by Dr. Paul Kennedy at Cayman Chemical Co., Ann Arbor, MI.

3.2.3.4 GPC

GPC analyses were performed using THF as a solvent on a Waters 440 system equipped with Waters Styragel columns (7.8 x 300, HT 0.5, 2, 3, 4) with RI detection using a Waters 2410 refractometer. The system was calibrated using polystyrene standards and toluene as reference. Data analysis was performed using GRAMS32 version 6.0 (Thermo-Scientific, Pittsburgh, PA). GPC was conducted by Phi Doan at the University of Michigan.

3.2.3.5 UV-Vis

UV-Vis spectra were obtained on a UV-1601PC UV-Vis Shimadzu Spectrophotometer. Thin plastic films were formed on the insides of quartz cuvettes by pipetting ~1 mL plastic solution inside the cuvettes using a glass pipette and pouring excess solution out. For the thin film preparation, the plastic solution procedure was identical to the method stated in the experimental section of this Chapter. The cuvettes were rinsed with ethanol and Millipore deionized water several times, dried with nitrogen gas, and then cleaned via plasma for 3 min prior to film preparation. For these experiments, one quartz cuvette was subjected to 5h 254 nm UV exposure in an identical manner to the UV experiments outlined previously. Clean quartz cuvettes were used as a background for all UV-Vis measurements. Special thanks are given to the members of the Gafni lab at the University of Michigan for allowing us use of and help with their UV-Vis instrument.

3.3 Results and Discussion

3.3.1 Surface Analysis Results

3.3.1.1 25 wt% DEHP Before UV Exposure

Similar to previous results in Chapter 2, the surface of plasticized PVC with 25 wt% DEHP was analyzed with SFG (Figure 3.2).[34] The result again shows the dominating methyl group signatures at 2880 cm^{-1} (CH_3(s)) and 2945 cm^{-1} (Fermi resonance) and a shoulder peak at 2860 cm^{-1} (CH_2(s)), all of which are associated with the DEHP molecule.[34,50] Again, the shoulder peak at 2915 cm^{-1} can be observed and corresponds to the CH_2(s) of PVC. This CH_2(s) peak can be seen in the SFG spectrum of pure PVC (Figure 3.3). [34,50,51]

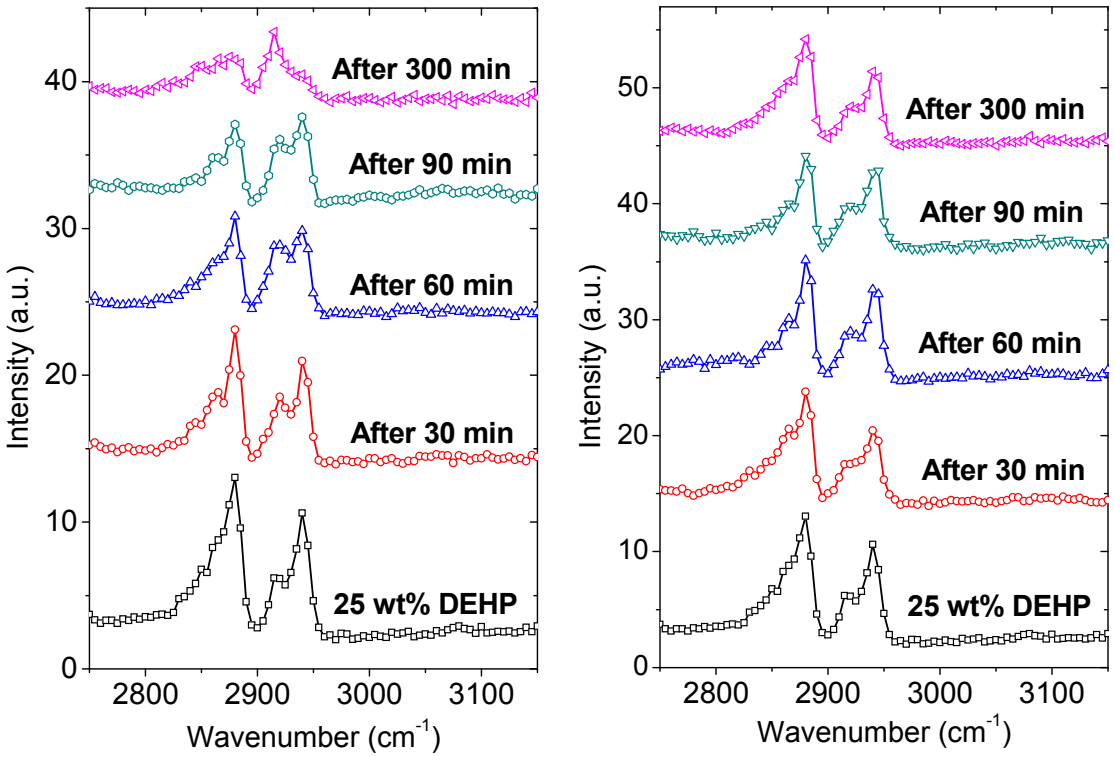

Figure 3.2. SFG ssp spectra collected from plasticized PVC with 25 wt% DEHP before and after 30 min, 60 min, 90 min, or 300 min of short (left panel) versus long (right panel) wave UV exposure.

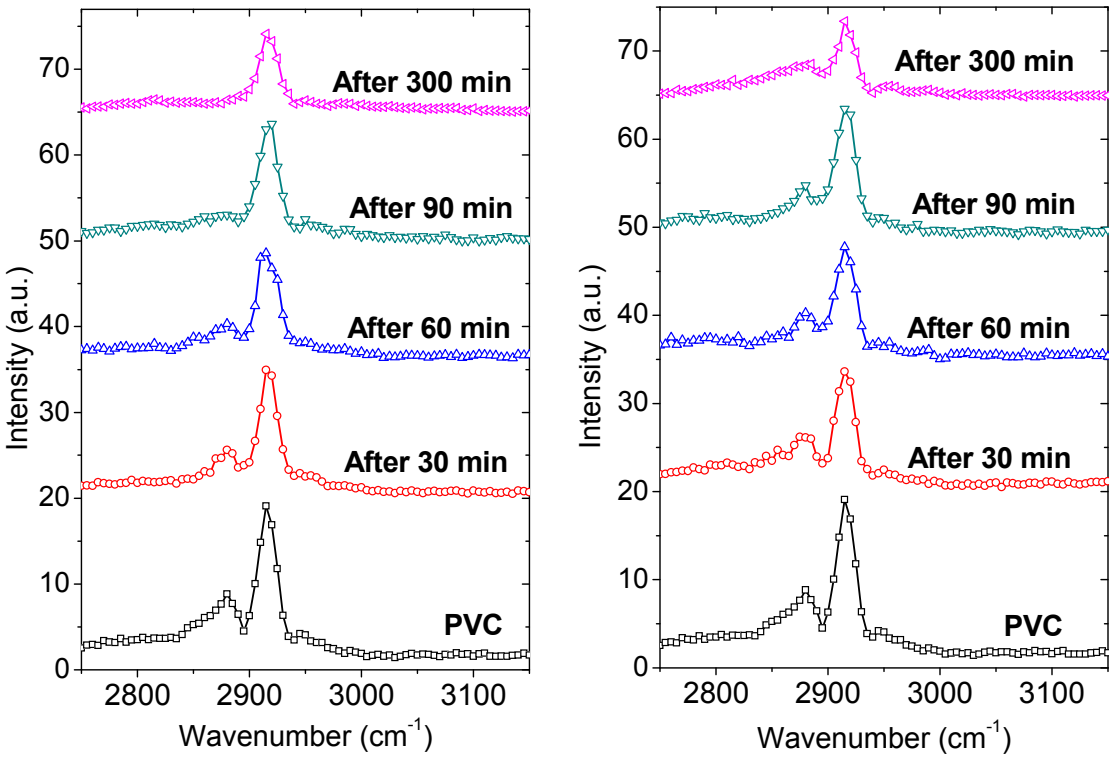

Figure 3.3. SFG ssp spectra collected from PVC before and after 30 min, 60 min, 90 min, or 300 min of short (left panel) versus long (right panel) wave UV exposure.

3.3.1.2 25 wt% DEHP After Short Wave UV Exposure

SFG spectra collected from PVC with 25 wt% DEHP after 30, 60, 90 and 300 min of short wave UV exposure can be found in Figure 3.2. After 60 min of short wave UV exposure, an obvious increase in intensity of the PVC CH_2(s) peak at 2915 cm^{-1} compared to the DEHP CH_3 peaks at 2880 and 2945 cm^{-1} can be observed. After 300 min, the PVC CH_2(s) signal dominates the spectrum, with comparatively small peaks present between 2840 cm^{-1} and 2880 cm^{-1} and a small shoulder at 2940 cm^{-1}. These spectral changes suggest the surface of the plastic dramatically changed after short wave UV exposure, likely due to reactions on the surface. The loss of CH_3 signals can be attributed to either DEHP-reacted surface molecules, the removal of DEHP, or a combination thereof, but SFG data alone cannot differentiate such possibilities.

To generate information on the surface energy changes of the plastics from UV exposure, experiments using contact angle goniometry were conducted before and after short wave UV exposure. In the top panel of Table 3.1, water contact angles of PVC, 10 wt% DEHP films and 25 wt% DEHP surfaces before and after 1 h or 5 h exposure to short wave UV are given. In turn, the bottom panel shows contact angles of PVC, 10 wt% DEHP films and 25 wt% DEHP surfaces before and after 1 h or 5 h exposure to long wave UV. The contact angle data indicated that the changes in SFG signals were not due to complete removal of DEHP surface molecules. After 60 min of UV exposure, the measured contact angle decreases from 86° to 79-80°, indicating the surfaces of the films became more hydrophilic, at a slightly lower contact angle than that of pure unadulterated PVC. After 5 h of exposure the contact angle further decreases to 70-71° as can be observed in Table 3.1. If the DEHP molecules were simply removed and pure PVC was exposed, the contact angle would likely return to that of pure PVC (80-81°). We can also observed in Table 3.1 that the contact angle decreases even lower than pure PVC after 300 min of UV exposure (77-79°).

Table 3.1. Water contact angle measurements before and after UV exposure

Short Wave	**PVC**	**10 wt% DEHP**	**25 wt% DEHP**
Before	80-81°	86-87°	86-87°
After 1 h	80-81°	82-84°	79-80°
After 5 h	77-79°	74-75°	70-71°

Long Wave	**PVC**	**10 wt% DEHP**	**25 wt% DEHP**
Before	80-81°	86-87°	86-87°
After 1 h	80°	85-86°	85-86°
After 5 h	79-80°	85-86°	85-86°

3.3.1.3 25 wt% DEHP After Long Wave UV Exposure

The SFG results after long wave UV exposure are much different from those after short wave UV exposure (right panel, Figure 3.2). No detectable changes were observed in the spectra from 30 min to 300 min of exposure, suggesting neither occurrence of major reactions, nor changes of PVC or DEHP molecular surface ordering. Water contact angles on the 25 wt% DEHP samples show virtually negligible surface hydrophobicity changes after 300 min of long wave UV treatment (Table 3.1).

3.3.1.4 10 wt% DEHP Before UV Exposure

As previously shown in this thesis, the SFG spectrum collected from the 10 wt% DEHP sample contains strong signals significant of both PVC at 2915 cm^{-1} and DEHP at 2880 cm^{-1} and 2945 cm^{-1} (Figure 3.4), indicating that both PVC and DEHP molecules are present on the surface. The water contact angle on this surface is slightly higher than pure PVC, at 84-85° (Table 3.1).

3.3.1.5 10 wt% DEHP After Short Wave UV Exposure

After 60 min of short wave UV exposure to PVC with 10 wt% DEHP (left panel, Figure 3.4), trends in SFG signal changes are similar to those found with PVC containing 25 wt% DEHP are found. The ratio of the intensity of the PVC CH_2(s) peak compared to the intensity of the DEHP-associated peaks increases from 60 min to 90 min, and again at 300 min. After 300 min of UV treatment, very little signal associated with DEHP remains, suggesting that almost all DEHP molecules may have been reacted and/or removed from the surface. The water contact angle after 300 min of UV exposure decreases from 85° to 74° as well.

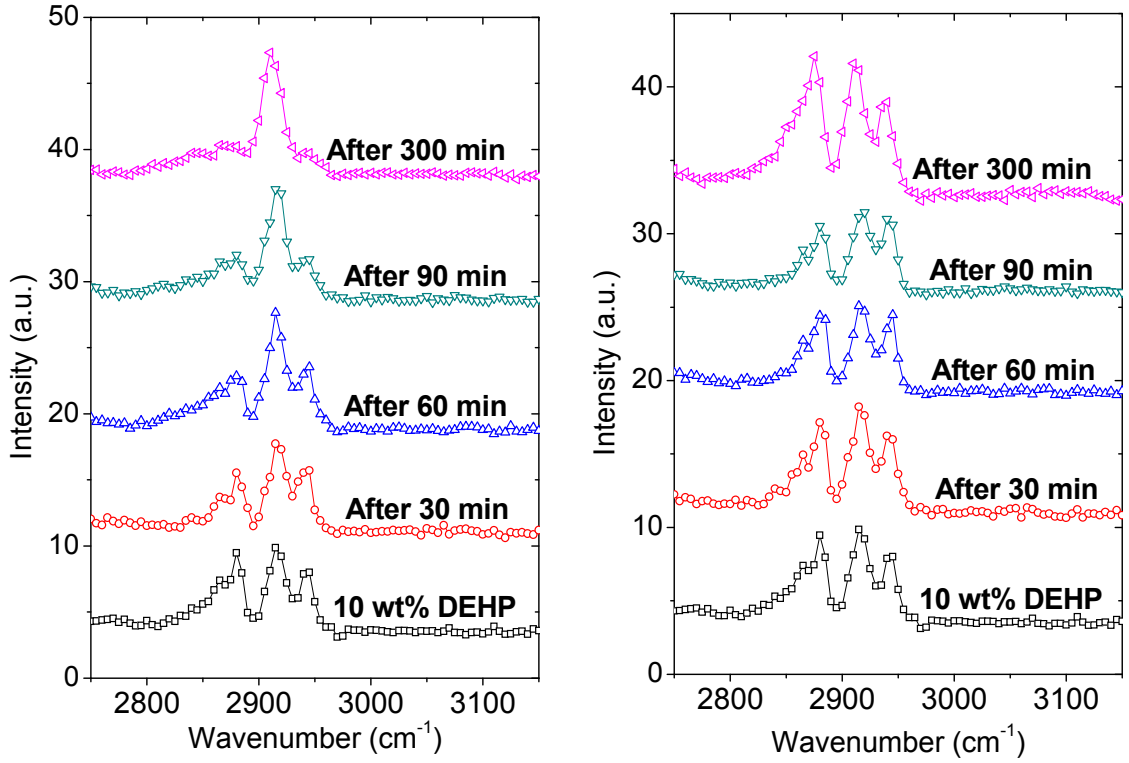

Figure 3.4. SFG ssp spectra collected from plasticized PVC with 10 wt% DEHP before and after 30, 60, 90, or 300 min of short (left panel) versus long (right panel) wave UV exposure.

We previously demonstrated that the increased addition of bulk DEHP to PVC from 10 wt% to 25 wt% also increased the number of DEHP molecules on the surface. Knowing that piece of information and that the water contact angle on the 25 wt% sample after UV exposure was lower than the 10 wt% sample, we believe that the UV induced reaction products from DEHP on the surface must increase the surface hydrophilicity. If the surface of the 10 wt% sample contained a lower surface concentration of DEHP molecules than the 25 wt% sample before UV exposure, likely there would be fewer UV induced reaction products on the 10 wt% sample, in agreement with contact angle changes. In addition, virtually no CH_3 groups were observed after 5h of short wave UV treatment on the 10 wt% sample, while some DEHP CH_3

signatures remained for the 25 wt% sample, suggesting not all DEHP molecules on the 25 wt% sample were reacted, while the majority of DEHP molecules on the 10 wt% sample reacted.

3.3.1.6 10 wt% DEHP after Long Wave UV Exposure

Once again long wave UV exposure appears to have very little effect on the CH groups of DEHP and PVC. The SFG spectra remain similar before and after UV exposure up to 300 min (right panel, Figure 3.4). The spectral features remain similar, and the relative peak intensities vary only slightly. In addition, the water contact angles are similar on the sample surface after 60 min or 300 min of UV treatment (again contact angles only change 1-2°), suggesting that the majority of DEHP molecules remain intact on the surface.

3.3.1.7 Pure PVC in Air

To recap the characteristic SFG spectra signature of PVC, two peaks can be clearly resolved in ssp polarization combination. The dominating signal at 2915 cm^{-1} is associated with the CH_2(s) stretch and the much smaller, broad peak at 2880 cm^{-1} is associated with the CH_3(s) chain end groups.

3.3.1.8 Pure PVC after Short Wave UV Exposure

SFG ssp spectra of PVC after short wave UV exposure can be observed in the left panel of Figure 3.2. Spectral changes can be observed after 30 min of UV exposure, with decreased intensity of the CH_3(s) peak compared to the CH_2(s) peak. The ratio of peak intensities continues to decrease over increasing exposure time, with only the CH_2(s) peak observed after 300 min of exposure. There are a few possibilities as to why the spectral changes may have occurred. Mainly, the CH_3 groups could have become completely disordered, removed, or reoriented such that they lie flat on the surface. It is highly likely that the CH_3 groups may have

been reordered and/or removed due to radical chemical reactions involving either crosslinking or minor chain scission. Evidence of such reactions will be presented later. The overall intensities of the signals decrease after increased short wave treatment times as well, suggesting there is either a higher degree of disorder among molecular groups in the C-H stretching vibrational range or that there are fewer of these C-H groups on the surface. In addition, a decreased contact angle from 81° to 78° suggests a slight increase in surface hydrophilicity after UV exposure. This increase in hydrophilicity was likely due to the molecular changes of C-H groups as well as increased oxygen content, as the 254 nm wavelength emitted from the lamp forms oxygen radicals in air. The combination of noted increase in hydrophilicity and decrease in SFG signal intensity is also highly indicative of increased C-H disorder on the surface.

3.3.1.9 Pure PVC after Long Wave UV Exposure

Figure 3.2 displays SFG spectra of pure PVC after long wave treatment. Similar to the short wave treatment, a decrease in the ratio of CH_3(s) to CH_2(s) intensities can be observed with as little as 30 min of exposure. However, this trend in signal decrease does not continue to the same extent. After 300 min of UV exposure, there is further decrease in this ratio, but, unlike the samples exposed to short wave UV light, the CH_3 signal does not completely disappear. This may suggest that whatever mechanism results in the disappearance of CH_3 signals from short wave UV occurs to a lesser extent with long wave UV. Similar to signals after short wave UV treatment, the SFG overall signal intensities decrease with increasing reaction times, again indicating either fewer CH groups are left on the surface or that they are more disordered. Additionally, there are no major differences between contact angles before and after treatment. This is supportive evidence that the surface of this film did not change as much as those exposed to short wave UV.

In summary, examining the surface information obtained from all three sample types, it is obvious that short wave UV induces greater surface changes for both PVC and DEHP than long wave UV. In addition, we can surmise that DEHP is affected more by short wave UV than PVC is, with more dramatic changes in SFG signals and greater decreases in water contact angle after UV exposure in comparison.

3.3.2 Bulk Analysis Results

To complement surface analysis results and generate a much more well-rounded picture on the molecular effects of long and short wave UV on the surface and majority of phthalate plasticized PVC films, FTIR, HPLC-MS and GPC results were obtained of all three sample types.

3.3.2.1 FTIR of Pure PVC

FTIR spectra of 25 wt% DEHP and pure PVC films before and after 60 min or 300 min of short or long wave UV exposure are found in Figure 3.5. In the pure PVC panel, we can see that short wave UV induces a decrease in intensity across the CH vibration region (2800-3000 cm^{-1}), which is more dramatic with increased UV exposure times from 1 h to 5 h. In more detail, there is a noted decrease in signal intensity from 2840 cm^{-1} to roughly 3000 cm^{-1}, which contains assignments from both CH_2 and CH_3 groups according to literature including the 2880 cm^{-1} (CH_3), 2860 cm^{-1} (CH_2), and 2845 cm^{-1} (CH_2(s)).[51,52] There is also an increase in signal intensity of a C=O stretch at 1725 cm^{-1} with increased reaction time. This peak is not present in pure PVC before UV exposure. The exact nature of the increase in C=O bonds cannot be determined directly from the FTIR spectrum, but it is likely caused by oxygen radicals reacting with carbon atoms in PVC chains.

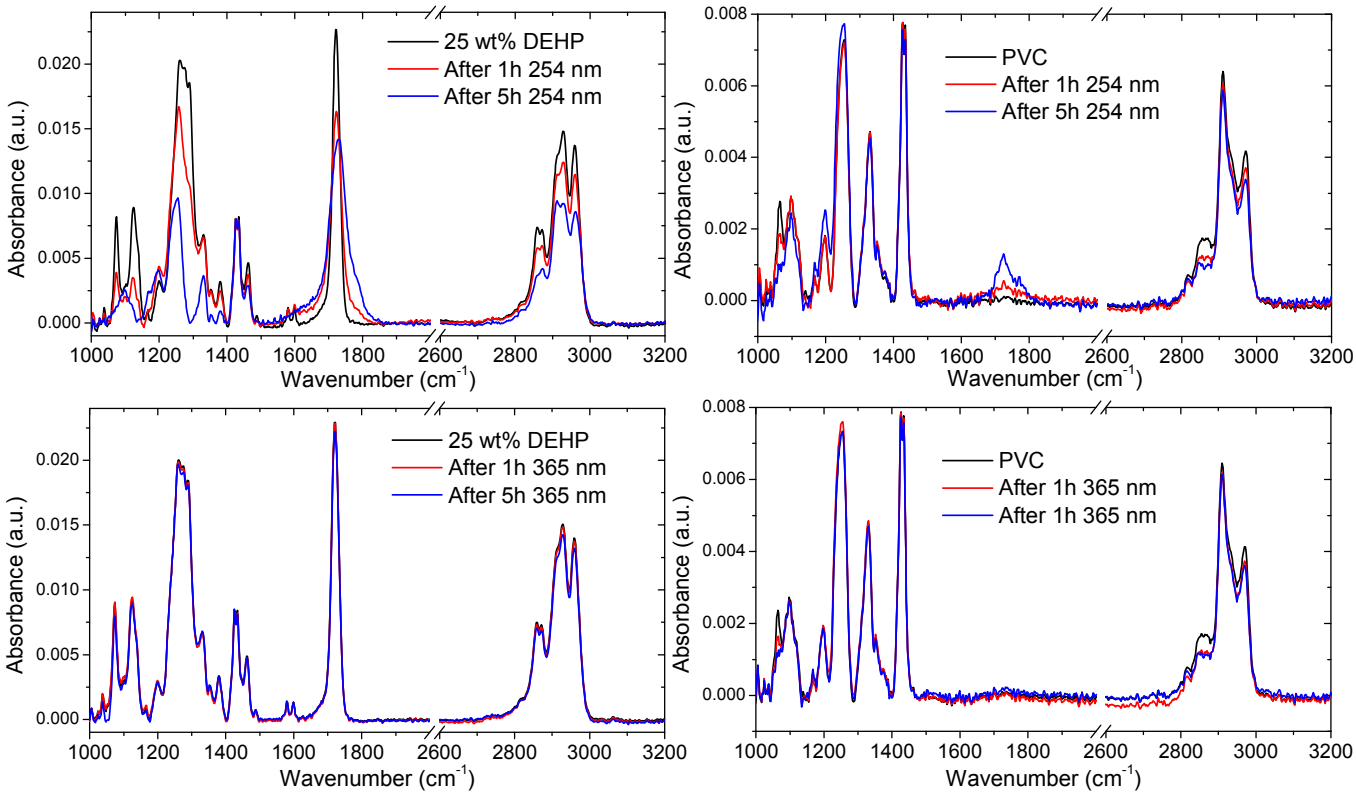

Figure 3.5. Left panel: FTIR data of PVC with 25 wt% DEHP before (black) and after 1 h (red) and 5 h (blue) UV exposure. Right panel: FTIR data of PVC before (black) and after 1 h (red) and 5 h (blue) UV exposure. The top row contains data obtained after short wave UV exposure, the bottom row from long wave UV exposure.

In comparison, the FTIR spectra of PVC after long wave exposure do not change nearly as dramatically as with short wave UV treatment. There are smaller decreases in signal intensity in the C-H region from 2840 cm^{-1} to 3000 cm^{-1}, and no observable formation of a peak at 1725 cm^{-1}. The observed changes in C-H vibrational resonances may be due to a number of chemical reactions including crosslinking, scission, or scavenging and removal of C-H bonds due to radical reactions. Similar to the results found with SFG and contact angle measurements, it appears both long and short wave UV induce minor chemical reactions involving C-H groups, but short wave UV induces much greater molecular changes overall than long wave UV.

3.3.2.2 FTIR of 25 wt% DEHP

After PVC with 25 wt% DEHP has been exposed to short wave UV, dramatic FTIR spectral bulk changes can be found across both C-H and C=O stretching frequency ranges which increase from 1h to 5 h of exposure (Figure 3.5). Decreases in the intensities of signals in the lower frequency range are of special interest, including decreases at 1027 and 1127 cm^{-1}, which have been previously assigned in literature to the aromatic O-CH_2 group of DEHP, 1280 cm^{-1}, which has been assigned to the conjugated aromatic ester COO group of DEHP, and 1462 cm^{-1}, which is associated with an aromatic C=C stretch. There is evidence that some aromaticity remains in molecules located in these films. However, the unchanged peak at 1428 cm^{-1} indicates that some phenyl rings remain intact.[53] There is also a dramatic decrease in intensity and broadening of the 1725 cm^{-1} C=O stretch, which indicates not only that the number of C=O groups decreased dramatically, but that the neighboring chemical environment surrounding the C=O bonds changed; there are multiple different environments surrounding the bond. Lastly, there are significant decreases in intensity across the C-H region of spectra, indicative of C-H bond elimination through radical attack.

Collectively the FTIR spectral changes indicate that short wave UV exposure results in degradation of DEHP molecules. Cleavage of the aromatic ester bond occurs, which removes the alkyl chain "legs" of DEHP, thus forming smaller molecules. It is likely that radical reactions led to the formation of phthalic acid. Evidence for this can be seen in the wide C=O stretching peak, which is observed in FTIR reference spectra of phthalic acid. Further possible reaction products include phthalic anhydride, phthalic monoesters, and phthalate-related molecules that have hydroxylated phenyl rings. It is unlikely, simply due to the nature of these radical reactions, that only one product type was formed, especially considering the FTIR spectra

after 5h of treatment do not indicate reaction to complete degradation of DEHP molecules. Unfortunately, the identity of the newly formed molecules could not be confirmed with the FTIR spectra alone.

In contrast, the FTIR spectra of PVC with 25 wt% DEHP obtained after long wave UV exposure yield virtually no changes, with minute decreases in intensity in the C-H stretching frequency region of spectra and no broadening of the C=O stretching signal observed (Figure 3.5). This indicates the plastic chemical integrity is protected by DEHP under long wave UV light, since the vibrational molecular changes of the plasticized sample were far less dramatic than for pure PVC. It is likely that the DEHP molecules absorb this wavelength of UV light with little resulting damage and reduce the amount of C-H cleavage or reaction in PVC. The UV absorbance from the plastic films was quantified using UV-Vis and details regarding DEHP UV absorption as well as the amount of UV absorbance vs. film thickness can be found in the next section. Recall the DEHP molecules are highly reactive under short wave UV, much more so than pure PVC, which can be observed by greater UV absorbance as well as FTIR.

3.3.2.3 UV-Vis of PVC Plastics

To further understand the chemical changes the plasticized PVC material may undergo due to absorption of UV light and the subsequent bond breaking, UV-Vis spectra of 25 wt% DEHP films were obtained before and after 5h exposure to 254 nm UV, as shown in Figure 3.6. First it is important to note that before exposure, with a film thickness upwards of 200 nm on all sides of the UV-Vis cuvette (400+ nm total) exposed to UV, there is low UV absorbance at 254 nm, indicating that the UV (at 254 nm) penetrates the bulk of the sample.

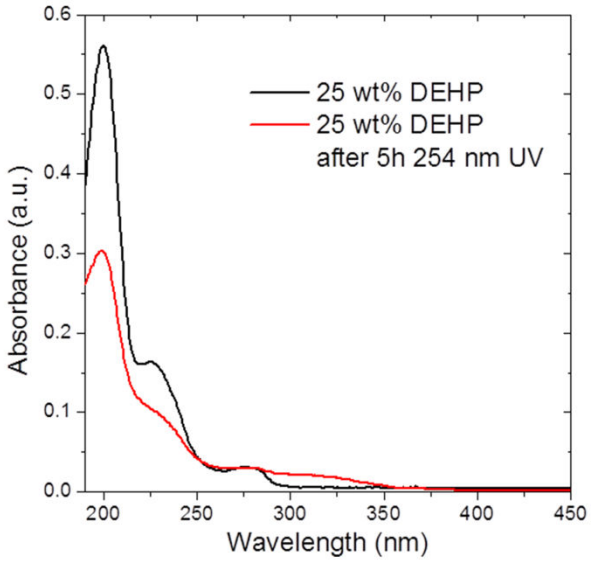

Figure 3.6. UV-Vis spectra of a thin film (400+ nm total thickness) of PVC with 25 wt% DEHP before and after 5h of exposure to 254 nm.

After short wave UV exposure, there is a marked decrease in signal intensity in the lower wavelength region, from ~190 nm-250 nm, and an increase in signal intensity at about 300 nm. The absorbances in the low wavelength UV region are associated with the phenyl ring of DEHP (possibly in combination with the conjugated C=O), suggesting that after exposure the conjugated bond network in and around some phenyl rings are no longer intact. In turn, there is an increase in absorption after reaction around 300 nm, which is associated with an increase in conjugation across PVC chains, strong evidence for double bond formation. Such bonds would result once chlorine was abstracted from the polymer, which is expected to occur from short wave UV exposure and has been well documented and reported in literature. A slight tail of increased absorption is also observable towards longer UV wavelengths, which can be associated with increased conjugation of the polymer system as well. It is important to note that not many absorbance changes are observed in the longest UV wavelengths tested, and although the film does not absorb much long wave UV or short wave visible light, a very small amount of

absorption is observed at 365 nm, the wavelength utilized for our long wave UV exposure experiments.

3.3.2.4 HPLC/MS of Phthalate Reaction Products

To further identity DEHP reaction products formed from UV exposure, HPLC/MS experiments were performed on small molecules extracted from PVC with 25 wt% DEHP after 300 min exposure to short or long wave UV. The molecules were extracted from the samples using acetonitrile and pure DEHP added to acetonitrile was used for the standard HPLC chromatogram and corresponding mass spectrum of DEHP itself. An HPLC chromatogram of the compounds extracted from 25 wt% DEHP after 300 min of short wave UV exposure using a UV detector at 210 nm can be seen in Figure 3.7. There is a major peak at 9.2 min associated with pure DEHP. The peak of interest eluted at 7.3 min, with the resulting mass spectrum of its contents shown at the lower half of Figure 3.7. Signals at 301.1 and 279.2 m/z have been identified as sodium and hydrogen adducts of phthalate monoesters, respectively. A peak at 167 m/z was assigned to a hydrogen adduct of phthalic acid, 149.1 m/z to the hydrogen adduct of phthalic anhydride, and a peak at 181.1 m/z to a hydrogen adduct of phthalic anhydride with a doubly hydroxylated phenyl ring.

It is important to note that the analysis of the obtained mass spectra in relation to proof of existence of molecules after reaction is not completely straight forward. For example, the presence of the signal at 167.0 m/z does not by itself prove that phthalic acid was formed from radical reactions, as this molecule may result from in-source decay of phthalate monoester. But since FTIR evidence suggests that phthalic acid was formed after 300 min of reaction time, as the vibrational resonance from the conjugated aromatic ester bond virtually disappeared, and we have additional evidence from HPLC/MS, it is safe to say that this molecule was indeed formed.

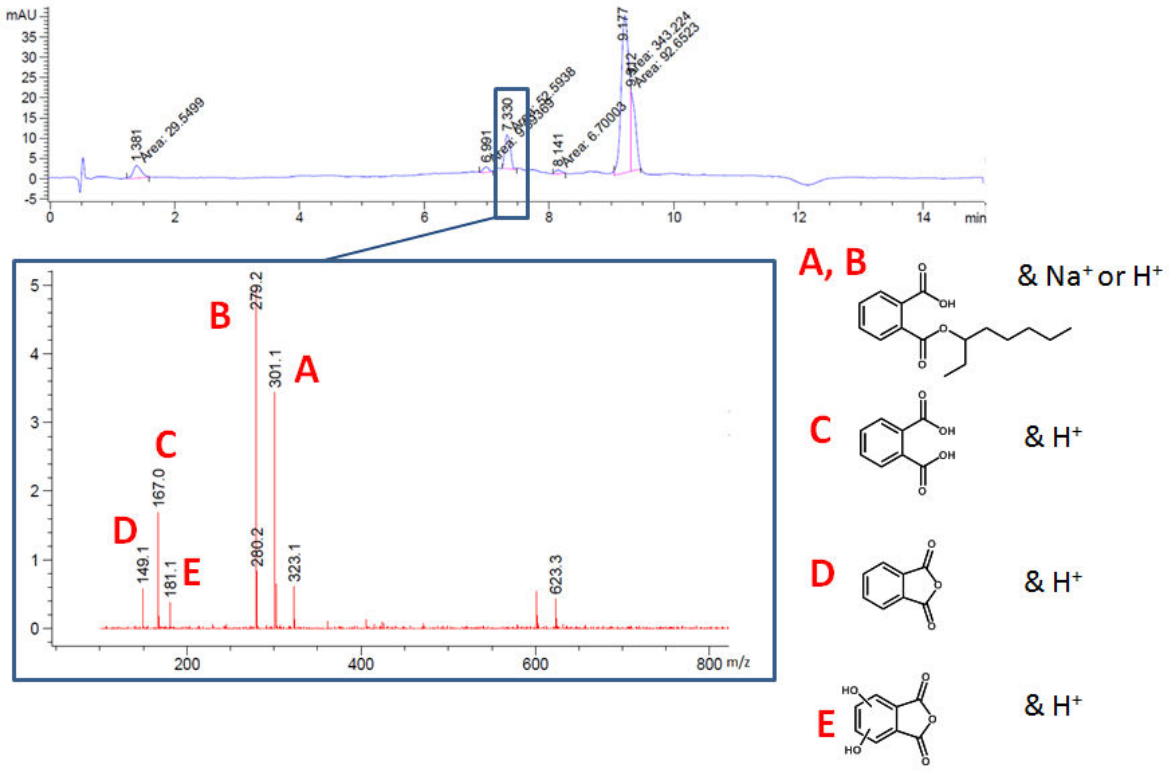

Figure 3.7. Top: HPLC chromatogram of extracted DEHP and DEHP related compounds after 5 h short wave UV treatment. Bottom: corresponding mass spectrum of the peak at 7.3 min in the UV chromatogram.

The use of combined techniques indicates in fact that both the monoester and diacid were formed. However, the formation of phthalic anhydride cannot be proven using mass spectrometry. It is possible that the anhydride was formed under the "harsh" ESI conditions and may not exist at higher humidity levels, like those found in normal room temperature air. Finally, the evidence of phenyl ring hydroxylation at 181.1 m/z is not surprising, but it is not definitive proof of any dominant type of hydroxylation since there was no direct evidence of this molecule by FTIR or SFG. We did observe a slight increase in intensity of a broad peak in the OH stretching frequency in FTIR (3300 cm^{-1} to 3700 cm^{-1}, data not shown here), but it is very difficult to assign this broad signal increase to a phenyl ring hydroxylation. The slight increase in signal in this region indicates some increase in hydroxyl or water stretching, but gives no

indication of the surrounding chemical environment. In addition, if some phenyl rings (but not a majority) underwent reactions with hydroxyl radicals, it is possible that very weak or no FTIR signal would be observed. Lastly, a peak in the OH stretching frequency region would only appear in SFG spectra if the OH molecular groups formed some order at the air interface. With varied hydroxylation across differently oriented molecules, it is not surprising that no OH SFG signal was observed. Previous research on free molecule phthalate degradation by UV/catalysts suggests that phenyl ring hydroxylation occurs on many different molecules.[29]

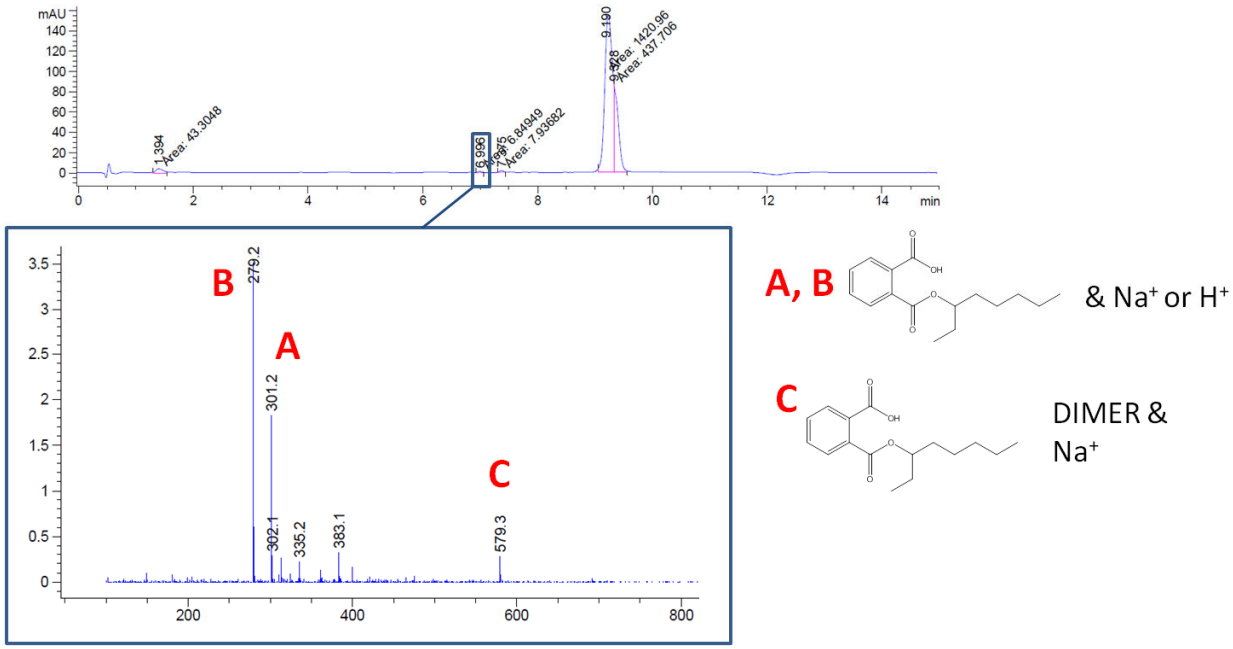

Figure 3.8. Top: HPLC chromatogram of extracted DEHP and DEHP related compounds after 5h long wave UV treatment. Bottom: corresponding mass spectrum of the peak at 7.0 min in the chromatogram.

For comparison, the HPLC chromatogram obtained from the acetonitrile extraction of PVC samples with 25 wt% DEHP after exposure to 300 min of long wave UV is shown in Figure 3.8. This chromatogram contains a much smaller peak at about 7.0 min in relation to the intensity of the pure DEHP peak (Figure 3.9). When the mass spectrum of this peak is evaluated, only

signals associated with the phthalate monoester are observable, and there is no evidence of phthalic acid formation. These results can be interpreted as due to two possible reasons: either phthalic acid was formed and extracted from films but in such low quantities that it could not be observed using the extraction/mass spectrometry technique, or that no phthalic acid was formed. In any case, the results found with mass spectra and HPLC chromatograms correspond to the results from FTIR well, indicating that more products were formed from short wave UV treatment than long wave UV treatment. Finally, note that the standard HPLC chromatogram of DEHP has only 1 peak (Figure 3.9) with a corresponding mass spectrum that contains signals only associated with the DEHP molecule, showing that the plasticizer is highly pure previous to UV exposures. One final note regarding the chromatographic separation of reaction products extracted from plastics films regards the ratio of the peak intensities. The ratios in the individual HPLC chromatograms may not directly correspond to the concentration of reaction products compared to intact DEHP molecules, since the extraction efficiency for pure DEHP versus reaction products was not characterized. Therefore the chromatograms and corresponding mass spectra were used strictly in a qualitative manner for this study.

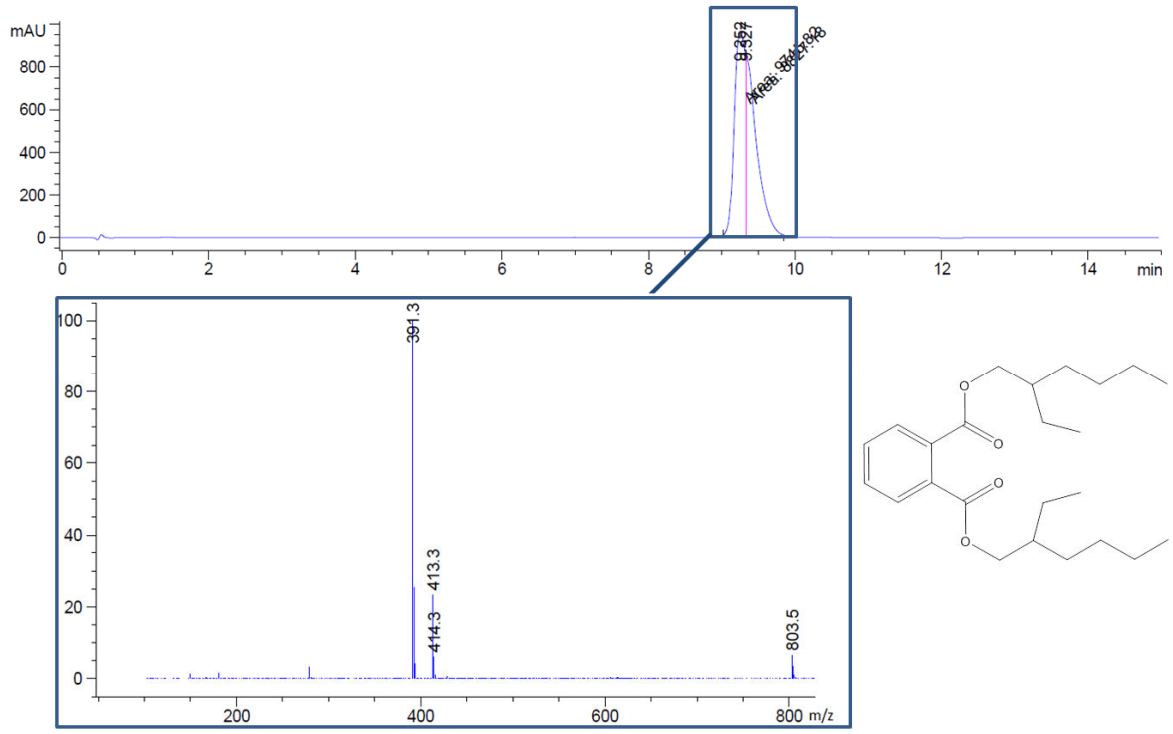

Figure 3.9. Top: HPLC chromatogram of pure DEHP. Bottom: corresponding mass spectrum of the peak at 9.4 min in the chromatogram.

Using the bulk data obtained of the plastic films (HPLC/MS and FTIR), we can surmise a simplified multi-step reaction scheme for DEHP degradation under short wave UV conditions that yields several different kinds of stable molecular products before complete degradation to CO_2 and water (Figure 3.10). The details in this reaction scheme will be elaborated upon in the next section of this thesis once surface data from time of flight secondary ion mass spectrometry (ToF-SIMS) of plasticized PVC films after UV/radical reactions is analyzed.

The following is a general description of the reaction of DEHP molecules in plastic under short wave UV light under normal room temperature conditions. The high energy 254 nm UV light generates more radicals in air than 365 nm, including ozone and OH radicals which contribute towards the major reactions of DEHP. Absorption of photons of light and attack by OH radicals lead to the removal of one chain "leg" at a time to form monoesters. Under dry

conditions, this could yield phthalaldehyde or phthalic anhydrides. However, under atmospheric conditions, it is much more likely that hydrates (i.e. phthalic acid) are formed. The molecules formed in these first steps are relatively stable, as evidence for the existence of partially degraded DEHP was found with both FTIR and HPLC/MS.

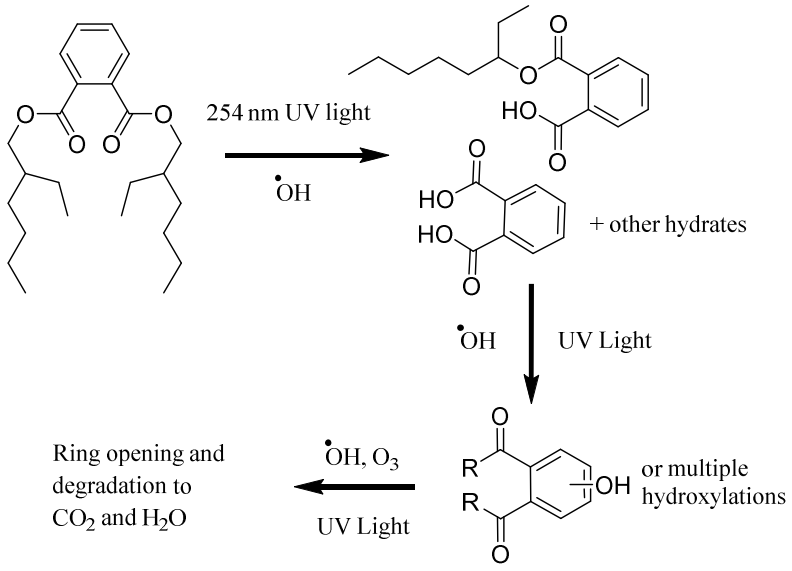

Figure 3.10. Simplified reaction scheme for DEHP degradation under 254 nm UV light.

The generated OH radicals could attack the phenyl ring, and lead to such hydroxylation products as observed with HPLC/MS. It is likely that hydroxylation occurred at all steps in the reaction process, although the evidence for such hydroxylation events will not be given until later. Further reactions with OH radicals and ozone would lead to phenyl ring opening and degradation to CO_2 and water. While some of the complete degradation occurred, as evidenced by decreased FTIR signals over both C=O and C-H regions of spectra, it appears as though many molecules remained only partially degraded after 5h of exposure. Under normal atmospheric conditions, the formation of gas-phase ozone molecules would be highly favored over the formation of hydroxyl radicals. Therefore, it is somewhat surprising that many partially

degraded molecules with relatively intact phenyl rings were observed with bulk techniques. It is possible that many ozone reactions did occur compared to hydroxyl radical reactions but the products of ozonolysis are much more difficult to observe with the applied techniques. Extensive radical chemistry studies must be performed to concretely answer this question.

If we then combine data analysis from HPLC/MS and FTIR and from SFG, we can confirm that the disappearance of CH_3 signals on the surface of samples was not only due to molecular rearrangement, but chemical reactions as well, since we can infer that some or all of the products found in the bulk were present on the surface of the plastic. Additionally, the formation of phthalic acid may also explain the disappearance of CH_3 surface signals. Fewer CH_3 groups would be present on the surfaces of the plasticized PVC film after the removal of CH alkyl chains at the aromatic ester bond. The new reaction products likely also aided to increase the hydrophilicity of the plastic surfaces, which further substantiate the contact angle data.

3.3.2.5 GPC of Pure PVC

Lastly, gel permeation chromatography (GPC) was utilized to determine if major crosslinking or scission occurred to the bulk of the pure PVC from either short or long wave UV exposure. The GPC chromatograms can be found in Figure 3.11. The following description aids in interpreting the peak changes in the chromatograms: an increase in elution time after UV treatment indicates that the molecular weight of the polymer decreased, suggesting chain scission occurred. In turn, shorter elution times indicate an increase in molecular weight, and are evidence for bulk PVC crosslinking.

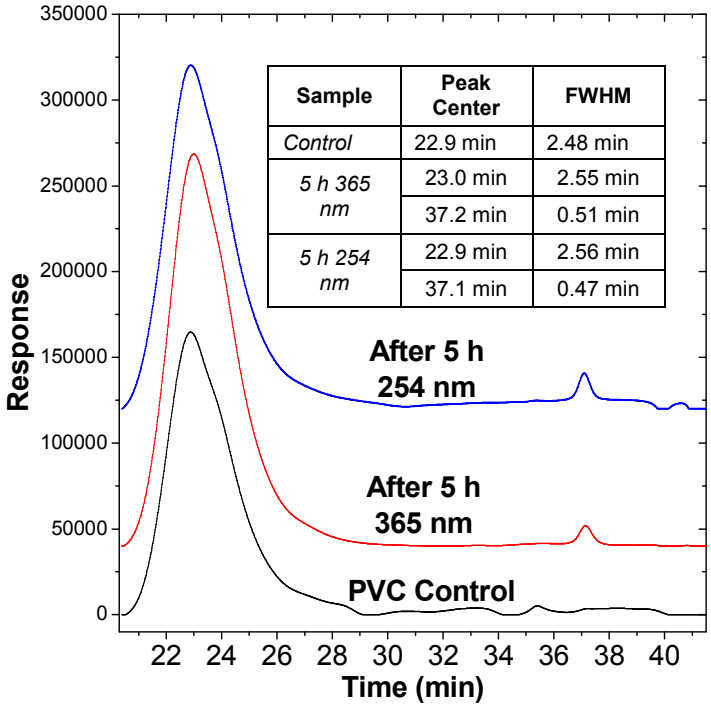

Figure 3.11. GPC chromatograms of pure PVC (black line), PVC after 5h exposure to long wave UV (red line) and PVC after 5h exposure to short wave UV (blue line).

After fitting the GPC peaks, it can be observed that pure PVC with no exposure to UV gives a large peak with peak maximum at 22.9 min. The full width at half maximum (FWHM) of this peak is at 2.48 min. Once the PVC has been exposure to 5h of long wave UV, the major PVC peak elutes at 23.0 min, which is not a significant difference in elution time. The FWHM max of this peak is slightly larger, at 2.55 min. From this information we can deduce long wave UV does not appear to cause major changes to the integrity of the pure polymer. The observed small change in peak center is not significant for a decrease in molecular weight and therefore this is not direct evidence of chain scission. However, there is formation of a new peak at 37.2 min after long wave UV which confirms that some chemical reactions did occur. This smaller peak may have been the result of either minor amounts of scission yielding small sections of chains, or recombination of small molecular weight PVC found in the mixture (possible evidence

of these smaller chains is found in the very small peaks around 35 min of pure PVC before UV exposure).

Likewise, after exposure to 5h of short wave UV, we can see the formation of a small peak eluting at 37.1 min, once again evidence of the formation of smaller molecular weight molecules. The major PVC peak elutes at a similar time as the pure PVC control (22.9 min) with a FWHM at 2.56 min. The slight increase in FWHM from 2.48 min may suggest a small amount of either chain scission or crosslinking occurred, leaving a slightly larger distribution of molecular weights.

In summary, the GPC data suggest the majority of PVC did not undergo major changes in molecular weight after UV exposure, e.g., major destruction of chains or the formation of ultra-high weight polymer did not occur. It is interesting that the surface vibrational spectral results demonstrated almost complete disappearance of CH_3 signals after exposure to short wave UV and decreases in CH_3 signal intensity after exposure to long wave UV. Collectively this suggests that either the presence of oxygen had a large influence on molecular group surface ordering (deposition of oxygen moieties induced CH_3 group disorder), or that a minor amount of PVC chain crosslinking occurred on the surface of films exposed to short wave UV which could not be detected using GPC.

By using analytical instruments HPLC/MS, FTIR, and GPC, we were able to better understand what major changes occur to phthalate plasticized PVC thin films from different UV exposures. In turn, surface techniques SFG and CA data yielded important information on what molecular changes occurred to the surface of these plastics. Finally, combining information from bulk and surface techniques allowed us to hypothesize what molecular products were formed on both the surface and throughout the majority of the plastic.

3.4 Conclusions

Several different analytical techniques were applied to determine the molecular changes on both the surface and the bulk of phthalate plasticized PVC from UV light exposure. We found that the addition of DEHP plasticizer to PVC increased molecular changes on the surface and throughout the plastic when exposed to short wave UV, with greater increase in surface hydrophilicity, the removal of surface CH_3 groups, and the formation of several DEHP-related products including phthalic acid and phthalic monoesters. In contrast, the addition of DEHP under long wave UV exposure resulted in reduced molecular breakdown, with no substantial changes on the surface or throughout the bulk of the film, excluding a minor increase in surface hydrophilicity.

From a more practical aspect, the results found in this Chapter illustrate that many phthalate plasticized PVC materials exposed to short wave UV light for cleaning, industrial, or experimental purposes, will eventually yield surfaces containing different molecules than pure plastic and plasticizer, even if UV absorbers have been added. While our models utilized for these experiments are extremely simple with no UV absorbers or fillers, similar reactions will occur to fully processed plastics, albeit at a much slower rate. As many PVC plastics are used for decades, it is highly likely that the surfaces (and in some cases involving clear or low density materials, the bulk) of these plastics undergo such reaction processes. In addition, the molecular degradation of the plastic is enhanced if phthalate plasticizers are present, yielding smaller toxic molecules available for contact before complete carbonization of the plasticizer. However, the addition of phthalates may be beneficial in protecting PVC films exposed to longer wavelengths of UV, as the molecules help protect the integrity of both the surface and bulk of the plastic. Our experimental results are especially relevant for understanding what molecular changes occur to

phthalate plasticized PVC materials left out in the environment exposed to sunlight for long periods of time, even before we can observe physical microscopic or macroscopic changes to the plastics such as yellowing, major loss of elasticity, and crack formation. In such cases we believe similar reaction products to those we found from short wave UV exposure will likely form in the bulk and surface of the plastic over a span of months to years, leaving living organisms susceptible to contact with phthalic acid, phthalate monoesters, and other phthalate-related products which are still toxic to different life forms.

3.5 References

1. Wypych, G. *Handbook of Plasticizers*; Chemtech Publishing: Toronto, 2004.
2. Koch, H. M.; Calafat, A. M. *Philos. Trans. R. Soc. Lond., Ser. B: Biol. Sci.* **2009**, *364*, 2063.
3. Halden, R. U. *Annu. Rev. Public Health* **2010**, *31*, 179.
4. Wilkes, C. E.; Summers, J. W.; Daniels, C. A.; Bernard, M. T. *PVC Handbook*; Hanser Gardner Publications Inc.: Cincinnati, OH, 2005.
5. Jaeger, R. J.; Rubin, R. J. *Lancet* **1970**, *2*, 35.
6. Hauser, R.; Meeker, J. D.; Singh, N. P.; Silva, M. J.; Ryan, L.; Duty, S.; Calafat, A. M. *Hum. Reprod.* **2007**, *22*, 688.
7. Ferguson, K. K.; Loch-Caruso, R.; Meeker, J. D. *Environ. Sci. Technol.* **2012**, *46*, 477.
8. Meeker, J. D. *Arch. Pediatr. Adolesc. Med.* **2012**, *166*, 952.
9. Sathyanarayana, S.; Karr, C. J.; Lozano, P.; Brown, E.; Calafat, A. M.; Liu, F.; Swan, S. H. *Pediatrics* **2008**, *121*, E260.
10. Oehlmann, J.; Schulte-Oehlmann, U.; Kloas, W.; Jagnytsch, O.; Lutz, I.; Kusk, K. O.; Wollenberger, L.; Santos, E. M.; Paull, G. C.; Van Look, K. J. W.; Tyler, C. R. *Philos. Trans. R. Soc. Lond., Ser. B: Biol. Sci.* **2009**, *364*, 2047.
11. Doyle, T. J.; Bowman, J. L.; Windell, V. L.; McLean, D. J.; Kim, K. H. *Biol. Reprod.* **2013**, *88,* 112.
12. Staples, C. A.; Peterson, D. R.; Parkerton, T. F.; Adams, W. J. *Chemosphere* **1997**, *35*, 667.
13. Gibb, W. H.; Maccallu.Jr *Eur. Polym. J.* **1971**, *7*, 1231.
14. Decker, C. *Eur. Polym. J.* **1984**, *20*, 149.
15. Chung, Y. C.; Chen, C. Y. *Water Air Soil Poll.* **2009**, *200*, 191.
16. Chen, C. Y. *Water Air Soil Poll.* **2010**, *209*, 411.
17. Xu, B.; Gao, N. Y.; Cheng, H.; Xia, S. J.; Rui, M.; Zhao, D. D. *J. Hazard. Mater.* **2009**, *162*, 954.
18. Al-Dossary, A. K.; Gilbert, M.; Hitt, D. *Adv. Mat. Res.* **2010**, *83-86*, 923.
19. Hollande, S.; Laurent, J. L. *Polym. Degrad. Stab.* **1997**, *55*, 141.
20. Nepotchatykh, O. V.; Power, J. F. *Polym. Eng. Sci.* **2000**, *40*, 1747.
21. Power, J. F.; Nepotchatykh, O. V.; Fu, S. W. *Appl. Spectrosc.* **2000**, *54*, 1782.
22. Torikai, A.; Hasegawa, H. *Polym. Degrad. Stab.* **1999**, *63*, 441.
23. Cho, S. M.; Choi, W. Y. *J. Photochem. Photobiol. A: Chem.* **2001**, *143*, 221.
24. Balandier, M.; Decker, C. *Eur. Polym. J.* **1978**, *14*, 995.
25. Skowronski, T. A.; Rabek, J. F.; Ranby, B. *Polym. Photochem.* **1984**, *5*, 77.
26. Kaczmarek, H.; Galka, P.; Wrzyszczynski, A.; Olszewski, K.; Janota, H. *Polimery* **2009**, *54*, 202.
27. Park, C. G.; Kim, J. C. *Desalin. Water Treat.* **2012**, *47*, 163.
28. Zhao, X.-K.; Yang, G.-P.; Wang, Y.-J.; Gao, X.-C. *J. Photochem. Photobiol. A: Chem.* **2004**, *161*, 215.
29. Ding, X.; An, T.; Li, G.; Chen, J.; Sheng, G.; Fu, J.; Zhao, J. *Res. Chem. Intermed.* **2008**, *34*, 67.
30. Hizal, G.; Zhu, Q. Q.; Fischer, C. H.; Majima, T.; Schnabel, W. *J. Photochem. Photobiol. A: Chem.* **1992**, *69*, 33.
31. Denizligil, S.; Schnabel, W. *Angew. Makromol. Chem.* **1995**, *229*, 73.

32. Balabanovich, A. I.; Denizligil, S.; Schnabel, W. *J. Vinyl Addit. Techn.* **1997**, *3*, 42.
33. Ito, R.; Seshimo, F.; Haishima, Y.; Hasegawa, C.; Isama, K.; Yagami, T.; Nakahashi, K.; Yamazaki, H.; Inoue, K.; Yoshimura, Y.; Saito, K.; Tsuchiya, T.; Nakazawa, H. *Int. J. Pharm.* **2005**, *303*, 104.
34. Hankett, J. M.; Zhang, C.; Chen, Z. *Langmuir* **2012**, *28*, 4654.
35. Hankett, J. M.; Liu, Y. W.; Zhang, X. X.; Zhang, C.; Chen, Z. *J. Polym. Sci., Part B: Polym. Phys.* **2013**, *51*, 311.
36. Zhang, C.; Myers, J. N.; Chen, Z. *Soft Matter* **2013**, *9*, 4738.
37. Ye, H. K.; Gu, Z. Y.; Gracias, D. H. *Langmuir* **2006**, *22*, 1863.
38. Aliaga, C.; Park, J. Y.; Yamada, Y.; Lee, H. S.; Tsung, C.; Yang, P.; Somorjai, G. A. *J. Phys. Chem. C.* **2009**, *113*, 6150.
39. Miyamae, T.; Nozoye, H. *J. Photochem. Photobiol. A: Chem.* **2001**, *145*, 93.
40. Liu, H. J.; Tong, Y. J.; Kuwata, N.; Osawa, M.; Kawamura, J.; Ye, S. *J. Phys. Chem. C.* **2009**, *113*, 20531.
41. Ye, S.; Osawa, M. *Chem. Lett.* **2009**, *38*, 386.
42. Ye, S.; Liu, G.; Li, H.; Chen, F.; Wang, X. *Langmuir* **2012**, *28*, 1374.
43. Ye, S. J.; Majumdar, P.; Chisholm, B.; Stafslien, S.; Chen, Z. *Langmuir* **2010**, *26*, 16455.
44. Li, Q.; Hua, R.; Chou, K. C. *J. Phys. Chem. B* **2008**, *112*, 2315.
45. Li, Q. F.; Hua, R.; Cheah, I. J.; Chou, K. C. *J. Phys. Chem. B* **2008**, *112*, 694.
46. Shen, Y. R. *The Principles of Nonlinear Optics*; Wiley: New York, 1984.
47. Shen, Y. R. *Nature* **1989**, *337*, 519.
48. Wang, J.; Chen, C.; Buck, S. M.; Chen, Z. *J. Phys. Chem. B* **2001**, *105*, 12118.
49. Chen, Z.; Shen, Y. R.; Somorjai, G. A. *Annu. Rev. Phys. Chem.* **2002**, *53*, 437.
50. Zhang, X. X.; Zhang, C.; Hankett, J. M.; Chen, Z. *Langmuir* **2013**, *29*, 4008.
51. Krimm, S.; Shipman, J. J.; Folt, V. L.; Berens, A. R. *J. Polym. Sci. Part A* **1963**, *1*, 2621.
52. Enomoto, S.; Asahina, M. *J. Polym. Sci. Part A* **1966**, *4*, 1373.
53. Ishiaku, U. S.; Ishak, Z. A. M.; Ismail, H.; Nasir, M. *Polym. Int.* **1996**, *41*, 327.

CHAPTER 4

ANALYZING THE MOLECULAR LEVEL EFFECTS OF SHORT WAVE UV LIGHT TREATMENTS DESIGNED TO DEGRADE PHTHALATES IN PLASTICIZED PVC

4.1 Background and Motivation

The previous Chapters focused more on understanding how phthalates and plastic structures change from various chemical stimuli. First, the effect of heat on the surface structures of PVC plastics was analyzed. Molecular-level surface changes caused by air plasma, intended to reduce phthalate leaching, were deduced. Chemical changes throughout the plastic and on the surfaces of plastic due to exposure to long and short wave UV light were analyzed in depth. In this Chapter, I move on from understanding how stimuli may affect potential exposure to phthalates, phthalate-related degradation products, or PVC products, to testing new UV light-based prevention methods that we designed to reduce phthalate environmental exposure. Once again, surface techniques SFG and SIMS were used to study surface phthalate degradation, and select bulk techniques FTIR and UV-Vis revealed how PVC and phthalates degrade within the layers of a thin plastic. Results from this Chapter have been adapted with permission from: Hankett, J.M.; Welle, A.; Lahann, J.; Chen, Z. **"**Evaluating UV/H_2O_2 Exposure as a DEHP Degradation Treatment for Plasticized PVC" *J. App. Polym. Sci.* **2014**, *131,* 40649 (1-10), Publisher John Wiley and Sons, Copyright Wiley Periodicals, Inc. 2014.

Due to the impending environmental and health threats that DEHP poses, the removal of DEHP after plastic disposal from the polymer matrix is vital.[1-17] Surface DEHP molecules on the

plastic often end up in water supplies, air currents, and soils as the plasticizers slowly leach out from the bulk.[2,4,6,17-20] This is especially a concern where both the utilization of phthalates as plasticizers and mishandling of plastic waste are common, which can be the case in developing countries. In such places, plasticizer alternatives to phthalates and proper plastic disposal and/or recycling facilities may not be available. Unfortunately, there currently exists no energy and cost efficient means to degrade plasticizers from PVC waste products and eliminate or reduce the risk of DEHP exposure after the plastic has been disposed of. Thus, it is of utmost importance to generate a means to remove as much DEHP as possible after disposal to prevent environmental contamination in a safe and green manner.

The model treatment systems presented were developed for the intention of degrading phthalates throughout flexible clear PVC materials, which typically contain the highest weight percentage of phthalates of PVC products. This includes medical tubing waste, which can often contain more plasticizer by weight than plastic. The treatments may also be applied to the surfaces of very old PVC materials in the cases where most phthalates have already migrated to the surface layers of the plastic, and opaque thin film PVC products. The proposed degradation methods are deliberately designed to be simple, so that disposed of plastics can be simply placed in a designated area under short wave UV lamps before disposal or stockpiling for recycling.

When we previously studied exposure of PVC materials to short wave UV, we found that DEHP rapidly degraded on the surface of the plastic and in the bulk to form products including mono-ethylhexyl phthalate, phthalic acid, hydroxylation of phenyl rings and complete breakdown of DEHP.[21] From an environmental perspective, this demonstrates that plastics exposed to short wave UV over time will form surfaces containing phthalate related molecules. These results helped inspire the idea that if short wave UV is applied to plastics for a pre-

determined amount of time, it may be possible to remove phthalate molecules from the surface or bulk almost completely.

Additionally, previous studies have shown free DEHP molecules in aqueous systems can be effectively removed by treatment with UV light and hydroxyl radicals.[22-27] The addition of oxygen radicals in H_2O_2 was believed to increase the pseudo first order degradation kinetics of phthalates compared to just using UV light alone, resulting in faster bulk removal of dimethyl phthalate from water treatment systems.[22,27] Therefore, I decided to test the effectiveness of adding aqueous phase OH radicals to the UV reaction system in degrading phthalate molecules. The hope here was that a higher concentration of OH radicals to the system would lead to faster DEHP degradation. While using gas-phase OH radicals would likely lead to much faster reaction times (gas-phase kinetics versus aqueous phase), the addition of aqueous phase OH radicals was much simpler and less dangerous to the user. For an end application, adding a liquid to plastics under a UV light in a safe ventilated enclosure would be much preferred over having to use a gas cylinder, not to mention, much cheaper and easier to set up. As a result, we studied photochemical reaction processes in the presence of 35 wt% H_2O_2 as well as a UV light treatment. To the best of our knowledge, this is the first time that UV and UV/H_2O_2 exposures have been studied as phthalate degradation treatments for phthalates on and within plastics.

Therefore, the first goal of this Chapter was to evaluate the effectiveness of H_2O_2/UV systems on removing or reducing the amounts of phthalate molecules from both the surface and bulk of plastics in comparison to short wave UV exposure alone. The second goal was to deduce how hydroxide radicals that could be present in an aqueous environment may affect plastics exposed to UV in an environmental setting.

SFG was utilized to deduce molecular-level surface changes to plastics without damage or disturbance to the samples. Once again SFG experiments were performed before and after UV treatments. We used SFG data to specifically gain information on molecular surface group type and ordering changes. In turn, time-of-flight secondary ion mass spectrometry (ToF-SIMS) was used to determine what stable molecules were formed on plastic surfaces after treatments. Since SIMS data were obtained several days after UV treatment, we were able to determine that all products found using SIMS were stable and persist on the surface of the plastic. FTIR was utilized to obtain additional information on molecular bulk changes.

4.2 Experimental Methods

4.2.1 Materials

Poly(vinyl) chloride (Mw 62,000, Mn 35,000), Tetrahydrofuran (THF) ≥99.9% purity, concentrated sulfuric acid (reagent grade), and potassium dichromate were obtained from Sigma Aldrich (St. Louis, Mo). Bis(2-ethylhexyl) phthalate (analytical standard) was obtained from Fluka (St. Louis Mo).

4.2.2 Sample Preparation

4.2.2.1 General Sample Preparation

Fused silica windows (ESCO Products, Inc.) were used for SFG measurements and were cleaned with a concentrated sulfuric acid bath saturated with potassium dichromate overnight, rinsed with deionized water, and dried under nitrogen gas. Then the windows were exposed to a glow discharge air plasma for 4 min using a PE-50 series Plasma System (Plasma Etch, Inc.) prior to plastic sample preparation. For FTIR experiments, calcium fluoride windows (ESCO

Products, Inc.) were used instead of silica. Calcium fluoride windows were soaked in THF and then cleaned with a dilute Contrex soap solution, rinsed with Milli-Q deionized water, dried under nitrogen gas and lastly cleaned with glow discharge plasma. For SIMS experiments, clean silicon wafers (Wafer World Inc., 250-300 μm thickness, (100) orientation, prime grade) were cut into 10x15 mm pieces and dusted off with nitrogen gas prior to film deposition.

PVC pellets were dissolved in THF to prepare the plastic thin films. A 30:1 weight ratio of THF/PVC was used for all plastic films. DEHP was added by weight percent to PVC. Solutions were prepared using a vortex mixer (Vortex-Genie 2T, Scientific Industries Inc.) which mixed components until the contents were clear. A P-6000 spin coater (Speedline Technologies) was used to prepare all PVC-based films. Samples were spin coated at 3000 rpm for 30 s on silica windows, calcium fluoride windows, or silicon wafers, depending upon the application. Film thicknesses were around 200 nm for all SFG, FTIR, and SIMS samples.

4.2.2.2 UV Treatment for Spectral Analysis

Sample films were placed in a chemical hood sealed from outside light sources in air and exposed to either a 60 watt short wave UV (254 nm) lamp (Cole Palmer, Inc.) at about 30 cm from the film surface ($I = 53\ W/m^2$) or a 100 watt long wave UV (365 nm) lamp (Ted Pella, Inc.) at about 30 cm from the film surface ($I = 88\ W/m^2$) for 30, 60, 90, 300, or 480 min. SFG spectra were collected from PVC-based thin films deposited on fused silica as reference spectra in air before UV exposure. After UV exposure, SFG spectra were obtained again at the air interface. Films spin coated on Si substrates were first placed on plasma cleaned glass slides and then exposed to UV light as mentioned above for 5 or 8h prior to SIMS analysis. For samples undergoing UV treatment with H_2O_2, 35 wt% H_2O_2 was added by glass pipette to cover film

surfaces. After UV exposure and before spectral analysis, remaining H_2O_2 liquid was removed by glass pipette.

4.2.3 Instrumentation

4.2.3.1 SFG

As previously described, SFG has been widely applied to gain information on molecular level changes of polymers at interfaces including air, water, and other buried interfaces.[28-38] The details of SFG theory and experimental setup have been extensively outlined in the introduction Chapter of this thesis and can be found in previous publications as well.[31,39,40] The SFG experiments conducted for this study were taken using the ssp (s-polarized signal, s-polarized 532 nm input beam and p-polarized tunable frequency IR input beam) polarization combination. All SFG spectra were obtained at the same visible and IR beam powers. SFG spectra in this paper were obtained in the C-H stretching frequency region.

4.2.3.2 SIMS

Time-of-flight secondary ion mass spectrometry was performed on a TOF.SIMS 5 instrument (ION-TOF GmbH, Münster, Germany). The instrument is equipped with a reflectron type time-of-flight analyzer and a Bi cluster liquid metal ion source. Short primary ion pulses (<1 ns) of Bi_3^+ with an energy of 25 keV were applied, providing high mass resolution secondary ion spectra together with a spot size of ~5μm (bunched mode). Experiments were performed on 500×500 μm fields of view under static SIMS conditions by limiting the primary ion dose to 10^{11} ions/cm^2. No charge compensation was required for these experiments. The pressure in the sample compartment of the spectrometer was < 2×10^{-9} mbar. Spectra were calibrated on omnipresent C^-, CH^-, and CH_2^- peaks. SIMS experiments and analyses were graciously

performed by Dr. Alexander Welle at KIT in Germany. SIMS is a well established technique and has been widely used to study molecular surface changes of polymer networks.[41-45]

4.2.3.3 FTIR

A Nicolet 6700 FTIR spectrometer was used to analyze the vibrational molecular signatures of the bulk of plastic films before and after UV exposure. The FTIR sample stage and optics were purged with nitrogen gas prior to and during data collection. Signatures of pure PVC films were compared to FTIR PVC reference spectra to insure sample purity. Spectra were obtained of pure PVC and 25 wt% DEHP plastic PVC films spin coated on calcium fluoride windows from 400 cm^{-1} to 4000 cm^{-1} before UV exposure and after 1, 5, or 8h of short or long wave UV or UV/H_2O_2 treatment. The UV treatment for FTIR studies was performed in an identical manner to the treatment for SFG analysis. Spectra are shown between 1000 and 3600 cm^{-1} in the following figures. The presented spectra were corrected for atmospheric water interferences and baseline anomalies as well.

4.2.3.4 UV-Vis

UV-Vis spectra were obtained on a UV-1601PC UV-Vis Shimadzu Spectrophotometer. Thick films were generated by squirting ~1 mL of plastic solution into quartz cuvettes two times, and pouring excess solution out. The sample preparation for the plastic solutions were the same as stated previously except the weight ratio of THF:PVC was 10:1. The cuvettes were rinsed with ethanol and Milli-pore deionized water several times, dried with nitrogen gas, and then plasma cleaned for 3 min prior to film preparation. A clean quartz cuvette was used as a background for UV-Vis measurements. Again I would like to thank the members of the Gafni lab at the University of Michigan for allowing us use of and help with their UV-Vis instrument.

4.3 Results and Discussion

4.3.1 UV-Depth Penetration

Before examining the bulk of the results for this Chapter, it is very important to discuss the applicability of this UV-based treatment to various hypothetical PVC materials. As previously stated, this simple treatment is specifically geared towards degrading DEHP molecules in clear PVC materials, opaque thin film PVC products, and treating the surfaces of decades old PVC materials in which most phthalates have already migrated to the surface layers of the plastic. Many clear PVC plastics contain a large concentration of plasticizers by weight. This includes PVC tubing, medical tubing and bags (which are known to be made with >70 wt% phthalates), assorted PVC films, and PVC utilized for packaging materials. Due to the limits of UV depth penetration, short wave UV cannot be used on all PVC materials to degrade phthalates throughout the plastic after disposal.

While determining the exact penetration depth of short wave UV into different types of plastics is beyond the scope of this study, we utilized UV-Vis to determine if 254 nm UV could penetrate the bulk of a thicker film. The UV-Vis setup used requires that the UV pass through the entirety of the cuvette to reach the detector so a 25 wt% DEHP loaded PVC plastic coated 20-30 μm thick on all sides of a quartz cuvette was effectively acting as a 40-60 μm thick film. As shown in Figure 4.1, this thick film absorbs only about 0.23 absorbance units at 254 nm. This indicates that UV light still penetrates through both layers of plastic at roughly 59% transmission. It may be reasonable to apply this technique, therefore, to both sides of clear thin PVC plastics to remove bulk phthalates, or to the surfaces of old PVC plastics.

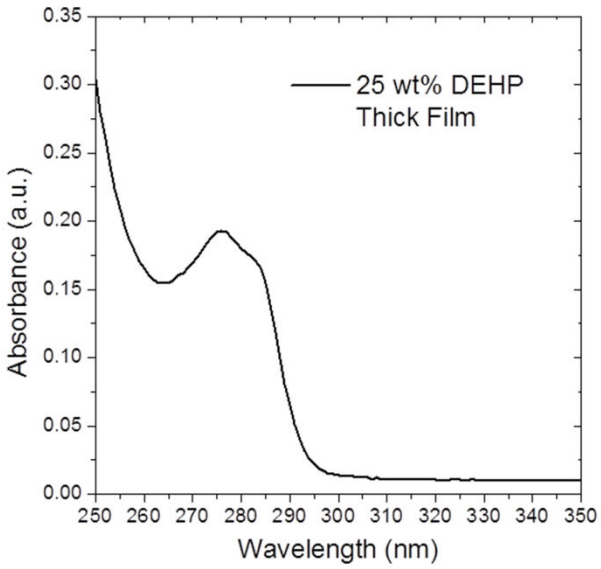

Figure 4.1. UV-Vis spectra near 254 nm of a thick film (40-60 µm total thickness) of PVC with 25 wt% DEHP.

4.3.2 SFG and SIMS Results on Short Wave UV Treated Materials

4.3.2.1 SFG Analysis of 25 wt% DEHP

Because the surface of PVC with 25 wt% DEHP before UV/H_2O_2 exposure has been characterized in depth in previous chapters, the spectrum will only be described here very briefly.[22,34] Two dominant peaks at 2880 and 2945 cm^{-1} correspond to the CH_3(s) and Fermi resonance of the DEHP molecule, whereas a smaller shoulder at 2915 cm^{-1} corresponds to the CH_2(s) stretch of PVC (Figure 4.2). The larger signal of DEHP compared to PVC indicates that DEHP molecules dominate the plastic surface.

After 30 min of exposure to short wave UV/H_2O_2, there is an increase in the SFG CH_2(s)/CH_3(s) peak intensity ratio (left panel, Figure 4.2). From the discussion in the previous Chapter studying UV-induced reactions of plasticized PVC films in air, we were able to associate this change in peak ratio with DEHP surface reactions.[22] Interestingly, in Chapter 3, it was after 1h exposure to short wave UV without H_2O_2 that this peak ratio change was observed

for 25 wt% DEHP. Here, with the only change being the addition of H_2O_2, the surface molecular changes are evident much faster at 30 min. This is indicative at first glance that the surface reactions may occur faster with the addition of hydroxyl radicals.

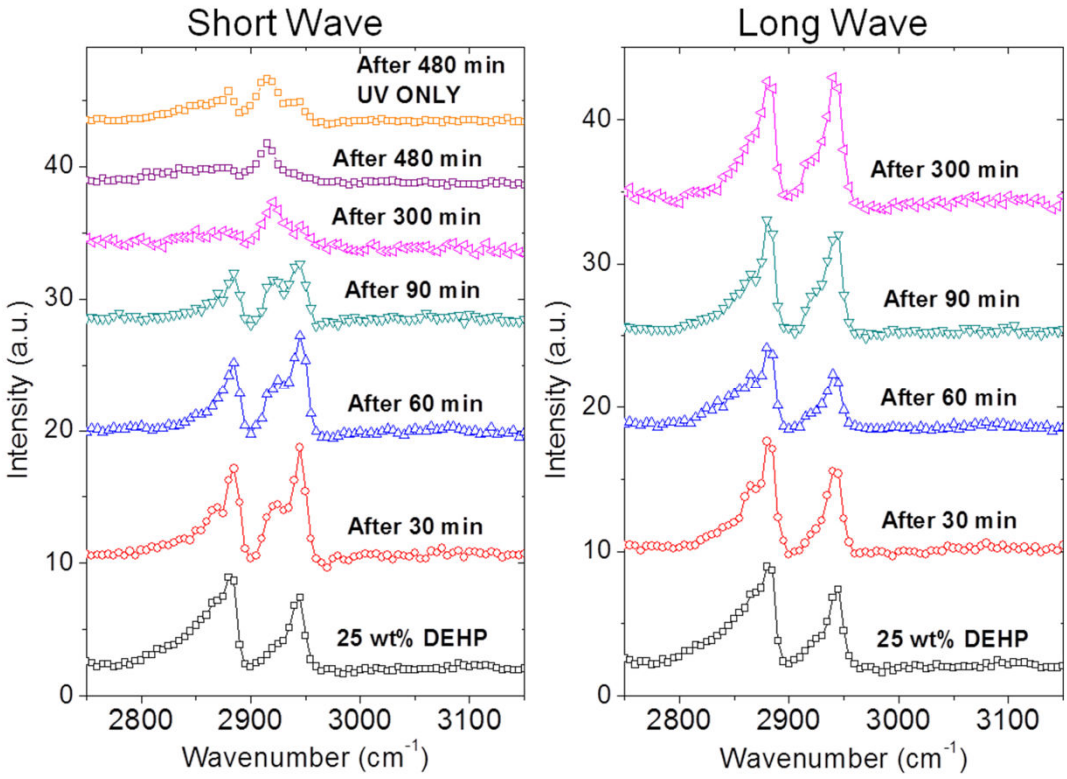

Figure 4.2. Left panel: SFG ssp spectra collected from plasticized PVC with 25 wt% DEHP before and after 30, 60, 90, 300, or 480 min of short wave UV exposure with H_2O_2 and after 480 min of short wave treatment with no H_2O_2. Right panel: SFG spectra of plasticized PVC with 25 wt% DEHP before and after 30, 60, 90, or 300 min long wave UV exposure with H_2O_2.

This CH_2(s)/CH_3(s) signal ratio change continues as the intensity of the CH_3(s) peak decreases more and more up to 5h of treatment, where the only peak distinguishable is the CH_2(s) peak (Figure 4.2), which indicates the CH_2 groups from PVC remain ordered on the plastic surface. The SFG data suggests after 5h of treatment, almost all DEHP molecules have either been removed or converted to different molecules. Unlike the spectrum taken after 5h of

short wave UV exposure in the previous Chapter (with no H_2O_2 added), there is no small 2880 cm^{-1} peak of CH_3(s) still clearly visible.[22]

After 8h of short wave UV/H_2O_2 treatment, only the CH_2(s) signal remains resolvable, indicating almost all CH_3 groups are disordered or have been removed. This is quite different than the surface of the plastic after 8h of short wave UV exposure only, where the CH_3 signals remain (Left panel, Figure 4.2). Recall from Chapter 3 that the surface of the plastic after 5h of short wave UV only yielded SFG surface signals dominantly from CH_2 groups. The increase in CH_3 signals after 8h of UV only may suggest that either the DEHP molecules have been reacted even further to yield small alkyl groups, or that the PVC surface itself is now beginning to undergo scission once a layer of DEHP molecules has been removed. However, this assumption cannot be made without further evidence, which will be discussed in the next section.

4.3.2.2 SIMS Analysis of 25 wt% DEHP

Since SFG results indicated that the surface removal and conversion of DEHP molecules may occur faster with the addition of H_2O_2 and may yield different surfaces after 5h and 8h of treatment, we obtained SIMS data after 5 or 8h of exposure to short wave UV only and compared these results to SIMS data obtained after short wave UV with the addition of 35wt% H_2O_2. SIMS data complements the molecular ordering data obtained by SFG by yielding information on the types of molecules that remained on surfaces after treatment, allowing us to identify molecular reaction products. A 25 wt% DEHP sample that was not exposed to reaction treatments was utilized as a control. The negative secondary ion spectrum of the control sample had a peak at 277.1 m/z, associated with a phthalic monoester, and attributed to the *in-situ* fragmentation of DEHP during the sputtering process initiated by the primary ion bombardment (Figure 4.3). A weaker signal found at 391.3 m/z, $[C_{24}H_{38}O_4+H]^-$, is from the parent DEHP

molecule. Although all samples were analyzed by applying a constant Bi_3^+ dose, the total secondary ion count rate in negative polarity is low in the case of the untreated sample compared to the UV treated samples. We believe this is mainly due to the introduction of oxygen by UV treatment, which would increase the ionization yield.

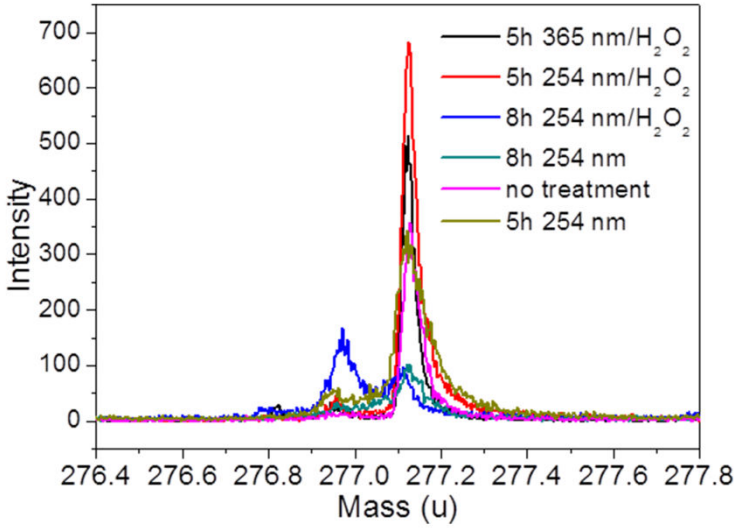

Figure 4.3. SIMS spectra of the phthalic monoester fragment before and after a variety of long or short wave UV treatments, with or without the addition of 35 wt% H_2O_2.

SIMS data obtained after 5h of exposure to short wave UV only revealed evidence of phthalic acid formation found at a 165.0 m/z, $[C_8H_5O_4]^-$, phenyl ring hydroxylation of phthalic acid at 181.0 m/z, the formation of a phthalate monoester at 277.1 m/z, hydroxylation of the monoester at 293.1 m/z, and hydroxylation of the parent molecule at 405.2 m/z (see Table 4.1). The evidence of phthalic acid formation and phenyl ring hydrogenation is consistent with results we previously found of molecules contained in the bulk after short wave UV exposure (Chapter 3, FTIR and HPLC/MS results). Now, however, there is additional evidence of multiple phenyl ring hydroxylation types.

Once the plastic was exposed to 5h of short wave UV and 35 wt% H_2O_2, large peaks at 165.0 m/z, 181.0 m/z, 277.1 and 405.2 m/z were found in SIMS spectra. The intensities of the

peaks associated with the monoester and hydroxylated parent molecule compared to the nontoxic molecules are larger than those observed after 5h of short wave UV exposure alone, indicating different reaction pathways.

After 8h of short wave UV exposure, peaks associated with phthalic acid at 165.0 m/z, hydroxylated phthalic acid at 181 m/z, and a hydroxylated phthalic monester at 293.1 m/z were apparent. The intensity of the peaks at 165.0 and 181.0 m/z were much larger in comparison to the intensity of the peak at 293.2 m/z collected on the same sample, indicating that a small percentage of the surface products were hydroxylated monoesters. The lack of signals at 391.3 and 405.2 m/z in turn suggest that most of the DEHP molecules present on the topmost surface layers were degraded to smaller molecules. Thus the surface contained very few molecules that are toxic to humans after treatment.

Table 4.1. Poisson corrected peak areas and total counts in neg. secondary ion mass spectra

Experimental Conditions	PVC with DEHP, Untreated	5h, Short UV	8h, Short UV	5h, Short UV with H_2O_2	8h, Short UV with H_2O_2
O [$\times 10^3$]	117	353	322	510	420
CCl, 47 m/z [$\times 10^3$]	28.0	15.4	36.4	24.7	27.5
$[C_8H_5O_4]^-$, 165 m/z [$\times 10^3$]	1.7	28.1	13.3	5.8	7.9
$[C_8H_5O_5]^-$ 181 m/z [$\times 10^3$]	n.d.	12.9	11.5	1.9	12.3
$[C_{16}H_{21}O_4]^-$ 277.1 m/z [$\times 10^3$]	6.1	8.6	2.4	16.2	2.1
$[C_{16}H_{21}O_5]^-$ 293.1 m/z [$\times 10^3$]	n.d.	4.3	2.4	1.6	n.d.
$[C_{24}H_{39}O_4]^-$ 391.3 m/z	500	n.d.	n.d.	900	n.d.
$[C_{24}H_{37}O_5]^-$ 405.2 m/z [$\times 10^3$]	n.d.	1.2	n.d.	11.0	n.d.
Total ions [$\times 10^6$]	7.5	15.3	16.0	14.2	25.3

The SIMS results after 8h of short wave UV exposure with 35 wt% H_2O_2 are similar to those obtained after 8h of pure UV. The intensities of the peaks at 165.0 and 181.0 m/z are still

quite large. However, the peak at 293.1 m/z is smaller than the sample after exposure to 8h of short wave UV only. These results indicate that there is still a small percentage of the hydroxylated monoester left on the surface (or possibly the hydroxylated parent before sputtering and fragmentation during secondary ion generation) but overall most of the surface DEHP molecules have been converted to smaller molecules.

At first glance, it may appear that the SIMS results after 5 or 8h of short wave treatment contradict the SFG results. For example, there are lower intensity SFG CH_3 peaks visible after 5h of UV/H_2O_2 treatment compared to short wave UV only[22], which tends to indicate that the addition of H_2O_2 has resulted in further reaction on the surface. However, SIMS results reveal there are actually more DEHP molecules on the UV/H_2O_2 treated surface than the UV treated surface. Similarly, there are lower intensity SFG CH_3 peaks for the UV/H_2O_2 treated surfaces after 8h compared to the UV treatment alone, but SIMS demonstrates that there are similar surface products after both 8h UV and UV/H_2O_2 treatments. What is key is that the assumption that the decrease in SFG CH_3 signals directly relate to DEHP content does not take into account the physical differences in UV treatment methods. With the addition of H_2O_2 in solution, two complications may result: the addition of liquid to the system may have increased the degree of disordering of hydrophobic groups on the surface, and/or the removal of the liquid by pipette prior to spectroscopic analysis may have aided in removing smaller aliphatic alkyl groups in water soluble degradation products.

Since SFG is sensitive to the ordering of the functional groups as well as the number of groups, it is most likely that the changes in SFG signals with UV/H_2O_2 treatment compared to UV treatment alone are due to increased surface disorder. It is likely that the few DEHP molecules and/or DEHP reaction products remaining on the surface after UV/H_2O_2 treatment

were disordered, giving lower or no CH_3(s) signals compared to treatment without the addition of liquid. With this in mind, the increase in the intensity of the CH_2 peak compared to CH_3 peaks observed after 30 min of UV/H_2O_2 exposure as discussed in the beginning of this section may arise from the different experimental conditions of UV/H_2O_2 treatment. Rather than an indication in increased reaction kinetics, the CH_2/CH_3 ratio change is more likely attributed to differing CH surface ordering.

The SIMS results indicate that the addition of hydroxyl radicals to the UV treatment for the purpose of additional DEHP removal is not immensely beneficial as there are no major differences in plastic surfaces after 8h of either treatment method. The SIMS results allow us to form a slightly more complex reaction scheme for the degradation of DEHP molecules at the air/film interface. Now we can confirm that the hydroxylation of the phenyl ring occurs at many steps in the degradation process and may occur multiple times on a single molecule for both reaction types, with or without H_2O_2. For the UV/H_2O_2 reactions, the DEHP molecules are expected to almost entirely cover the surface of the plastic, and therefore be readily available for reaction with OH radicals from H_2O_2. The increase in surface present OH radicals may compensate for the slower reaction kinetics in water compared to air, which could explain why the surfaces of films eventually contain similar reaction products after 8h of short wave UV treatment or UV/H_2O_2 treatment. The DEHP degradation process under UV/H_2O_2 conditions will be discussed in greater detail later in this chapter.

4.3.2.3 SFG Analysis of 10 wt% DEHP

Briefly, in order to make a direct comparison to the studies looking at the surface changes of plasticized PVC after short wave and long wave UV exposure only presented in the previous Chapter, we also obtained SFG data of PVC plasticized with a lower weight percentage of

DEHP, 10 wt% DEHP. In contrast to the dominating signals observed from DEHP in the 25 wt% sample, the intensities of the signals from DEHP and PVC in the 10 wt% sample are virtually the same, indicating that the surface contains both PVC and DEHP molecules (Figure 4.4). After 30 min of short wave/H_2O_2 treatment, the intensity of the CH_2(s) peak is larger than the CH_3 peaks, and by 5h, the only signal remaining is that of the CH_2(s) peak, showing that virtually all DEHP molecules have been converted to other molecules.

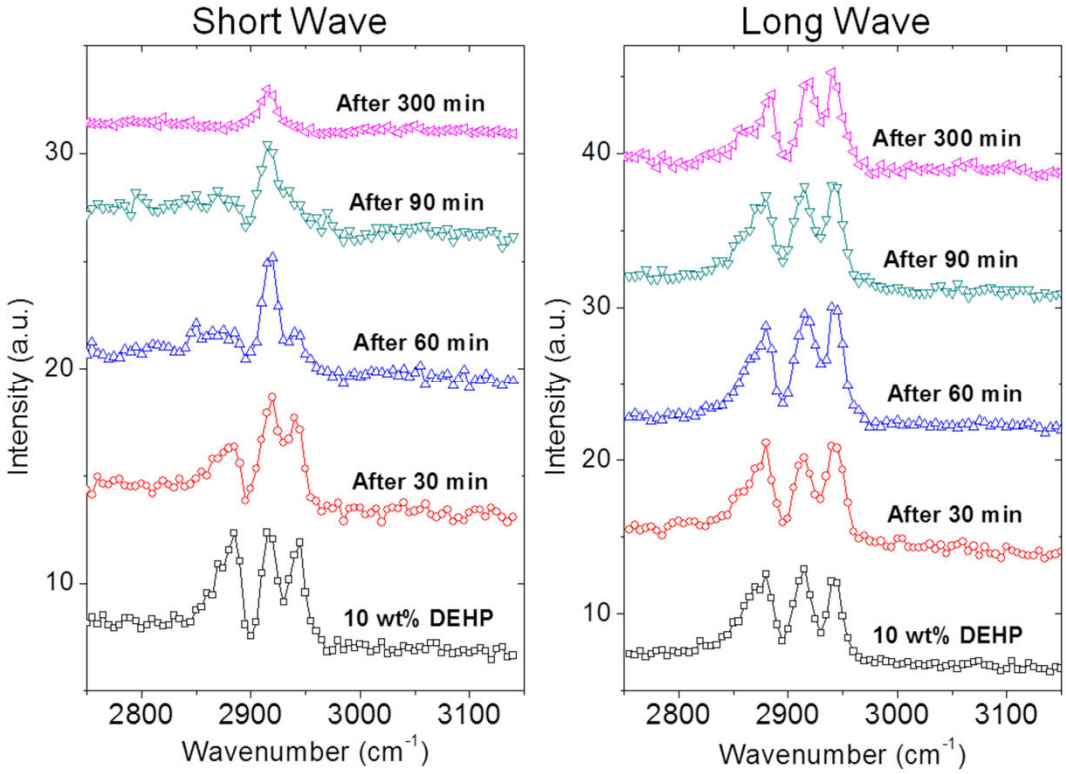

Figure 4.4. SFG ssp spectra collected from plasticized PVC with 10 wt% DEHP before and after 30 min, 60 min, 90 min, or 300 min of short (left panel) versus long (right panel) wave UV exposure with H_2O_2

The SFG spectra after 5h of treatment highly resembles the signal from pure PVC but without the peak from the CH_3(s) end group at 2880 cm^{-1} so it may be possible that the majority of the surface ordering observed is from PVC groups. Near complete removal or degradation of DEHP at this point would be expected. At this time, according to SFG and SIMS results in the

previous section, the 25 wt% DEHP samples contain few intact phthalate molecules and some smaller degraded ones. With a lower concentration of DEHP than 25 wt%, perhaps most of the DEHP reacted. In contrast, after 5h of long wave/H_2O_2 treatment, there are virtually no changes in the CH_2 to CH_3 ratio, similar to the spectra from the 25 wt% DEHP sample.

4.3.2.4 SFG Analysis of Neat PVC

SFG spectra were obtained before and after treatment to determine what surface molecular changes occurred to pure PVC due to short wave UV/ H_2O_2 treatment (Figure 4.5). After 60 min of exposure, the CH_3(s) peak decreases in intensity compared to the CH_2 peak. This trend continues after 1.5h of exposure. However, after 5h of exposure, the 2880 cm^{-1} peak reappears, and a peak near 2945 cm^{-1} appears as well. These two peaks are equal in intensity compared to that of the CH_2(s) peak. This indicates that now both CH_3 and CH_2 groups are ordered on the plastic surface. We may conclude that at first, susceptible CH_3 end groups are removed from the PVC surface by radical reactions. Then once all of the end groups are removed, the chains themselves undergo radical attack, resulting in scission, removal of chlorine, and double bond formation. With ozone present and readily formed under short wave UV conditions, these double bonds were likely attacked to form more CH_3 groups. In addition to the peak intensity changes, the 2915 cm^{-1} peak red-shifts after 30-90 min of short wave UV exposure. This peak shift is likely due to the differing chemical environments surrounding the CH_2(s) bond resulting from the aforementioned radical reactions, although the exact nature of the surrounding environment after different reaction times remains unknown.

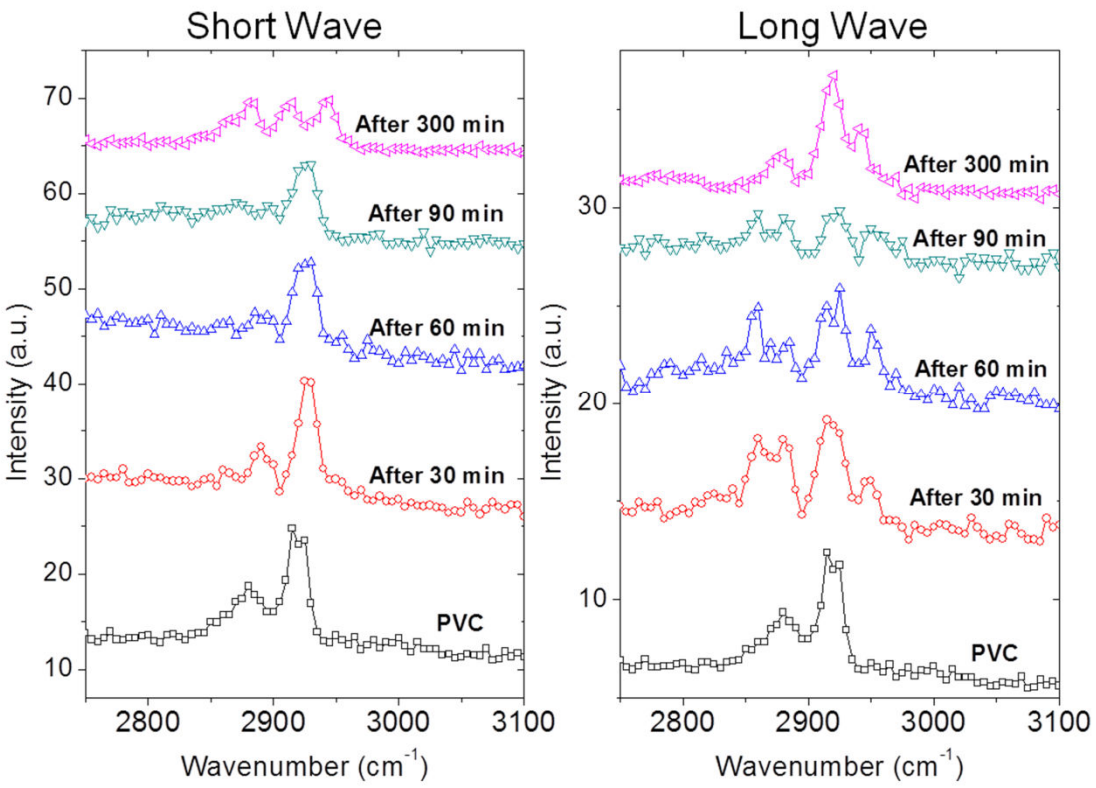

Figure 4.5. SFG ssp spectra collected from PVC before and after 30 min, 60 min, 90 min, or 300 min of short (left panel) versus long (right panel) wave UV exposure with H_2O_2.

4.3.3 SFG and SIMS Results on Long Wave Treated Materials

4.3.3.1 SFG Analysis of PVC and 25 wt% DEHP

To determine the surface molecular trends occurring from long wave UV/H_2O_2 treatment, SFG data was obtained before and after long wave UV/H_2O_2 exposure to 0 and 25 wt% DEHP films. Exposure to UV/H_2O_2 for 25 wt% DEHP films, even after 5h, did not induce any observable changes in the CH_2(s) to CH_3 ratios in SFG spectra (Figure 4.2), indicating that the molecular surface ordering of CH groups did not occur to any major extent.

Results from pure PVC exposure to long wave UV/H_2O_2, (Figure 4.5), demonstrate that there is likely a complex reaction process occurring at the PVC surface. After 30 minutes of treatment, increase in the intensity of the CH_3(s) peak, Fermi resonance, and a CH_2(as) peak at

2860 cm^{-1} is quite evident. Additionally, the C-H signal intensities overall decrease with increasing reaction time up to 90 min, indicative of increased C-H disorder across the plastic surface. After 5h, however, there is a dramatic increase in CH_2(s) in comparison to the intensity of the other CH region peaks.

The differences observed in SFG spectral trends for long wave UV/H_2O_2 treatment versus short wave treatment may be due to different equilibrium reactions between hydroxide radicals and ozone radicals. Unlike the environment under short wave UV exposure, the long wave system contained a much lower concentration of ozone in air. A change in the balance of radical reactions between ozone and hydroxyl radicals may have led to increased surface chain scission (hence the increase in intensity of the CH_3(s) peak) and chlorine removal, and eventually more double bond formation with the elimination of the chlorine atoms. The double bonds would not be as susceptible to further scission with less ozone present. Unfortunately, this theory is difficult to prove with our current evidence and it is unclear as to exactly why CH_3 peaks are dominant at the surface after shorter treatment times.

4.3.3.2 SIMS Analysis of 25 wt% DEHP

To determine what molecular products, if any, may have been formed on the surface of the plastics from long wave exposure, SIMS data was obtained after long wave UV exposure to 25 wt% DEHP films (See Table 4.2) and after long wave UV/ H_2O_2 exposure. SIMS results after 5h of exposure to long wave UV just have peaks at 277.1 m/z and 391.3 m/z, the phthalic monoester and parent molecule. The addition of hydrogen peroxide appears to make little difference in surface reactions, with major peaks at 277.1 and 391.3 m/z, and a very small signal at 181.0 m/z, the hydroxylated phthalic acid after 5h long wave UV/H_2O_2 treatment. The SFG and SIMS results both demonstrate that the addition of OH radicals to the long wave UV

treatment did not help induce major surface reactions on DEHP molecules. Thus we can determine that long wave UV should not be used for any DEHP-removal process and will do little to affect the surface of PVC films.

Table 4.2. Poisson corrected peak areas and total counts in neg. secondary ion mass spectra

Experimental Conditions	PVC with DEHP, untreated	5h, Long UV	5h, Long UV, with H_2O_2
O [$\times 10^3$]	117	122	426
CCl, 47 m/z [$\times 10^3$]	28.0	25.7	26.6
$[C_8H_5O_4]^-$, 165 m/z [$\times 10^3$]	1.7	1.6	2.7
$[C_8H_5O_5]^-$ 181 m/z [$\times 10^3$]	n.d.	n.d.	1.1
$[C_{16}H_{21}O_4]^-$ 277.1 m/z [$\times 10^3$]	6.1	6.0	7.2
$[C_{16}H_{21}O_5]^-$ 293.1 m/z [$\times 10^3$]	n.d.	n.d.	n.d.
$[C_{24}H_{39}O_4]^-$ 391.3 m/z	500	350	400
$[C_{24}H_{37}O_5]^-$ 405.2 m/z [$\times 10^3$]	n.d.	0.2	0.6
Total ions [$\times 10^6$]	7.5	14.2	14.4

4.3.4 Evidence for Bulk Reactions from UV Treatments

FTIR spectra were obtained before and after long or short wave UV/H_2O_2 exposure to pure PVC and 25 wt% DEHP (Figure 4.6 and Figure 4.7). PVC with 25 wt% DEHP films after short wave UV exposure with H_2O_2, similar to our previous results after short wave UV only (Chapter 3), contained dramatic spectral bulk changes across both C-H and C=O stretching frequency regions (Figure 4.6, top panel). We are able to obtain information about molecular structural changes of the plastic by closely studying peak ratio changes. Large decreases in signal intensities were observed at 1027 and 1127 cm^{-1} (contributed by the aromatic O-CH_2 group of DEHP), and 1280 cm^{-1} (conjugated aromatic ester COO group of DEHP). Additionally,

a decrease in intensity and broadening of the 1725 cm^{-1} C=O stretch suggests that not only did the number of C=O groups decrease but that the neighboring chemical environment around the C=O bond changed, similar to evidence found in the previous Chapter.

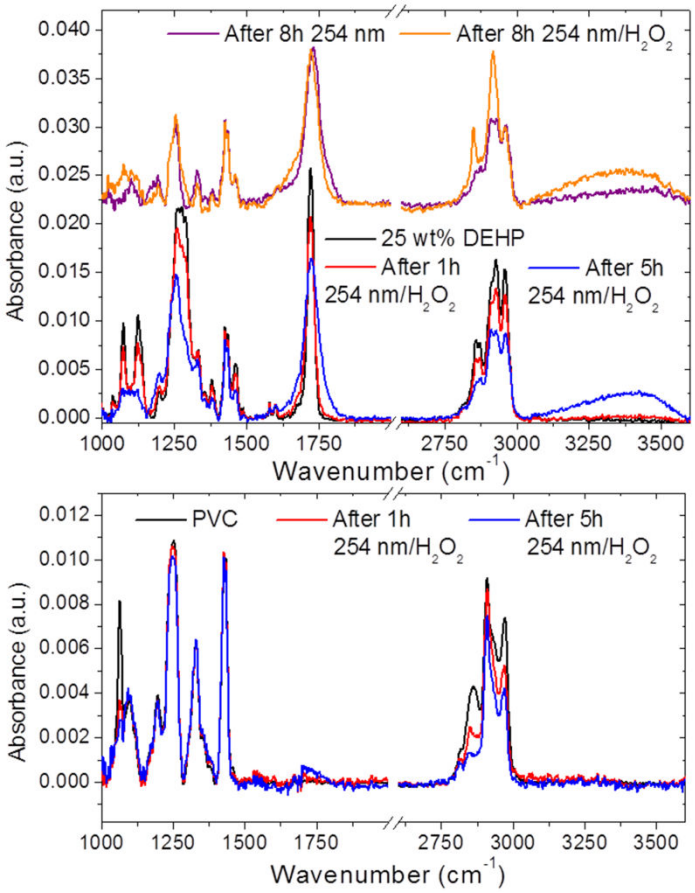

Figure 4.6. Top panel, top row: FTIR data of PVC with 25 wt% DEHP after 8h of short wave UV exposure (purple) and 8h short wave UV exposure with H_2O_2. Top panel, bottom row: PVC with 25 wt% DEHP before (black) and after 1h (red) and 5h (blue) UV exposure with H_2O_2. Bottom panel: FTIR data of PVC before (black) and after 1h (red) and 5h (blue) short wave UV exposure with H_2O_2.

Again, these spectral changes are indicative that the ester bond of DEHP was reacted to form smaller molecules. Likely formed molecules include phthalic acid, phthalic monoesters, and phthalate-related molecules with hydroxylated phenyl rings as observed with HPLC/MS in the previous Chapter and with SIMS here. Interestingly, the decrease in intensities in the C=O region of spectra in Figure 4.6 is not as dramatic as previously found with exposure to short

wave UV only. However, there are greater decreases in intensity across the C-H region of spectra, indicative of C-H bond elimination. Collectively this is evidence that more reactions may have occurred with PVC molecules over DEHP molecules.

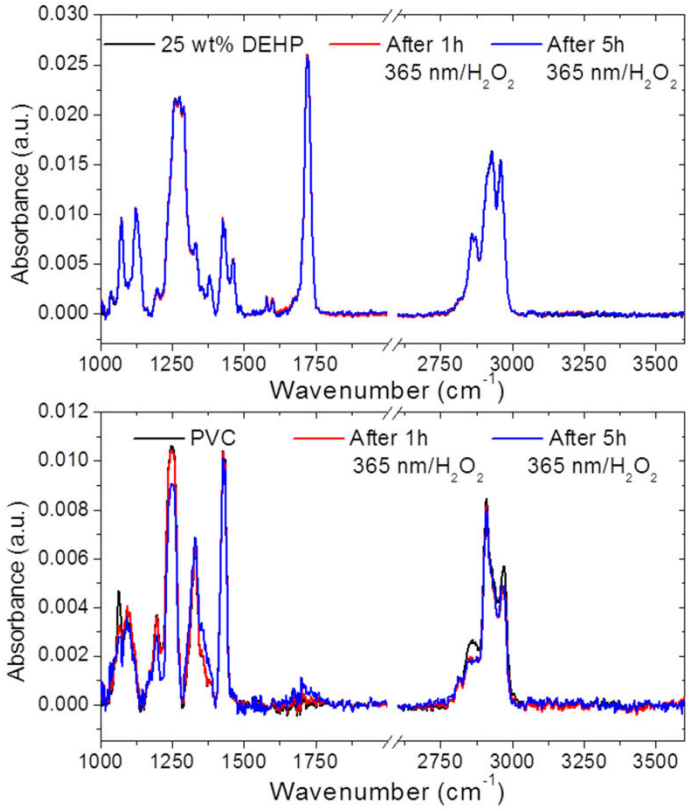

Figure 4.7. Top panel: FTIR data of PVC with 25 wt% DEHP before (black) and after 1h (red) and 5h (blue) long wave UV exposure with H_2O_2. Bottom panel: FTIR data of PVC before (black) and after 1h (red) and 5h (blue) long wave UV exposure with H_2O_2.

This suspicion was confirmed by studying the FTIR spectra of pure PVC before and after 1 or 5h short wave UV/H_2O_2 treatment. There is a major decrease in intensity of the C-H stretching frequency region signals which increases with longer treatment times from 1h to 5h. Decreases in signal intensity include both CH_2 and CH_3 groups at 2880 cm^{-1} (CH_3), 2860 cm^{-1} (CH_2), and 2845 cm^{-1} (CH_2(s)). These decreases in signal intensities for pure PVC are much larger than the signal decreases previously observed in Chapter 3. Thus, the addition of

hydroxide radicals to our treatment system demonstrated preferential radical reactions with PVC chains rather than DEHP molecules, leading to a larger amount of bulk polymer breakdown.

Lastly, FTIR data obtained after 8h of 25 wt% DEHP treatment reveal that exposure to short wave UV only results in almost complete removal of DEHP in the bulk (up to the FTIR detection limit) with no DEHP signals, whereas 8h short wave UV/H_2O_2 exposure does not result in elimination and DEHP FTIR signals remain. It is at this point that the pure UV reaction is still faster than UV/H_2O_2 and is successful in removing almost all DEHP molecules from the bulk (Figure 4.6, top panel). It is interesting that this means the surface and bulk reaction kinetics for DEHP degradation are different. Recall that at this point on the surface of the plastic, SIMS results reveal that the removal of DEHP via UV or UV/H_2O_2 is virtually the same.

We additionally obtained FTIR data to compare the bulk molecular changes for DEHP plasticized and pure PVC exposed to long wave UV/H_2O_2 compared to the surface changes. Pure PVC exposure to long wave UV treatment resulted in some C-H signal decreases, likely due to crosslinking, scission, or radical scavenging. Again, the decrease in signal intensity after long wave UV treatment was less dramatic than that after short wave UV treatment. Also there are virtually no changes in FTIR signal intensity when the DEHP was added to the PVC matrix, demonstrating that the molecules have a protecting effect on both the surface (from SFG data) and throughout the bulk (Figure 4.7). This is concrete evidence that the use of long wave UV is not effective for either surface or bulk DEHP removal in these plastics.

We can deduce from FTIR results that reaction processes for DEHP molecules in the bulk due to short wave UV/H_2O_2 exposure are similar to reaction processes induced from short wave UV exposure only, but are complicated by preferential hydroxyl and ozone radical reactions with PVC chains. Compiling information from all three analytical techniques, it is clear that the

addition of hydrogen peroxide was less effective in degrading DEHP molecules located within the plastic matrix than UV exposure alone, and was comparable at converting DEHP on the surface of the plastic. Using the data from Chapters 3 and 4, the following is a simplified reaction scheme for the degradation of DEHP in the short wave UV/H_2O_2 system (Figure 4.8).

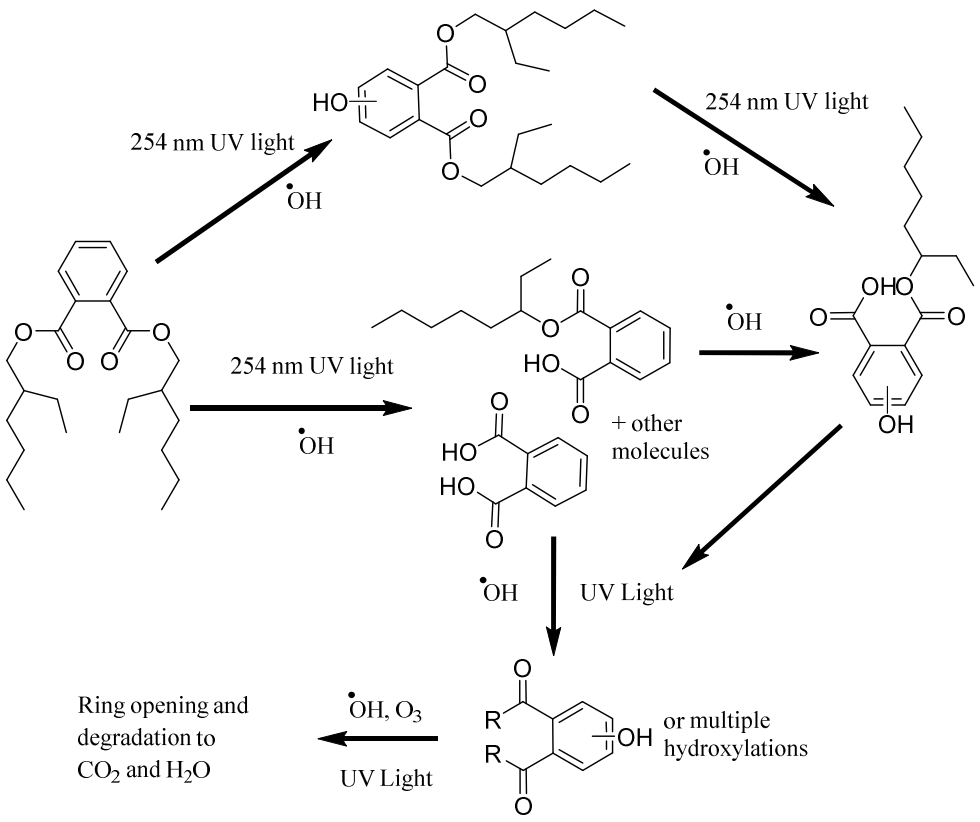

Figure 4.8. Simplified reaction scheme for DEHP degradation at 254 nm UV light with 35 wt% H_2O_2(aq).

Within the plastic, a competing reaction pathway with PVC and OH radicals results but the pathway is not shown here. Hydroxylation of the phenyl ring occurred at all steps of degradation. Major stable products include hydroxylated DEHP, and the formation of MEHP and hydroxylated MEHP. These products would give way to phthalic acid, hydroxylated phthalic acid, and other smaller molecules formed from the breaking of the CO ester bond of the

phthalate. The small alkyl legs of the molecule may have volatilized or been removed with the removal of the H_2O_2 liquid after treatment. The addition of O_3 in the system from the short wave UV would break open phenyl rings at a fast rate, with further radical attack leading to complete degradation of the plasticizer. A similar molecular degradation would likely result for phthalates in plastics exposed for long periods of time to short wave UV in aqueous environments with hydroxyl radicals as well.

Again, it is unclear of the rate of ozone reactions versus hydroxide reactions with DEHP, given that the concentration of OH to O radicals has changed with the addition of hydrogen peroxide compared to the UV only treatment. Evidence of products formed by phenyl ring ozone reactions were not widely observed with SIMS in either case. It is possible that many ozone reactions were quenched by reaction with PVC, that these smaller products readily left the PVC matrix by evaporation, or are simply difficult to observe with our analytical techniques. Thus a concrete description of how OH/O radical kinetics changed with the addition of aqueous H_2O_2 cannot be ascertained.

We can, however, hypothesize a few reasons as to why the bulk DEHP removal was less effective with a treatment involving the addition of hydrogen peroxide. The first reason is most obvious: these bulk reactions took place in aqueous media rather than air. The aqueous phase kinetics would therefore be much slower than gas phase in the bulk of the plastic, yielding slower initial OH radical reactions with DEHP. This can help explain why FTIR results show much more DEHP degradation at 5h for UV reactions in air, and only a small difference at 8h.

Second, the influx of water into the PVC system would swell the polymer matrix further than the plasticizers already had and increase the regions in which PVC chains are susceptible to radical attack. The behavior of water to act as a plasticizer has been previously demonstrated in

published polymer systems.[46,47] Perhaps the influx of radicals at new regions within the plastic helped lead to the preferential attack on the PVC chains rather than the DEHP molecules.

4.4 Conclusions

The molecular structural surface and bulk changes of plasticized PVC materials after UV/H_2O_2 exposure via UV lamps were studied using analytical techniques SFG, SIMS, and FTIR. The results are summarized as follows:

The addition of 35 wt% H_2O_2 to short wave UV exposure for the purpose of improving DEHP degradation was found to yield comparable phthalate-related products on plastic surfaces exposed to short wave UV only after 8h of treatment. Surface products formed from both treatments include phthalic acid, hydroxylated phthalic acid, MEHP, and hydroxylated MEHP. By 8h, most toxic surface molecules were eliminated using either treatment methods. Surface CH_3 groups were found to order to a lesser extent on samples exposed to short wave UV/H_2O_2 compared to short wave UV exposure alone. This change in surface structure was induced by the addition and removal of H_2O_2 aqueous solution during the reaction process which increased molecular disorder on the surface and likely also physically removed small alkyl reaction products, respectively.

In contrast to surface reactions, the short wave UV/H_2O_2 treatment was less effective in degrading DEHP molecules in the bulk of the plastic compared to short wave UV exposure only up to 8h of treatment. This was determined to have occurred due to preferential radical reactions with the PVC plastic. Lastly, for plastics exposed to long wave UV/H_2O_2 treatments, the addition of DEHP to PVC was found to protect the surface and bulk of the plastic from damage. Without DEHP, the polymer was susceptible to radical attack by OH radicals, resulting in increased CH_3 surface groups after exposure and minor chain scission in the bulk.

Results from this Chapter indicate that extended short wave UV exposure may be an effective means to degrade toxic DEHP and MEHP molecules after plastic disposal, and the addition of H_2O_2 to this treatment system is only beneficial if additional degradation of the polymer bulk of thin film plastics is desired. Therefore the H_2O_2/UV treatment may be best applied to plastics that cannot be recycled and will later be disposed in a landfill. Here, the minor polymer chain degradation can lead to increased degradation kinetics under landfill conditions, as hypothesized in many previous studies. In contrast, short wave UV exposure alone is the simpler and safer treatment, and may be appropriate for both plastics temporarily stored for recycling and regularly disposed plastics, by changing the exposure time as needed. It is worth mentioning that commercial UV absorbers are typically added to the plastic matrix during plastic processing for multiple types of PVC products. If this is the case, the treatment times indicated in this study are not directly applicable, and longer UV exposure times must be used to achieve the same amount of DEHP degradation.

4.5 References

1. Wilkes, C. E.; Summers, J. W.; Daniels, C. A.; Bernard, M. T. *PVC Handbook*; Hanser Gardner Publications Inc.: Cincinnati, OH, 2005.
2. Wang, X. L.; Lin, Q. X.; Wang, J.; Lu, X. G.; Wang, G. P. *Ecol. Eng.* **2013**, *51*, 10.
3. Hopewell, J.; Dvorak, R.; Kosior, E. *Philos. Trans. R. Soc. Lond., Ser. B: Biol. Sci.* **2009**, *364*, 2115.
4. Chen, C. W.; Chen, C. F.; Dong, C. D. *Soil. Sediment. Contam.* **2013**, *22*, 119.
5. Zhou, Y. C.; Yang, N.; Hu, S. Y. *Resour. Conserv. Recy.* **2013**, *73*, 33.
6. Staples, C. A.; Peterson, D. R.; Parkerton, T. F.; Adams, W. J. *Chemosphere* **1997**, *35*, 667.
7. Ferguson, K. K.; Loch-Caruso, R.; Meeker, J. D. *Environ. Sci. Technol.* **2012**, *46*, 477.
8. James-Todd, T.; Stahlhut, R.; Meeker, J. D.; Powell, S. G.; Hauser, R.; Huang, T. Y.; Rich-Edwards, J. *Environ. Health Perspect.* **2012**, *120*, 1307.
9. Hauser, R.; Meeker, J. D.; Singh, N. P.; Silva, M. J.; Ryan, L.; Duty, S.; Calafat, A. M. *Hum. Reprod.* **2007**, *22*, 688.
10. Meeker, J. D.; Calafat, A. M.; Hauser, R. *J. Androl.* **2009**, *30*, 287.
11. Rael, L. T.; Bar-Or, R.; Ambruso, D. R.; Mains, C. W.; Slone, D. S.; Craun, M. L.; Bar-Or, D. *Oxid. Med. Cell Longev.* **2009**, *2*, 166.
12. Halden, R. U. *Annu. Rev. Public Health* **2010**, *31*, 179.
13. Oehlmann, J.; Schulte-Oehlmann, U.; Kloas, W.; Jagnytsch, O.; Lutz, I.; Kusk, K. O.; Wollenberger, L.; Santos, E. M.; Paull, G. C.; Van Look, K. J. W.; Tyler, C. R. *Philos. Trans. R. Soc. Lond., Ser. B: Biol. Sci.* **2009**, *364*, 2047.
14. Doyle, T. J.; Bowman, J. L.; Windell, V. L.; McLean, D. J.; Kim, K. H. *Biol. Reprod.* **2013**, *88,* 112.
15. Kasahara, E.; Sato, E. F.; Miyoshi, M.; Konaka, R.; Hiramoto, K.; Sasaki, J.; Tokuda, M.; Nakano, Y.; Inoue, M. *Biochem. J.* **2002**, *365*, 849.
16. Tetz, L. M.; Cheng, A. A.; Korte, C. S.; Giese, R. W.; Wang, P. G.; Harris, C.; Meeker, J. D.; Loch-Caruso, R. *Toxicol. Appl. Pharmacol.* **2013**, *268*, 47.
17. Okamoto, Y.; Hayashi, T.; Toda, C.; Ueda, K.; Hashizume, K.; Itoh, K.; Nishikawa, J.; Nishihara, T.; Kojima, N. *Chemosphere* **2006**, *64*, 1785.
18. Zieminski, K. F.; Peppas, N. A. *J. Appl. Polym. Sci.* **1983**, *28*, 1751.
19. Colombani, J.; Herbette, G.; Rossi, C.; Joussot-Dubien, C.; Labed, V.; Gilardi, T. *J. Appl. Polym. Sci.* **2009**, *112*, 1372.
20. Lardjane, N.; Belhaneche-Bensemra, N. *J. Appl. Polym. Sci.* **2009**, *111*, 525.
21. Hankett, J. M.; Collin, W. R.; Chen, Z. *J. Phys. Chem. B* **2013**, *117*, 16336.
22. Xu, B.; Gao, N. Y.; Cheng, H.; Xia, S. J.; Rui, M.; Zhao, D. D. *J. Hazard. Mater.* **2009**, *162*, 954.
23. Chen, C. Y. *Water Air Soil Poll.* **2010**, *209*, 411.
24. Park, C. G.; Kim, J. C. *Desalin. Water Treat.* **2012**, *47*, 163.
25. Chung, Y. C.; Chen, C. Y. *Water Air Soil Poll.* **2009**, *200*, 191.
26. Zhao, X.-K.; Yang, G.-P.; Wang, Y.-J.; Gao, X.-C. *J. Photochem. Photobiol. A: Chem.* **2004**, *161*, 215.
27. Tawabini, B. S.; Al-Suwaiyan, M. S. *J. Environ. Eng. Sci.* **2004**, *3*, 289.
28. Gracias, D. H.; Chen, Z.; Shen, Y. R.; Somorjai, G. A. *Acc. Chem. Res.* **1999**, *32*, 930.
29. Zhang, C.; Myers, J. N.; Chen, Z. *Soft Matter* **2013**, *9*, 4738.

30. Ye, S.; Osawa, M. *Chem. Lett.* **2009**, *38*, 386.
31. Chen, Z.; Shen, Y. R.; Somorjai, G. A. *Annu. Rev. Phys. Chem.* **2002**, *53*, 437.
32. Hankett, J. M.; Liu, Y. W.; Zhang, X. X.; Zhang, C.; Chen, Z. *J. Polym. Sci. Part B: Polym. Phys.* **2013**, *51*, 311.
33. Hankett, J. M.; Zhang, C.; Chen, Z. *Langmuir* **2012**, *28*, 4654.
34. Ye, H. K.; Gu, Z. Y.; Gracias, D. H. *Langmuir* **2006**, *22*, 1863.
35. Aliaga, C.; Park, J. Y.; Yamada, Y.; Lee, H. S.; Tsung, C. K.; Yang, P. D.; Somorjai, G. A. *J. Phys. Chem. C.* **2009**, *113*, 6150.
36. Miyamae, T.; Nozoye, H. *J. Photochem. Photobiol. A: Chem.* **2001**, *145*, 93.
37. Li, Q.; Hua, R.; Chou, K. C. *J. Phys. Chem. B* **2008**, *112*, 2315.
38. Beaman, D. K.; Robertson, E. J.; Richmond, G. L. *Langmuir* **2012**, *28*, 14245.
39. Wang, J.; Chen, C.; Buck, S. M.; Chen, Z. *J. Phys. Chem. B* **2001**, *105*, 12118.
40. Shen, Y. R. *Nature* **1989**, *337*, 519.
41. Benninghoven, A. *Angew. Chem.* **1994**, *33*, 1023.
42. Mahoney, C. M. *Mass Spectrom. Rev.* **2010**, *29*, 247.
43. Schwarz, S. A.; Wilkens, B. J.; Pudenzi, M. A. A.; Rafailovich, M. H.; Sokolov, J.; Zhao, X.; Zhao, W.; Zheng, X.; Russell, T. P.; Jones, R. A. L. *Mol. Phys.* **1992**, *76*, 937.
44. Karim, A.; Slawecki, T. M.; Kumar, S. K.; Douglas, J. F.; Satija, S. K.; Han, C. C.; Russell, T. P.; Liu, Y.; Overney, R.; Sokolov, O.; Rafailovich, M. H. *Macromolecules* **1998**, *31*, 857.
45. Pauloehrl, T.; Welle, A.; Oehlenschlaeger, K. K.; Barner-Kowollik, C. *Chemical Science* **2013**, *4*, 3503.
46. Clarke, M. L.; Chen, C.; Wang, J.; Chen, Z. *Langmuir* **2006**, *22*, 8800.
47. Wang, J.; Woodcock, S. E.; Buck, S. M.; Chen, C. Y.; Chen, Z. *J. Am. Chem. Soc.* **2001**, *123*, 9470.

CHAPTER 5

SURFACE AND BURIED INTERFACE RESTRUCTURING OF PVC AND PLASTICIZED PVC IN WATER

5.1 Background and Motivation

Chapter 5 focuses on two major concepts: understanding how plasticized PVC surfaces change from water contact at a molecular level, and advancing a theoretical understanding of multiple interface SFG signal interferences from polymeric film systems. In these studies, several different kinds of PVC plastic were probed *in situ* before, during, and after water contact using SFG. An SFG method platform for studying the transfer of small molecules from surface to surface via liquid was developed in these studies as well. Dr. Xiaolin Lu from Southeast University was vital in furthering quantitative understanding of SFG signal interferences and determined Fresnel coefficient contributions under different experimental conditions for different interfaces, completed SFG fits for multiple interface signals and aided in data analysis. His collaboration on this project is greatly appreciated. Results from this Chapter are adapted from the following publication: Hankett, J.M.; Lu, X.; Liu, Y.; Seeley E.; Chen, Z. "Interfacial Molecular Restructuring of Plasticized Polymers in Water" *Phys. Chem. Chem. Phys.* **2014**, *16,* 20097-20106 with permission from the PCCP Owner Societies.

Here we focus on the concern of the instability of phthalates and potential leaching hazards from plastic to water at a molecular level. It has been well established that human produced plastic components profusely permeate natural ecosystems through many means,

including the leaching and transfer of plasticizers into liquids in the surrounding environment.[1-6] Phthalates are susceptible to leach from the entangled polymer chains due to their small size and the lack of covalent bonding to PVC. Over the plastic's lifetime, plasticized PVC may be exposed to air and water frequently. This means phthalate leaching into water may occur as the plastic is being used and after it is disposed. Therefore it is important to obtain a molecular-level understanding of the surface structures of phthalate plasticized PVC upon water contact. The analytical technique SFG is extremely well suited for this task. There are very few other analytical techniques suitable for studying the molecular behaviors of polymers at aqueous interfaces *in situ*. Cryogenic x-ray photoelectron spectroscopy (cryo-XPS) allows for polymer strands to be effectively frozen in place when in contact with an aqueous environment so that surface compositional changes may be observed.[7,8] This can be compared to data from XPS measurements taken in dry conditions. However, XPS is performed under ultra-high vacuum and it is nearly impossible to determine any molecular ordering changes a homo-polymer undergoes over increasing contact time with a liquid. Near Edge X-Ray Absorption Fine Structure (NEXAFS), another very powerful spectroscopic technique, may allow for the determination of molecular orientation changes upon water contact, but the use of a synchrotron is required.[9-11] Using SFG we probed the solid/aqueous interface *in situ* and in real time without physically breaking apart the system of study. Although SFG has been used to extensively study other polymers in water, PVC has not yet been studied *in situ* in water at a molecular level. [12-21]

This Chapter presents a fundamental study on the behaviors of PVC and phthalate (DEHP) surface functional groups in air, the ordering changes of these C-H groups over time when in contact with D_2O (utilized to avoid spectral confusion between the water O-H stretching and the plastic C-H stretching signals) and the following C-H functional group restructuring in

air after water contact using SFG. The behaviors of surface molecular structures on pure PVC films are compared to those on PVC plasticized with 10 wt% and 25 wt% DEHP. In order to obtain molecular vibrational information at the water interface *in situ*, a prism experimental geometry is used, where PVC thin films are spin coated on right angle silica prisms and D_2O droplets are contacted to the films on the bottom of the prisms (Figure 5.1). Such an experimental geometry setup yields larger signals when liquids are contacted to substrates (no signals could be obtained with a flat window substrate rather than a prism geometry), but also may lead to interfacial signal interferences and/or different spectra than window geometry, as found in this research. In fact, when the spectra obtained under the prism geometry were originally fit with the traditional fitting method outlined in Chapter 1 accounting for signals originating from a single surface, the resulting calculated CH_2 and CH_3 surface orientations were very similar for every prism sample type before and after water contact, even though the window spectra indicated major structural changes. These results left us to conclude that the SFG signals obtained on plastics under the prism geometry may not solely originate from the plastic surfaces.

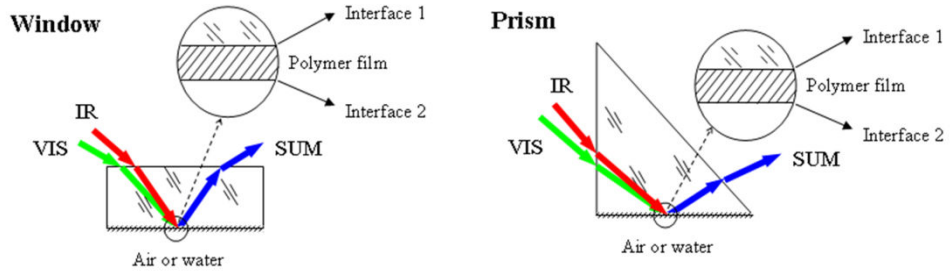

Figure 5.1. The window and prism geometries for SFG experiments in this study.

Therefore, this Chapter also focuses on resolving SFG signals of the silica/polymer interface from those resulting from the polymer/water or polymer/air interface, allowing us to further understand the molecular-level behaviors of PVC and phthalates in aqueous conditions and to give a quantitative answer as to why different SFG signals were observed in window

versus prism geometry. Finally, the leaching of DEHP molecules into D_2O and their reorganization at a new interface is briefly studied, demonstrating the instability of the PVC films and furthering our understanding of the surface molecular structural changes of these plastics when in contact with water.

5.2 Experimental Methods

5.2.1 Materials

Poly(vinyl chloride) (M_w 62,000; M_n 35,000, pellet form), tetrahydrofuran (THF) ≥99.9% purity, toluene ≥99.3% purity, concentrated sulfuric acid (reagent grade), potassium dichromate, and deuterium oxide were obtained from Sigma Aldrich (St. Louis, MO). Deuterated poly(styrene)-d_8 (PS-d_8) was purchased from Polymer Source, Inc. (Dorval, QC Canada). Bis 2-ethylhexyl phthalate (analytical standard) was purchased from Fluka (St. Louis, MO).

5.2.2 Sample Preparation

Right angle fused silica prisms (Altos Photonics, Inc.) and fused silica windows (ESCO Products, Inc.) were used for SFG measurements and were sequentially cleaned with a concentrated sulfuric acid bath saturated with potassium dichromate overnight, rinsed with deionized water, dried with nitrogen gas and then cleaned by exposing substrates to a glow discharge air plasma for 5 min with a PE-50 series Plasma System (Plasma Etch, Inc.) to remove any excess organic material before sample preparation. PVC pellets were dissolved in THF to prepare the PVC-based thin films. A 30:1 weight ratio of THF/PVC was used for all PVC-based films. DEHP was added by weight percent to PVC. PVC plastic film thicknesses were ~200 nm. 1 wt% PS-d_8 solutions were prepared by dissolving PS-d_8 in toluene. Solutions were mixed using a vortex mixer (Vortex-Genie 2T, Scientific Industries Inc.) until clear.

A P-6000 spin coater (Speedline Technologies) was used to prepare all plastic thin films. Plastics were spin coated at 3000 rpm for 30 s on silica prisms or windows depending upon the application. PVC plastic films were spin coated on both windows and prisms. PS-d_8 solutions were spin coated on prisms only.

5.2.3 SFG D_2O Experiments

5.2.3.1 SFG Model Water Interface Experiments

For the SFG experiments, samples were placed film-face down in a custom made sample holder so that the film surfaces were initially open to air. PVC films were exposed to D_2O for approximately 1.25 h by contact to a droplet of D_2O in a clean holder pushed upwards to samples using a lab jack. After 1.25 h the jack was lowered and the films were exposed to air to dry for approximately 1 h. SFG spectra were taken before and during D_2O contact, and after 1 h of drying time in air. Two sample geometries, window and prism geometries, were used in this study (Figure 5.1). *In situ* measurements and measurements taken before and after D_2O contact were performed with prism geometries (using right angle prisms as substrates). Window geometries were used for measurements before and after water exposure, but not during since spectra could not be obtained in this geometry *in situ* (signal to noise ratio was too low to observe spectral peaks conclusively). The consequences of using these two different geometries to obtain SFG measurements will be discussed in more detail later.

5.2.3.2 SFG Phthalate Migration Experiments

For SFG phthalate migration experiments, samples spin coated on windows were contacted to a droplet of D_2O in the same manner as stated above for approximately 1.5h. Afterwards the jack was lowered and the D_2O holder containing the droplet was transferred to

contact a new prism with a PS-d_8 spin coated film. SFG spectra were obtained before, during, and after "dirty" D_2O contact to PS-d_8.

5.2.4 Instrumentation

5.2.4.1 SFG

The details of SFG theory and experimental setup have been extensively outlined in the introduction of this thesis and elsewhere.[32,40,41] SFG has been previously applied to gather molecular-level information of a variety of surfaces and interfaces like polymers in aqueous environments.[12,22-30] The SFG experiments conducted for this Chapter were taken using ssp (s-polarized signal, s-polarized 532 nm input beam and p-polarized tunable frequency IR input beam) and ppp polarization combinations.

5.2.4.3 FTIR

A Nicolet 6700 FTIR spectrometer was used to determine whether or not remaining D_2O was trapped in PVC films after exposure to D_2O. The FTIR sample stage was purged with nitrogen prior to and during obtaining sample spectra to reduce water content present in the atmosphere. Pure PVC films were compared to FTIR PVC reference spectra. Spectra were obtained from 400 cm^{-1} to 4000 cm^{-1}. Spectra are shown in a range of 1000-3600cm^{-1} for image clarity.

5.2.5 Spectral Deconvolution Analysis

In our SFG experiments, we could not detect SFG ppp signals at the air interface using a face-down window geometry (Figure 5.1), nor could we generate ssp or ppp signals at the polymer/water interface with a window geometry, as previously mentioned. Therefore, we

obtained SFG spectra using a prism geometry (Figure 5.1), where both cases (in air and contacting water) generated strong signals. However, the ssp prism air/polymer interface spectra were markedly different from the window air/polymer spectra, indicating that there were complications with the spectra obtained in prism geometry. For the previous three Chapters, the vast majority of SFG experiments were performed in window geometry, and so these complications were not observed and not an issue in interpreting surface spectra.

Here, it is believed that the SFG spectral differences between spectra obtained on prisms versus windows arise from signal interferences that occurred with prism geometry for this system. Since a polymer film on a supported substrate has two interfaces, whether it is a polymer film on a silica window or a prism, both interfaces (silica/polymer interface and polymer surface in air or polymer/water interface) can generate SFG signals. Generally, for SFG spectra of polymers in air, the signal at the air interface is often much larger than at the buried substrate/polymer interface, due to differences in local Fresnel coefficients (as well as functional group orientation or ordering) at the two interfaces. It is this local field correction for each interface that influences the relative interfacial SFG signal intensity. However, if signals at the buried substrate/polymer interface are strong, i.e. when using the prism geometry with an appropriate film thickness, it is possible that these signals may dominate the air or water/polymer interfacial signals. Therefore it was vital to complete Fresnel coefficient calculations and also use a two-interface thin film spectral fitting model to determine if signals at the air or water interface were convoluted with the buried substrate interfacial signals.

For our fitting calculations, we used the ssp SFG spectra in air in window geometry as the basis for plastic surface signal contributions because the spectra are dominated by surface signals in this geometry. Evidence to support this claim can be found in our Fresnel coefficient

calculations in the following section. Then, we deduced the ssp SFG signals of the buried polymer/substrate interface generated from the prism geometry in air by fitting spectra (which contain signals generated by both the polymer surface in air and the polymer/substrate interface). Finally, knowing the buried polymer/substrate ssp SFG signals and having collected the ssp SFG spectra from the prism geometry in water, we deduced the SFG signals of the polymer surface in water. Likewise, we were able to deduce the SFG ppp spectra from the polymer surface in water, in air and from the buried polymer/substrate interface.[31-38] Dr. Xiaolin Lu performed all fits using the multi-interface model he wrote based on well established theoretical calculations, determined Fresnel coefficients at various film thicknesses and sample geometries, and aided greatly in data analysis and interpretation for this Chapter. Fitting results in this Chapter are given in A_q / Γ_q values (strength of the q_{th} vibrational mode divided by the damping coefficient of the q_{th} vibrational mode), which are generated after fitting peaks and are directly correlated to the observed SFG signals. We can directly correlate relative A_q / Γ_q ratios at the two interfaces to the relative contributions of a functional group at these interfaces. The multi-interface analysis will be described in detail below.

The Fresnel coefficients responsible for both interfaces were first calculated using a thin-film model. The calculated Fresnel coefficients were plotted as a function of the polymer film thickness under ssp and ppp polarization combinations and are shown in Figure 5.2 (window face-down contacting air and window face-down contacting water), and Figure 5.3 (prism contacting air and prism contacting water). As presented in the introduction Chapter of this thesis, ssp spectra probe χ_{yyz}, while ppp spectra probe multiple χ components. From these curves, important perspectives can be gained on which interface may contribute more to the collected SFG spectra and the spectra can be analyzed quantitatively. It should be mentioned that

the values of Fresnel coefficients used for quantitative analysis of spectra in this Chapter correspond to a polymer film thickness of ~200 nm, which holds true for our PVC thin film samples.

First the Fresnel coefficients of the window geometry are discussed in detail. Specifically for the window face-down geometry with air as the bottom contacting medium (Figure 5.2), the Fresnel coefficient of the polymer surface in air for the ssp polarization combination (~0.94) is much larger than that of the silica/polymer interface and the Fresnel coefficients for the ppp polarization combination. This indicates that SFG signals from the surface may dominate window spectra. In addition, for this Chapter we studied methylene and methyl functional groups, hydrophobic groups which at polymer surfaces in air tend to orientate more towards the surface normal than those at the polymer buried interfaces. This orientation behavior yields a larger corresponding second-order nonlinear susceptibility tensor component, i.e. χ_{yyz}, at polymer surfaces than at polymer buried interfaces, and therefore a larger signal.

These two reasons explain why the ssp SFG resonant signals of hydrophobic molecular groups located near the buried silica/polymer interface in window geometry can generally be considered negligible compared to those arising from the polymer surface in air. In turn, the much smaller Fresnel coefficients for the ppp polarization combination help explain why no ppp resonant signals were collected for this window geometry. With the window face-down geometry with water as the bottom contacting medium (Figure 5.2), the Fresnel coefficients for both ssp and ppp polarization combinations are also very small, and therefore it is quite reasonable that no SFG resonant signals were collected.

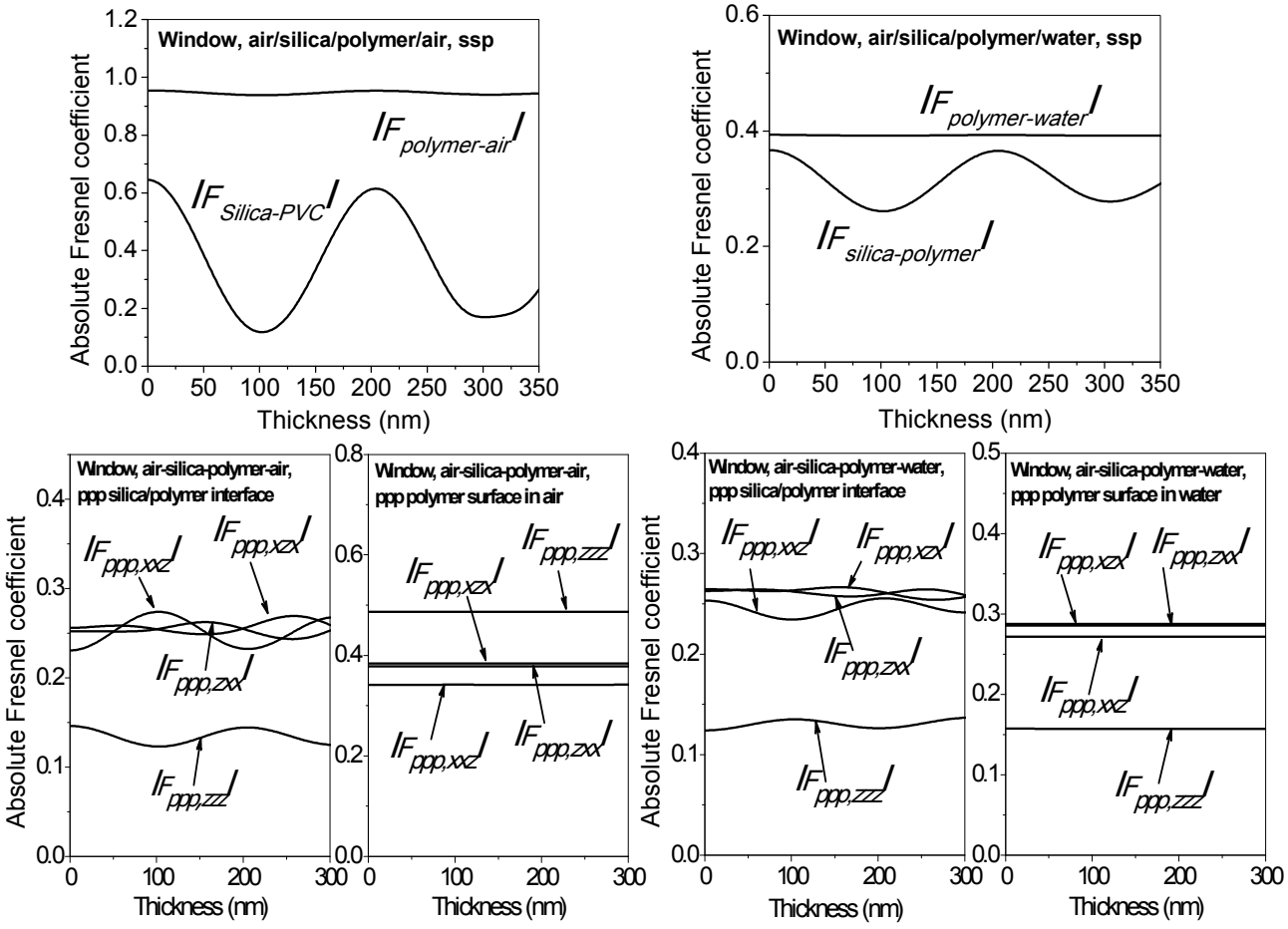

Figure 5.2. (Left) The calculated Fresnel coefficients for the window face-down geometry with air as the bottom contacting medium. (Right) The calculated Fresnel coefficients for the window face-down geometry with water as the bottom contacting medium.

As it turns out, the Fresnel coefficients of the prism geometry are quite different from those of the window geometry. If the Fresnel coefficients of the prism geometry with air as the bottom contacting medium (Figure 5.3) are inspected, specifically for the ssp polarization combination of a 200-nm-thick polymer film, the Fresnel coefficient of the silica/polymer interface (~2.21) is much larger than that of the polymer surface in air (~0.66). This indicates that the ssp spectra of the prism geometry with air as the contacting medium are composed of both contributions from the silica/polymer interface and the polymer surface in air but the

contribution from the silica/polymer interface likely prevails over that of the polymer surface in air. The Fresnel coefficient differences are the intrinsic reasons as to why the ssp spectral features for the window geometry with air as the bottom contacting medium and the prism geometry with air as the bottom contacting medium are different (these trends can be observed later in the discussion section of this Chapter).

For the ppp polarization combination in prism geometry, the Fresnel coefficient of the χ_{zzz} component of the silica/polymer interface (~2.40) is much larger than the seven other coefficients, i. e. the χ_{xxz}, χ_{xzx}, χ_{zxx} components for the silica/polymer interface and χ_{xxz}, χ_{xzx}, χ_{zxx}, χ_{zzz} components for the polymer surface in air. This strongly suggests that for the prism geometry with air as the contacting medium, the ppp spectrum is dominated by the χ_{zzz} second-order nonlinear susceptibility tensor component at the silica/polymer interface rather than the surface.

If the Fresnel coefficients of the prism geometry with water as the bottom contacting medium rather than air (Figure 5.3) are inspected, for the ssp polarization combination, the Fresnel coefficient of the silica/polymer interface (~0.98) is much smaller than that of the polymer/water interface (~2.56). This indicates the ssp spectra collected from prism geometry with water as the contacting medium are composed of contributions from both the silica/polymer interface and the polymer/water interface, but the contribution from the polymer/water interface will likely prevail over that of the silica/polymer interface.

For the ppp polarization combination, the Fresnel coefficients of the χ_{zzz} components for both the silica/polymer interface (~1.15) and the polymer/water interface (~2.50) are much larger than the six other coefficients, i. e. χ_{xxz}, χ_{xzx}, and χ_{zxx} components for both the silica/polymer interface and the polymer/water interface. This again indicates the collected ppp spectra obtained in prism geometry with water as the contacting medium are composed of both contributions from

the silica/polymer interface and the polymer/water interface. However in this case the contribution from the polymer/water interface will likely prevail over that of the silica/polymer interface.

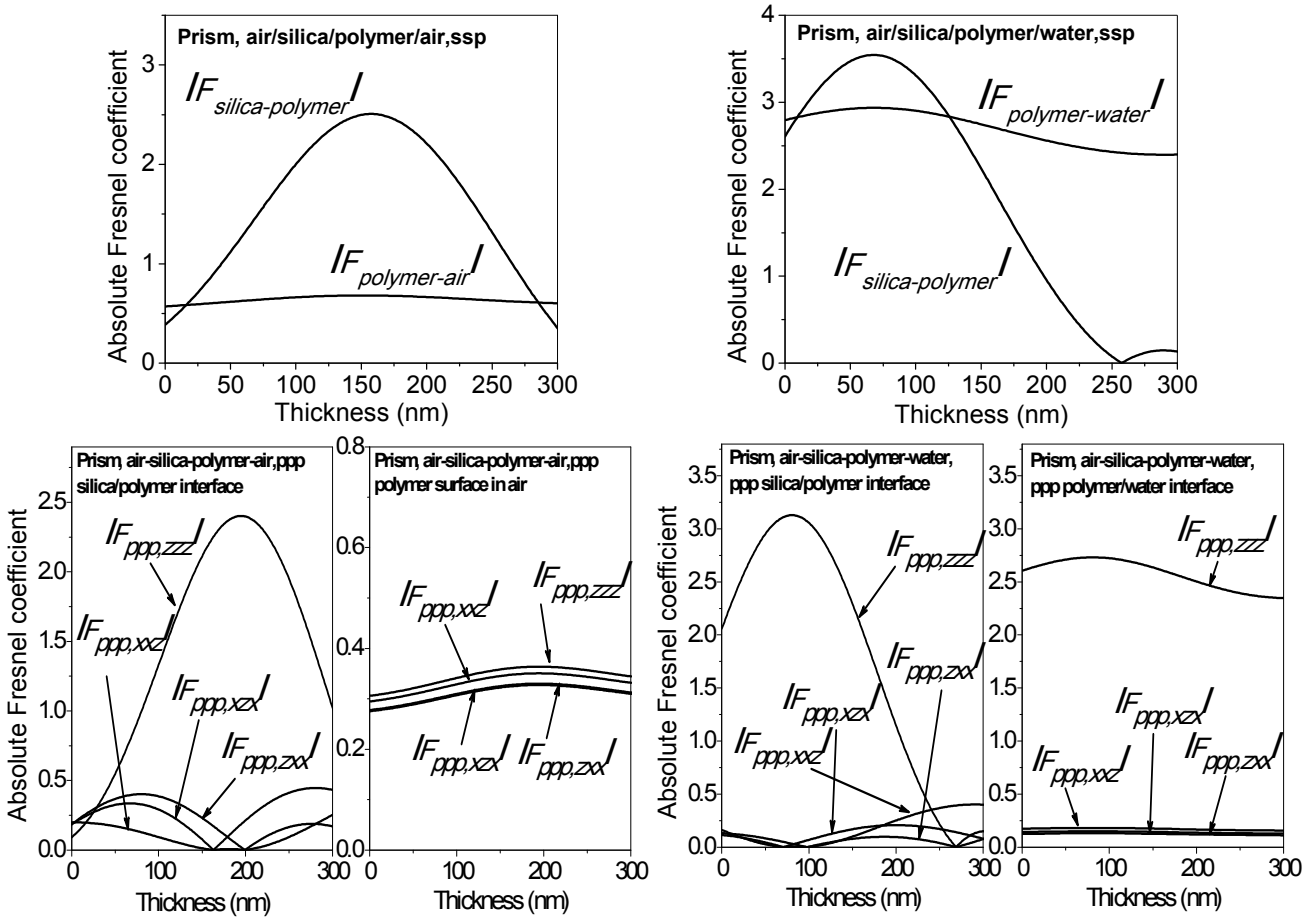

Figure 5.3. (Left) The calculated Fresnel coefficients for the prism geometry with air as the bottom contacting medium. (Right) The calculated Fresnel coefficients for the prism geometry with water as the bottom contacting medium.

Whether using ssp or ppp polarization combinations in the prism geometry, only one second-order nonlinear susceptibility tensor component has substantial contribution to the collected spectrum. This makes quantitative analysis practical and feasible for both ssp and ppp spectra. The following equation was used to fit spectra that are composed of contributions from two interfaces for an SFG spectrum of a 200-nm thick polymer thin film:

$$I_{SFG} \propto \left|\chi_{eff,ijk}\right|^2 = \left|\chi_{NR} + F_{ijk,\text{int}erface1}\sum_q \frac{A_q e^{i\alpha}}{\omega - \omega_q + i\Gamma_q} + F_{ijk,\text{int}erface2}\sum_q \frac{B_q}{\omega - \omega_q + i\Gamma_q}\right|^2 \quad \textbf{Eq. 5.1}$$

Here χ_{NR} is the non-resonant background, ω_q and Γ_q are the resonant infrared frequency and damping coefficient of the q_{th} vibrational mode, respectively, and A_q and B_q are the strengths of the q_{th} vibrational mode at the two interfaces, respectively. Once the spectral peaks were fitted, generated A_q/Γ_q ratios directly correlate to $\chi^{(2}{}_{eff}$ and therefore directly relate to the observed signals. Hence, we can directly correlate the relative A_q/Γ_q ratios obtained from fitting results to the relative contributions of a functional group at two different interfaces.[31-36,38,39]

5.3 Results and Discussion

5.3.1 PVC in Air and D_2O

5.3.1.1 Window Geometry: PVC in Air

First the ssp SFG spectrum of pure PVC in air obtained in window geometry is analyzed (Figure 5.4). Similar to previous Chapters, the largest peak at 2915 cm^{-1} belongs to the methylene symmetric (CH_2(s)) stretch and a small peak at 2880 cm^{-1} is assigned to the end group methyl symmetric stretch (CH_3(s)).[16,40,41] From our previous discussion in the experimental section, we know that such a window spectrum originates from C-H groups on the PVC surface in air. Therefore, we can confirm the PVC surface is dominated by methylene groups.

5.3.1.2 Prism Geometry: PVC in Air

As discussed in the previous section, the ssp SFG signal (Figure 5.5) generated from the PVC on silica prism in air may be dominated by the contribution from the buried PVC/silica

interface since the absolute Fresnel coefficient of the silica/PVC interface is ~2.21 and that of the PVC surface in air is ~0.66 for a film thickness around 200 nm. To obtain the signal contribution from the buried PVC/silica interface, the ssp spectrum of the PVC surface in air is needed. This was collected from the window geometry measurements. Detailed fitting results are given in Table 5.1 below.

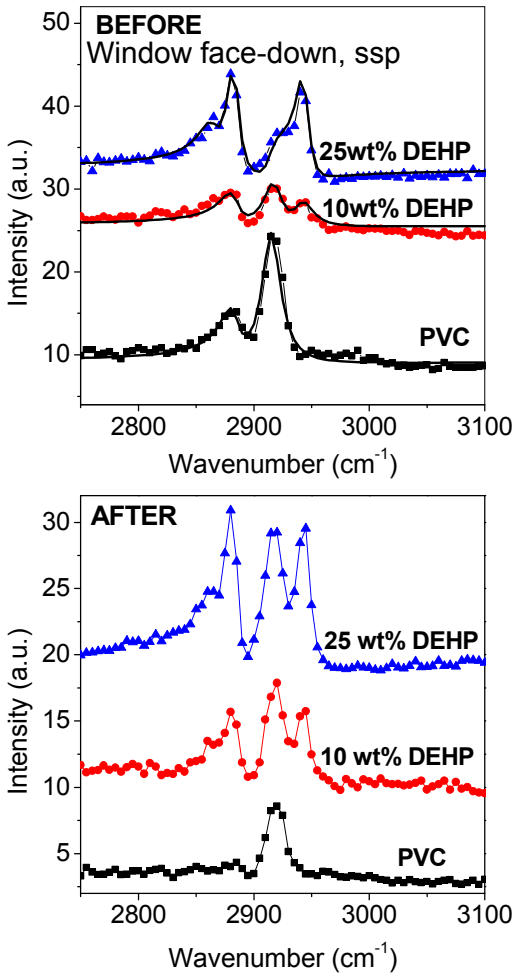

Figure 5.4. SFG ssp face down window spectra of pure PVC, PVC with 10 wt% DEHP and PVC with 25 wt% DEHP in air before D_2O contact (top) and after D_2O contact (bottom). The spectra before D_2O contact have been fitted. The fits are shown on the spectra in the top panel as solid black lines and the experimental data as points only.

Table 5.1. Spectral fitting results for PVC in air in window geometry

Window in air, PVC, ssp						
Assignment	**PVC surface in air**			**PVC/silica interface**		
	Wavenumber (cm^{-1})	A_q	Γ_q	*Wavenumber (cm^{-1})*	A_q	Γ_q
CH/CH_2	2860	-	-	-	-	-
CH_3 (s)	2880	17	10	-	-	-
CH_2 (s)	2915	40	10	-	-	-
CH_2 (as)	2950	-	-	-	-	-
Fitting Details: $F_{ssp,yyz}$=0.95, χ_{NR}=-0.4						

Surprisingly, the major contribution from the prism measurement arises from the surface methylene signal. Only two very weak resonant peaks were determined to originate from the buried silica interface with A_q/Γ_q ratios of 0.3 and -0.2 (see Table 5.2 for more information). So for the ssp spectrum collected from the prism geometry in air, the surface signals dominate the spectrum even though the buried silica interface has a larger Fresnel coefficient than that of the PVC surface in air. This likely occurred because the molecular groups at the silica/PVC interface are highly disordered in comparison to the groups at the air interface.

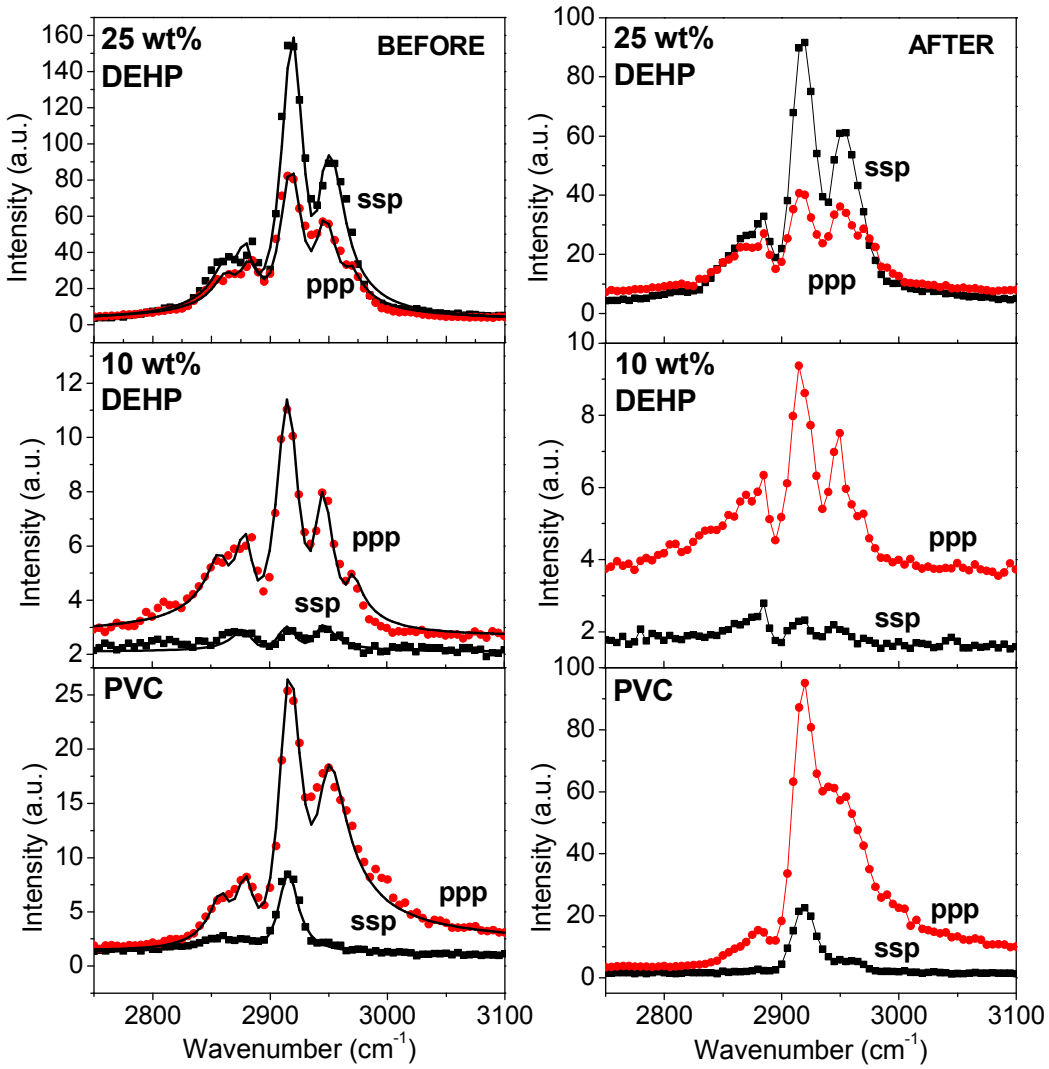

Figure 5.5. SFG prism spectra of plastics in air before (left side) and after (right side) D_2O exposure with 1h drying time. The spectra before D_2O contact found in the left panel have been fitted. The fits are shown on the spectra as solid black lines and the data as points only.

Since no SFG signals were collected from the window geometry in the ppp polarization combination and strong ppp SFG signals were collected from the prism geometry, and since the Fresnel coefficients of the buried interface dominate in prism geometry are known (see experimental section), we can conclude that the strong ppp SFG signals from PVC on prisms in air were only generated from the silica/PVC interface. Unsurprisingly, the spectrum could be fitted using signals from the buried silica interface only (Table 5.2). In prism ppp spectra, as well

as the previous PVC peak assignments, we can observe a small peak at 2860 cm^{-1}, assigned to CH/CH_2 contributions in accordance with IR studies[42,43] (see Figure 5.5). From the discussed fitting results, we can conclude that the PVC ssp spectrum on prisms yields information on both the PVC surface in air and the buried PVC/substrate interface, whereas the ppp polarization gives information only on the C-H functional groups at the buried silica interface. This in fact may be a benefit for some studies. For thin films of a select refractive index and thickness, we may be able to use ppp SFG signal in prism geometry to selectively probe the buried interface. In this case we can specifically study the PVC/silica interface in ppp and use different experimental setups to study the surface molecular behaviors of the plastic film.

Table 5.2. Spectral fitting results for PVC in air in prism geometry for ssp polarization (left) and ppp polarization (right) combinations

Prism in air, PVC, ssp							Prism in air, PVC, ppp						
	PVC surface in air			PVC/silica interface				PVC surface in air			PVC/silica interface		
	cm^{-1}	A_q	Γ_q	cm^{-1}	A_q	Γ_q		cm^{-1}	A_q	Γ_q	cm^{-1}	A_q	Γ_q
CH/CH_2	2860	-	-	2860	3	10	CH/CH_2	2860	-	-	2860	5	10
CH_3 (s)	2880	17	10	2880	-2	10	CH_3 (s)	2880	-	-	2880	7	10
CH_2 (s)	2915	40	10	2915	-	-	CH_2 (s)	2915	-	-	2915 (2916)	22	12
CH_2 (as)	2950	-	-	2950	-	-	CH_2 (as)	2950	-	-	2950 (2947)	16	15
200 nm, $F_{PVC/Air}$ =0.66, $F_{Silica/PVC}$=2.21, χ_{nr}=-0.2							200 nm, $F_{Silica/PVC}$= 2.40, χ_{nr}=0.25						

5.3.1.3 Prism Geometry: PVC in D_2O

To study the molecular surface changes of PVC from water contact, PVC samples were contacted with D_2O (used in place of water to avoid spectral confusion) and SFG spectra were collected *in situ* in the prism geometry. Figure 5.6 shows ssp and ppp prism spectra collected from PVC as a function of D_2O contact time. The major signal detected in water for both ssp

and ppp spectra is the CH_2(s) peak at 2915 cm^{-1}. Upon contact with deuterated water, the 2915 cm^{-1} signal increases slightly in intensity compared to the signal in air. However, as contact time increases, the PVC peaks decrease in intensity and are significantly smaller than those in air in both ssp and ppp spectra. Interestingly, the 2880 cm^{-1} signal from CH_3 disappears immediately. In addition, a new peak at 2970 cm^{-1} appears, which we have previously assigned to the CHCl stretch from PVC.[44] This peak is barely observable in ssp but clearly present in ppp spectra.

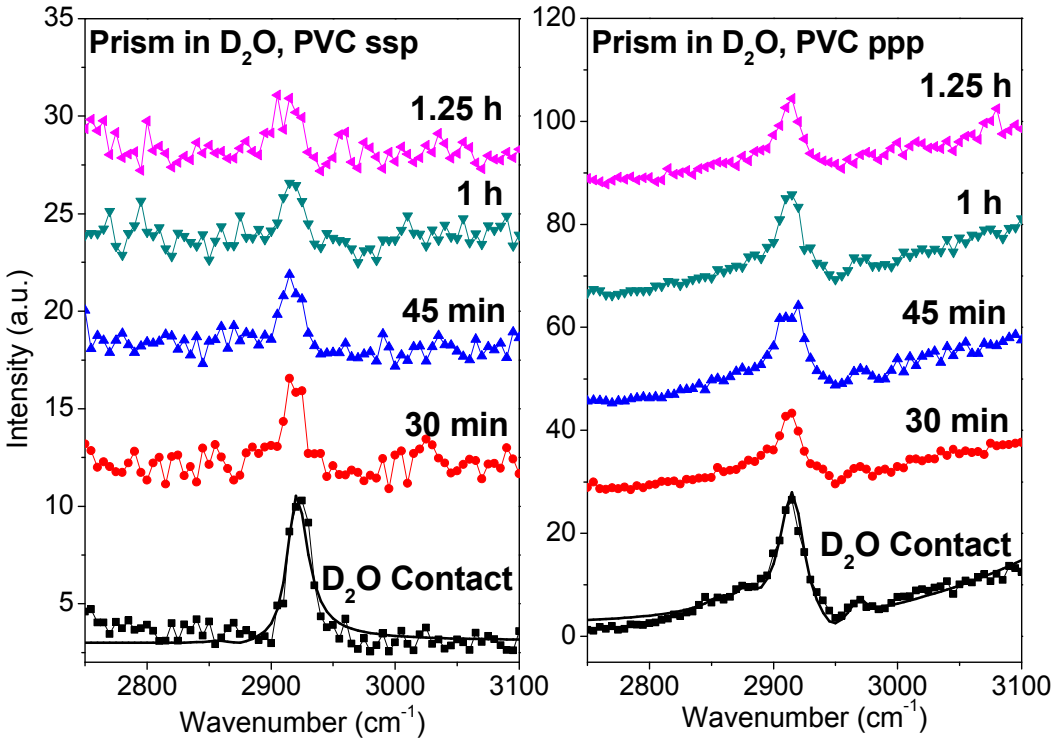

Figure 5.6. SFG prism spectra of PVC in D_2O interface over increasing contact time from first contact to 1.25h. On the left is the ssp spectra series and the right the ppp series. The spectral fits of the peaks upon water contact are represented as black lines.

Since we know the buried silica prism/PVC interfacial ssp SFG signal from the study in air (Table 5.3), we can obtain the ssp SFG signal contributed from the PVC/silica interface versus the PVC/water interface by fitting the ssp SFG spectrum collected from the PVC on a prism in D_2O as seen in Table 5.3. The fitting results indicate that the main signal at 2915 cm^{-1}

in ssp spectrum for the prism in water (Figure 5.6) must come from the PVC/water interface since the only contributed resonant signals from the silica/PVC interface are very weak. These weak signals are located at 2860 cm^{-1} and 2880 cm^{-1} with 0.3 and -0.2 A_q/Γ_q ratios, respectively. When the same fitting logic is applied for the ppp spectra, the observed resonant signals can only be fit well when both interfaces are accounted for (Figure 5.6, Table 5.3). As an example, A_q/Γ_q for CH_2(s) at the PVC/water interface is -2.4, whereas it is 1.8 for the silica/PVC interface. Therefore the SFG signals must originate from both the silica/PVC and PVC/water interfaces. Here OH vibration (which may be from incomplete deuteration) shifts the line shape.

The decrease in 2915 cm^{-1} intensity over time in ssp spectra (dominated by PVC/water interface contributions) could either indicate a change in methylene group orientation or an increase in surface methylene disorder (or orientation distribution) at the PVC/water interface. Since both ssp and ppp polarization combinations showed a decrease in methylene signals, it is more likely that the PVC surface continues to disorder with increasing contact time with water. Thus with the information from our spectral fitting, we concluded that the observed spectral changes of CH groups in ssp were indicators of increased CH disorder over a span of minutes at the polymer/water interface. The spectra from ppp, which arise from both the water and silica buried interfaces, also indicate increased CH disorder over time. However, it is apparent that some ordering at the polymer/water interface remains after 90 min of water exposure. We are not able to make definitive statements about ordering changes at the buried polymer/silica interface from water contact with our spectra obtained *in situ* in D_2O. This research indicates that even though we could not detect SFG signals from the PVC/water interface using a window geometry, it is still feasible to follow the surface structural changes as a function of time using a prism geometry.

Table 5.3. Spectral fitting results for PVC in D_2O in prism geometry for ssp polarization (left) and ppp polarization (right) combinations

Prism in D_2O, PVC, ssp							Prism in D_2O, PVC, ppp						
	PVC/water interface			PVC/silica interface				PVC/water interface			PVC/silica interface		
	cm^{-1}	A_q	Γ_q	cm^{-1}	A_q	Γ_q		cm^{-1}	A_q	Γ_q	cm^{-1}	A_q	Γ_q
CH/CH_2	2860	-	-	2860	3	10	CH/CH_2	2860	-3.9	10	2860	5.1	10
CH_3 (s)	2880	-	-	2880	-2	10	CH_3 (s)	2880	-6.0	10	2880	7.0	10
CH_2 (s)	2915 (2919)	29	10	2915	-	-	CH_2 (s)	2915 (2916)	-29	12	2915 (2916)	22	12
CH_2 (as)	2950	-	-	2950	-	-	CH_2 (as)	2950	-	-	2950 (2947)	16	15
							CHCl	2970	-2.3	10	2970	-	-
							OH	3200	-320	170	3200	-	-
200 nm, $F_{PVC/Water}$ =2.56 , $F_{Silica/PVC}$=0.95, χ_{NR}=0.1, α=-0.11, β=0							$F_{PVC/Water}$ = 2.50, $F_{Silica/PVC}$=1.15, χ_{NR}=0.4, α= -0.11, β=3.14						

5.3.1.4 Window Geometry: PVC in Air after D_2O Contact

After exposure to D_2O, the PVC films were dried in air for one hour and SFG spectra were obtained again at the air interface. Spectra were obtained on both windows and prism substrates. The ssp spectra of PVC in air on windows after drying can be observed in Figure 5.4. Note that the 2915 cm^{-1} CH_2(s) peak still dominates. However, the 2880 cm^{-1} CH_3 (s) peak is now lower in intensity compared to 2915 cm^{-1} than previously, suggesting some functional group rearrangement after water contact, and ultimately indicating that the exposure to water contact for hours results in stable surface restructuring changes (on a scale of hours). The more hydrophobic end methyl groups move to the bulk of the PVC sample after water contact.

5.3.1.5 Prism Geometry: PVC in Air after D_2O Contact

Looking at the ssp prism spectrum after D_2O contact, the 2915 cm^{-1} signal dominates, but the 2880 cm^{-1} signal is not observed, and an increase in intensity for the 2950 cm^{-1} methylene asymmetric (CH_2(as)) peak is clearly observed (Figure 5.5). We believe that the CH_2(as) peak

originates from the surface since the contributions from the buried silica interface before water contact were very small in comparison. The decrease of the CH_3(s) signal and increase of CH_2(as) signal is further evidence that water contact changed the surface of the material. In ppp prism spectra, there is an obvious decrease in intensity of the CH_3(s) peak at 2880 cm^{-1}. We previously determined that this peak originated from CH_3 groups at the silica/polymer interface. This indicates there is buried interface restructuring as well as surface restructuring, which could occur if the water penetrated all the way to the bottom of the film.

To summarize, the PVC surface exhibits restructuring upon contacting water. At the PVC/water interface, the plastic surface is still dominated by the methylene groups, but the end methyl groups are not observed. The PVC surface becomes more and more disordered as a function of water contact time, and the resulting surface restructuring is irreversible on a scale of hours. After the removal of PVC from water, the surface is still dominated by the methylene groups, but end methyl groups are no longer ordered on the surface. In addition, irreversible buried film/silica interface restructuring occurred from water contact as well, which indicates that water eventually penetrated the entirety of the plastic.

5.3.2 10 wt% DEHP/PVC in Air and D_2O

5.3.2.1 Window Geometry: 10 wt% DEHP in Air

First to refresh what the SFG spectra for pure DEHP involves: there are two major peaks at 2880 cm^{-1} and 2945 cm^{-1} belonging to CH_3(s) and Fermi resonance vibrational modes, respectively, and a shoulder around 2860 cm^{-1} assigned to the CH_2(s) mode of DEHP. For mixtures of PVC and 10% DEHP by weight, the film/air interfacial ssp spectra on windows contain vibrational resonances from both PVC's CH_2(s) groups at 2915 cm^{-1} and CH_3(s) at 2880

cm^{-1}. The CH_3(s) from PVC overlaps with the dominating CH_3(s) signal from DEHP at the same wavenumber. The addition of DEHP also yields a Fermi resonance signal (2945 cm^{-1}), and a 2865 cm^{-1} CH_2(s) shoulder from DEHP can be resolved as well in Figure 5.4. Again, ssp window spectra tell us that the surface in air is covered by both PVC and DEHP at 10 wt% DEHP loading. Fitting results for 10 wt% DEHP on windows can be found in Table 5.4.

Table 5.4. Spectral fitting results for 10 wt% in air in window geometry

Window in air, 10 wt% DEHP, ssp						
Assignment	**10 wt% DEHP surface in air**			**plastic/silica interface**		
	cm^{-1}	A_q	Γ_q	cm^{-1}	A_q	Γ_q
CH/CH_2 (PVC)	2860	-	-	-	-	-
CH_3 (s) (PVC)	2880	-	-	-	-	-
CH_2 (s) (PVC)	2915	21	10	-	-	-
CH_2 (as) (PVC)	2950	-	-	-	-	-
CH_2 (s) (DEHP)	2860	-	-	-	-	-
CH_3 (s) (DEHP)	2880	15	10	-	-	-
CH_3 (Fermi) (DEHP)	2945	14	10	-	-	-
200 nm, $F_{ssp,yyz}$=0.95, χ_{nr}=-0.4						

5.3.2.2 Prism Geometry: 10 wt% DEHP in Air

SFG spectra on prisms appear similar to those on windows (Figure 5.5) although the peak ratios of methylene to methyl groups are different in ssp versus ppp polarization. In the ssp spectrum, the CH_3 peaks are about equally intense compared to PVC's CH_2 peak. However in the ppp spectrum, the CH_2(s) peak is much larger than the CH_3 peaks.

This trend can be explained once again, by fitting the SFG spectra with regards to Fresnel coefficient contributions and the known fitting parameters of the ssp signals in air from the windows spectrum. As seen in Table 5.5, for the ssp prism spectrum in air, both interfaces contribute to the spectrum. As seen with the pure PVC sample, the silica/PVC interface

contribution is small although it has a large Fresnel coefficient. To demonstrate this, the A_q/Γ_q ratio of the CH_2(s) peak at the air interface is 2.1 compared to -0.28 at the buried silica interface.

Table 5.5. Spectral fitting results for 10 wt% DEHP in air in prism geometry for ssp polarization (left) and ppp polarization (right) combinations

Prism in air, 10 wt% DEHP, ssp							Prism in air, 10 wt% DEHP, ppp						
	plastic surface in air			plastic/silica interface				plastic surface in air			plastic/silica interface		
	cm^{-1}	A_q	Γ_q	cm^{-1}	A_q	Γ_q		cm^{-1}	A_q	Γ_q	cm^{-1}	A_q	Γ_q
CH/CH_2 (PVC)	2860	-	-	-	-	-	CH/CH_2 (PVC)	2860	-	-	2860	2.8	10
CH_3 (s) (PVC)	2880	-	-	-	-	-	CH_3 (s) (PVC)	2880	-	-	-	-	-
CH_2 (s) (PVC)	2915	21	10	2915	-3.3	12	CH_2 (s) (PVC)	2915	-	-	2915 (2916)	13	12
CH_2 (as) (PVC)	2950	-	-	-	-	-	CH_2 (as) (PVC)	2950	-	-	-	-	-
CH_2 (s) (DEHP)	2860	-	-	-	-	-	CH_2 (s) (DEHP)	2860	-	-	-	-	-
CH_3 (s) (DEHP)	2880	15	10	2880	-1.0	10	CH_3 (s) (DEHP)	2880	-	-	2880 (2881)	4.9	10
CH_3 (Fermi) (DEHP)	2945	14	10	2945 (2944)	-0.7	10	CH_3 (Fermi) (DEHP)	2945	-	-	2945 (2944)	6.6	10
							CHCl (PVC)				2970 (2969)	1.6	7
$F_{PVC/Air}$ =0.66, $F_{Silica/PVC}$=2.21, χ_{nr}=0, β=0, α=0							$F_{PVC/Air}$ =0.36, $F_{Silica/PVC}$=2.40, χ_{nr}=0.4, β=3.14, α=-0.11						

However, in the ppp prism spectrum, the CH_2(s) peak is much larger than the CH_3 peaks, because only the silica/PVC interface contributes to the spectrum, according to the fitting results (Table 5.5, A_q/Γ_q ratios only generated for the buried interface). On a mechanistic level, it makes sense that there are larger CH_2 signals at this interface. It is highly likely that the CH_2 groups on the PVC chains are more ordered at the buried solid hydrophilic interface than the more hydrophobic CH_3 groups on the small DEHP molecules. Once again, we have an opportunity to determine what happens to both the surface and buried interface of the plastic film from water

contact by inspecting both ssp and ppp spectra. Previous to water contact, we now know the 10 wt% DEHP plasticized PVC surface in air is covered by both DEHP and PVC, while the PVC CH_2 group dominates at the buried polymer/silica interface.

5.3.2.3 Prism Geometry: 10 wt% DEHP in D_2O

Once the 10 wt% DEHP films on prisms were contacted to D_2O, similar spectral trends as those with PVC contacted to D_2O occur (Figure 5.7). Again, the 2915 cm^{-1} CH_2(s) peak increases in intensity upon contact and then decreases over increasing contact time. The CH_2(s) peak also dominates both ssp and ppp spectra the entire 1.25 hours of D_2O contact. The major difference between pure PVC and the 10 wt% mixture in contact with D_2O is the overall intensity of the CH_2(s) peak. Looking at the scale on Figures 5.6 and 5.7, it is obvious that the intensity of the 2915 cm^{-1} peak is larger in the PVC phthalate mixture than the pure PVC in D_2O for both ssp and ppp prism spectra. This may indicate that the CH_2(s) groups were ordered to a higher degree on the surface of the polymer mixture compared to the surface of the pure PVC sample.

The fitting results for the ssp spectra in D_2O upon water contact (Table 5.6) reveal that the dominant CH_2(s) peak originates mainly from the polymer/water interface with an A_q/Γ_q ratio of 3.5 versus -0.28 at the buried silica/polymer interface. We believe that the strong CH_3 signals from the 10 wt% DEHP sample present in air before D_2O contact, immediately disappear because of almost immediate disorder of the CH_3 DEHP groups at the polymer/water interface. Most barely resolvable residual CH_3 signals upon contact and increasing contact times are from the still ordered CH_3 molecules at the buried silica/film interface.

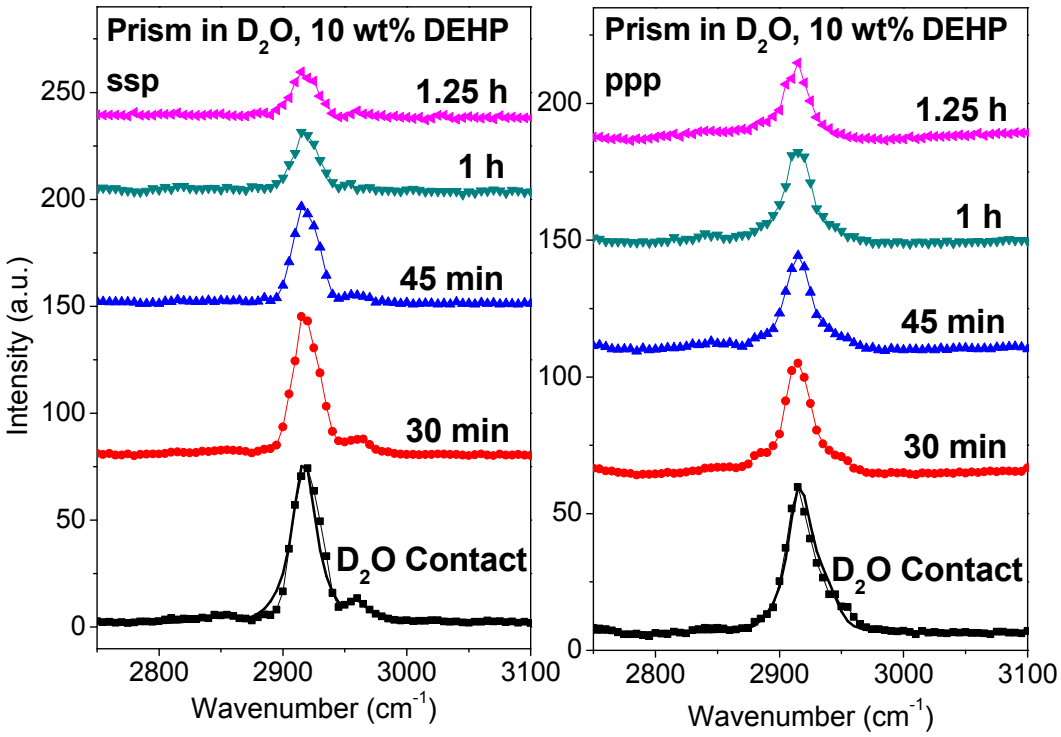

Figure 5.7. SFG prism spectra of 10 wt% DEHP plasticized PVC in D_2O over increasing contact time from first contact to 1.25h. On the left is the ssp spectra series and the right the ppp series.

Then, by studying the fitting results for the ppp spectra of 10 wt% DEHP in D_2O, we can see that both interfaces contribute to the spectrum. In Table 5.6, A_q/Γ_q ratios for 2860, 2880, 2945, and 2970 cm^{-1} peaks are only generated from the buried silica interface. However, the strong 2915 cm^{-1} peak mainly arises from the PVC/water interface with an A_q/Γ_q ratio -3.5 versus 1.1. Particular attention should be focused on the signs of the CH_2(s) mode. The signs of the signals at the PVC/water interface (-42) and the silica/PVC interface (13) are opposite, indicating the absolute orientations of these functional groups at the two interfaces are different. On one side the functional groups are pointing up and on the other they are pointing down. Once again we can conclude that the addition of water increases and then decreases CH_2 ordering of the PVC molecules at the water interface, and that the CH_3 molecules from DEHP at this interface are almost instantly disordered.

Table 5.6. Spectral fitting results for 10 wt% DEHP in D_2O in prism geometry for ssp polarization (left) and ppp polarization (right) combinations

Prism in D_2O, 10 wt% DEHP, ssp							Prism in D_2O, 10 wt% DEHP, ppp					
plastic/water interface				plastic/silica interface			plastic /water interface				plastic/silica interface	
	cm^{-1}	A_q	Γ_q	cm^{-1}	A_q	Γ_q		cm^{-1}	A_q	Γ_q	cm^{-1}	A_q	Γ_q
CH/CH_2 (PVC)	2860	4.0	10	2860	-	-	CH/CH_2 (PVC)	2860	-	-	2860	2.8	10
CH_3 (s) (PVC)	2880	-	-	-	-	-	CH_3 (s) (PVC)	2880	-	-	-	-	-
CH_2 (s) (PVC)	2915 (2917)	42	12	2915 (2916)	-3.3	12	CH_2 (s) (PVC)	2915	-42	12	2915 (2916)	13.1	12
CH_2 (as) (PVC)	2950	-	-	-	-	-	CH_2 (as) (PVC)	2950	10	15	-	-	-
CH_2 (s) (DEHP)	2860	-	-	-	-	-	CH_2 (ss) (DEHP)	2860	-	-	-	-	-
CH_3 (s) (DEHP)	2880	-	-	2880 (2881)	-1.0	10	CH_3 (s) (DEHP)	2880	-	-	2880 (2881)	4.9	10
CH_3 (Fermi) (DEHP)	2945	-	-	2945 (2944)	-0.7	10	CH_3 (Fermi) (DEHP)	2945	-	-	2945 (2944)	6.6	10
Unassi-gned	2955	3.8	7	2955	-	-	CHCl (PVC)	2970	-	-	2970	1.6	7
$F_{PVC/Water}$ =2.56, $F_{Silica/PVC}$=0.95, χ_{nr}=0.1, β=0, α=-0.11							$F_{PVC/Water}$ =2.50, $F_{Silica/PVC}$=1.15χ_{nr}=0.1, β=3.14, α=-0.11					

5.3.2.4 Window Geometry: 10 wt% DEHP in Air after Water Contact

The windows spectrum of 10 wt% DEHP film/air interface after water contact is found in Figure 5.4. The ssp window spectrum appears remarkably similar to the film/air interface before water contact except for one element: the DEHP CH_3 to PVC CH_2 peak intensity ratio. After water contact, the 2880 cm^{-1} peak is always lower in intensity than the 2915 cm^{-1} peak. This is in comparison to before water contact, when the peak ratios are almost evenly matched. This suggests either CH_3 irreversible reorientation or the dislodging of CH_3 groups from the surface in some form.

5.3.2.5 Prism Geometry: 10 wt% DEHP in Air after Water Contact

For ssp spectra on prisms, the opposite peak ratio trend holds true (Figure 5.5). The 2880 cm^{-1} peak increases in intensity in comparison to the 2915 cm^{-1} peak after water contact. This change in trend can be easily justified. An increase in molecular disorder on the surface of the film with minor changes to the buried silica/PVC interface or increased ordering at the buried interface may result in a larger CH_3 to CH_2 intensity ratio after water contact. This means once again that some form of irreversible molecular surface reorientation occurred. And for the prism ppp spectrum, which only contains signals from the buried interface, we can conclude that some, but not many ordering changes occurred. There is a slight change in the CH_3 to CH_2 intensity ratio after water contact, with an increase in the CH_3 intensity, which corroborates the conclusions with the ssp prism spectra in that the CH group reordering changes on the surface of this PVC system were much larger than the changes at the buried silica/film interface.

To summarize, the surface of 10 wt% DEHP plasticized PVC in air is covered by both DEHP and PVC functional groups but the buried polymer/silica interface is dominated by PVC methylene groups. The CH_3 groups of DEHP are disordered almost immediately upon water contact and as a function of time, PVC surface order decreases. After removing the 10 wt% DEHP plasticized PVC from water, there was only partial recovery of surface methyl groups likely due to loss of molecules and/or permanent surface restructuring. Minor restructuring behavior of the buried polymer/silica interface was also observed.

5.3.3 25 wt% DEHP/PVC in Air and Water

5.3.3.1 Window Geometry: 25 wt% DEHP in Air

As previously reported, the SFG ssp window spectrum of the PVC/DEHP mixture in air contains signals assigned to both PVC and DEHP functional groups, with DEHP molecules dominating the surface, and will not be discussed further here (Figure 5.4).[16,40] Fitting results for the window geometry can be found in Table 5.7.

5.3.3.2 Prism Geometry: 25 wt% DEHP in Air

Once again, the spectra in air on prisms are quite different from the ssp spectra on windows as seen in Figure 5.5. In the ssp spectrum, the 2915 cm^{-1} peak is much larger than the 2880 and 2945 cm^{-1} peaks whereas in the ppp spectrum the 2915 cm^{-1} peak is only slightly larger than the methyl resonances. This time, the fitting results indicate that both the air and buried silica interfaces contribute to ssp spectra, but the silica/PVC interface dominates the spectrum (Table 5.8). Here, the CH_2(s) A_q/Γ_q ratio in air is -2, and 5.7 at the buried silica interface. Once again, this indicates that the PVC methylene groups are more ordered at the hydrophilic silica interface than the hydrophobic air interface.

Table 5.7. Spectral fitting results for 25 wt% DEHP in air in window geometry

Window in air, 25 wt% DEHP, ssp						
	25 wt% DEHP surface in air			plastic/silica interface		
	cm^{-1}	A_q	Γ_q	cm^{-1}	A_q	Γ_q
CH/CH_2 (PVC)	2860	-	-	-	-	-
CH_3 (s) (PVC)	2880	-	-	-	-	-
CH_2 (s) (PVC)	2915	-20	10	-	-	-
CH_2 (as) (PVC)	2950	-	-	-	-	-
CH_2 (s) (DEHP)	2860 (2865)	10	10	-	-	-
CH_3 (s) (DEHP)	2880	24	7	-	-	-
CH_3 (Fermi) (DEHP)	2945 (2944)	23	7	-	-	-
200 nm, $F_{ssp,yyz}$=0.95, χ_{nr}=-0.4						

In contrast, the ppp spectrum only contains signals from the PVC/silica interface which originate from both PVC methylene groups and DEHP groups. This case is clearly different than pure PVC and 10 wt% DEHP, where we were still able to generate information mainly from the surface in ssp polarization. Here, most information arises from the buried interface in both ssp and ppp spectra, which will be very important in our analysis of water penetration into the film later.

Table 5.8. Spectral fitting results for 25 wt% DEHP in air in prism geometry for ssp polarization (left) and ppp polarization (right) combinations

Prism in air, 25wt% DEHP, ssp							Prism in air, 25 wt% DEHP, ppp						
	plastic surface in air			plastic/silica interface				plastic surface in air			plastic/silica interface		
	cm^{-1}	A_q	Γ_q	cm^{-1}	A_q	Γ_q		cm^{-1}	A_q	Γ_q	cm^{-1}	A_q	Γ_q
CH/CH_2 (PVC)	2860	0	-	-	-	-	CH/CH_2 (PVC)	2860	-	-	-	-	-
CH_3 (s) (PVC)	2880	0	-	-	-	-	CH_3 (s) (PVC)	2880	-	-	-	-	-
CH_2 (s) (PVC)	2915	-20	10	2915 (2919)	68	12	CH_2 (s) (PVC)	2915	-	-	2915 (2918)	39	12
CH_2 (as) (PVC)	2950	0	-	-	-	-	CH_2 (as) (PVC)	2950	-	-	-	-	-
CH_2 (s) (DEHP)	2860 (2865)	10	10	2860 (2865)	5.9	10	CH_2 (s) (DEHP)	2860 (2865)	-	-	2860 (2865)	7.3	10
CH_3 (s) (DEHP)	2880	24	7	2880 (2883)	8.0	12	CH_3 (s) (DEHP)	2880	-	-	2880 (2885)	17	12
CH_3 (Fermi) (DEHP)	2944	23	7	2945 (2950)	28	12	CH_3 (Fermi) (DEHP)	2944	-	-	2945	25	12
							CHCl (PVC)	2967	-	-	2967	4	7
$F_{PVC/Air}$ =0.66, $F_{Silica/PVC}$=2.21, α=0, β=0, χ_{NR}=0							200 nm, $F_{PVC/Air}$ =0.36, $F_{Silica/PVC}$=2.40, α=-0.11, β=0, χ_{nr}=0						

5.3.3.3 Prism Geometry: 25 wt% DEHP in D_2O

The ssp prism spectrum of 25 wt% DEHP upon contact with D_2O shows the appearance of an intense 2915 cm^{-1} CH_2(s) peak (Figure 5.8). A second strong peak at 2950 cm^{-1} in ssp spectra is also present, which is assigned to the CH_3(s) Fermi resonance. However, after 30 min of water exposure, almost no peaks can be resolved. This indicates that either the plastic surface first became highly ordered and then disordered, or that multiple interfacial signals are initially observed, and then disappear with increasing water contact time.

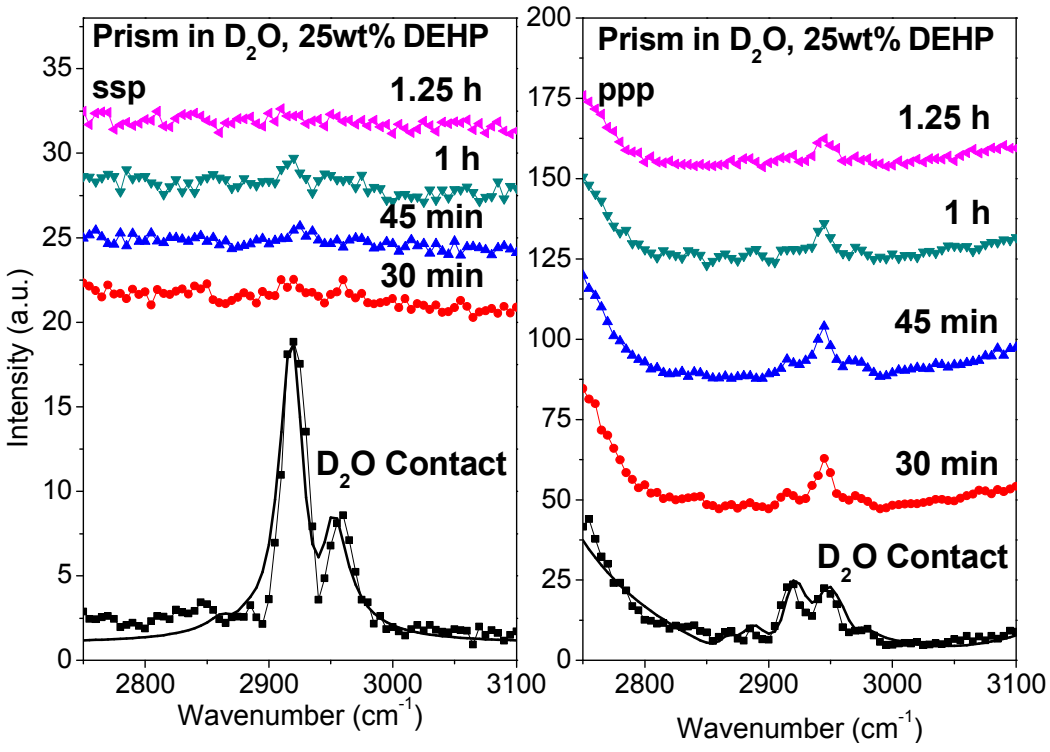

Figure 5.8. SFG prism spectra of 25 wt% DEHP plasticized PVC in D_2O over increasing contact time from first contact to 1.25h. On the left is the ssp spectra series and the right the ppp series. The spectral fits of the peaks upon water contact are represented as black lines.

The ssp spectrum obtained upon initial water contact (Table 5.9) can be fit with the parameters of the buried interface in air. As such, we believe that the plastic's surface ordering is destroyed right after contacting water. With increased plasticization from the DEHP molecules, the water quickly diffused to the buried interface and destroyed silica/PVC interfacial ordering as well. This conclusion is supported by ppp spectra as well.

The ppp spectrum upon water contact was fit well with contributions from the buried silica interface and weak surface signal contributions from the water interface (Table 5.9), agreeing with the observation of the disappearance of the ssp plastic surface signals immediately after water contact. The ppp SFG signal also decreases as a function of increasing contact time, which means the silica/PVC interfacial ordering must be destroyed due to increased water

diffusion through the plasticized polymer film. Again, because the plasticizer bulk content is high in this sample, the water can more easily diffuse through the film.

5.3.3.4 Window Geometry: 25 wt% DEHP in Air after D_2O Contact

The trends in changes to CH_3 to CH_2 peak ratios in plasticized PVC due to water contact can be more clearly observed with the ssp window spectrum of 25 wt% DEHP in air after water contact (Figure 5.4). Before water contact, the CH_2(s) peak of PVC is observed as a shoulder in the 25 wt% DEHP mixture. After water contact, however, a clear large 2915 cm^{-1} peak is present. This again suggests that there may have been functional group reorientation and/or loss of CH_3 groups on the surface.

Table 5.9. Spectral fitting results for 25 wt% DEHP in D_2O in prism geometry for ssp polarization (left) and ppp polarization (right) combinations

Prism in D_2O, 25 wt% DEHP, ssp							Prism in D_2O, 25 wt% DEHP, ppp						
plastic/water interface				plastic/silica interface			plastic/water interface				plastic/silica interface		
	cm^{-1}	A_q	Γ_q	cm^{-1}	A_q	Γ_q		cm^{-1})	A_q	Γ_q	cm^{-1}	A_q	Γ_q
CH/CH_2 (PVC)	2860	-	-	-	-	-	CH/CH_2 (PVC)	2860	-	-	-	-	-
CH_3 (s) (PVC)	2880	-	-	-	-	-	CH_3 (s) (PVC)	2880	-	-	-	-	-
CH_2 (s) (PVC)	2915 (2919)	-7	-	2915 (2919)	68	12	CH_2 (s) (PVC)	2915 (2918)	-3.3	12	2915 (2918)	39	12
CH_2 (as) (PVC)	2950	0	-	-	-	-	CH_2 (as) (PVC)	2950	-	-	-	-	-
CH_2 (s) (DEHP)	2860 (2865)	-1	-	2860 (2865)	5.9	10	CH_2 (s) (DEHP)	2860	-	-	2860 (2865)	7.3	10
CH_3 (s) (DEHP)	2880 (2885)	-1	-	2880 (2885)	8.0	12	CH_3 (s) (DEHP)	2880 (2885)	-1.2	12	2880 (2885)	17	12
CH_3 (Fermi) (DEHP)	2944 (2950)	-2	-	2945(2950)	28	12	CH_3 (Fermi) (DEHP)	2945	-2.5	12	2945	25	12
							Unassigned	2967	-3.2	7	2967	4	7
							CHCl (PVC)	2975	1.0	7	2975	-	-
							O-D vibration	2570	600	50	2570	-	-
							O-H vibration	3200	200	100	3200	-	-
$F_{PVC/Water}$ =2.56, $F_{Silica/PVC}$=0.95, α=-0.11, β=0, χ_{nr}=0.0							$F_{PVC/Air}$ =2.50, $F_{Silica/PVC}$=1.15, α=-0.11, β=0, χ_{nr}=0						

5.3.3.5 Prism Geometry: 25 wt% DEHP in Air after D_2O Contact

Prism ssp spectra reveal again, only very small changes before and after water exposure (Figure 5.5). Since it was found that the silica/polymer interface dominates ssp spectra with this sample type, we believe that there were only small ordering changes at this buried interface. The spectrum of ppp prisms after water exposure slightly changes. Recall for ppp prism spectra, the buried silica interface completely dominates the spectrum. The buried solid interface must undergo slight irreversible ordering changes from water contact. It is now known that both the surface and the bottom of this plastic film were altered from water contact. It is interesting that

this film has roughly the same thickness as the other two sample types (~200 nm), but the signal contributions from the film surface versus buried interfaces are different for the 25 wt% DEHP prisms in air and D_2O compared to the pure PVC and 10 wt% DEHP samples. It can be reasonably concluded that this occurs because the material with 25 wt% DEHP is intensively plasticized, compared to the other two samples. The increased plasticizer content increases the free volume within the polymer matrix, therefore changing the dynamic reordering behavior of the C-H functional groups at the two interfaces.

Nevertheless, the results demonstrated that the surface of the 25 wt% DEHP plasticized PVC underwent dramatic surface restructuring in water. Both the surface and the buried polymer/silica interface became disordered in water. After the water was removed from the sample, the surface structure did not completely recover. For both plasticized samples, it is not yet clear if the surface signal changes after water contact are due to phthalate or PVC surface reorientation, disorder, or loss of phthalates on the surface to water. As the next section of this discussion reveals, all of those behaviors may have occurred.

5.3.4 Phthalate Disorder and Leaching

To test the stability of phthalates in PVC/plasticizer mixtures due to contact with water, phthalate-leaching experiments were conducted. For these experiments, a PVC film containing 45 wt% DEHP was contacted to D_2O for about 1.5 hours. The D_2O droplet was then contacted to a new clean polymer surface (PS-d_8) and SFG spectra were obtained at the PS-d_8 interface. The SFG spectra of the clean deuterated polystyrene polymer surface before, during and after "dirty" D_2O contact can be seen in Figure 5.9. With this system there is no worry about interfacial signal interferences due to the fact that any deposited molecules will not form a thick

enough film where interface interference will occur, and that the deposited PS-d_8 yields no SFG signal in the CH stretching frequency range of interest.

Upon immediate contact with the "dirty" D_2O, spectral shapes significant of DEHP at the D_2O/polymer interface are observed. The unique shape of the three major peaks at the PS-d_8/dirty D_2O interface matches that of pure DEHP in air, but the peaks are red shifted in D_2O: near 2855 cm^{-1}, 2870 cm^{-1}, and 2935 cm^{-1}, rather than at the normal frequencies located 10 cm^{-1} higher. We found this same frequency shift trend with a solution of known concentration of DEHP in D_2O contacted to a PS-d_8 sample (data not shown), confirming that indeed phthalate molecules transferred from the plastic matrix to the water even though the molecules are considered hydrophobic in nature.

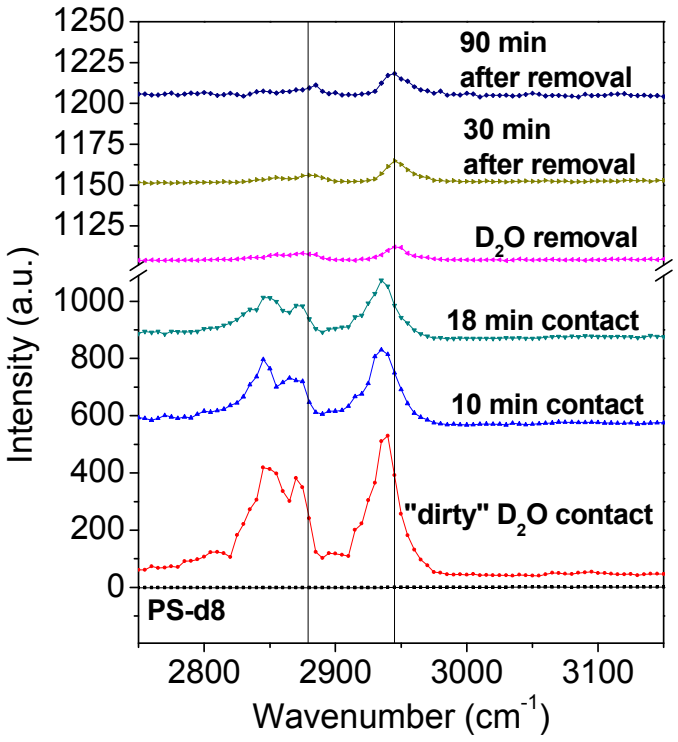

Figure 5.9. SFG prism ssp spectra of PS-d_8 film contacted with "dirty" D_2O containing phthalate molecules for up to 20 minutes and the resulting spectra of the PS-d_8 air interface after removal of the D_2O. The two black lines are provided for reference and centered at 2880 and 2945 cm^{-1}.

In addition, there are observed trends in phthalate reordering over time, with decreasing signal at the water/polymer interface, suggesting either disorder or adsorption into the PS matrix. Once the D_2O was removed and the surface was air-dried, a clear peak at 2880 cm^{-1} and a peak around 2945 cm^{-1} remain at the polymer/air interface. To make sure the signals observed were not from the D_2O or PS-d_8 itself, the experiments were not only repeated numerous times but conducted using pure D_2O as blank experiments. No signals were observed for the blank experiments. Attempts to observe the leaching of phthalates from plastic films using FTIR and ATR-FTIR were unsuccessful (see Figure 5.10 for FTIR results before and after water contact), which indicates that the amounts of leached phthalates were too low to be detected using these traditional spectroscopic techniques.

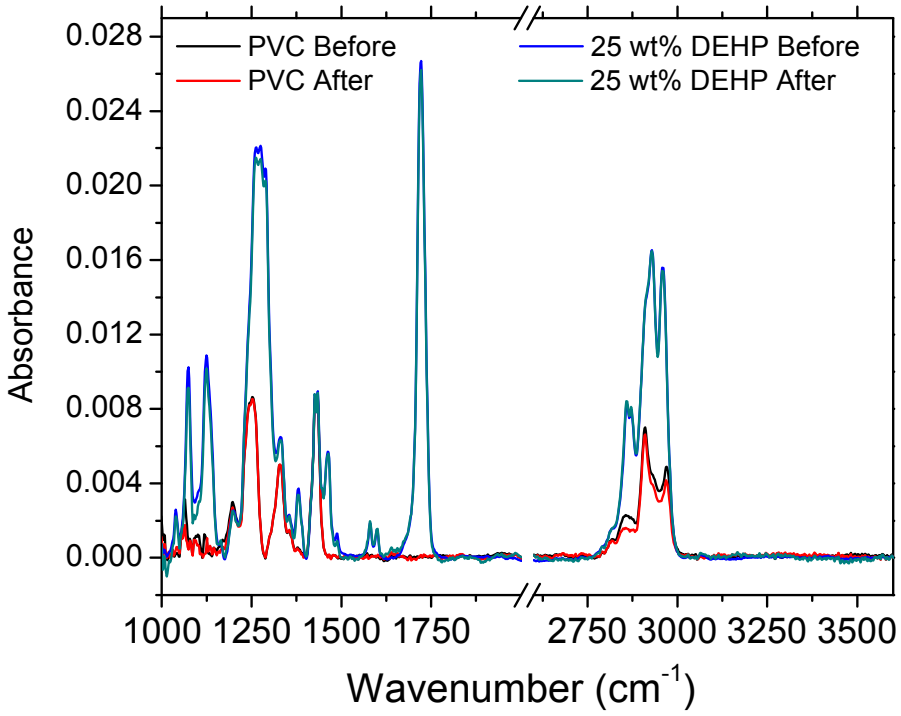

Figure 5.10. FTIR spectra obtained before and after water contact for pure PVC (black and red lines, respectively) and 25 wt% DEHP (blue and green lines, respectively).

To elaborate briefly on the FTIR results, first looking at FTIR spectra of the 25 wt% DEHP plasticized sample, it is obvious that not many spectral changes are observed between spectra obtained before and after water contact and air drying. Therefore, the amount of DEHP that leached from the sample was too small to observe with FTIR. Interestingly, in the lower frequency region for pure PVC, hardly any signal differences are observed before and after water contact, but there are some obvious signal intensity differences across the C-H region of spectra. There are two likely scenarios for the decrease of C-H signals. It is possible that some small contaminants or smaller fragments of PVC chains were removed from water contact. And/or, the process of water penetrating the PVC film changed the density of the film itself, yielding slightly different FTIR signals.

The phthalate leaching studies demonstrate that the surface phthalate molecules were not stable upon contact with water even at relatively "short" contact times, and help explain the differences in peak ratios between CH_3 and CH_2 groups on windows after water contact. DEHP molecules were likely disordered, and some molecules were removed from the water contact. Like most water/polymer SFG studies, the movement of functional groups at the surface likely occurred due to drives to lower the interfacial free energy of the system.

5.4 Conclusions

In this Chapter, the molecular effects of water contact on pure and plasticized PVC surfaces were studied *in situ* using SFG spectroscopy. First it was found the surface end CH_3 molecular groups on pure PVC were instantly disordered upon water contact and the dominating CH_2 groups disordered in water over increasing exposure time. Addition of 10 wt% DEHP changed the surface structure in air and upon water contact, yielding increased CH_2 and CH_3 disorder with increased water exposure time. All surface C-H molecular groups on PVC with 25

wt% bulk DEHP disordered almost immediately with water contact. Eventually, water migrated through the plastic bulk of all the films to reach the buried substrate/polymer interface, where water induced CH group disorder. This was most clearly observed with the 25 wt% DEHP sample, which indicates that more water penetrated this film than the other two sample types. After removal from water and drying in air, all films demonstrated irreversible surface functional group changes. For the first time, through SFG-based leaching tests, it was found that the phthalate molecules are capable of transferring into D_2O and can be transferred from D_2O to reorganize and reorient on new surfaces very quickly (in minutes). It is believed that the DEHP molecules transferred onto water in contact with a plasticized PVC surface remain mostly on the surface of the water to transfer quickly to new surfaces. Irreversible buried interface reordering was also observed.

During this study, it was found that SFG spectra obtained in prism geometry appeared different from spectra taken in window geometry. It was determined that the spectra obtained in window geometry in air only contained signals from the air interface. Using a deconvolution analysis and the fitted parameters of the window spectra, we quantified the spectral contributions from the buried polymer/silica interface in the prism spectra. It was concluded that prism SFG signals generated from different samples originated from different interferences (either surface signal dominated, buried interface dominated, or both interfacial signals contributed to spectra, depending on the plastic type and the experimental environment). We therefore were able to generate a very good understanding of molecular ordering changes from water contact at the polymer/water and polymer/silica interfaces at the same time. The molecular changes to both the top and bottom plastic films during water contact are summarized in Table 5.10 below.

Table 5.10. Description of molecular changes to plastics at the water/plastic interface and plastic/optical substrate interface during water contact

	PVC	10 wt% DEHP	25 wt% DEHP
Plastic/Water Interface	• ~Instant CH_3 disorder • Initial ↑ then gradual ↓ in PVC CH_2 order • Some C-H order remains at 1.5h	• ~Instant DEHP CH_3 disorder • Initial ↑ then gradual ↓ in CH_2 order (CH_2 more ordered than in pure PVC) • CH_2 remains ordered at 1.5h	• ~Instant surface disorder • Some DEHP leached into water
Plastic/Silica Interface	• Gradual CHCl disorder • CH_3/CH_2 changes unclear	• CH_2 point in opposite direction of CH_2 on surface • Gradual water penetration • Some DEHP CH_3 remains ordered at 1.5h	• Water penetrates film quickly • Gradual ↓ in order of all C-H groups from water • Little C-H order remains at 1.5 h

More importantly, this method of analysis aids in explaining a signal phenomenon in the SFG field where SFG studies of polymers yield different spectral signals under different sample geometries. Through quantitative analysis we have proven that in some cases, SFG prism spectra of thin films are different than window spectra not because of bulk signal contribution, but because of multi-interface signal convolution. This analysis can be applied to many other thin-film systems analyzed using SFG to identify the interfacial origins of SFG signals and/or study molecular group behaviors at two interfaces simultaneously.

Lastly, the films studied were simple models of PVC plastics, but it is well known that many PVC plastics contain leached plasticizers present on surfaces available to contact water. Therefore, the results from these studies suggest that when real PVC plastics are contacted with water, the molecular surfaces of the plastics may change drastically and if plasticizers are present on the surface, small amount of plasticizer molecules may escape from the plastic and permanently transfer to other surfaces through water contact. Thus, this transfer process has the potential to occur every time a plastic containing surface phthalates comes into contact with water. Small amounts of phthalates can be transferred from plastic surfaces into water many

times over the plastic lifetime and the cumulative events have the potential to transfer many phthalates to new environments via a previously unreported transfer route.

5.5 References

1. Staples, C. A.; Peterson, D. R.; Parkerton, T. F.; Adams, W. J. *Chemosphere* **1997**, *35*, 667.
2. Wang, X. L.; Lin, Q. X.; Wang, J.; Lu, X. G.; Wang, G. P. *Ecol. Eng.* **2013**, *51*, 10.
3. Zieminski, K. F.; Peppas, N. A. *J. Appl. Polym. Sci.* **1983**, *28*, 1751.
4. Oehlmann, J.; Schulte-Oehlmann, U.; Kloas, W.; Jagnytsch, O.; Lutz, I.; Kusk, K. O.; Wollenberger, L.; Santos, E. M.; Paull, G. C.; Van Look, K. J. W.; Tyler, C. R. *Philos. Trans. R. Soc. Lond., Ser. B: Biol. Sci.* **2009**, *364*, 2047.
5. Jaeger, R. J.; Rubin, R. J. *Science* **1970**, *170*, 460.
6. Chen, C. W.; Chen, C. F.; Dong, C. D. *Soil. Sediment. Contam.* **2013**, *22*, 119.
7. Chen, L.; Hook, D. J.; Valint, P. L.; Gardella, J. A. *J. Vac. Sci. Technol. A* **2008**, *26*, 616.
8. Delcroix, M. F.; Zuyderhoff, E. M.; Genet, M. J.; Dupont-Gillain, C. C. *Surf. Interface Anal.* **2012**, *44*, 175.
9. Hahner, G. *Chem. Soc. Rev.* **2006**, *35*, 1244.
10. Yoon, T. H. *Appl. Spec. Rev.* **2009**, *44*, 91.
11. Leung, B. O.; Brash, J. L.; Hitchcock, A. P. *Materials* **2010**, *3*, 3911.
12. Hankett, J. M.; Liu, Y. W.; Zhang, X. X.; Zhang, C.; Chen, Z. *J. Polym. Sci. Part B: Polym. Phys.* **2013**, *51*, 311.
13. Hsiao, E.; Barnette, A. L.; Bradley, L. C.; Kim, S. H. *ACS Appl. Mat. Int.* **2011**, *3*, 4236.
14. Zuo, B.; Hu, Y.; Lu, X.; Zhang, S.; Fan, H.; Wang, X. *J. Phys. Chem. C* **2013**, *117*, 3396.
15. Chen, Z.; Shen, Y. R.; Somorjai, G. A. *Annu. Rev. Phys. Chem.* **2002**, *53*, 437.
16. Hankett, J. M.; Collin, W. R.; Chen, Z. *J. Phys. Chem. B* **2013**, *117*, 16336.
17. Shen, Y. R. *Nature* **1989**, *337*, 519.
18. Clarke, M. L.; Chen, C.; Wang, J.; Chen, Z. *Langmuir* **2006**, *22*, 8800.
19. Rangwalla, H.; Schwab, A. D.; Yurdumakan, B.; Yablon, D. G.; Yeganeh, M. S.; Dhinojwala, A. *Langmuir* **2004**, *20*, 8625.
20. Miyamae, T.; Akiyama, H.; Yoshida, M.; Tamaoki, N. *Macromolecules* **2007**, *40*, 4601.
21. Miyamae, T.; Yokoyama, H.; Han, S.; Ishizone, T. *e-J. Surf. Sci. Nanotech.* **2006**, *4*, 515.
22. Beaman, D. K.; Robertson, E.J.; Richmond, G. L. *PNAS* **2011**, *109*, 3226.
23. Beaman, D. K.; Robertson, E. J.; Richmond, G. L. *Langmuir* **2012**, *28*, 14245.
24. Hu, D.; Yang, Z.; Chou, K. C. *J. Phys. Chem. C.* **2013**, *117*, 15698.
25. Li, G.; Dhinojwala, A.; Yeganeh, M. S. *J. Phys. Chem. C* **2011**, *115*, 7554.
26. Prasad, S.; Zhu, H.; Kurian, A.; Badge, I.; Dhinojwala, A. *Langmuir* **2013**, *29*, 15727.
27. Ni, H. G.; Li, X. H.; Hu, Y. Y.; Zuo, B.; Zhao, Z. L.; Yang, J. P.; Yuan, D. X.; Ye, X. Y.; Wang, X. P. *J. Phys. Chem. C.* **2012**, *116*, 24151.
28. Leung, B. O.; Yang, Z.; Wu, S. S. H.; Chou, K. C. *Langmuir* **2012**, *28*, 5724.
29. Chen, C.; Clarke, M. L.; Wang, J.; Chen, Z. *PCCP* **2005**, *7*, 2357.
30. Noguchi, H.; Hiroshi, M.; Tominaga, T.; Ping Gong, J.; Osada, Y.; Uosaki, K. *PCCP* **2008**, *10*, 4987.
31. Feller, M. B.; Chen, W.; Shen, Y. R. *Phys. Rev. A* **1991**, *43*, 6778.
32. Wilk, D.; Johannsmann, D.; Stanners, C.; Shen, Y. R. *Phys. Rev. B* **1995**, *51*, 10057.
33. Lambert, A. G.; Neivandt, D. J.; Briggs, A. M.; Usadi, E. W.; Davies, P. B. *J. Phys. Chem. B* **2002**, *106*, 10693.
34. McGall, S. J.; Davies, P. B.; Neivandt, D. J. *J. Phys. Chem. B* **2004**, *108*, 16030.

35. Tong, Y. J.; Zhao, Y. B.; Li, N.; Osawa, M.; Davies, P. B.; Ye, S. *J. Chem. Phys.* **2010**, *133*.
36. Tong, Y. J.; Zhao, Y. B.; Li, N.; Ma, Y. S.; Osawa, M.; Davies, P. B.; Ye, S. *J. Chem. Phys.* **2010**, *133*.
37. Lu, X. L.; Clarke, M. L.; Li, D. W.; Wang, X. P.; Xue, G.; Chen, Z. *J. Phys. Chem. C.* **2011**, *115*, 13759.
38. Backus, E. H. G.; Garcia-Araez, N.; Bonn, M.; Bakker, H. J. *J. Phys. Chem. C.* **2012**, *116*, 23351.
39. Lu, X.; Clarke, M. L.; Li, D.; Wang, X.; Xue, G.; Chen, Z. *J. Phys. Chem. C* **2011**, *115*, 13759.
40. Hankett, J. M.; Welle, A.; Lahann, J.; Chen, Z. *J. Appl. Polym. Sci.* **2014**.
41. Zhang, X.; Chen, Z. *Langmuir* **2014**.
42. Krimm, S.; Shipman, J. J.; Folt, V. L.; Berens, A. R. *J. Polym. Sci. Part A* **1963**, *1*, 2621.
43. Enomoto, S.; Asahina, M. *J. Polym. Sci. Part A* **1966**, *4*, 1373.
44. Zhang, X. X.; Zhang, C.; Hankett, J. M.; Chen, Z. *Langmuir* **2013**, *29*, 4008.

CHAPTER 6

MOLECULAR INTERACTIONS OF NONYLPHENOL WITH PLASTIC UNDER MODEL ENVIRONMENTAL CONDITIONS

6.1 Background and Motivation

The research in Chapter 6 changes from studying molecular behaviors of a specific plastic type to investigating how prominent environmental toxins may interact with hydrophobic plastic surfaces under different ecological platforms, mainly dry land versus the headspace above a body of fresh water. SFG was used to probe the surfaces of common hydrophobic plastic poly(styrene) (PS) during and after exposure to gas phase environmental toxin molecules nonylphenols (NP)s. The role of water on the deposition of toxins was studied with SFG, ATR-FTIR, and QCM. In addition, a new SFG sample stage setup was developed to study gas-phase deposition and/or reactions on surfaces. This research was performed as part of a multidisciplinary effort at the University of Michigan to elucidate the effects of microplastics on the ecological health of the Great Lakes, led by research scientist Dr. Melissa Duhaime.

Two major factors in understanding how microplastics influence biota in the great lakes involve quantifying and cataloging microbial communities supported by microplastics, and gathering information on how/what local toxins deposit and desorb from the plastics under different conditions including lake water, atmosphere, and inside living organisms. The presented research here aims to start addressing the latter factor. Here one type of model toxin of interest is studied in detail. This category of toxin, the nonylphenols (NPs), has not only been

prominent in the Great Lakes for decades, but NPs have similar physical properties and molecular structures to many other categories of toxins found in the Lakes' ecosystems. The following paragraphs explain in more detail the impact of NP on the Great Lakes, our model of study, and the intent of the research.

NPs are a class of endocrine disrupting alkylphenols manufactured industrially at large volumes as precursors and additives for a wide variety of products including industrial detergents, emulsifiers, paints, lubricants, personal care products, and nonionic surfactants. [1,2] NPs are acute and chronic toxicants for aquatic organisms and highly suspected human reproductive toxicants. NP structure varies from a linear nine carbon alkyl chain to branch conformations off of a phenol ring. (See Figure 6.1 for a structure of a generic NP isomer.) Industrially, no single isomer of NP is utilized for surfactant production and a mixture of isomers can be found in both manufactured products and natural environments including aquatic ecosystems, agricultural and urban environments.[3-7] The branched isomers tend to dominate isomer mixtures.[8,9]

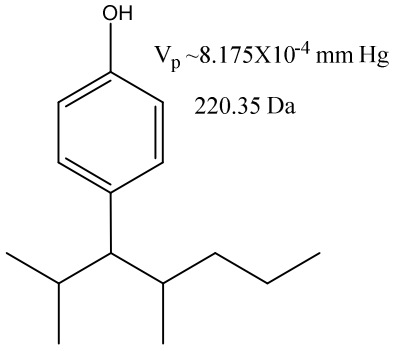

Figure 6.1. 4-nonylphenol molecular structure of a branched isomer.

In 2014, due to the proliferation of NPs in natural aquatic ecosystems and the molecule's potential adverse effects on the environment, the EPA added the category of nonylphenols to the Toxic Release Inventory list of reportable chemicals, officially highlighting these molecules as a

danger to aquatic organisms and adding mandated action plans to reduce NP production and evaluate NP sources.[10] NPs also appear on many pharmaceuticals and personal care products indicator lists as marine endocrine disruptors and xenoestrogens. Correlations between the feminization of male fish with NP environmental exposure indicate that NP potentially poses a large threat to the reproduction of fish species. Ecosystems especially of concern are watersheds where large volumes of NPs may collect after manufacturing, production, and use.[3] As can be expected, the Great Lakes in the United States meet such criteria. Here, not only are ppm levels of NP and other alkylphenol concentrations reported in and above river estuaries, in the surface waters of Great Lake basins and in wastewaters, but there exist artificial sinks in the form of microplastics for NPs to adsorb and/or transfer through different ecosystem platforms.[4,11-17]

These microplastics, which often originate from personal care product waste, synthetic clothing, consumer waste products, and industrial plastic manufacturing, are most commonly found in the epipelagic (surface) layer of the water column. The low density of the plastic materials allows for buoyancy, and thus microplastics can provide large surface areas for toxin adsorption at the water/air interface. Collected microplastics from marine water systems have been previously reported to contain NP and endocrine disruptor toxins with similar K_{ow} values to NPs such as phthalates, bisphenol A and PCBs. However, freshwater microplastics remain comparatively less studied.[15,18-24]

The lack of information on freshwater microplastics does not indicate that there are no scientists researching the impacts of microplastics on freshwater ecosystems. Rather, this field is much newer, and many studies are in their infancy. Currently, determining the role of these non-native materials in toxin collection and subsequent release in local biota is an increasingly popular field of study.[25-27] As of yet, little is currently understood as to the behaviors of toxin

deposition, adsorption, and desorption on microplastics. This includes knowledge of where and how toxins like NP may deposit on these artificial sinks and the permanence of such deposition. Information beyond basic applied and theoretical adsorption studies generated from K_{ow} values of toxin and surface energies of plastics is greatly lacking.[18]

In this Chapter, SFG studies reveal that the headspace above calm (fresh) water provides an excellent environment for NP deposition onto poly(styrene) plastic surfaces. NP is studied as an environmentally relevant model toxin, and PS as a model hydrophobic plastic. Experiments were designed to mimic the addition of a new NP point source under an environment consisting of a microplastic floating on a freshwater lake surface at warm temperatures, and a microplastic located on land under dry and warm conditions as closely as possible. To validate our Laurentian model, a set of experiments used water collected from Lake Erie spiked with a known concentration of nonylphenol. In this manner, we demonstrate that even a calm environment (lack of waves and/or high winds) may result in gaseous phase NP deposition on plastic.

In addition, we surmise that humidity can dramatically affect how NP molecules deposit on plastic surfaces and aim to show that deposition may occur differently on plastics over land mass rather than water or in high humidity environments. We demonstrate different NP deposition behaviors depending on humidity and study the presence of interfacial water on plastics during the deposition. Lastly, we test the permanence of NP deposition on PS under humid or dry environments by adding agitating factors after deposition including exposure of the plastic with toxin to clean air and to moving water. Once again, SFG is the analytical tool of choice for the main experiments, probing the gas-phase deposition of NP on plastics *in situ* in real time. SFG has been proven well suited to study the *in situ* deposition and ordering of toxins on plastics at a molecular level in real time.[28-30] Additionally, SFG is capable of yielding key

insights into how molecules deposit and re-order during and after deposition processes.[31-36] Lastly, this Chapter also presents a new sample chamber designed to study gas-phase adsorption/desorption and reactions at interfaces under standard atmospheric conditions, applied vacuum, or regulated vapor generation. The basis for this setup follows traditional SFG sample chambers previously used for high pressure experiments.[37] By combining information from SFG, quartz crystal microbalance (QCM), and attenuated total internal reflectance-Fourier transform infrared spectroscopy (ATR-FTIR) measurements, the effects of plastic surface structure, water content, and environmental factors on the quantity and ordering behaviors of NP molecules adsorbed and desorbed from plastic surfaces were determined.

6.2 Experimental Methods

6.2.1 Materials

Deuterated Poly(styrene) PS-d_8 (M_w 198000; M_n 165000) and poly(ethylene terephthalate) PET-d_4 (M_v 72000; M_w/M_n broad) were obtained from Polymer Source Inc (Dorval, QC Canada). Solvents toluene ≥99.3% purity, 2-chlorophenol (99+%) and deuterium oxide (99.9% atom D) were obtained from Sigma Aldrich (St. Louis, MO). 4-nonylphenol (analytical standard, technical mixture, CAS 84852-15-3) was purchased from Fluka (St. Louis, MO). All chemical materials were used as received.

6.2.2 Sample Preparation

Right angle calcium fluoride prisms (Altos Photonics) were utilized for SFG measurements and were cleaned with a Contrex soap solution, rinsed with deionized water (Millipore), dried with a stream of nitrogen gas (N_2) and then exposed to glow discharge air plasma for 4 min with a PE-50 series Plasma System (Plasma Etch, Inc.). Zinc selenide (ZnSe)

crystals were used for ATR-FTIR experiments and were cleaned using an Alconox soap solution, water, ethanol, acetone, deionized water (Millipore), dried with a stream of nitrogen gas and exposed to air plasma for 1 min. 10 MHz quartz crystals, etched surface, Au electrode (International Crystal Manufacturing) were used for QCM experiments and crystals were immersed in toluene, extensively rinsed with toluene and ethanol, and then dried with a stream of N_2 for at least 5 min prior to film deposition.

1.5 wt% solutions of PS-d_8 were prepared with toluene in glass vials to prepare the plastic thin films. Solutions were mixed using a vortex mixer (Vortex-Genie 2T, Scientific Industries Inc.) until clear. A P-6000 spin coater (Speedline Technologies) was used to prepare all plastic films. Samples were spin coated at 3000 rpm for 30 s on calcium fluoride prisms for SFG experiments, at 2000 rpm for 40 s on a ZnSe crystal for ATR-FTIR experiments, and at 1500 rpm for 30 s on quartz crystals for QCM experiments. All films were prepared one day prior to experiments. After films were prepared on optical substrates, a stream of N_2 was applied for 3-5 min to help remove trapped solvent. Prepared substrates were then placed in a clean petri dish purged with N_2 which was put in a chemical hood overnight. The day of SFG, ATR-FTIR, or QCM experiments, N_2 was again applied to plastic films for 2-3 min to ensure solvent removal. Deuterated polymer was utilized to avoid spectral overlap of toxin and plastic for SFG experiments, and the same polymer was utilized for ATR-FTIR and QCM experiments for consistency.

6.2.3 Experimental Chamber Preparation

To prepare the experimental chamber for SFG experiments, extensive cleaning steps were performed 1 day prior to analysis. The two glass pieces (top and bottom of the chamber) were

cleaned as follows: washed with Contrex soap solution, rinsed with deionized water, rinsed with methanol, ethanol, and then ~1L Millipore water before drying with nitrogen gas. The quartz windows (SPI Industries) were cleaned with Contrex soap solution, deionized water, quickly rinsed with methanol, ethanol, and Millipore water, dried with nitrogen gas, and then further cleaned by application of glow discharge air plasma for 2 min on both sides of the quartz windows. The screw cap and o-ring were cleaned with Contrex soap solution, deionized water, ethanol, and rinsed with Millipore water before drying with nitrogen gas. After all parts were cleaned, the chamber windows were assembled using silicone-free polyimide tape and the chamber was placed on clean room paper and covered with plastic to prevent contamination. The prism holder and optic pole were cleaned the day of analysis. The prism holder was cleaned in the same manner as the two glass chamber pieces. The optic pole was cleaned with ethanol and Millipore water and then dried.

6.2.4 Instrumentation

6.2.4.1 SFG

The details of SFG theory and experimental setup have been extensively outlined in the introduction Chapter of this thesis and elsewhere.[32,40,41] SFG has been widely applied to gather molecular-level information of a variety of surfaces and interfaces like plastics exposed to model environmental conditions and in aqueous environments.[28-30,38-41] The SFG experiments were taken using ssp and ppp polarization combinations. The surface area of analysis is approximately 0.19 mm^2, ideal to model the appropriate surface area of a microplastic. All presented SFG spectra in this Chapter were normalized to the intensity of the visible and IR beams except for water spectra (Figure 6.11) which were normalized to visible only to avoid

creating false peaks. All spectra were obtained with a short pass 532 nm filter placed in the signal beam path to block visible light scattering from the detector. The spectra obtained in D_2O (Step 3 of SFG experiments) were not corrected for changes in Fresnel coefficients. Details on SFG setup for these particular experiments can be found in the next section as well.

6.2.4.2 ATR-FTIR

ATR-FTIR experiments were performed on PS-d_8 to further study the presence of interfacial water (water on the plastic surface) during nonylphenol deposition under humid conditions. FTIR spectra were obtained on a Nicolet 6700 spectrometer with a golden gate trough-style ATR accessory stage. A ZnSe ATR prism coated with PS-d_8 was used as background.

6.2.4.3 QCM

The QCM instrument was an RQCM, Model 246H (Maxtek, Inc., Cypress, CA). The Maxtek RQCM data logging software from Inficon was used during data collection. Post collection, frequency data was converted to mass according to the well-known Sauebrey equation using OriginLab 9.0. The plotted mass shown in the paper was normalized to the surface area of the prism utilized for SFG, (0.25 in^2).

6.2.5 Experimental Details

6.2.5.1 SFG Chamber Setup Details

The custom made sealed chamber system used at the SFG sample stage was held at ambient conditions and consisted of glass with two 1 mm thick quartz windows to allow penetration of input and output laser beams (Figure 6.2). Windows were held on with silicone-

free 3M polyimide tape applied to the outer edges of the windows as previously mentioned. No vacuum or external gases were applied to the chamber and gas inlet and outlet were sealed during SFG experiments. Prisms were held film-face down in a custom made sample holder open to air. The prism holder was attached to the lid of the chamber using an o-ring and as such the bottom of the chamber could be easily removed without disturbing the placement of the prism. To seal the bottom of the chamber to the top, the edges of the flanged glass were pinned shut with metal clips. Prisms were set to hang 3 mm above the toxin source which was applied to the floor of the chamber for all experiments (see experimental diagram). To check the integrity of deuterated plastic films, prisms were placed inside the clean chamber and spectra were obtained "*in situ*" under normal conditions prior to adding toxin. Standardized experiments to quantify the loss of spectral signals from absorption by the quartz windows revealed about a 10% reduction in signal intensity.

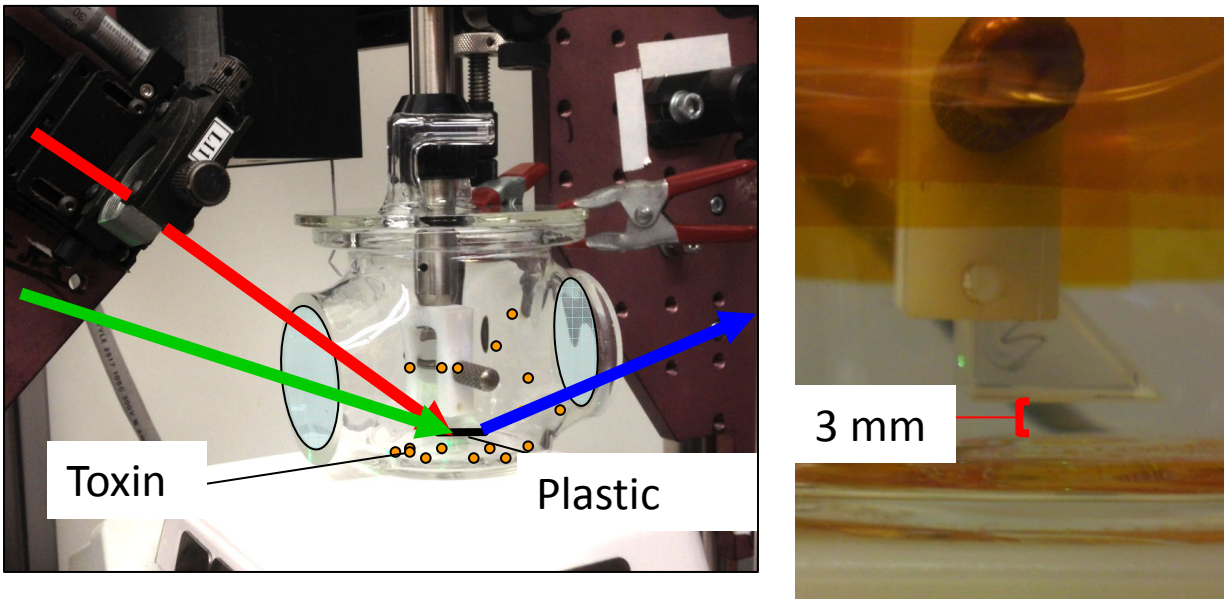

Figure 6.2. (Left) Picture of chamber set up on the SFG sample stage. Here, the prism with spin coated plastic is held above a toxin point source on the bottom of the chamber. Note that the quartz windows and some metal clips have been removed for image clarity. (Right) Zoom in on height of prism with spin coated plastic at 3 mm above toxin source.

6.2.5.2 Model Deposition of NP on Plastics Under Dry Environments

For all SFG experiments, prisms were placed inside the sealed custom made sample chamber at ambient conditions. To test the deposition of gaseous phase NP on polystyrene plastic under "dry" conditions, three droplets of NP (~50 μL) were added to the bottom of the chamber directly underneath the prism with PS-d_8 plastic film. A needle was used to spread the NP across the bottom of the chamber to an area of ~1 cm^2. Under these conditions, the maximum concentration of NP in air is ~1 ppm. Due to the low volatility of NP, the experiments model a case where a plastic is exposed to a new point source of NP under dry conditions.

The experiment consisted of four main steps: 1. ~3 min after the bottom chamber was prepared with NP, it was re-attached to the top of the chamber and SFG spectra were obtained as soon as the chamber was secured. The sample was left in the chamber for a total of 2.5h. 2. The bottom half of the chamber was removed and the prism exposed to lab air for 1h. 3. ~1 mL of D_2O in a clean Teflon holder was pushed upwards to touch the plastic film using a lab jack for 30 min. A small stir bar was run at 125 rpm to agitate the system. 4. The D_2O was lowered and the plastic film was again exposed to lab air for 1h. SFG spectra were obtained *in situ* in all conditions, and in this manner we were able to develop insights into how NP molecules deposit on plastics under dry conditions, and test the permanence of deposition after the plastic has been exposed to different agitating environments (clean air, moving water, and air again). All experiments were conducted with a room humidity of 19-21%.

6.2.5.3 Model Deposition of NP on Plastics Under Humid Environments

SFG experiments for the deposition of gaseous phase NP on PS-d_8 under humid conditions were completed in an identical manner to the dry condition experiments, except that

the pure NP droplets were substituted with 3 mL of a super saturated (micelle) 100 ppm solution of NP in D_2O (H_2O was used in separate interfacial water ordering studies). The plastic film was placed 3 mm above the toxin source (water surface). Under these humid model conditions, the maximum concentration of NP is estimated to be much lower (9 ppt) due to the competing evaporation of water. These sets of experiments allowed us to better understand how NP interacts with plastics that exist just above a water surface or under very humid conditions (i.e. plastic particles that float on a body of water) and how the addition of humidity can alter toxin deposition on plastics.

To visually summarize the setup for SFG experiments, an experimental diagram outlining the 4 steps can be seen below in Figure 6.3:

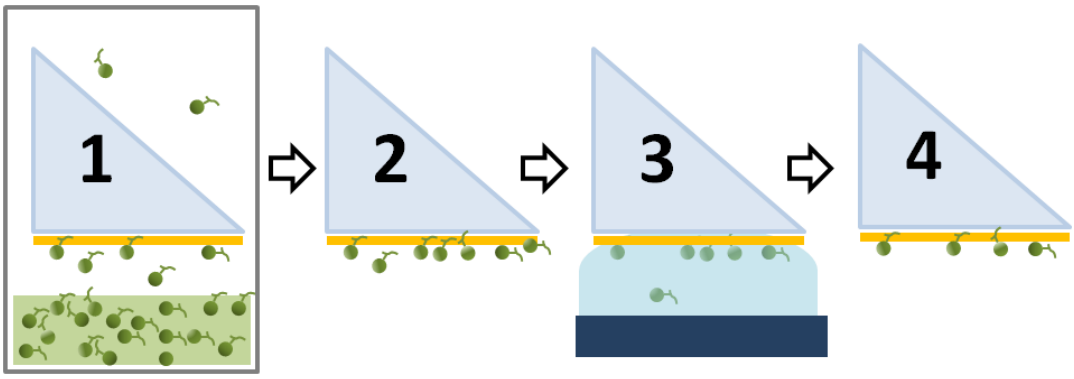

Figure 6.3. SFG experimental setup: 1. Plastic surface is introduced to gas phase NP molecules either by placing neat NP or NP/D_2O mixture under optical prism for 2.5h; 2. Chamber containing NP or NP/D_2O is removed and plastic is exposed to clean air for 1h; 3. To agitate system, plastic is contacted to D_2O stirred at 125 rpm for 30 min; 4. Water is removed and plastic is exposed to air for 1h.

6.2.5.4 QCM Experimental Details

To gain an estimate on the mass of NP molecules deposited on PS-d_8 under both dry and humid situations, QCM experiments were conducted in a similar manner to steps 1-2 of SFG experiments using a custom made crystal holder that fit exactly in the experimental chamber. Baseline QCM frequencies were measured in lab air prior to toxin introduction. Quartz crystals with plastic coatings were held 3 mm above pure NP, 100 ppm NP solutions, or 3 mL of D_2O. QCM measurements were obtained for 3h of NP exposure under dry conditions, humid conditions, or exposure to humidity alone (D_2O). Afterwards the bottom of the chamber was removed and the crystal exposed to clean air and QCM measurements were obtained for approximately 20 min.

6.2.5.5 ATR-FTIR Experimental Details

To prepare the humid environment, a solution of 100 ppm nonylphenol in D_2O was applied to a glass slide and excess liquid shaken off. This slide was placed approximately 3 mm above the surface of the ATR prism with plastic coating, and the system was roughly sealed. Non-polarized spectra were obtained from 650 cm^{-1} to 4000 cm^{-1}. Spectra were obtained upon addition of the slide, and every 3 min until 35 min. Spectra have been corrected for CO_2 absorption and are presented in the range of 1900-3100 cm^{-1} for clarity.

6.3 Results and Discussion

6.3.1 QCM Studies of NP and D_2O Deposition on PS

QCM experiments were performed to estimate the mass of NP deposited on PS-d_8 plastic under model dry and humid conditions. To summarize, one face of a QCM crystal coated with plastic was exposed to a "point source" of gas-phase NP under dry conditions (19% humidity), humid conditions (3 mm above water/NP solution), and humid conditions with no NP present (above water only) in the experimental chamber. Representative QCM mass deposition and desorption curves can be found in Figure 6.4. The data in this figure have been normalized to the theoretical mass deposited on the surface area of a plastic film on a calcium fluoride prism utilized in the SFG experiments.

A representative QCM mass deposition curve for NP deposited on PS-d_8 under dry conditions is found in Figure 6.4a. As expected, under dry conditions, a monotonic curve indicating increase in mass deposited on the plastic covered crystal is observed. At 2.5h, when the chamber with NP is removed for SFG experiments, QCM results yield an estimate that approximately 195 ng of NP have been deposited. Repeated experiments revealed total NP mass deposited under dry conditions varied from 136 to 213 ng. Both QCM and SFG results (shown later) indicate a constant rate of deposition from start to 2.5h.

In order to correctly interpret the QCM and SFG results in this Chapter, the masses given by QCM must be compared to the mass of a single layer of NP deposited on the plastic. The minimum mass of a single monolayer on the surface of the plastic was calculated twice using a simple sum of triangles to estimate the surface area of two completely flat NP isomers. Both calculations yielded similar estimates in masses, on the order of 170 ng. Because both

calculations assumed a planar surface area of contact, the calculated mass of a monolayer must be the minimum value. Therefore, the deposited mass of NP on PS under dry conditions varies from slightly under to slightly greater than that of the calculated single monolayer of NP molecules.

More importantly, every mass deposition/desorption curve collected under dry conditions revealed that much less than a monolayer of NP molecules remained on the plastic surface after the point source was removed and the plastic exposed to clean air for ~20 min (the deposition and desorption curve shown in Figure 6.4b is from one sample). If the deposition and desorption amounts are subtracted, after 20 min of clean air exposure approximately 65 ng of NP remain on the plastic. Repeated experiments show a stabilized mass deposited from 19 to 65 ng.

Next, the QCM results of the deposition of D_2O only on PS under humid conditions are studied. The sorption of D_2O is not monotonic, and consists of a very rapid initial increase and a plateau followed by a slower increase towards equilibrium (Figure 6.4a). Because we are modeling the appearance of a point source of molecules rather than studying a system already at vapor equilibrium or with constant vapor generation, our QCM measurements are actually representations of both adsorption and evaporation of molecules from the plastic surface. This is dependent on many factors, including evaporation rate of D_2O from the bulk source, the partition coefficient of D_2O into the PS-d_8 film, and the equilibrium between surface sorption and desorption. The rapid increase is due to the large vapor phase concentration difference between room air (19% humidity) and the sealed chamber. The slower approach to equilibrium is likely dependent on the evaporation of D_2O and the equilibrium between the vapor phase D_2O and the film. Virtually no water is left in/on the plastic once the system is exposed to air for 20 min, as can be seen in the D_2O desorption curve in Figure 6.4b. In fact, most of the D_2O leaves the

system within the first minute of exposure to dry room air. Repeated experiments revealed a varying mass of D_2O deposited on the surface, which likely occurred due to slight changes in humidity and plastic surface dryness. Results varied from deposition of 500 to 1005 ng. Theoretically a monolayer of water should weigh more than 1230 ng, so less than a monolayer of water is deposited during this time. Regardless of initial mass deposited, virtually all water evaporated, with no evidence of increased mass after 20 min of air exposure.

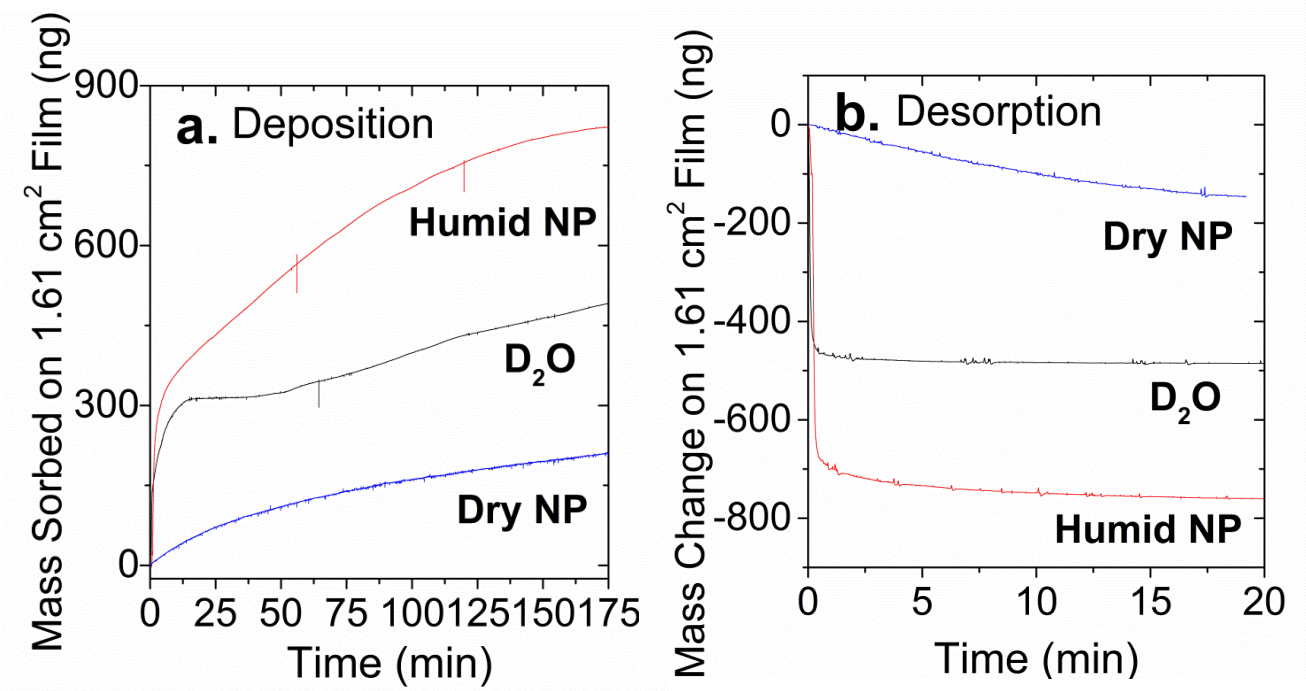

Figure 6.4a. QCM curves of mass deposition on PS-d_8: NP only under dry conditions; D_2O only under humid conditions; NP under humid conditions; 6.4b. Corresponding QCM curves of mass desorption once the three systems are exposed to clean air.

When studying the curve generated when NP is deposited on PS-d_8 under humid conditions, the rate changes seen with the water deposition are no longer observed. Once again a constant rate of mass is deposited upon the crystal denoted by a smooth curve. Total mass deposited varied from 330 to 824 ng, and deposition of mass was always constant, although the total mass is statistically insignificant to the runs of water only. Once again this is because small

changes in surrounding environments changed the mass of water deposited on a given experiment. More important is the result from the humid/NP desorption curve (Figure 6.4b). Here after 20 min of air exposure approximately 62 ng of mass remains. Regardless of initial deposition of NP under humid conditions, the mass remaining after 20 min of drying is similar, varying from 33 to 62 ng.

This means a similar amount of total NP molecules remain in/on the PS plastic when the NP source is located in a model lake system compared to dry conditions, according to the QCM mass desorption curves (Figure 6.4b), even though NP was present in ppt concentrations under humid conditions rather than ppm concentrations calculated in the absence of D_2O. This was unexpected, given the much lower number of available NP molecules in the former case. But results indicate enough mass of NP was deposited under both conditions such that an equilibrium concentration of NP in/on PS was reached. This value does not represent a potential maximum NP concentration, however. If the point source of NP remains for longer periods of time, more mass may be deposited on the PS and sorb into the plastic, increasing the amount of stable deposited NP molecules.

6.3.2 Introduction to NP and Analysis of SFG Results

Before studying the SFG spectra obtained in these experiments, it is important to show the ssp SFG spectra of the isomer mixture of NP itself, displayed in Figure 6.5. Important signatures to note are the CH_3(s) peak at 2875 cm^{-1}, clearly observed above the CH_2 signatures and Fermi resonance, and the phenyl ring signatures observed around 3030 cm^{-1} and 3050 cm^{-1}. The 3030 cm^{-1} peak is specifically assigned to a C-H stretching mode of the phenyl ring: v_{20b} mode in accordance with previous SFG literature.[42] The SFG signals associated with two

functional groups on NP: 2880 cm^{-1} and 3030 cm^{-1} are used to monitor NP deposition and desorption in real time. These two functional group signatures are chosen for this study because NP typically yields very strong 2880 cm^{-1} signal which has minimal spectral overlap with other C-H range NP peaks (as shown in Figure 6.5) and the NP 3030 cm^{-1} is observable on deuterated PS surfaces and deuterated PET surfaces which were studied as well (results not shown in this thesis, however).

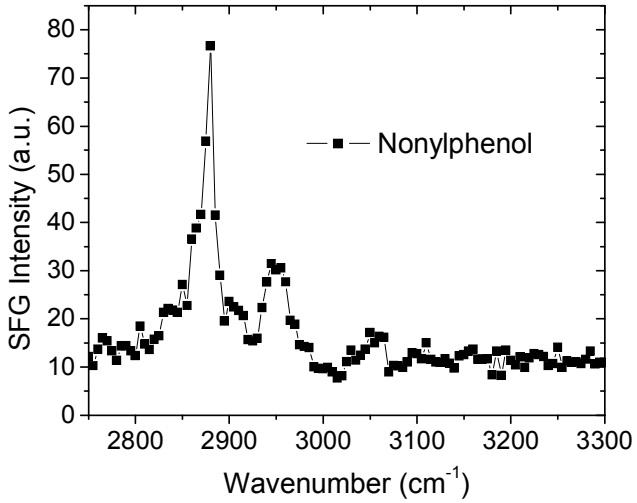

Figure 6.5. SFG ssp spectra of nonylphenol spin coated on a CaF_2 prism in air.

6.3.3 NP Adsorption/Desorption on PS Under Dry Conditions

SFG experiments were completed to model molecular surface changes of PS microplastic exposed to a new point source of NP air-borne molecules under dry conditions. The SFG time-dependent spectra obtained during exposure of PS-d_8 to NP in air for 2.5h can be seen in Figure 6.6a. Here, the NP SFG signals 2880 cm^{-1} (CH_3 (s)) and 3030 cm^{-1} (C-H stretching of the phenyl ring v_{20b} mode) are tracked for two hours.

It can be clearly observed that the CH_3(s) signal increases steadily similar to a gas phase mass deposition curve, indicating a consistent rate of deposition which matches QCM results.

The phenyl signature, however, remains low in intensity and only slightly increases, suggesting that the phenyl rings are highly disordered during the deposition process but the CH_3 groups remain at least somewhat ordered. After about 1.75h the signal intensities of the CH_3(s) and phenyl group no longer change, indicating a stabilized surface structure.

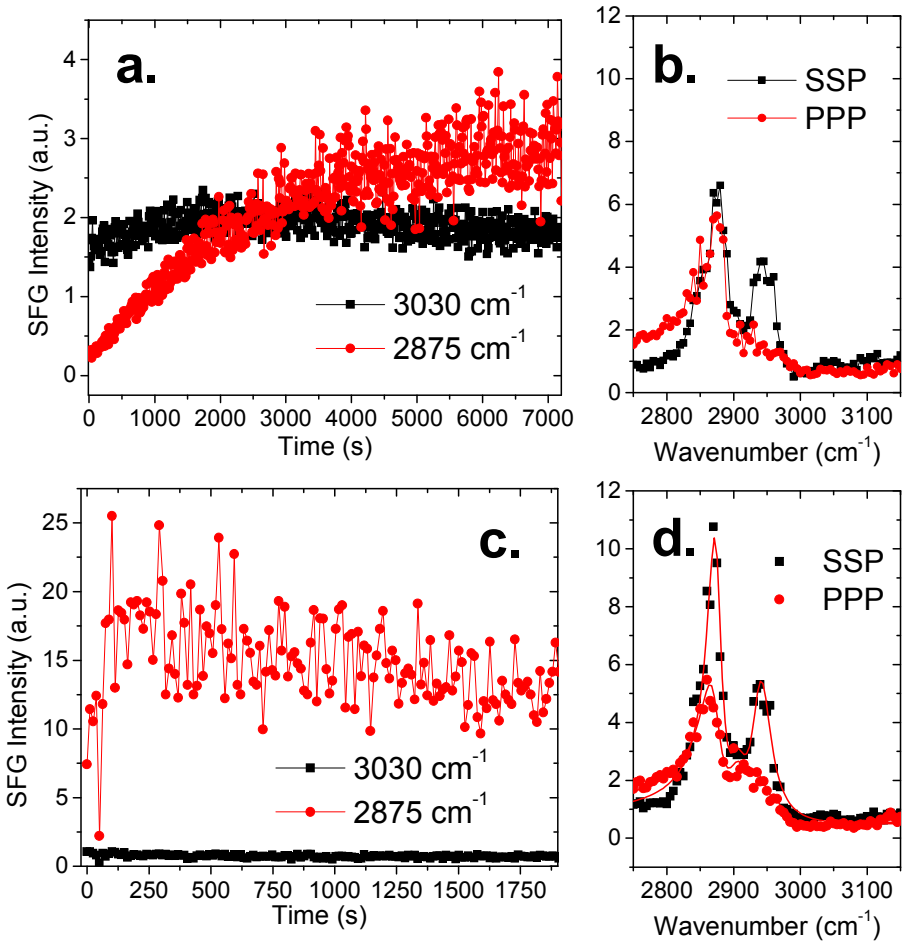

Figure 6.6. SFG results: 6.6a. Time dependent ssp signals during NP deposition process on PS-d_8 in dry chamber; 6.6b. The ssp and ppp spectra obtained after 2h of exposure in chamber; 6.6c. Time dependent ssp signals obtained once chamber is removed; 6.6d. The ssp and ppp spectra obtained after 40 min of exposure to clean air with fits shown as red lines and data as points.

At about the 2h mark of the deposition process, ssp and ppp SFG spectra are obtained in the chamber and can be seen in Figure 6.4b. If we recall the conclusions for mass deposition

studied with QCM, it is likely that more than a monolayer of NP molecules is present on the plastic at this point. Therefore, quantitative calculations regarding the orientation of any functional groups may not accurately reflect surface group behaviors. SFG spectra can reveal however, how the NP molecules are generally ordered on the PS surface under dry conditions with NP gas-phase molecules present in air. The SFG results show the presence of strong CH_3 peaks but very weak phenyl signal. This indicates that during the deposition process the CH_3 groups on NPs are generally ordered, but the phenol rings of NP lay relative flat on the plastic surface or are buried.

Next, the point source of NP was removed and the plastic surface exposed to clean air for 1h through the removal of the bottom of the sample chamber. Figure 6.6c shows the time-dependent SFG signals of this process. The initial decrease in intensity, due to the removal of the chamber and temporary blocking of laser beams, is followed by a dramatic increase in intensity (note a.u. of 25 versus 4 in the chamber). While some of the increase is due to the removal of quartz windows from the incoming and outgoing beam paths, the remaining increase is due to molecular reordering, indicating that the CH_3 groups stand up more toward the hydrophobic air surface upon exposure to clean air. Decreases in signal with increased air exposure time can be attributed to the loss of surface molecules through evaporation (as shown in QCM results). SFG signals show a stable surface structure is reached at about 30 min, when methyl and phenyl signals remain constant. This indicates at this time point, once some NP molecules on the topmost surface have been removed to leave less than a monolayer of NP molecules, a more stable, ordered layer of NP remains. SFG spectra taken after 45 min of clean air exposure show clear CH_3(s) and corresponding Fermi resonance signals. SFG calculations reveal the CH_3(s) groups order with an average tilt angle of 44° to the surface normal. This

number does not reflect a single orientation across all CH_3 groups, but an average since 12 isomers of NP will likely yield multiple CH_3 orientations. We can conclude that the NP molecules are oriented such that phenol rings lying flat on the plastic and CH_3 groups pointed towards the air.

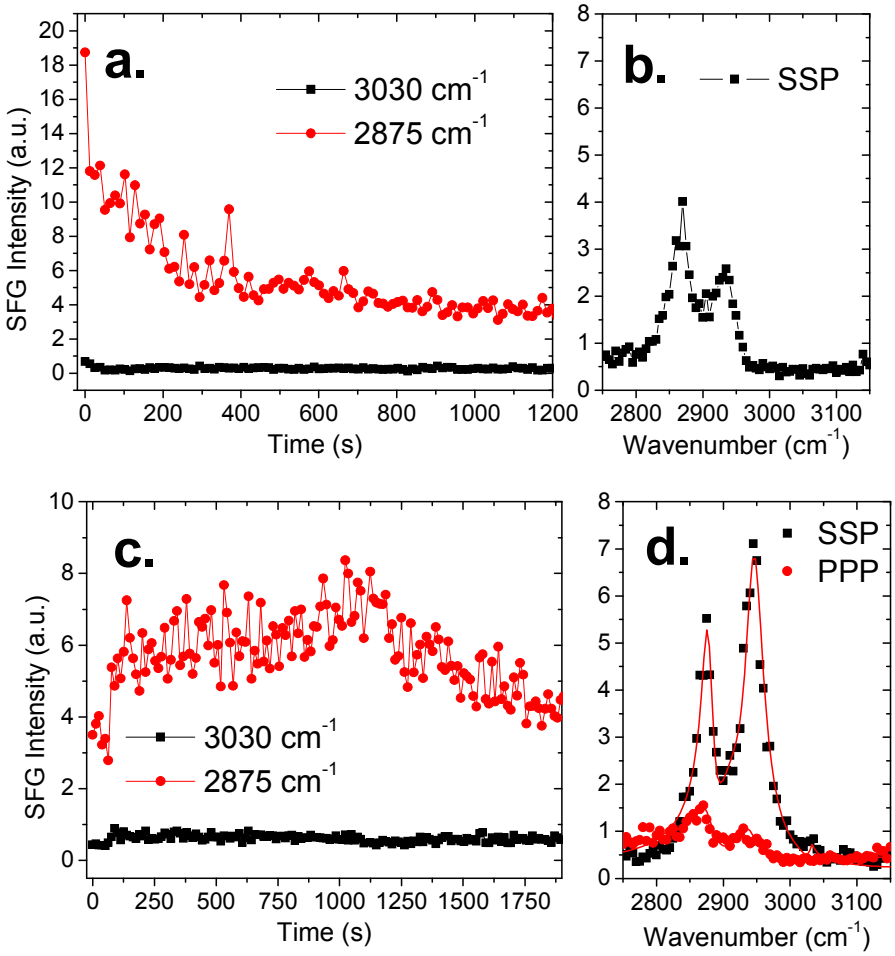

Figure 6.7. SFG results: 6.7a. Time dependent ssp signals detected during contact of PS-d_8 with NP to D_2O; 6.7b. The ssp spectra obtained after 20 min in D_2O; 6.7c. Time dependent ssp signals obtained after plastic is removed from D_2O; 6.7d. The ssp and ppp spectra obtained after 40 min of exposure to clean air with fits shown as red lines and data as points.

To further test the stability of the deposited NP molecules, the plastic was exposed to moving water for 30 min in the form of D_2O stirred at 125 rpm, and SFG time-dependent spectra were obtained *in situ* (Figure 6.7a). Almost immediately a decrease in CH_3(s) intensity is

observed, from both loss of molecules and increased disorder. At 20 min of water contact, SFG ssp spectra show CH_3 and CH_2 groups remain somewhat ordered at the water interface (Figure 6.7b).

After water contact, the plastic is re-exposed to air for 1 h. At this point, there should be even fewer NP molecules on the surface of the plastic. Time dependent SFG signals (Figure 6.7c) show an increase and decrease in SFG signal over increasing drying time, indicating molecular rearrangement as the hydrophobic methyl groups first stand up and then relax as the plastic surface dries. The final ssp and ppp spectra in Figure 6.7d indicate that the CH_3 groups are highly ordered. Fitting results indicate that the methyl groups tilt at an average of approximately 43° to the surface normal, similar to their previous orientation in air before water contact. The lack of large phenyl signal indicates that the phenol rings lie down or are buried in the plastic. Looking at the total intensity of the ssp spectra at the end stage versus after removal from the chamber (a.u. of 5.5 vs. 11 for the CH_3(s) mode) and at the decrease in time dependent spectra after in Figure 6.7c, we can insinuate that there are fewer molecules present after the agitating steps. Most importantly, we can conclude that even after agitating steps modeling a plastic re-exposed to moving water, there are still NP molecules present on the surface of the plastic.

6.3.4 NP Adsorption/Desorption on PS Under Humid Conditions

SFG experiments were also completed to model molecular surface changes of PS plastic exposed to a new point source of NP air-borne molecules under humid conditions like those near a body of water. SFG time dependent signals obtained during deposition of NP above water show an interesting signal trend (Figure 6.8a). Instead of a steady increase in CH_3(s) signal, the

signal increases overall, but there are two areas of faster signal increase at around 700 s and 2400 s as well as a much higher signal intensity than the dry conditions (note maximum a.u. of 20 versus 3.5). The phenyl ring signal changes can be observed and an increase then decrease in the 3030 cm^{-1} signal is seen at around 2500 s.

After two hours of exposure, ssp and ppp SFG spectra were obtained inside the deposition chamber (Figure 6.8b). Here, weak phenyl signal can be observed as well. CH_3 signals are present under both polarizations, indicating methyl group ordering once again. However, no calculations for orientation were completed since we know that at this point, more than a monolayer of NP molecules may be present on plastic (according to the QCM data presented above). We can assume that if water molecules were also present on the surface of the plastic, the rearrangement of CH_3 groups away from the surface would be likely.

A similar pattern to the low humidity case arises once the chamber is removed and the system exposed to clean air (Figure 6.8c). A clear initial signal increase and then decrease is observed for the CH_3(s) group as the chamber is removed and NP molecules evaporate. After 30 min, SFG signals remain similar in intensity. Note that the NP SFG signals are much higher after exposure to air for 1h in the humid case than the dry case, which may be indicative of better molecular ordering on the surface of the plastic exposed to a humid environment.

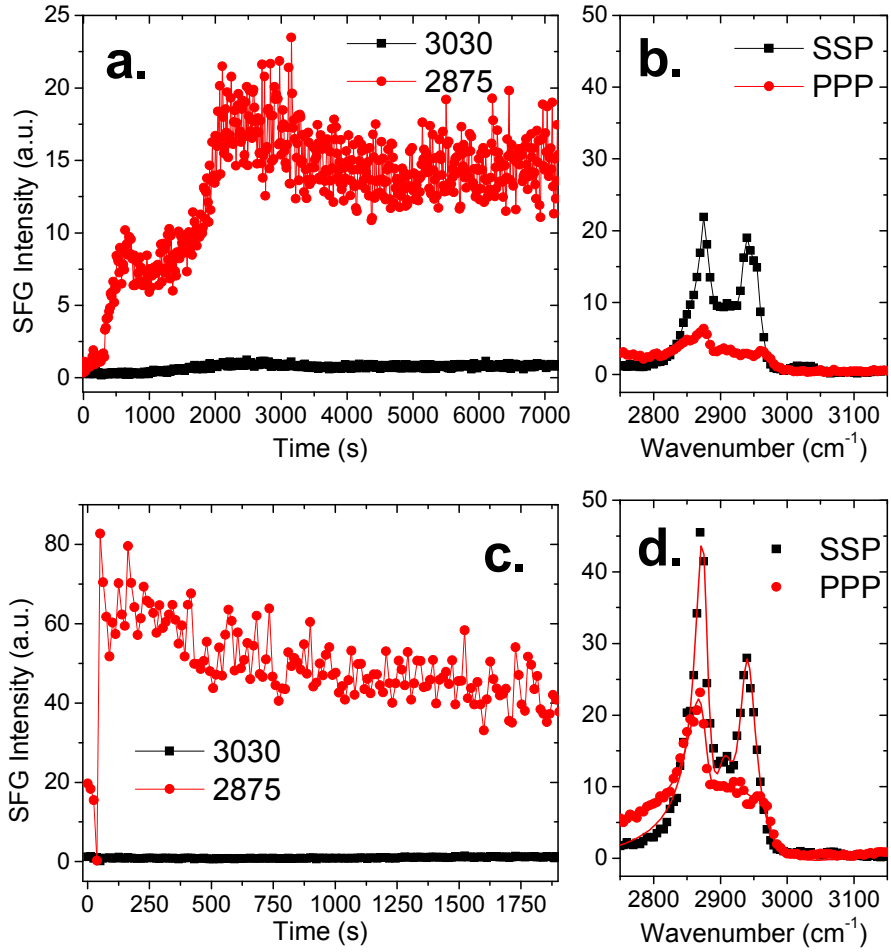

Figure 6.8. SFG results: 6.8a. Time dependent ssp signals during the NP deposition process on PS-d_8 in humid chamber; 6.8b. The ssp and ppp spectra obtained after 2 h of exposure in chamber; 6.8c. Time dependent ssp signals obtained once chamber is removed; 6.8d. The ssp and ppp spectra obtained after 40 min of exposure to clean air with fits shown as red lines and data as points.

At 45 min of clean air exposure, SFG spectra are obtained (Figure 6.8d). Calculations reveal that the CH_3 molecular groups tilt at an average of 44° to the surface normal, very similar to the calculated orientation of CH_3 groups 45 min after NP deposition under low humidity. Interestingly, the overall SFG signal intensities are still much higher after the humid deposition compared to the dry deposition. This contrasts with QCM results, which indicate a similar number of NP molecules remain on the plastic surface after 20 min of exposure to clean air, regardless of deposition environment.

It is believed that the presence of water on the plastic plays a role in these increased SFG signal intensities during and after humid NP deposition. With more water present during deposition, forming a more hydrophilic surface, more methyl groups on the 12 isomers of NP will become ordered and tilt away from the plastic surface, or in other words, there are fewer NP groups that point inward to the plastic, are disordered, or lie flat due to hydrophobic/hydrophilic molecular interactions. Thus, we do not see dramatic changes in average methyl orientation after the NP is deposited in a humid environment, but still see an overall increase in methyl signal intensities.

Upon exposure to the agitating water system, CH_3(s) signals drop dramatically, (Figure 6.9a and 6.9b) but increase once the plastic is re-exposed to air and reach a stable surface structure after 30 min (Figure 6.9c and 6.9d). Owing to a loss of surface molecules, the SFG signals are much lower than first exposure to air, and it is apparent that CH_3(s) groups are still well ordered, with an average orientation of 33° to the surface normal after 45 min of drying time. This indicates that the NP molecules adopt different orientations at equilibrium after they were deposited under humid conditions compared to dry conditions. We also conclude that NP molecules remain on the plastic surface after agitation.

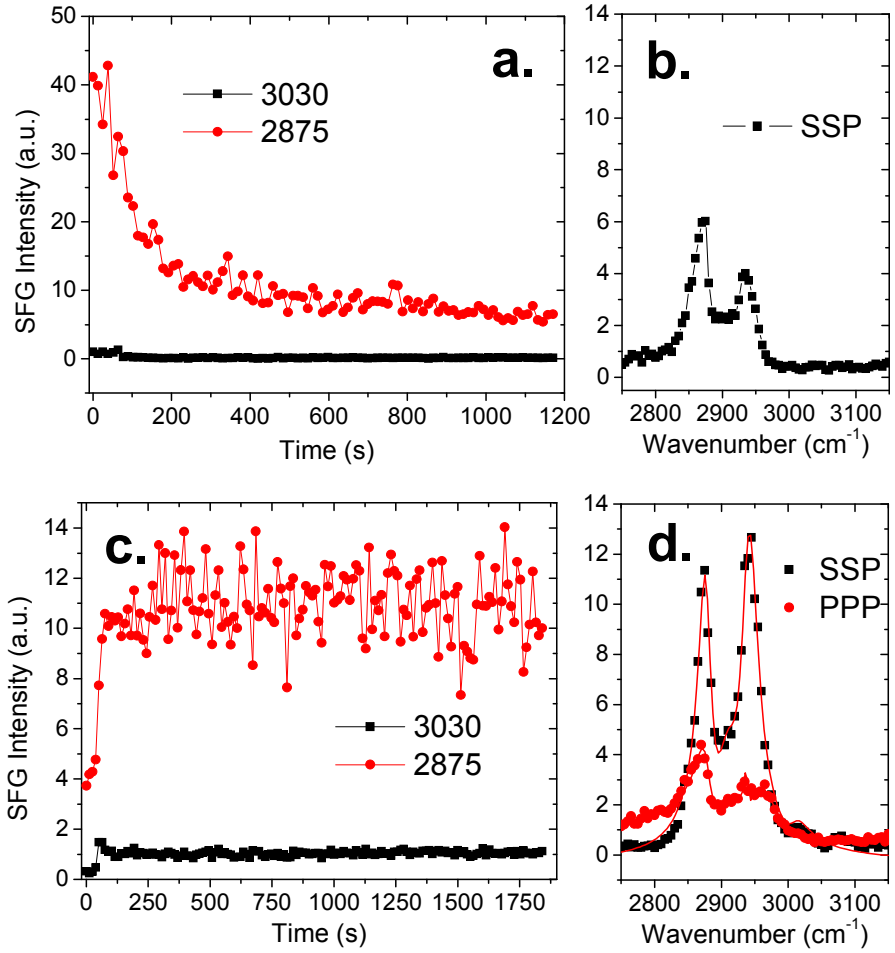

Figure 6.9. SFG results: 6.9a. Time dependent ssp signals during contact of PS-d_8 with NP to D_2O; 6.9b. The ssp spectra obtained after 20 min in D_2O; 6.9c. Time dependent ssp signals obtained after plastic is removed from D_2O; 6.9d. The ssp and ppp spectra obtained after 40 min of exposure to clean air with fits shown as red lines and data as points.

6.3.5 NP Adsorption/Desorption on PS Under Humid Conditions with Lake Water Solution

To demonstrate the validity of NP deposition on plastic under a lake environment, the humid NP deposition experiments were repeated with lake water collected from Lake Erie instead of purified and/or heavy water. As can be seen in Figure 6.10a., the same sort of CH_3(s) signal intensity pattern occurs. And with the lake water experiments, all SFG signals are on the same order or higher than those found with the humidity NP model deposition experiments.

After 2h of NP exposure in the chamber (Figure 6.10b.), it can be observed that the CH_3(s) groups tilt towards the surface normal, and the phenyl rings do not lie completely flat, similar to the experiments with D_2O solutions. There is also evidence of a small amount of water ordering on the surface of the plastic; O-H stretching signals between 3100 and 3700 cm^{-1} can be seen. After removal of the chamber (Figure 6.10c.) there is a slight decrease in signal, indicating some surface NP loss. A second NP deposition experiment can be seen in Figure 6.10d. Here, the change in CH_3(s) signal is more obvious. This experiment demonstrates that in a real lake environment, NP may not deposit exactly the same on different plastic samples, but the same type of ordering behaviors may occur.

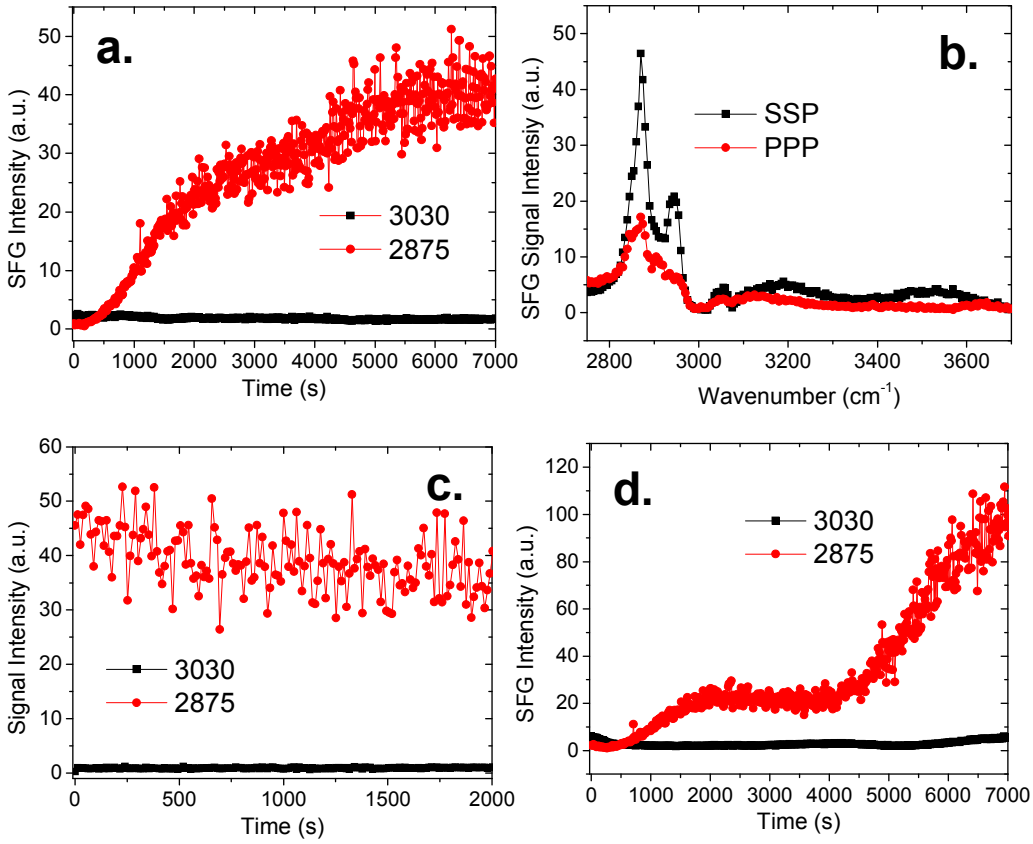

Figure 6.10. SFG results: 4a. Time dependent ssp signals during NP deposition process on PS-d_8 in humid chamber using lake water instead of purified water; 6.10b. The ssp and ppp spectra obtained after 2h of exposure in chamber. Note small signals from ordered water present (evidenced by the O-H stretching signals between 3100 and 3700 cm^{-1}); 6.10c. Time dependent ssp spectra obtained once chamber is removed; 6.10d. Time dependent ssp spectra during NP deposition process for a second sample. Note changes in intensity but same basic signal pattern.

6.3.6 Studies on Water Presence and Ordering During NP Humid Deposition

To try and pinpoint the presence and role of interfacial water ordering on NP deposition behaviors under humid conditions, SFG spectra were obtained of the humid condition model using H_2O instead of D_2O. Results can be seen in Figure 6.11a. Upon introduction of the 100 ppm NP water mixture to the sample chamber, some ordered water signature is observable with a peak center around 3300 cm^{-1}. The large signal seen at 2900 cm^{-1} is partially attributed to non-resonant signal of PS-d_8 under ppp SFG conditions. The spectra obtained in ppp polarization at

the plastic surface were normalized to green light only and a dip at 3200 cm^{-1} occurs because of fluctuation in IR intensity. At the end of 2.5 h of exposure, the surface of the plastic reveals intense signals from NP and not much change in the ordered water signal. No pattern of multiple increases and decreases in water signal were observed like in the case of CH_3(s) signal during humid deposition. However, the presence of some tightly bound interfacial water molecules on the surface of the PS plastic during NP deposition is confirmed. There is no evidence of decrease in ordered water signal throughout the NP deposition process as well. Throughout the deposition process, theoretical mass calculations coupled with QCM data indicate that less than a monolayer of water should be present on the surface of the plastic. Therefore it is likely that the observed SFG water signals originate from the ordered water molecules near the surface of the plastic and give a good representation of interfacial water structure.

To prove that the spectral peaks observed in the previous figure are indeed due to ordered water, the same experiments with 100 ppm nonylphenol solution were completed with D_2O and spectra were again obtained *in situ* (Figure 6.11b). Note that an increase in signal is observed (this time the first spectrum demonstrates a much lower non-resonant ppp signal) but no peaks in the water O-H stretching region of the spectrum are observed throughout the process from start to 2.5h. Here the spectra are corrected for green only again to avoid generating false peaks in the background.

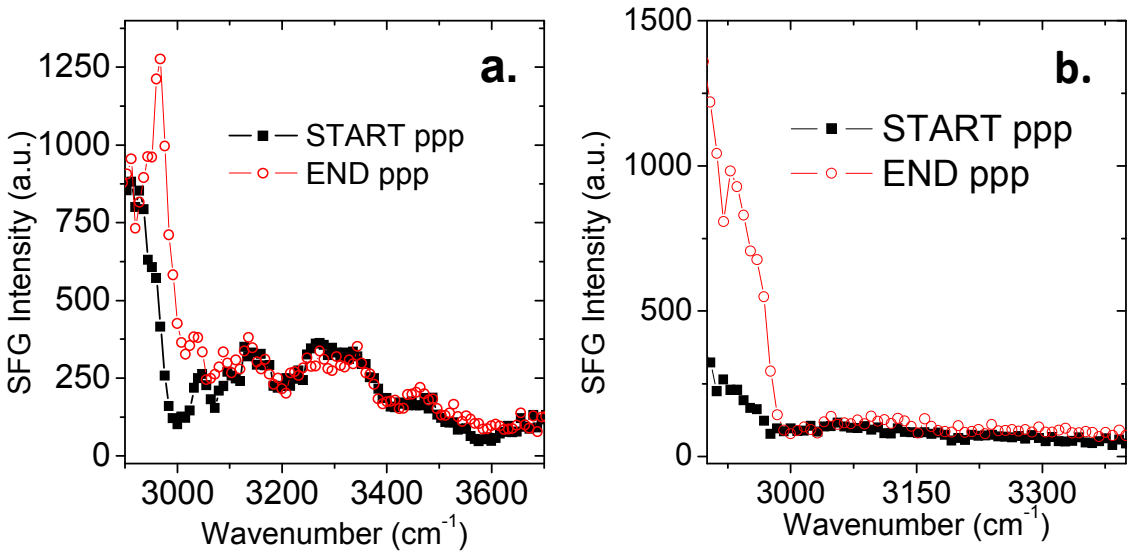

Figure 6.11. SFG Results: 6.11a. SFG water ppp spectra obtained during humid NP deposition process on PS-d_8 in humid chamber using H_2O instead of D_2O. Starting spectra obtained upon chamber enclosure and final spectra after 2h; 6.11b. SFG ppp spectra obtained during humid NP deposition process on PS-d_8 in humid chamber using D_2O. Starting spectra obtained upon chamber enclosure and final spectra after 2h.

ATR-FTIR data reveal that D_2O molecules are present on the PS plastic surface very quickly upon the addition of a glass slide with 100 ppm nonylphenol in D_2O 3 mm above the plastic-coated ATR crystal. Only one broad peak centered at about 2500 cm^{-1} can be observed, and a trend in the increase of D_2O signal, and therefore number of molecules, is observed up to about 35 min, indicating that D_2O molecules continue to deposit during the NP deposition process (Figure 6.12). At 35 min and thereafter a decrease in signal occurs at the same time that a decrease in the amount of solution on the slide is observed, indicating that in this loosely closed system the volume of water used is not sufficient to reach saturation equilibrium. If more solution is added (data not shown), the D_2O signals increase once again, confirming this hypothesis. Thus the ATR-FTIR experiment is not completely similar to the SFG and QCM experiments, which contain enough water molecules to be able to reach saturation equilibrium. However, ATR-FTIR data does agree with the QCM data presented previously, which shows the

quick start of deposition of water and contiguous deposition during the time that NP is also deposited. The ATR data also demonstrates the power of our SFG technique. For ATR-FTIR, heavy water dominates the spectrum and it is extremely difficult to observe peaks associated with NP, whereas with SFG we can single out NP vibrational signatures and observe them at T < 1min.

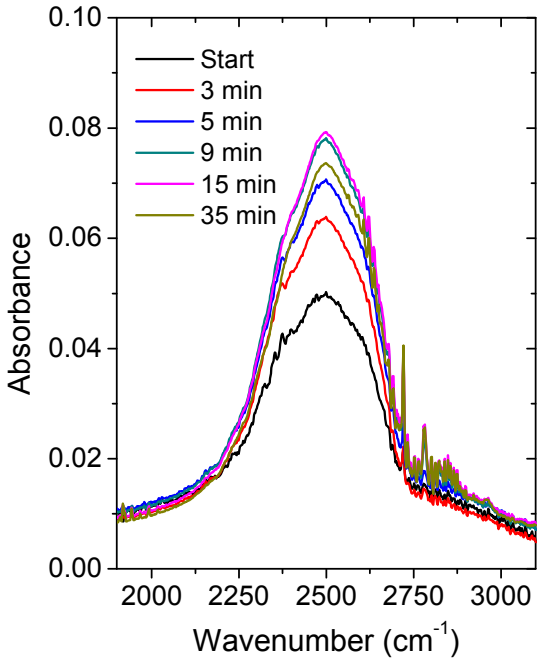

Figure 6.12. ATR-FTIR spectra obtained during humid deposition of NP on PS-d_8.

QCM data and ATR-FTIR data indicate a steady deposition of water molecules during the humid NP deposition, but the SFG signals of ordered water do not change over time. This means that we cannot conclude the degree of water ordering is the underlying reason for SFG signal changes during NP humid deposition. We can reasonably conclude that the presence of surface water molecules induces changes that result in SFG signal fluctuations since the

increased number of water molecules (and decreased number of NP(g)) is the major difference between the two deposition systems. It is likely that hydrophilic/hydrophobic interactions between the plastic, NPs and water induced SFG CH_3(s) signal changes but a more detailed investigation into the physical mechanism behind the SFG signal fluctuation, should be conducted in the future.

6.4 Conclusions

In this study we found that NP quickly and semi-permanently deposits on PS plastic under both dry and humid conditions, modeling environments over land mass, and lake water, respectively. Surprisingly, a similar number of stable NP molecules are deposited on PS under humid conditions and dry conditions even though the initial concentration of NP(g) molecules under the former condition was orders of magnitude lower. NP molecules reorder in a unique manner during deposition on plastics under humid conditions, most likely due to the presence of interfacial water molecules and changing surface energy of the plastic. In addition, C-H groups of NP surface molecules deposited under humid conditions were more ordered at all stages of investigation than those of NP molecules deposited under dry conditions. Agitating conditions (moving water and re-exposure to air) remove NP molecules from PS, but some surface NP molecules deposited under humid or dry conditions remain on the surface of the plastic at all stages of testing.

Realistically, our results indicate that a prolific environmental lake toxin, nonylphenol, may quickly and semi-permanently deposit on very small pieces of hydrophobic plastics above lake water even under extremely low air concentrations (lower than 9 ppt) and calm weather conditions. In a matter of hours under these model lake conditions, tens to hundreds of

nanograms of gas phase NP can sorb on an area of plastic less than half a millimeter and major NP deposition on the plastic surface occurs in less than 1 min. The presence of atmospheric water induces unique molecular restructuring at the plastic surface over minutes to hours, changing how the NP deposits. In the case of polystyrene plastic, there is great potential for just as much NP to sorb and collect in great numbers on plastic in a humid environment compared to a dry one with a much higher concentration of gas-phase NPs. Overall, NP deposition on plastics occurs much differently at a molecular level above bodies of water compared to on land. If NP or similar environmental toxins deposit on hydrophobic plastics in a freshwater system, it is highly likely that some toxins will remain in the surface layers of the plastic (and not sorb completely into the plastic) until transfer to a more favorable amphiphilic environment is available.

6.5 References

1. *Nonylphenol (NP) and Nonylphenol Ethoxylates (NPEs) Action Plan*, U.S. Environmental Protection Agency, 2010.
2. *SVHC Support Document-4-Nonylphenol, Branched and Linear*, European Chemicals Agency, 2012.
3. Soares, A.; Guieysse, B.; Jefferson, B.; Cartmell, E.; Lester, J. N. *Environ. Int.* **2008**, *34*, 1033.
4. Bennett, E. R.; Metcalfe, C. D. *Environ. Toxicol. Chem.* **2000**, *19*, 784.
5. Hung, Y. T.; Wang, L. K.; Shammas, N. K. *Handbook of Environment and Waste Management: Air and Water Pollution Control*; World Scientific, 2012.
6. Lichtfouse, E.; Schwarzbauer, J.; Robert, D. *Environmental Chemistry: Green Chemistry and Pollutants in Ecosystems*; Springer, 2005.
7. Giger, W.; Brunner, P.; Schaffner, C. *Science* **1984**, *225*, 623.
8. Bidleman, T. F.; Renberg, L. *Chemosphere* **1985**, *14*, 1475.
9. Ieda, T.; Horii, Y.; Petrick, G.; Yamashita, N.; Ochiai, N.; Kannan, K. *Environ. Sci. Technol.* **2005**, *39*, 7202.
10. Federal Register, 2014; Vol. 79, p 58686.
11. Bennie, D. T.; Sullivan, C. A.; Lee, H. B.; Peart, T. E.; Maguire, R. J. *Sci. Total Environ.* **1997**, *193*, 263.
12. Li, H.; Helm, P. A.; Metcalfe, C. D. *Environ. Toxicol. Chem.* **2010**, *29*, 751.
13. Kavanagh, R. J.; Balch, G. C.; Kiparissis, Y.; Niimi, A. J.; Sherry, J.; Tinson, C.; Metcalfe, C. D. *Environ. Health Perspect.* **2004**, *112*, 898.
14. Dachs, J.; Van Ry, D. A.; Eisenreich, S. J. *Environ. Sci. Technol.* **1999**, *33*, 2676.
15. Castañeda, R. A.; Avlijas, S.; Simard, M. A.; Ricciardi, A. *Can. J. Fish. Aquat. Sci.* **2014**, *71*, 1767.
16. Gouin, T.; Roche, N.; Lohmann, R.; Hodges, G. *Environ. Sci. Technol.* **2011**, *45*, 1466.
17. Eriksen, M.; Mason, S.; Wilson, S.; Box, C.; Zellers, A.; Edwards, W.; Farley, H.; Amato, S. *Mar. Pollut. Bull.* **2013**, *77*, 177.
18. Wagner, M.; Scherer, C.; Alvarez-Munoz, D.; Brennholt, N.; Bourrain, X.; Buchinger, S.; Fries, E.; Grosbois, C.; Klasmeier, J.; Marti, T.; Rodriguez-Mozaz, S.; Urbatzka, R.; Vethaak, A.; Winther-Nielsen, M.; Reifferscheid, G. *Env. Sci. Eur.* **2014**, *26*, 12.
19. Eerkes-Medrano, D.; Thompson, R. C.; Aldridge, D. C. *Water Res.* **2015**, *75*, 63.
20. Frias, J. P. G. L.; Sobral, P.; Ferreira, A. M. *Mar. Pollut. Bull.* **2010**, *60*, 1988.
21. Antunes, J.; Frias, J.; Micaelo, A.; Sobral, P. *Estuar Coast Shelf S* **2013**, *130*, 62
22. Ivar do Sul, J.; Costa, M. *Environ. Pollut.* **2014**, *185*, 352.
23. Andrady, A. L. *Mar. Pollut. Bull.* **2011**, *62*, 1596.
24. Lorena Rios Mendoza, P. J. *Environ. Chem.* **2015**, *Just Accepted*.
25. Bakir, A.; Rowland, S.; Thompson, R. *Mar. Pollut. Bull.* **2012**, *64*, 2782.
26. Bakir, A.; Rowland, S. J.; Thompson, R. C. *Environ. Pollut.* **2014**, *185*, 16.
27. Cole, M.; Lindeque, P.; Halsband, C.; Galloway, T. *Mar. Pollut. Bull.* **2011**, *62*, 2588.
28. Hankett, J. M.; Lu, X. L.; Liu, Y. W.; Seeley, E.; Chen, Z. *PCCP* **2014**, *16*, 20097.
29. Hankett, J. M.; Zhang, C.; Chen, Z. *Langmuir* **2012**, *28*, 4654.
30. Zhang, X. X.; Li, Y. X.; Hankett, J. M.; Chen, Z. *PCCP* **2015**, *17*, 4472.
31. Lis, D.; Backus, E. H. G.; Hunger, J.; Parekh, S. H.; Bonn, M. *Science* **2014**, *344*, 1138.

32. Wang, T.; Li, D. W.; Lu, X. L.; Khmaladze, A.; Han, X. F.; Ye, S. J.; Yang, P.; Xue, G.; He, N. Y.; Chen, Z. *J. Phys. Chem. C.* **2011**, *115*, 7613.
33. Stokes, G. Y.; Chen, E. H.; Walter, S. R.; Geiger, F. M. *J. Phys. Chem. A* **2009**, *113*, 8985.
34. Song, S. H.; Koelsch, P.; Weidner, T.; Wagner, M. S.; Castner, D. G. *Langmuir* **2013**, *29*, 12710.
35. Kristalyn, C. B.; Watt, S.; Spanninga, S. A.; Barnard, R. A.; Nguyen, K.; Chen, Z. *J. Colloid Interface Sci.* **2011**, *353*, 322.
36. Ebben, C. J.; Ault, A. P.; Ruppel, M. J.; Ryder, O. S.; Bertram, T. H.; Grassian, V. H.; Prather, K. A.; Geiger, F. M. *J. Phys. Chem. A* **2013**, *117*, 6589.
37. Cremer, P. S.; Su, X.; Shen, Y. R.; Somorjai, G. A. *J. Am. Chem. Soc.* **1996**, *118*, 2942.
38. Hankett, J. M.; Collin, W. R.; Chen, Z. *J. Phys. Chem. B* **2013**, *117*, 16336.
39. Hankett, J. M.; Liu, Y. W.; Zhang, X. X.; Zhang, C.; Chen, Z. *J. Polym. Sci., Part B: Polym. Phys.* **2013**, *51*, 311.
40. Hsiao, E.; Barnette, A. L.; Bradley, L. C.; Kim, S. H. *ACS Appl. Mater. Interfaces* **2011**, *3*, 4236.
41. Hu, D.; Yang, Z.; Chou, K. C. *J. Phys. Chem. C.* **2013**, *117*, 15698.
42. Lu, X. L.; Han, J. L.; Shephard, N.; Rhodes, S.; Martin, A. D.; Li, D. W.; Xue, G.; Chen, Z. *J. Phys. Chem. B* **2009**, *113*, 12944.

CHAPTER 7

SUMMARY AND FUTURE DIRECTIONS

Research in this thesis investigated the *in situ* molecular interactions between common plastics and surrounding matter including chemical reactions, plasticizer leaching, surface structural changes, and toxin adsorption in order to better understand how plastics impact the environment at a molecular level. Much emphasis was placed on studying changes to phthalate-plasticized PVC plastics from harsh chemical environments and proposed plasticizer treatment methods. The effects of changes in environment (humidity) on toxin sorption on common plastics were also elucidated. A brief summary of research conclusions, achievements and impacts is given below.

7.1 Thesis Summary

Chapter Two marks the onset of research probing the molecular behaviors of phthalate-plasticized PVC plastics *in situ*. Together with Dr. Chi Zhang, we developed sample and experimental methodology to study both the surface and bulk structures of polymer materials in the same environment near simultaneously using Chi's CARS/SFG combined laser setup. Such general methods may be applied to study the surface and bulk structures of a wide range of complex polymer systems in the same chemical environment.

We demonstrated that DEHP, a common PVC plasticizer, can be present on the surfaces of model PVC plastics under normal atmospheric conditions even if very little DEHP was added to the plastic by weight (5 wt%). Annealing of the plastics leads to phthalate leaching, which was observed with both SFG and CARS spectroscopies. The power and sensitivity of analytical nonlinear optical technique SFG was demonstrated by early observation of phthalate leaching occurring at a scale of hours rather than days or weeks. Because of the inherent sensitivity of the SFG process, we are able to use this spectroscopy as a predictive technique for fundamental studies on surface chemical reactions, ultimately saving time and resources during the process of surface treatment selection.

We also elucidated the surface and bulk molecular effects of surface leaching treatment air plasma exposure on PVC plastics plasticized with different concentrations of phthalates. Results include surface scission of PVC chains, removal of chlorine, and deposition of oxygen moieties. The C-H groups of surface DEHP molecules remained relatively intact compared to the PVC polymer. No major changes were observed to occur throughout the bulk of the plastics, leaving us to conclude that at appropriate exposure times, air plasma treatment induces chemical reactions only at the topmost surface layers of PVC plastics. An understanding of how leaching treatments like plasma exposure change plastics at a molecular level can greatly aid in improving and developing new treatments and methodologies.

In Chapter Three, I investigate the molecular changes induced to PVC plastics from short and long wave UV exposure, with intent to understand how plastic structure and content change from exposure to UV lamps and sunlight at a fundamental level. It was determined that phthalate-plasticized PVC materials were greatly affected by short wave UV exposure on a scale of hours, leading to the degradation of phthalates on both the surface and bulk of the plastic

through reactions with ozone and hydroxyl radicals. Stable surface products formed from short wave UV exposure include monoesters, diacids, and alkyl products before complete degradation. PVC plastics that did not contain phthalates were less affected by short wave UV, leading only to minor reactions of PVC chains throughout the plastic, increased surface hydrophilicity, and some deposition of surface oxygen moieties. In contrast, exposure of phthalate-plasticized PVC to long wave UV induced no chemical changes, as the phthalates protected the PVC chains from damage. Results from this Chapter aid in demonstrating how plastics may be altered after exposure to harsh chemical environments even when no macroscopic or microscopic physical changes can be observed. In addition, the fundamental insights gained in this study aid in environmental research on plastics, elucidating which surface products may now interact with surrounding wildlife.

In Chapter Four, we take the information gained in Chapter Three and push it forward towards real-life applications of treating plastics after disposal. The goal in this Chapter was to evaluate the effectiveness of two UV-based plastic treatment methods designed to degrade phthalates in plastic and thus reduce or eliminate the risk of phthalate leaching after the plastic is no longer usable. Spectroscopic techniques SFG and SIMS evaluated the molecular surface structure changes, and surface content changes, respectively, after plastics were treated with short wave UV, or short wave UV/35 wt% H_2O_2. It was found that both methods left similar phthalate degradation products up to 5h of treatment, with only surface structural changes varied due to the introduction of liquid in the latter treatment method. Bulk spectroscopic technique FTIR revealed molecular changes throughout the majority of the plastic. Interestingly, short wave UV exposure appeared to degrade more phthalates up to 8h of treatment in the bulk of the plastic compared to the UV/H_2O_2 treatment. This was found to occur because the aqueous-phase

hydroxyl radicals from H_2O_2 preferentially reacted with polymer chains over phthalates. Finally, a basic degradation scheme of DEHP reactions from the two treatment methods was proposed, highlighting stable step degradation products MEHP, diacids, and molecules with hydroxylated phenyl rings.

Thus, we evaluated simple short wave UV exposure as a successful methodology to degrade phthalates in used clear and/or thin PVC plastics, with minimal damage to the polymer itself. This may be applicable for plastics designated for recycling and landfills. In contrast the UV/H_2O_2 treatment was slightly less successful in degrading phthalates in the allotted time, but also induced polymer reactions to partially degrade the PVC polymer. Therefore, the UV/H_2O_2 treatment may be applied to clear and/or thin PVC plastics which will be disposed of rather than recycled, due to the added benefit of pre-degradation of the polymer network which aids in speeding up the breakdown of the plastic itself. One must take into account, however, the safety and ease of treatment methods, in which case short wave UV exposure alone is the clear choice. The methods developed in this thesis for plasticizer degradation forward research in environmental detoxification, and if polished and combined with current practices, may be helpful in regions where proper disposal routes may be lacking

The research in Chapter Five led us to understand how PVC plastic surfaces change from water contact using SFG, and advanced SFG theory on post-processing multiple-interface signals. For all PVC plastics, water contact induced irreversible surface molecular ordering changes. But, it was determined that the degree of surface order and speed of water penetration through PVC thin films was directly dependent upon the concentration of phthalate added to the plastic. A small percent of DEHP (10 wt%) added to PVC actually increased CH_2 order at the plastic/water interface compared to pure PVC, but left all CH_3 groups almost instantly disordered

as was seen in the case of pure PVC as well. With a larger percent of DEHP added to PVC (25 wt%), the surface of the plastic was almost instantly disordered at the water interface, and water migrated through the film quickly, to induce almost complete molecular disorder on the opposite side of the film. Newly developed SFG-based leaching tests revealed that in the process of surface disordering, some DEHP leached into water and could be transferred permanently to new materials by water contact within minutes. Therefore using this platform we can observe how toxins release and transfer from surface to surface through liquid contact.

During this process, we found that it is possible to gain information on two interfaces of a thin-film system at the same time, provided the conditions for the sample are appropriate. The developed multi-interface methodology we utilized to deconvolute multi-interface SFG signals is general and can be applied to numerous thin-film systems *in situ* and in real time. In addition, it aids in explaining signal differences observed when the same thin-film sample is probed with SFG under two different sample geometries.

Lastly, in Chapter Six I investigate the interaction of prominent environmental toxins nonylphenols with hydrophobic microplastic surfaces under model lake vs. land conditions using SFG with a new sample stage chamber, QCM, and ATR-FTIR. With SFG, we could observe NP deposition *in situ*, and found gas-phase NP molecules depositing on plastics in seconds under both environments. It was determined that the humid air space above a calm lake surface provides an excellent environment for NP deposition on hydrophobic plastics. We determined increases in humidity, and thus the presence of water molecules on the surface of the plastic in the model lake conditions changed how NPs deposited on plastic surfaces at a molecular level. In the case of PS, this led to a similar amount of NP deposition and greater molecular ordering under model lake conditions compared to dry land with much fewer available NP molecules.

This may have occurred because the increase in surface hydrophilicity provided a better environment for adsorption and packing on the PS surface. Under the humid environment, more CH_3 groups on NP were highly ordered toward the plastic surface normal, again attributed to changes in surface energy. The permanence of NP deposition on plastic was tested by inducing agitating conditions (air exposure, moving water exposure and re-exposure to air) and it was found that each agitating step reduced the number of NP molecules on the plastic surface, but NP molecules were present on plastic surfaces at all steps, regardless of deposition environment.

From these studies we can conclude that very hydrophobic microplastics located in a humid environment with toxin point sources (as is the case with the Great Lakes), may collect and adsorb similar amounts of toxins like NP over extended amounts of time compared to plastics located on land with a much higher number of available NPs nearby. We can also predict that some plastic-bound toxin molecules will evaporate once the point source is removed, but that the plastic will likely retain some surface toxin molecules until a more favorable hydrophobic environment is presented. By understanding how prominent toxins adsorb, desorb, and pack on microplastic surfaces, we may further elucidate the impact of microplastics on freshwater organism life cycles.

7.2 Future Research

As has been stated throughout this thesis, the work performed here was fundamental in nature, and while we do provide vital information forwarding applied research, there are also very many future research avenues that can branch off from these projects. Here, I will briefly outline a few research opportunities which I believe should be addressed in the future.

7.2.1 Fundamental Nonlinear Optical Spectroscopy on Bio-Polymers

It can be clearly concluded from this thesis that while investigation of methods to reduce the negative impact of PVC plastics on the environment are warranted, the future application of polymer alternatives should also be considered. The institution of new plastics that may be manufactured with fewer or no petrochemicals is particularly desirable as the depletion of non-renewable energy resources continues. Viable alternatives to PVC and medical plastics include bio-plastics, which may be synthesized and even degraded by bioorganisms.[1-3] As of yet, no promising bio-produced plastics have been thoroughly studied using SFG and CARS. Lack of surface nonlinear optical studies on these materials may be attributed to bio-polymer thin-film structures, which tend to be crystalline and generate bulk SFG signals. But there is great promise in studying the surface and bulk structures of bio-plastic polymer blends, which are often more stable, robust, and less crystalline materials than the bio-plastic alone. I believe that SFG/CARS studies can again be utilized to predict in which model situations bio-plastics degrade or remain unaltered, in efforts to advance future plastic formulation.

7.2.2 Advancing Analytical Research on Lake-bound Microplastics

As previously mentioned, environmental research on the impact of microplastics on freshwater ecosystems is currently in its infancy. Thus, there are many research directions within this field varying from field ecology work to fundamental physical studies. Some potential projects however, are of particular interest to me. These include UV-degradation studies on plastics within the surface layers of water, enhanced bio-degradation of common plastics, and combinatory analytical research on plastic bio-films.

Briefly, to address the former research study, it is important to elucidate the effects of aging and UV/radical degradation on lake-bound microplastics for two major reasons. First, the surface and bulk of the plastics may dramatically change at a molecular level and knowing how plastics change can yield what molecules and molecular fragments are now introduced to the surrounding ecosystem. Second, the induced molecular changes may provide different environments for microbial growth and toxin adsorption, due to changes in hydrophobicity and surface energy. Currently, it is difficult to predict the age of a microplastic collected from a freshwater system. But, if there are means to correlate microbial strains with degree of plastic degradation through model spectroscopic studies, researchers may be able to gain important information on the lifetime of microplastics and their role in the surrounding environment. Spectroscopic studies on real plastics in a model lake environment exposed to UV light, toxins, and/or microbes, may help address the two proposed concerns.

On a related note, studies on the effects of microbial colonies and biofilms on hydrophobic plastics may reveal an energy efficient means to purposely degrade plastics under a variety of different environments. Introduction of complex microbial colonies or single strains of biofilm producing microorganisms to plastics for the purpose of bio-degradation has been previously performed with some success.[4-7] Research in this field could be furthered by studying the effects of colonies cultured from collected freshwater microplastics on plastics in-house. With the isolation of successful biofilm colonies, it may be feasible to someday utilize local biota to degrade plastics.

The mechanism of plastic biodegradation may vary depending upon both plastic type and microbial strain.[8] Microplastics collected from the field have shown surface pitting and erosion where microbial communities are present.[9] However, it is often difficult to decipher if micro-

pitting occurs from mechanical action or chemical reaction. Using analytical techniques like FTIR, SIMS, and SFG/TIRF, it may be possible to deduce possible chemical reactions between biorganism secretion and the molecular components of plastic surfaces, thus providing new details on the microbial life/plastic relationship.

7.3 Concluding Remarks

Conclusions on research topics tend to be difficult to write, if only for the fact that research in one's field of choice is never really finished. But if I can say anything at all regarding the enclosed Chapters, it is this: starting off as a budding young scientist with naive, if not overly ambitious goals, it has been both a pleasure and hardship to search for answers to the unknown. I take no attempt to profess that I am a much older, wiser person with regards to analytical and material science, but I can say that we did have some success in research achievements which I list here. The major goals of this research included the advancement of knowledge regarding the environmental impact of plastics, surface changes of plastics under varying conditions, future green plastic treatments, and the improvement and/or application expansion of non-linear optical analytical techniques. I can happily say that we have made progress in all four categories and have therefore collectively aided in the ongoing improvement of polymers and plastics. And as long as scientists as a whole continue the search to learn about materials integral to society at large, our abilities of improving and designing safer, greener, and more favorable future materials will continue to increase.

7.4 References

1. Chen, G. Q.; Patel, M. K. *Chem. Rev.* **2012**, *112*, 2082.
2. Martin, D. P.; Williams, S. F. *Biochem. Eng. J.* **2003**, *16*, 97.
3. Venkatraman, S.; Boey, F.; Lao, L. L. *Prog. Polym. Sci.* **2008**, *33*, 853.
4. Mor, R.; Sivan, A. *Biodegradation* **2008**, *19*, 851.
5. Cacciari, I.; Quatrini, P.; Zirletta, G.; Mincione, E.; Vinciguerra, V.; Lupattelli, P.; Sermanni, G. G. *Appl. Environ. Microbiol.* **1993**, *59*, 3695.
6. Ghosh, S. K.; Pal, S.; Ray, S. *Environ. Sci. Poll. Res.* **2013**, *20*, 4339.
7. Sivan, A. *Curr. Opin. Biotechnol.* **2011**, *22*, 422.
8. Shah, A. A.; Hasan, F.; Hameed, A.; Ahmed, S. *Biotechnol. Adv.* **2008**, *26*, 246.
9. Zettler, E. R.; Mincer, T. J.; Amaral-Zettler, L. A. *Environ. Sci. Technol.* **2013**, *47*, 7137.